Modeling the transport of *Escherichia coli* through the subsurface environment

By

Lee Burdenuk

A Thesis Submitted to the Faculty of Graduate Studies
In Partial Fulfillment of the Requirements for the degree of

Masters of Science in Environmental Engineering

Engineering Department
Lakehead University
Thunder Bay, Ontario
Fall 2009

Supervisors: Dr. B. Kjartanson and Dr. K. Leung

Abstract of the Thesis

Subsurface microbial transport is an important concern in many engineering projects. Expanding the knowledge of this process is important for the risk assessment of sites capable of releasing pathogenic bacterial species into the environment, as well as remediation efforts that involve bacterial injections into the subsurface.

Within the literature, most studies have focused on one-dimensional flow through columns containing soil of a uniform sandy texture. While such systems may be modeled relatively accurately through methods such as classic colloid filtration theory, the required assumptions of this and similar models are often grossly violated in real world situations. For example, such modeling techniques are unsuitable for soils of a heterogeneous texture or clayey soils where water flow is predominantly through soil fractures.

Studies examining the transport of bacteria through fractured clay soils are poorly represented in the literature. This research is of interest as such soils have been found to possess an elevated risk of bacterial infiltration relative to coarser soils such as sand. To investigate this phenomenon, our research group has conducted several experiments in the last few years. A modeling methodology was thus sought which could describe and extrapolate the recorded observations of these experiments. Based on the available data, an equilibrium model, and a mobile-immobile liquid phase model were developed by fitting the relevant transport parameters to the observed data using the CXTFIT software

package. Estimates of the associated transport parameters were found through bromide permeation, batch sorption, and fracture-flow analysis experiments.

The results indicate that the bacterial transport observed in the experimental compacted sand columns, and a subset of the experimental freeze-fractured compacted clay columns may be adequately modeled using a non-dimensional, basic equilibrium transport model with a decay coefficient fit to the experimental data. All freeze-fractured clay columns were best modeled using the CXTFIT mobile-immobile model. It is assumed in applying this modeling technique that bacterial transport occurred entirely within the fractured network of the experimental columns. The observed bacterial transport through compacted mixed 90% sand / 10% silt experimental columns, and compacted silts columns could not be adequately represented with any model used in this study.

Acknowledgements

The author would first like to acknowledge the expertise and guidance of his supervisors, Dr. B. Kjartanson and Dr. K. Leung, and all of the undergraduate and graduate students who have generated the data used in this project. C. Hagstrom for his assistance and guidance in preparing the column experiments. B. Rosa, M. Yim, C. Buonocore for their assistance in the collection of the microbiological data. And my former supervisor, Dr. E. Cholewa, for guiding me down the research path.

Table of Contents

List of Tables

List of Figures

Nomenclature, abbreviations and column labels

Latin symbols

$2b$ – fracture aperture (cm)

$2B$ – fracture spacing (cm)

A – cross sectional area of the soil column (cm^2)

a – first order kinetic rate coefficient (t^{-1})

C – solute concentration

c_{avg} – average *E. coli* concentration over an experimental data set

C_e - concentration of solute within the aqueous phase

c_i – measured *E. coli* concentration at a given time (C/C_o)

C_m – mean number of *E. coli* colonies in the given plate counting sample

c_{mi} – modeled *E. coli* concentration at a given time (C/C_o)

C_o – concentration of contaminant solute in the influent

d – diameter of the PVC cylinder (10.1 cm)

D – dispersion coefficient (Length^2 / time)

d_{10} – 10th percentile of the cumulative grain size distribution (m)

d_{50} – mean soil particle diameter

D_{brom} – Optimized dispersion coefficient as fit in the bromide breakthrough analysis

D_f – dilution factor of the given plate counting sample

d_m – diameter of bacteria (m)

D_{mim} – Optimized dispersion coefficient as fit within the mobile–immobile model

f_r – inverse of the flow rate in seconds/pore volume

g – acceleration due to gravity (cm/s^2)

Gs – specific gravity (unitless)

H – total head (dimensional length units)

h – head loss (cm)

i – hydraulic gradient (cm/cm)

k – hydraulic conductivity (cm/s)

K – slope parameter of the Freundlich sorption isotherm

k_{att} – first order kinetic attachment coefficient

K_d – distribution coefficient ($M^{-1}L^3$)

k_{det} – first order kinetic detachment coefficient

K_f – Hydraulic conductivity of fracture (cm/s)

K_L – adsorption constant in Langmuir sorption isotherm

k_m – measured hydraulic conductivity of the clay matrix

k_{str} – first order kinetic straining coefficient

k_{xy} – measured hydraulic conductivity of the fractured sample (cm/s)

k_y – hydraulic conductivity in the y–direction

k_z – hydraulic conductivity in the z–direction

L – transport distance (Length units or non–dimensional relative height)

L_c – total height of PVC column (m)

L_s – average height of space between top of soil column and top of PVC cylinder (m)

M – concentration of solute (dimensionless or dimensional g/g)

M_d – mass of oven dried soil sample (g)

M_e – mass of assembled soil apparatus without soil (kg)

M_L – maximum amount of contaminant that may be sorbed to the solid phase in the Langmuir sorption isotherm

M_s – mass of soil sample (kg)

M_{se} – mass of soil sample and assembled compaction apparatus (kg)

m_w – slope of the water storage curve used within SEEP/W

M_w – mass of moist soil sample (g)

N – unitless power constant of the Freundlich sorption isotherm

n_f – fracture porosity

PV – cumulative pore volumes at a given time (unitless)

Q – applied boundary flux

q – discharge per unit length of fracture (ml/s/cm)

Q – effluent volume (ml)

Q_t – cumulative effluent volume at a given time (ml)

R – retardation factor (unitless)

R^2 – coefficient of determination

S – concentration of cells attached to the solid phase (CFU / g)

t – dimensional time (seconds)

T – dimensionless time (PV)

$t_{1/2}$ – decay half life (time units)

u – flow viscosity of the fluid (g/cm/s)

v – average pore–water seepage velocity

V – volume of soil sample in m^3

V_v – volume of voids (ml)

w – moisture content (%)

x – independent variable in Geostudio addins

Greek symbols

α – attachment efficiency
β – dimensionless partitioning parameter (ratio of mobile pore fluid to immobile pore fluid)
γ – zero–order production coefficient
γ_w – unit weight of water (g/ml)
ζ – spatial distribution fitting parameter for the calculation of ψ_{str}
η – porosity
Θ – geometrical suffusion security (dimensionless)
θ – volumetric water content
μ – first–order decay coefficient
μ_{dim} – decay coefficient ($hour^{-1}$)
ρ_b soil dry density (Mg/m^3)
ρ_T – soil total density (Mg/m^3)
ρ_w – fluid density (g/ml)
ψ_{str} – depth dependant straining function
ω – dimensionless mass transfer coefficient

Abbreviations
CCFT – Classic Colloid Filtration Theory
CFU – Colony Forming Unit
Clay – Kam red clay
DLVO – Derjaguin–Landau–Verwey–Overbeek theory
LB – Luria–Bertani
M FC – membrane fecal coliform
MSM – Minimum salt media
NAPL – non–aqueous phase liquid (such as oil)
rpm – revolution per minuet
TSA – tryptic soy agar

Column labels

CC Control – Compacted intact clay control.
CCA – Freeze-fractured compacted clay column A.
CCB – Freeze-fractured compacted clay column B
CCC – Freeze-fractured compacted clay column C
CCD – Freeze-fractured compacted clay column D
NC Control – Normally consolidated intact clay control
NCC – Freeze-fractured normally consolidated clay column C
NCD – Freeze-fractured compacted clay column D

NCE – Freeze-fractured compacted clay column E
Silt R – Compacted silt column R
Silt S – Compacted silt column S
SnA – Compacted sand column A
SnB – Compacted sand column B
SP1 – Compacted sand pulsed column 1
SP2 – Compacted sand pulsed column 2
SP3 – Compacted sand pulsed column 3
SSC – Compacted 90% sand / 10% silt column C
SSD – Compacted 90% sand / 10% silt column D
SSP1 – Compacted 90% sand / 10% silt pulsed column 1
SSP2 – Compacted 90% sand / 10% silt pulsed column 2

Chapter 1 - Introduction

1.1 Project background

Bacteria and other microorganisms are common inhabitants of the subsurface environment. Where environmental conditions are beneficial for microbial growth, rich and ecologically complex communities may develop (Kölbel-Boelke *et al*, 1988). Understanding the factors that influence the fate and transport of these subsurface microbes is important for the improved understanding of waste impoundment construction, septic system setback distances (Pang *et al*, 2003, Foppen *et al*, 2008), or contaminant remediation efforts, involving microbial injections into the subsurface (Gross and Logan, 1995).

The subsurface transport of disease causing microbes, such as pathogenic strains of *Escherichia coil* (*E. coli*), is a particular concern. This bacterium is a cosmopolitan inhabitant of the digestive systems of most warm blooded animals. Because of this, *E. coli* and similar coliform bacteria have historically been used as biological indicators of fecal contamination from both animal and human sources (Yates and Yates, 1988. Feng *et al*, 2002). Because *E. coli* is quickly disabled by chlorination, it's presence in a treated water system is also indicative of recent fecal infiltration (Ontario Ministry of the Environment, 2003). It is also worth noting that *E. coli* and similar coliform bacteria may also thrive within organic rich industrial effluents, or within decaying biological materials (Foppen and Schijven, 2006, Gauthier and Archibald, 2001).

E. coli are rod shaped, approximately 0.8 x 2 μm in size, and may occur singly or in pairs. They may be motile or non-motile and are facultative anaerobes capable of survival in both aerobic and anaerobic environments (Bergey and Holt, 1994). Several hundred identified serotypes have evolved within a variety of hosts, and these may be broadly classified as either pathogenic or non-pathogenic types. The defining characteristic of this separation is the ability of the serotype to cause disease in humans. Exposure to these strains, primarily through fecal contaminated water supplies (Macler and Merkle, 2000), may result in life threatening illness. Some researchers predict that 750,000 - 5.9 million annual cases of illness within the United States may be attributed to microbiological contamination of groundwater drinking supplies (Macler and Merkle, 2000).

One common pathogenic *E. coli* strain typically associated with farming operations is the O157:H7 serotype. The toxin produced by O157:H7 requires specific cellular receptors in the host organism to cause disease, and many animals may act as asymptomatic carriers of this serotype. The highest prevalence of O157:H7 and other similar Shiga-like toxin producing serotypes are found within the digestive tracts of sheep, goats and cattle (Beutin *et al*, 1993). In humans, oral exposure to O157:H7 results in characteristic bloody diarrhea, which may progress to serious and even deadly complications such as microangiopathic hemolytic anemia, thrombocytopenia, renal failure, and disruption of the central nervous system (Boyce *et al*, 1995). In one case study of an O157:H7 outbreak, 23 percent of infected individuals required hospitalization, 6 percent went on to develop serious and life threatening complications and 1.2 percent died as a result of exposure (Griffin, 1995).

Because of their potential to cause disease, Ontario drinking water standards set limits of zero detectable colonies for *E. coli* and other fecal coliforms within treated water supplies (Ontario Ministry of the Environment, 2003). Private water supplies, such as private groundwater wells, are not connected to water treatment facilities, and are at an elevated risk of becoming infected with undesirable microorganisms. Studies have observed the presence of potentially pathogenic bacteria in up to 40% of privately owned wells in some localities (Macler and Merkle, 2000). It is no surprise then that contamination of these untreated wells accounts for the majority of waterborne disease outbreaks (Craun, 1985). Understanding the properties that enhance or inhibit bacterial transport in constructed wells and their surrounding locations can be used to improve well construction practices to reduce the risk of bacterial infiltration.

Perhaps one of the more locally known *E. coli* related waterborne disease outbreaks occurred in the town of Walkerton Ontario, in May 2000. This outbreak was sourced from a contaminated well that was infiltrated by farm runoff, and subsequently entered into the water distribution system without being adequately treated. While it was known in advance that this particular well was at a high risk of bacterial contamination due to surface water infiltration, specific protection efforts were never implemented (Hrudey *et al.* 2002. O'Connor, 2002). This outbreak resulted in the reported illness of 2300 residents and the subsequent death of 7 (Hrudley et al, 2002).

While pathogenic *E. coli* is ultimately sourced from the feces of infected animals or humans, significant quantities are required to permeate into and pollute groundwater supplies. The most significant point source of pathogenic bacteria in the subsurface is from septic tank effluent (Yates and Yates, 1988). Surface application of municipal

sewage, farm runoff and animal feed operations are other important contamination sources (Yates and Yates, 1988, Gerba and Smith, 2005). Typical *E. coli* concentrations measured within raw municipal sewage ranges between 1×10^6 -1.5×10^6 CFU (Colony Forming Units)/ml (Grant et al, 1996).

The application of municipal or farm sewage to soil surfaces has several benefits, such as improving soil properties or increasing crop yields (Abu-Ashour *et al*, 1994). This is also a cost effective method of recycling the nutrients contained within these wastes (Gagliardi and Karns, 2000). Because infectious population levels of *E. coli* may survive for over 60 days on surface vegetation (Avery *et al*, 2004) these microbes may become rapidly mobilized following rainfall. Stoddard *et al* (1998) measured *E. coli* densities of up to 100 CFU/ml, at a depth of 90cm in a loamy soil after one such rainfall event. Studies observing subsurface bacterial migrations of up to 830 meters from the surface application site have also been cited in the literature (Abu-Ashour, 1994).

To minimize the risk of pathogenic bacteria moving from a surface application site into subsurface drinking water resources, several common practices may be used. For example, frequent soil tilling may be utilized to disrupt continuous pore channels in the upper soil regions, which can reduce the availability of preferential flow paths for bacteria to move to the groundwater table (Conboy and Goss, 2000, McMurry *et al*, 1998). In areas where surface runoff is deemed a larger transport risk factor than groundwater infiltration, subsurface injections of bacterial contaminated effluent may be utilized instead of surface application (Schijven and Hassanizadeh, 2000). It should be noted that while intentionally contaminating a subsurface system with pathogenic bacteria would seem counter productive; this may be a viable treatment option to

minimize surface water transport in locations where the untreated groundwater will not be utilized for drinking purposes.

As soil may be composed of a wide variety of particle sizes, investigating the transport of bacteria through a variety of soil textures is important to improve the understanding of bacterial transport processes in differing conditions. The transport of bacteria through engineered clay barriers is one field of research that is quite underrepresented in the literature relative to transport through uniform sands or intact field samples. Soil liners, composed of at least 10% clay, are commonly constructed to contain liquid wastes and leachates within waste impoundments (Rosa *et al*, 2007). Regulatory agencies may outline several requirements of a compacted soil liner, including material properties and a maximum saturated hydraulic conductivity. For example, *the Ontario Ministry of Agriculture, Food and Rural Affairs* provide an acceptable range of soil grain sizes, Atterberg limits, and a maximum saturated hydraulic conductivity of $1x10^{-9}$ m/s, and a minimal thickness of 1m (OMAFRA, 2002).

Weathering and fracture formation within these liners is a potential cause of containment failure. Fracture flow may be described as preferential flow through cracks within the soil system, as opposed to matrix flow which occurs through aggregates within the intact matrix (Phifer *et al*, 1994). As flow rate within a fracture is often many times higher than the surrounding matrix, this fracture system can raise the effective hydraulic conductivity of a clay barrier by 1-3 orders of magnitude compared to the freshly constructed condition (Vargas and Ortega-Guerrero, 2004. Abichou *et al*, 2002).

Within Canada, an important risk factor for fracture formation within clay barrier systems is seasonal freezing and thawing. This process, known as frost action, may cause

fracture formation through both desiccation (U.S. National Research Council, 2007) and via the formation, growth, and subsequent melting of ice lenses. Freeze-thaw cycles can increase the measured hydraulic conductivity of laboratory compacted clay columns by 3-4 orders of magnitude and silt columns by 2 orders of magnitude (Kjartanson *et al*, 2005). This process may be expected to occur in the field at any soil depth exposed to freezing temperatures and a source of water (Sharma and Reddy, 2004).

A hypothetical scenario for a feedlot sewage lagoon is shown in Figure 1.1. Seasonal freeze-thaw action to a depth of the frost line may subject these soil regions to intensive physical weathering. This can result in the formation of fractures, which act as preferential water flow paths. Liquid waste containing pathogenic bacterial species may leak from the sewage lagoon through these fractures and be transported considerable distances, potentially to drinking water wells. Note that the upper zone in both the compacted clay liner and the natural clay can be subject to intense physical weathering, including freeze-thaw effects. This can lead to fractures of both the compacted and natural clay in this system.

Pachepsky *et al* (2006) and Shijven and Hassanizadeh (2000) suggest that most soils are efficient filters, and only in situations where extensive macroporosity exists is subsurface microbial transport expected. Macroporosity may be described as preferential flow paths composed of continuous and relatively large diameter pores. Studies have demonstrated that the drinking wells most at risk for pathogenic bacterial infiltration are located within aged limestone or dolomite bedrock, followed by those located in clay or clay loam soils (Conboy and Goss, 2000). As clay rich soils would be expected to filter bacteria more effectively than coarse soils such as sand, these results are puzzling. The

likely explanation for these observations is that bacterial transport occurs primarily via preferential flow paths within these soils.

An unresolved issue is the extent to which freeze-thaw fractured clay barriers provide preferential flow networks that would allow bacteria transport to occur. To investigate this, a number of studies have been conducted by both undergraduate and graduate students at Lakehead University, under the supervision of Drs. Kjartanson, Eigenbrod and Leung.

The first such project to investigate these processes was conducted by Miller (2004), under the supervision of Dr. Eigenbrod. The goal of this project was to investigate the transport of *E. coli* through freeze-fractured normally consolidated clay barriers. The normally consolidated clay columns are intended to simulate naturally forming clay soils, such as those surrounding the hypothetical sewage lagoon shown in Figure 1.1. This project also laid the groundwork procedures for subsequent projects, including microbiological preparation methodology, column preparation, and data collection procedures.

Subsequent research conducted by Scott and Nguyen. (2006), Lukacs *et al.* (2007) and Rosa *et al.* (2007) expanded upon this research by investigating bacterial transport through freeze-fractured compacted clays, compacted sand, and a compacted sand-silt mixture. The compacted sand and 90%sand / 10% silt mix columns tests were conducted to investigate and contrast *E. coli* transport through a porous medium in which most of the soil porosity contributed to the primary flow, as opposed to the fractured clays in which most of the flow would occur through the fracture network. These columns were not subjected to freeze-thaw cycles because such action would not generate preferential

fracture flow paths in these soils, as opposed to the clays. Batch sorption experiments were also conducted by Rosa (2007) on the clay, silt, and sand soils used in the column tests.

1.2 Project objectives

While the experiments referenced above have generated a large amount of data to describe the transport of *E. coli* through a variety of soils, corresponding numerical and analytical models have not been investigated in significant detail. To fill this knowledge gap, the objectives of this project are:

1. Review, summarize and assess microbial fate and transport theory, modeling approaches and corresponding software that can be used for bacterial fate and transport modeling. After assessment, select software applicable to model the results of the column tests based on the column test and batch sorption data.

2. Critically assess the existing column test data and design and conduct additional column tests, as required, to complement the existing database and provide additional data for the selected models. In particular, pulse-type column permeation tests will be designed and conducted.

3. Model the column test data using the selected methods, and determine the relevant *E. coli* fate and transport processes and parameters for each of the tested soil types. Asses the application of laboratory batch sorption data to model transport through the soil columns.

4. Simulate microbial transport from a potential pathogenic bacteria source, such as leaking sewage lagoon, leaking septic system, or other real world scenario. Compare simulation results to available field or laboratory data if available.

1.3 Thesis organization

This thesis is organized in the following manner. Chapter 2 and Chapter 3 provide a brief overview of the unique properties of bacterial movement in the subsurface, and introduce various modeling theories that have been applied to assess this transport. Chapter 4 and Chapter 5 introduce the methodologies used to investigate bacterial transport in column experiments, and summarize the results. Chapter 6 introduces the various software packages used in bacterial transport modeling, with detailed review of the software that was selected to be used in this study. Chapter 7 summarizes and contrasts the modeled results with the experimental data. Chapter 8 discusses the suitability and shortcomings of the models used for this research project, and possible interpretations of the experimental data. Chapter 9 summarizes the conclusions of this research project, and possible avenues for future research efforts. A summary of the

commonly used nomenclature is contained within the nomenclature, abbreviations and column label section.

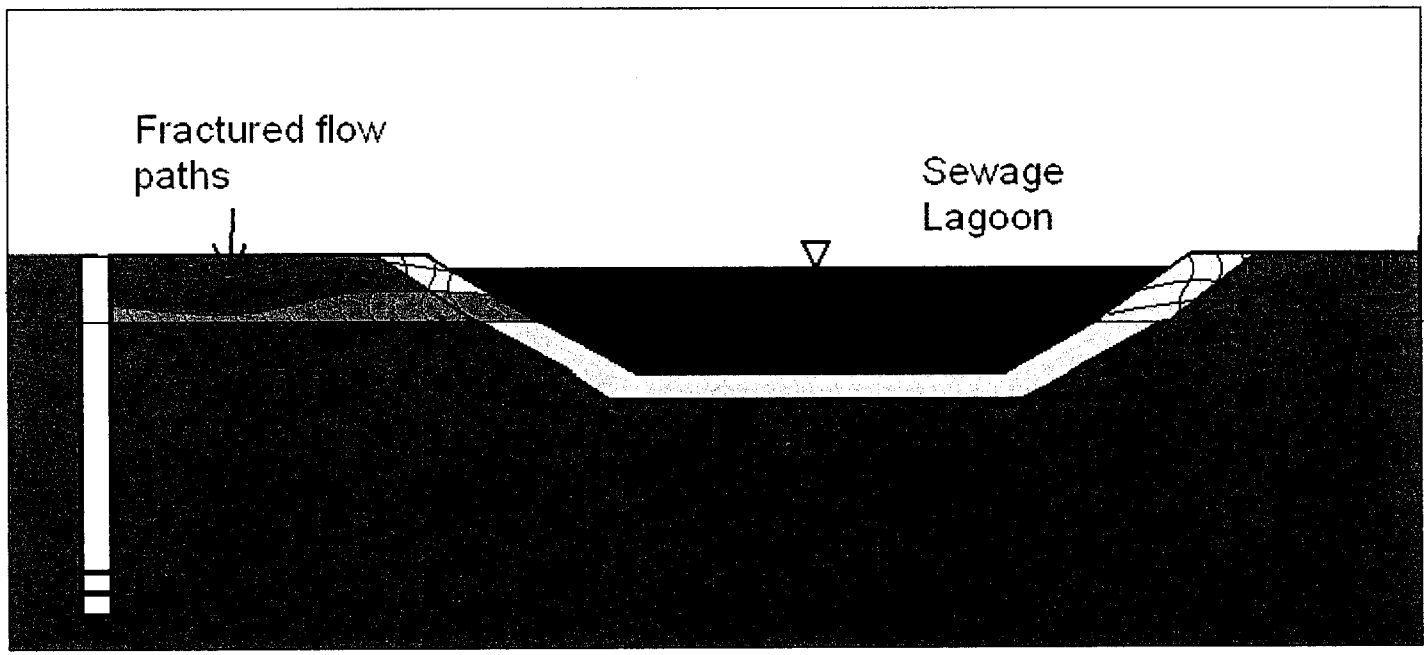

Figure 1.1 – Hypothetical scenario for a feedlot sewage lagoon containment failure due to freeze-thaw processes.

Chapter 2 - Literature Review: Microbial fate and Transport Processes

2.1 Unique properties of bacteria relative to dissolved solutes and colloids

As bacterial cells differ in many ways from both dissolved chemical compounds and suspended colloids, they possess many unique properties that must be taken into account when considering fate and transport processes. For modeling purposes, bacteria resemble colloids much more closely than dissolved chemical compounds. These similarities to colloids include: a similar size, similar density, negative net charge and hydrophobicity (Marshal, 1992). These "living colloids" are also physically very near the 1μm size threshold for colloid particles and the 2μm threshold for clay particles (Pachepsky *et al*, 2006). As bacteria are living organisms, they also respond quite differently to several environmental factors compared to non-living colloids.

2.1.1 Growth, nutrient availability and survivability in the natural environment

Under conditions of nutrient stress, many bacterial species undergo biochemical changes that result in the transformation of the cell into a starvation state. This state is characterized by reduced metabolic activity, size, and an increase in hydrophobicity. This change in hydrophobicity allows the bacteria to attach easier to the substrate in an attempt

to gain access to more nutrients (Marshal, 1992). Actively growing cells were also found to have a larger concentration of acidic, polar protein molecules on the cell surface than stationary growth phase cells (Walker *et al*, 2005) which may explain the observed differences in hydrophobicity between these populations. Typically, cells in the stationary growth phase exhibit higher sorption rates than cells in the actively growing phase (Chen and Strevett, 2001). These observations are not universal, as some authors have also found that bacterial attachment rates are higher during the exponential growth phase (Pekdeger and Matthess, 1983. Gargiulo *et al*, 2007a). It should also be noted that the zeta-potential, which is an indication of the flocculation potential of a suspended colloid in solution, is indistinguishable between growing and stationary-phase cells (Walker *et al*, 2005).

Individual nutrient availability also has an important effect on the surface structure and sorptive characteristics of *E. coli*. Two nutrients found to have a profound effect on bacterial sorptive properties are carbon and nitrogen. When nitrogen is limited, *E. coli* generates a more hydrophilic cell membrane. When carbon is limited, *E. coli* generates a more hydrophobic cell membrane (Chen and Strevett, 2003, Gagliardi and Karns, 2000). This results in carbon starved cells demonstrating higher sorption rates than nitrogen starved cells.

As bacteria such as *E. coli* are adapted to survival in the digestive systems of warm blooded animals, they are at a competitive disadvantage when released into the subsurface environment compared to naturally present, autochthonic bacterial species (Pekdeger and Matthess, 1983). Typically, *E. coli* cannot compete effectively with native bacteria species, and are gradually eliminated in the subsurface. An exception to this

occurs in locations where a warm organic rich environment is present. This can occur in locations exposed to pulp and paper mill effluent (Gauthier and Archibald, 2001) or other similar wastes. Sjogren (1994) estimated that the time required for total *E. coli* population decay in their soil microcosm experiments was on the order of 20.7-23.3 months at a temperature of 5°C.

2.1.2 Heterogenic cell surface

The bacterial cell surface is composed of a wide variety of organic molecules. The exact properties of this layer are subject to many influences, both environmental and biological. These may include co-contaminants such as non-aqueous phase liquids (NAPLS) and surfactants, ionic concentrations, temperature, nutrient availability, growth phase, and genetic variability (Gross and Logan, 1995, Abu-Ashour *et al*, 1994, Chen and Strevett, 2003, Vidal *et al*, 1998, Yates and Yates, 1988).

Complicating matters further, there is not a distinct transition between the cell membrane and the surrounding liquid medium (Figure 2.1). Rather than possessing a solid surface layer such as a mineral colloid, the cell surface is impregnated with a variety of extra-cellular molecules which may have either or both hydrophobic and hydrophilic properties. Surface appendages such as flagella may also extend up to 1μm from the cell surface (Bos *et al*, 1999). This variety of surface structures, including secreted adhesive compounds, undoubtedly interact to some degree with the surrounding soil particles before the phospholipid layer comprising the cell membrane surface.

Expression of the "CSA" gene, which governs distinctive pili-like "curli" structures on the cell surface have been observed to be important to the attachment

characteristics of *E. coli* cells (Vidal *et al*, 1998). Over expression of this gene may result from spontaneous mutation or unknown environmental factors. Pili-like structures were observed by Maurer *et al* (1998) in colonies of the O157H7 *E. coli* serotype grown at room temperature. Olsen *et al* (1989) also observed the preferential formation of these structures at ambient temperatures. As the digestive tract of warm blooded animals are typically a higher temperature than the local ambient conditions, this environmental change may enhance the production of genes such as CSA, which could increase the attachment characteristics as a possible survival mechanism. Bacteria are also capable of regulating gene expression and thus sorptive and metabolic properties in response to local population density. One system that bacteria use to control and respond in this manner is through Quorum signaling (Surette *et al*, 1999).

Extra-cellular structures also have the potential to cause bacteria in solution to interact, and bind to one another forming aggregated bacterial clumps. Aggregated colonies of *E. coli* isolated from the digestive tracts of avian species were all found to contain curli structures (Maurer, 1998). However, curli structures were not found on enterohemorrhagic or uropathogenic isolates also investigated during the course of that study. Aggregated clumps of *E. coli* cells would be transported at a different rate than mono-dispersed cell (Bradford *et al*, 2006b) further complicating transportation modeling. This can for example make it difficult to relate *E. coli* transport when uncontrolled environmental conditions cause the cells to aggregate (i.e. *E. coli* cells may possess different sorptive characteristics at different temperatures due to this one property).

2.1.3 Biofilm production, blocking and ripening

Unlike colloids, bacteria are capable of producing an extra cellular biofilm matrix. This structure may be described as a layer of cells anchored to the subsurface stratum and embedded within a matrix of biologically derived organic molecules (Bos *et al*, 1999). Thin, patchy biofilms are common in pristine subsurface environments, while thicker and more complex biofilms are common in engineered or nutrient rich systems (Leon-Morales *et al*, 2004). The binding of a bacterial cell to a collector surface via extra cellular adhesive proteins is also a defining characteristic of irreversible sorption.

During initial sorption, bacteria bind to a layer of hydrophobic molecules which form a conditioning film on soil surfaces. This conditioning film first alters the charge and free energy characteristics of the soil particle surface (Marshall, 1992) decreasing the repulsive properties between the soil and bacteria. Bacteria cells may then bind to the soil particles more efficiently. These sorbed bacteria may then act to inhibit (blocking) or enhance (ripening) the sorption of subsequent bacteria (Camesano and Logan, 1998).

Biomass accumulation has been linked to changes in both the physical and hydraulic properties of the soil system (Rockhold *et al*, 2004). Biofilms may trap both organic and inorganic compounds, which can then be metabolized by the inhabiting bacteria. The rapid formation of these films under flowing conditions allows these bacteria to filter nutrients from the passing water (Marshal, 1992). As *E. coli* and similar microbes are not well adapted to survival in the subsurface environment, sorption to soil particles provides another benefit. Besides the potential to have higher access to nutrients, the bacteria attached to soil particles are protected somewhat from abrupt changes in the local environmental condition (Pekdeger and Matthess, 1983). Interestingly, evidence

also exists to suggest that sorption is detrimental to bacterial survival. For example, Pang *et al* (2003) found death rates for the *E. coli* were 5 – 28 times greater for the bacteria sorbed compared to those in the free solution.

Biofilms are also subject to unique desorption processes compared to singly sorbed microbes. These include erosion, which may be defined as the continuous removal of deposited particles as a result of the shear forces caused by moving liquid, or sloughing, which is the removal of large biomass sections within older more mature systems via abrupt changes in the local conditions (Clement *et al*, 1997). These processes may result in unpredictable changes in measured desorption or bacterial production over time.

2.1.4 Bacterial motility

Bacteria may exhibit a variety of mechanisms for self propelled movement, or they may lack these mechanisms and essentially be immobile. Within a liquid medium, motility is expected to increase the apparent diffusion rate of a bacterial culture. Diffusion rate constants for *E. coli* within a free solution may range from 2×10^{-13} m^2/s for non-motile cells, to 2×10^{-9} m^2/s for fast swimming mutants (Berg, 2003). These fast swimming mutants may diffuse at roughly the same rate as bromide ions in free solution (2.08×10^{-9} m^2/s). Within the soil pore network, bacterial motility is limited to the local pore space, and is expected to have an insignificant contribution to overall transport.

Variations in bacterial motility may affect transport by influencing sorption. When compared to immobile colloids, mobile cells may be able to overcome the

repulsive charges between soil surfaces and the cell surface through momentum, thus increasing the collision rate between the cells and soil particles. Mobile cells may also be able to overcome sorption, and desorb at a higher rate than non-motile cells (Becker *et al*, 2004). Ultimately, increased cell motility tends towards increasing the rate of sorption, and decreasing the rate of desorption (Becker *et al*, 2004).

Motile bacteria are also capable of exhibiting chemotaxis, which may be defined as movement in response to a chemical gradient. It was demonstrated mathematically by Olsen *et al* (2006) that bacteria are capable of moving from high permeability soil regions, and congregating in lower permeability regions containing elevated levels of a diffusing contaminant.

2.1.5 Bacterial and chemical co-contamination

Co-contamination of a site with both bacteria and chemical waste has some interesting implications. This is especially important in the field of environmental remediation, where the injection of bacterial strains capable of metabolizing subsurface contaminants is frequently investigated. Several studies have indicated that co-contamination can affect the transport properties of bacteria cells in the subsurface without affecting the survivability of the cells.

Chemical treatments that increase the hydrophobicity or the electrostatic charge of the soil particles have been found to increase the attachment rate of bacteria (Gross and Logan, 1995). This situation may occur through an increase in the ionic concentration of the permeating solution. Sorbed bacteria may also be partially remobilized by depleting

the ionic strength of the pore water (Leon-Morales *et al*, 2004). The presence of surfactants on the other hand can strongly decrease cell hydrophobicity, which will decrease the sorptive potential of an exposed cell (Gross and Logan, 1995). Co-contamination with non-aqueous phase liquids (NAPL)s does not significantly affect the sorption of bacteria (Rogers and Logan, 2000). This is in contrast to their hypothesis that the hydrophobic bacteria would more easily partition into the hydrophobic NAPL contaminated regions.

The effect of solution pH on bacterial sorption appears to be dependant on the soil medium. Within columns containing 40 μm borosilicate beads or silica spheres, the effects of pH and buffer concentration are apparently negligible on bacterial sorption (Gross and Logan 1995. Jewett *et al*, 1995). Hassen *et al* (2003) reported the opposite, finding that bacterial sorption was affected by pH in the smectite clay material used in their study. It was speculated by Rosa (2007) that soil surface charge strongly influences bacterial sorption characteristics, which is dependant on the pH of the solution permeating the soil system.

2.1.6 Heterogenic bacterial populations

Besides the effect of variability in both the environmental conditions and lifecycle stages of individual bacteria, genetic variability can play a pronounced role in bacterial fate and transport. Subsurface transport would be comparably low for highly sorbing individuals, and high for poorly sorbing individuals (Gannon *et al*, 1990). These subpopulations may be easily isolated by column passage experiments, where the "fast"

subpopulation will proceed through the column at a faster rate than the "slow" population (Foppen *et al*, 2008).

To further complicate the role of genetic variation on bacterial transport, monoclonal cell cultures have been observed to generate subpopulations of cells that demonstrate significantly different transport properties than the original population. For example, non-sorbing *E. coli* strains have been observed to generate subpopulations of cells capable of attaching to both hydrophobic and hydrophilic surfaces (Vidal *et al*, 1998).

2.2 *Fate and transport processes*

To describe the transport of bacteria and other contaminants through the subsurface, several common terms are utilized. The most basic contaminant fate and transport terms include: advection, dispersion, diffusion, sorption, production and decay.

2.2.1 Advection, mechanical dispersion and diffusion when applied to bacteria transport

Advection is perhaps the most fate and transport basic process, and describes the transport of a contaminant with water flowing in response to a hydraulic gradient (Sharma and Reddy, 2004). Within the subsurface, this water flows through an interconnected network of pore spaces.

Mechanical dispersion describes the spreading of a contaminant front due to variations in pore water velocities at the microscale or macroscale level. This may be

caused by variations in pore size, transport path length, frictional forces or changes in soil lithology (Sharma and Reddy, 2004). The spreading of the contaminants within the plume by this mixing action may be both parallel to the flow direction, resulting in longitudinal dispersion, or perpendicular to the flow path, resulting in transverse dispersion.

Diffusion describes the transport of a contaminant under a concentration gradient. This results in the movement of a contaminant from an area of high concentration to an area of low concentration as a result of the random movement of molecules within the solvent medium. Diffusion is often deemed insignificant when considering bacterial transport, as the diffusion coefficients of suspended particles are typically much smaller than dissolved chemicals (White, 1984. Peterson and Ward, 1989). Bacterial diffusion coefficients also tend to be too small to contribute to the overall dispersion coefficients seen in many models (Reddy and Ford, 1996) and may even be safely removed from consideration (Peterson and Ward, 1989). Consequently, bacterial transport may be described using only the advection and dispersion terms.

2.2.2 Transport limiting processes - sorption, filtration and straining

In a situation where a contaminant does not experience decay, production, or any significant interaction the subsurface soil medium, transport may be described entirely using advection, dispersion and diffusion. This is the expected behavior of some chemicals such as bromide, which are commonly used as a conservative (i.e. non-sorbing) tracer in contaminant migration experiments. As the majority of contaminants interact in some significant degree with the solid phase, it is important to account for the

effects of this interaction on the transport process. These may be roughly classified into processes that result from a chemical or electrical charge interaction, or processes which result in physical interaction between the contaminant and the soil grains.

Sorption is the most commonly used term to describe this interaction, and may be defined as the partitioning of a solute from the permeating liquid to the solid soil phase. This term encompasses the sum contributions of adsorption, chemisorption, and absorption (Sharma and Reddy, 2004). Several methods have been utilized to estimate bacterial sorption rates in advance; however, as these methods are commonly based on theories that are violated when considering bacteria, they are often flawed when applied to this situation. For example, the assumptions of Derjaguin-Landau-Verwey-Overbeek (DLVO) theory, which is utilized to describe the interacting forces between a colloid and a collector surface, are violated with bacteria. This results in significant deviations between experimental observations and theoretical predictions when this theory is applied to bacteria (Ginn *et al*, 2002). Evidence exists that bacteria attach to surfaces primarily via chemical interactions rather than through the existence of specific surface structures (Gross and Logan, 1995) and that adhesion likely occurs in the secondary energy minimum. (Redman *et al*, 2004). It should be noted that Gross and Logan (1995) utilized a non-motile strain of the bacteria *Alcaligenes paradoxus* which may or may not exhibit the variety of surface structures identified in section 2.1.2, and may not be comparable to *E. coli*.

Physical transport limiting processes are those which predominantly are a result of physical interactions between the bacteria and surface grains. This method of attachment does not involve chemical bonding between the bacterial cell and the soil

surface, unlike physiochemical sorption. Physical processes will occur at a similar rate in a given soil independent of the chemical conditions of the permeating fluid (Tufenkji *et al*, 2004). However, physical processes may preclude adhesive chemical interactions by facilitating contact between the bacterial cell and soil surface. These processes are also dependant on the pore water velocity, with higher removal rates observed at lower velocities (Bradford *et al*, 2006b). Physical processes may be broadly classified into two general categories: filtration and straining. The defining characteristic which separates these processes is the colloid to pore diameter ratio. Because *E. coli* is a rod shaped microorganism, it is expected to behave similarly to a sphere at a diameter of its total length (White, 1984) which would be approximately 2 μm.

Mechanical filtration may be defined as the situation where colloids cannot penetrate a soil matrix due to these particles being larger than available pore spaces (Bradford *et al*, 2006a. Mcdowell-Boyer *et al*, 1986). This effect is best illustrated visually by the formation of a bacterial layer at a soil-water/textural interface, with little or no infiltration of the microorganisms into the soil matrix. This effect is predicted to occur when the pore diameter to colloid length ratio is smaller than 10:1 (Mcdowell-Boyer *et al*, 1986). As a demonstration, filtration would be expected to occur in soil textures containing pores of less than 20 μm diameter permeated with a 2 μm bacteria. Pekdegar and Matthess (1983) describe a soil meeting this criterion as being a "coarse loam" of a uniform texture. While *E. coli* cells are larger than these pore spaces, frictional drag, ripening and related processes can act to prevent significant transport within these spaces. Deposited particles are expected to form a cake-like layer on the surface of the

soil matrix which can also overwhelm and clog previously available pore spaces (Bradford *et al*, 2006a).

Straining is the next step in the physical removal process that may occur within pore spaces. Straining occurs when particles are deposited in pore channels that are physically smaller than a critical size (Bradford *et al*, 2002). Research suggests that straining is an important factor in bacterial transport when the bacterial size is greater than 5% of the median grain size, or when the pore to colloid length ratio is between 10:1 and 20:1 (Mcdowell-Boyer *et al*, 1986. Tufenkji 2007). Strained colloids can potentially fill a large amount of the available soil pore network in this size range, potentially in excess of 30% of the total pore spaces. (Sakthivadivel, 1969). When the pore to colloid length ratio is larger than 20:1, removal processes begin to favour physiochemical sorptive processes instead of physical removal processes (Mcdowell-Boyer *et al*, 1986).

A method of estimating the trapping of microbes through straining related processes is the geometrical suffusion security, estimated using the equation (Foppen *et al* 2005):

$$\Theta = \frac{d_m}{0.12 d_{10}}$$

Eqn 2.1

Where (Θ) is the geometrical suffusion security, a measure of the potential for straining in a soil material, (d_m) is the diameter of the bacteria (meters), and (d_{10}) is the 10^{th} percentile of the cumulative grain size distribution (meters). It is hypothesized that straining will only occur when $\Theta > 1.5$. This occurs when the bacteria is larger than 18% of the d_{10} grain size.

Variations in the pore sizes through the soil matrix may also act to exclude bacteria and other colloids from the majority of the total pore volume. This process, known as size exclusion, is a straining related principle that constrains bacteria and related colloids to pore networks that are physically accessible to them. (Bradford *et al*, 2006a). Size exclusion is also neglected in most transport models, though this principle can explain why in many cases, colloids such as bacteria, are detected in effluent before a conservative tracer (Bradford *et al*, 2002) especially at higher cell concentrations (Bradford and Bettahar, 2006. Camesano *et al*, 1999).

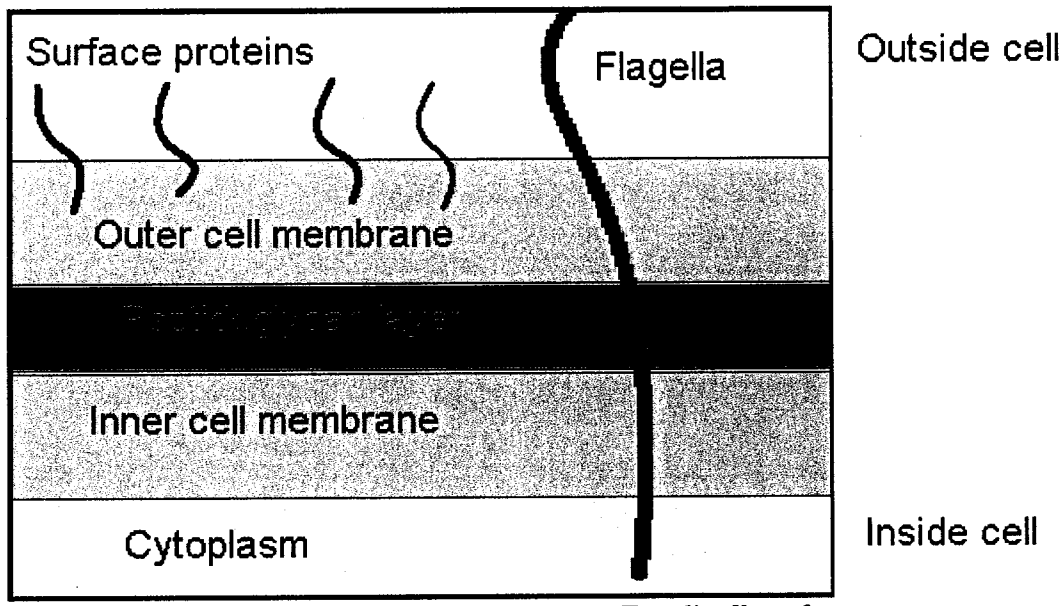

Figure 2.1 - Schematic of surface structures on *E. coli* cell surface

Chapter 3 - Modeling Approaches for Bacterial Fate and Transport

3.1 Introduction

The modeling of bacterial fate and transport through the subsurface environment has a fairly long history in the scientific literature. This has resulted in a variety of models based on several sorptive theories. Bacterial transport modeling is generally concerned with two goals: the modeling of effluent transport rate and breakthrough at certain distances from a contaminant source, and the modeling of a deposition profile within a test system. Ideally, a given model should be able to predict both the effluent concentration and deposition profile with a high level of accuracy (Bradford *et al*, 2003). For the purposes of this research, these models may be roughly classified into equilibrium, kinetic and straining dominated processes along with classic colloid filtration theory. A summary of the required parameters, advantages, and disadvantages of the various modeling theories is shown in Table 3.1. As this section contains a variety of mathematical symbols, a list of the nomenclature is provides in appendix 1.

3.2 General one-dimensional advection-dispersion model

Contaminant transport in column experiments and through clay waste containment liners is generally described using the one-dimensional advection-dispersion equation (Tufenkji, 2007):

$$\frac{\partial C}{\partial t} + \frac{\rho_b}{\theta}\frac{\partial S}{\partial t} = D\frac{\partial^2 C}{\partial L^2} - v\frac{\partial C}{\partial L}$$

Eqn. 3.1

Where (C) is the solute concentration (g/ml), (S) is the concentration of attached microbes (g/g), (D) is the dispersion coefficient (Length^2 / time), (t) is time (seconds or pore volumes of flow (PV)), (v) is the average pore-water seepage velocity (Length / time), (L) is the transport distance, (θ) is the volumetric water content which is equal to porosity in saturated conditions, and (ρ_b) is the soil dry density (g/g). This equation may be modified to incorporate different modeling parameters depending on the modeling theory. This formula also assumes steady state fluid flow and uniform soil water content (van Genuchten, 1981).

Dispersion is one variable that has interesting effects within different models. In colloid filtration theory, this term has a limited or negligible effect on attachment rates and transport through the model system, and may safely be ignored (Unice and Logan, 2000. Logan *et al*, 1999). However this term may be used to describe the shape of an advancing contaminant plume on the field scale (Unice and Logan, 2000). Dispersion is best incorporated into analytical solutions by using an effluent boundary condition located at infinity. This is because dispersion does not end at the edge of the soil column (Unice and Logan, 2000).

3.3 Equilibrium sorption models

Equilibrium sorption models are those that use the retardation factor term, where the transport of a solvent of interest is related to that of a non-sorbing tracer (Tufenkji, 2007). This transport model is commonly used to estimate the transport of dissolved chemical contaminants in the subsurface. The "sorptive" process assumes that the concentration of a contaminant in the solid phase is determined by the concentration of the contaminant in the liquid phase. This assumption predicts instantaneous and completely reversible mass transfer between the solid and liquid phases. While best suited to model the fate and transport of dissolved contaminants, the equilibrium sorption model has good application to scenarios where the contaminant is many times smaller than the particles within the soil medium (i.e. bacteria moving through a sandy soil). Fate and transport may be described by the equation (Tufenkji, 2007):

$$R\frac{\partial C}{\partial t} = D\frac{\partial^2 C}{\partial L^2} - v\frac{\partial C}{\partial L}$$

Eqn. 3.2

Where (R) is the retardation factor, defined as the transport rate of a solute relative to that of a conservative tracer. Typically, the retardation factor may be defined using Eqn 3.7.

To account for the potential growth or decay of a contaminant, additional coefficients may be included within the general equilibrium equation, such as (Toride *et al*, 1995):

$$R\frac{\partial C}{\partial t} = D\frac{\partial^2 C}{\partial L^2} - v\frac{\partial C}{\partial L} - \mu C + \gamma L$$

Eqn. 3.3

Where (μ) is a kinetic first-order decay term, while (γ) is a kinetic zero order production coefficient.

To describe the sorption of a solute from the liquid phase to soil particles, various sorption isotherms may be employed. These are typically linear, Freundlich or Langmuir isotherms, which may be shown by (Sharma and Reddy, 2004):

Linear isotherm

$$S = K_d C$$

Eqn. 3.4

Freundlich Isotherm

$$S = KC^N$$

Eqn. 3.5

Langmuir Isotherm

$$S = (K_L M_L C) / (1 + (K_L C))$$

Eqn. 3.6

Where (S) is the mass of contaminant sorbed per unit of dry soil, (C) is the concentration of contaminant in the liquid medium at equilibrium, (K_d) is the distribution coefficient ($M^{-1}L^3$), (K) is the slope of the Freundlich isotherm and, (N) is a unitless power constant of the Freundlich isotherm, (K_L) is the adsorption constant of the Langmuir isotherm relating to the binding energy, and (M_L) is the maximum amount of contaminant that may be sorbed to the solid phase.

Corresponding retardation factors may be calculated from the above isotherms using a number of equations (Sharma and Reddy, 2004).

Linear

$$R = 1 + \frac{\rho_b}{\eta} K_d$$

Eqn. 3.7

Freundlich

$$R = 1 + \frac{\rho_b}{\eta} KNC^{N-1}$$

Eqn. 3.8

Langmuir

$$R = 1 + \frac{\rho_b}{\eta}\left(\frac{K_L M_L}{(1 + K_L C)^2}\right)$$

Eqn. 3.9

Where (ρ_b) is the soil dry unit weight (g/g), (η) is the soil porosity, and (C) is the concentration of the permeating contaminant in the liquid phase (g/ml).

The Linear sorption isotherm assumes that the amount of contaminant sorbed is directly proportional to the amount of contaminant in solution. The Freundlich isotherm describes sorption via a non-linear power line plot, which is approximate to a linear isotherm when N is approximately equal to one. Both the Linear and Freundlich model have no upper limit for maximum sorptive capacity (Yates and Yates, 1988). In contrast, the Langmuir sorption isotherm assumes a finite number of available sorption sites, and a maximum sorptive capacity where these sites are saturated with a contaminant. Langmuir sorption assumes that all sorption sites are of equal strength, sorbed particles are non-interacting, and that the maximum sorptive condition may be described as a saturated monolayer of particles upon the collector surface (Yates and Yates, 1988).

The potential of a bacterial species to affect the sorption of subsequent bacteria may be the most important factor in determining the suitability of the various sorption models. Site blocking occurs when previously sorbed cells limit or prevent subsequent sorption, while ripening occurs when previously sorbed cells enhance the subsequent sorbing of bacteria (Camesano and Logan, 1998). Species which demonstrate significant blocking of sorption sites may show a sorption isotherm similar to the Langmuir model, while bacterial species that form a polylayer on collectors may be more accurately

represented using the Freundlich model. Evidence for polylayer sorption may be verified by an observed increase in the sorption rate with increasing cell concentration, which may indicate that previously sorbed cells act as preferential sorption sites compared to the natural soil (Camesano and Logan, 1998). It stands to reason that an observed decrease under these conditions would provide evidence for sorption blocking. As a polylayer biofilm production is more typical than a bacterial monolayer within most environments, this would favour utilizing the Freundlich sorption isotherm. This may indirectly account for the formation of biofilms on the collector surface, and also give a more general approximation of the bacterial sorptive behaviour in a soil.

Many shortcomings of the equilibrium model have been demonstrated when it is applied to colloids and bacteria. Because chemical contaminants possess far different properties than colloids, it is difficult to relate the behaviour of one to the other. Bacterial sorption is also unlikely to follow equilibrium-like models, and is far more likely to be a kinetically controlled process (Hornberger *et al*, 1992). However, in the absence of physical removal processes such as straining and filtration, batch sorption experiments should be in agreement with column effluent experiments (Bradford *et al*, 2006a).

3.4 Kinetic sorption model

Kinetic sorption differs from equilibrium sorption primarily by describing the sorptive process as a function of time, rather than occurring instantaneously. In the simplest situation, known as one-site kinetic sorption, this process is assumed to occur at identical sorption sites throughout the soil matrix. This means that all sorption sites are

expected to behave in an identical, time dependant manner (van Genuchten, 1981). Similar to the equilibrium sorption model, the kinetic sorption model is best applied in situations where there is a large size difference between the contaminant and soil grains. The governing equation is identical to the general advection-dispersion equation (Eqn 3.1), with the second term being described with the equation (Tufenkji, 2007):

$$\frac{\rho_b}{\theta}\frac{\partial S}{\partial t} = k_{att}c - \frac{\rho_b}{n}k_{det}S$$

Eqn. 3.10

Where (k_{att}) is the first-order kinetic attachment coefficient (t^{-1}), and (k_{det}) is the first-order kinetic detachment coefficient (t^{-1}). The remaining terms are described in the previous sections.

The detachment rate coefficient is often found to be 4-5 orders of magnitude lower than the attachment rate coefficient (Bales *et al*, 1997). Because of this, detachment is often assumed to be insignificant relative to attachment, and may be safely ignored in most models.

Because kinetic models utilize many of the same variables as the equilibrium model, many of these terms are both interchangeable and valid when used in both models. For example, Reddy and Ford (1996) utilized identical dispersivity values in their equilibrium and kinetic models for bacterial transport, which produced similar modeling results. As the kinetic and equilibrium models (Eqn 3.3) may give similar results, investigation of the tail region of an effluent curve is required to distinguish the relative rate of sorption and desorption (Schijven and Hassanizadeh, 2000). The tailing

region is the part of an effluent curve following the onset of permeation with a contaminant free solution, and is explained further in section 3.8.

3.5 Classic colloid filtration theory model

Classic colloid filtration theory (CCFT) is a special model technique commonly used to calculate the transport of colloids and bacteria through porous media. The model describes sorption as a two part process; the transport of colloids from the liquid phase to the surface of the collector (soil particles) followed by the attachment of a portion of these colloids to the collector via physiochemical processes (Tufenkji, 2007. Nelson *et al*, 2007). The earliest often cited filtration theory approach regarding bacterial transport is the Yao model (Yao *et al*, 1971) which has also been used to calculate colloid particle removal, and the feeding of aquatic organisms within experimental systems (Logan *et al*, 1995). This model is formed by applying a theoretical solution of colloid removal by an isolated collector in a clean and infinite medium (Logan *et al*, 1995). This modeling theory is best applied to soils composed of a uniform grain size, and where the colloids are unlikely to experience significant straining.

In this model, the solutions to the general advection-dispersion equation (Eqn 3.1) assuming a continuous contaminant injection (at L = 0, i.e. the start of the model system) over a given time period are given as (Tufenkji 2007):

$$C(L) = C_0 \exp\left[-\frac{k_{att}}{v} L\right]$$

Eqn 3.11

$$S(L) = \frac{t_0 \eta k_{att} C_0}{\rho_b} \exp\left[-\frac{k_{att}}{v} L \right]$$

Eqn 3.12

Where (t_0) is the length of time permeation is conducted, and (C_0) is the contaminant concentration in the influent (permeating fluid). The remaining terms are described in the preceding sections and summarized in appendix 1.

The kinetic attachment rate term in this model is described using the formula (Tufenkji, 2007):

$$k_{att} = \frac{3(1-\eta)v}{2d_c} \eta_o \alpha$$

Eqn. 3.13

Where (d_c) is the average soil grain size, (η_o) is the single collector contact efficiency, and (α) is the attachment efficiency. Contact efficiency is defined as the rate particles strike the collector divided by the rate particles flow by the collector (Yao *et al*, 1971). Collision efficiency is defined as the ratio of the number of particles that stick to the collector relative to the number of particles that strike the collector (Rogers and Logan, 2000. Gross *et al*, 1995). As attachment is considered irreversible in this modeling theory, the portion of bacteria predicted to pass through the column are those that have either not come into contact with the soil particles, or those that have failed to stick to the soil particles after a given number of collisions.

Regarding bacterial transport, the value of (α) must be a value below 0.01 to allow bacterial transport over 100 m with less than a two log reduction in colony forming

unit (CFU) concentrations (Gross and Logan, 1995). Desorption is assumed to occur at a much slower rate than sorption, and for modeling purposes, is assumed to be insignificant. The CCFT model does not consider equilibrium sorption (Tufenkji, 2007) and ionic strength is not predicted to play an important role in the sorptive characteristics (Hornberger *et al*, 1992).

The single collector contact efficiency (η_0) is the most important term for this equation, and may be calculated using a variety of methods (Yao *et al*, 1971. Rajagopalan and Tien, 1976. Logan *et al*, 1995. Tufenkji and Elimelech, 2004). The collector contact efficiency term is typically calculated in advance, with the assumption that the bacteria behave similarly to an inorganic colloid. As there are no acceptable theories to predict the attachment efficiency term (α), this variable is typically fitted to a given experimental data set after the single collector contact efficiency is calculated (Nelson *et al*, 2007).

While this model would seem to accurately describe colloid transport in many experiments, deviations from these expectations have been demonstrated in many real world applications involving bacteria. This theory assumes a homogenous, saturated soil media where all bacteria and soil particles interact identically, and that deposited colloids do not affect the sorption of additional colloids (Logan, 1999. Nelson *et al*, 2007). These assumptions are obviously violated in any soil of a non-uniform soil particle size distribution, and subject to any degree of pore exclusion or filter ripening. It has also been reported that surface charge heterogeneity on the bacterial cell surface can have a pronounced effect on fitted (α) values (Baygents *et al*, 1998). Heterogeneity among the colloid population likely drives much of the observed deviations from CCFT (Tong and Johnson, 2007).

CCFT also compresses the sorptive potential between the bacteria and soil into the collector efficiency term (η_o). With such complicated and encompassing methodologies to calculate this term, such as those presented by Tufenkji and Elimelech (2004), the validity of this model is questionable with bacteria that may exhibit a range of sorptive behaviors within a well graded soil that may not be properly represented by the median grain size. The presence of fines or organic matter in field samples has also been found to cause significant variations from model predictions (Levy *et al*, 2007). As non-spherical bacteria are also assumed using this modeling technique to behave (sorption wise) like spherical bacteria, this may also render CCFT invalid (Hornberger *et al*, 1992).

Colloid filtration theory also breaks down at low pore fluid velocities when mobile cells are considered (Camesano and Logan, 1998). These cells may potentially overcome sorption at these velocities, or come into contact with soil particles at a higher than predicted rate through self propelled momentum. Estimating the collector contact efficiency term (η_o) may be further complicated by the motility and tendency of bacteria to move based on an additional chemical gradient within the soil (Harvey, 1991. Olsen *et al*, 2006).

To overcome some of the limitations of CCFT, modifications to the governing equations have been proposed by some researchers. For example, dual deposition parameters may be incorporated to account for the kinetic attachment of subpopulations of bacterial cells with both high and low sorption rates (Tufenkji 2007. Fuller *et al*, 2000). This may for example be used for mixed populations of cells influenced by the factors described in section 2.1. Other methods of calculating the attachment terms used in CCFT have been proposed. One such example used by Levy *et al* (2007) used a

regression method which accounted for 89% of the observed variability in their experimental observations..

Colloid filtration theory cannot at this time account for soil heterogeneity (Tufenkji, 2007). This filtration theory is based on the Happel sphere-in-cell model which assumes the liquid is a continuous sheath surrounding isolated particles, and neglecting the soil matrix pore structure (Bradford *et al*, 2006a). Subsequently, the usefulness of CCFT in heterogeneous soil models is not clear at this time (Levy *et al*, 2007). CCFT is also weak when applied to new situations without first calibrating the parameters using bacterial permeation tests (Levy *et al*, 2007).

Possible discrepancies in colloid filtration theory may be answered by incorporating a straining term into the model, as this process is overlooked in most colloid transport models (Bradford *et al*, 2002). CCFT does not consider straining or other physical removal processes (Nelson *et al*, 2007). CCFT also has difficulty predicting the deposition profile when colloid diameter / mean soil grain diameter is greater than 0.005 (Bradford *et al*, 2006a).

3.6 Straining model

Models which incorporate straining attempt to remedy shortcomings in the previous models where the influence of physical size exclusion, filtration, straining, and blocking are ignored. This also addresses the suggestion that sorption is not the primary removal mechanism in many situations, which was demonstrated through various means (Bradford *et al*, 2006a). This modeling theory is best applied to soils composed of a

uniform grain size, where straining is believed to occur (i.e. soils at or finer than a fine sand when considering bacteria permeation). Similar to the kinetic sorption model (Eqn 3.10), the governing equation is a modification of the general advection-dispersion equation (Eqn 3.1) where the second term is defined as (Tufenkji, 2007):

$$\frac{\rho_b}{\theta}\frac{\partial S}{\partial t} = k_{att}c - k_{str}\psi_{str}c$$

Eqn. 3.14

Where (k_{str}) is the first-order kinetic straining coefficient, and (ψ_{str}) is the depth dependant straining function, described using the function (Tufenkji, 2007):

$$\psi_{str} = \left(\frac{d_{50} + L}{d_{50}}\right)^{-\zeta}$$

Eqn. 3.13

Where (d_{50}) is the mean soil diameter, (L) is the column length, and (ζ) is a fitting parameter that controls the shape of the contaminant spatial distribution.

Models based on straining related processes have significant similarity to kinetic based models. When the parameters are calculated separately, kinetic sorption is typically assumed to be the reversible component of the overall sorption process, while filtration is considered to be a first-order type irreversible process (Pang *et al*, 2003. Tufenkji, 2007). The relative influence of both processes may be investigated by varying the ionic strength of the influent solution, or by backwashing the soil column (Foppen *et al*, 2007b.

Tufenkji *et al*, 2004). Straining may also be demonstrated by conducting experiments at low ionic concentrations, which would minimize chemical sorption processes (Tufenkji *et al*, 2004).

Straining based models have several advantages over equilibrium, kinetic, and CCFT based models. Within finer soils, such as those classified as a coarse loam or finer, mechanical filtration is expected to be the dominant removal mechanism for bacteria (Pekdeger and Matthess, 1983). Straining is also expected to be dominant at the top of the column, being surpassed by attachment deeper in the system (Bradford et al, 2003). This may be attributed to colloids being predominantly transported through the larger diameter, interconnected pores deeper in the column, which limits the availability of smaller pore spaces where straining can occur. Because of this, straining models tend to have superior deposition pattern predictions than similar sorption models (Bradford *et al*, 2004). Straining is also expected to be more important as a removal mechanism in compacted soils as opposed to undisturbed field samples (Levy *et al*, 2007).

While straining models, in particular those proposed by Bradford *et al* (2003) are typically more accurate than equilibrium and kinetic attachment / detachment models (Tufenkji, 2007) they also have several limitations. Similar to CCFT, heterogeneous attachment characteristics within a solute population can confuse the influences of straining and attachment (Foppen *et al*, 2007b). Straining is also not likely the primary explanation for the deviations from CCFT, as the colloid collector ratio in a test system may be much lower than that which would be expected for straining to occur (Tong and Johnson, 2007). Colloid removal through straining is an evolving research area, and

further experimentation is needed to refine and relate this model to the older models which utilize collector efficiency parameters (Bradford *et al*, 2006a).

3.7 Special modeling considerations for bacterial transport

Because subsurface bacterial transport is a more complicated process than chemical or colloidal transport, many environmental factors can greatly affect the transport of bacteria through the subsurface relative to the expectations of available models. Numerical modeling approaches commonly present a series of simplified system assumptions which are unlikely to represent real world field conditions. Few if any models incorporate a range of physical, chemical and biological influences on bacterial transport in the subsurface (Yates and Yates 1988). Typical model assumptions include: Soil is homogenous and isotropic, the flow rate is constant and steady, Darcy's law is valid, flow is unidirectional, and that the sorbed and suspended microbes are in equilibrium (Ashour *et al*, 1994). These models typically ignore the influence of size exclusion and straining (Simunek *et al*, 2006). In addition, diffusion, growth/death, chemotaxis, filtration and sedimentation are commonly assumed to be negligible. When applicable, dispersion is predicted to be constant with a varying flow rate, and measured deviations from this suggest that the classic advection-dispersion model is not valid for these scenarios (Becker *et al*, 2004). Many models are also limited to one-dimensional flow, and cannot account for time dependant changes in permeability or porosity due to biomass accumulation (Rockhold *et al*, 2004).

Filter ripening or blocking is also likely to occur over extended permeation times, which will have many effects on the model transport parameters. This can affect both the sorption rates (Camesano *et al*, 1999) and hydraulic properties of the experimental system. This is likely to occur in nearly all environments where bacteria permeate as it is beneficial for these colonies to group together and form defensive biofilm structures (Gargiulo *et al*, 2007a. Marshall, 1992).

Biofilms may also contribute to higher than predicted bacterial removal rates in some soils. Filter efficiencies may also drop due to pore clogging at the influent surface due to suspended solids and biofilm formation. This can act to limit access to the pore network for the permeating bacteria (Pang *et al*, 2003).

Many bacterial species are more readily sorbed to other cells or biofilm structures compared to soil particles. Because of this, a significant amount of the bacterial population within a given soil could form aggregates. The straining of these aggregated colonies could potentially be the dominant removal mechanism in many soils, including sands (Gariulo *et al*, 2007b). Aggregated cells may also affect bacteria enumeration techniques, as plated cells may overlap, underestimating the number of CFUs within a given sample.

As bacteria are subject to population growth and decay, this may result in experiment deviations from model predictions. The population growth rate for *E. coli* within the subsurface is difficult to estimate as this depends on many factors, such as water content, pH, nutrient availability and predation. To control this parameter, many studies utilize nutrient stressed cultures. These cultures can then be presumed to be at the stationary or resting growth phase, rather than an unknown mixture of both growing and

resting cells. As bacteria are capable of metabolizing a variety of substrates to support their metabolic activities, models based upon cells permeating a nutrient stressed environment may not accurately represent real world scenarios. The transport of metabolically active bacterial cells in the subsurface is particularly important for bioaugmentation research (Gargiulo *et al*, 2007a).

Bacterial population decay (die-off) is subject to many different influences. Studies have shown that the population decay rate of *E. coli* populations in soil ranges from between 0.025-0.36 d^{-1} (Abu-Ashour *et al*, 1994. Foppen *et al*, 2008. Sjogren, 1994). The die off rate is also dependant on the solution pH and temperature (Sjogren, 1994) among other influences. Comparably, the population doubling times of autochthonic bacteria isolated from aquifers, such as *Comamonas* and *Acidovorax* species, are estimated to be approximately every 15 days under conditions similar to the aquifer environment (Mailloux and Fuller, 2003). Non-sorbing processes such as predation or population decay may also cause an overestimate of the sorption rate and sticking efficiency (Harvey, 1991). These processes may also cause significant variations from model predictions that do not consider these influences.

The estimation of the sorption parameters for a bacterial population proves problematic for many modeling theories. This may be due to heterogeneity in the sorption rates of bacteria within a given population. While influences such as nutrient availability, growth phase, genetic variability and related parameters may be accounted for and controlled in laboratory studies, subpopulations of both quickly sorbing and non-sorbing cells may develop (Vidal *et al*, 1998). Through test systems, the majority of observed *E. coli* transport occurs via the more mobile, less adhesive population, while the less mobile,

more adhesive population is sorbed quickly near the inlet (Albinger *et al*, 1994). This is a particular problem with straining models, as both physical straining or a subpopulation of highly sorbing cells can explain high bacteria retention at the system inlet.

De-sorbing processes are also of special concern. Because sorption rates are considered to be many times greater than desorption rates, this term is often omitted from many models. Despite this, desorption does occur, and some proposed mechanisms include hydrodynamic shearing processes such as erosion and sloughing (Clement *et al*, 1997) diffusion-like processes (Morley *et al*, 1998) and kinetically dominated processes (Levy *et al*, 2007). Experiments where flow was interrupted for various time periods have indicated that hydrodynamic shearing forces have a limited roll in desorption compared to diffusion or kinetically controlled desorption processes. This conclusion was reached as the magnitude of desorption was found to be dependant on the length of flow interruption. Hydrodynamic shear would theoretically give similar results regardless of the interruption period due to similarities in the post-interruption flow rate (Schelde *et al*, 2002).

Computational assumptions of soil homogeneity may be of limited concern when applied to small laboratory controlled scales; however, this can become a problem when the simplified model is applied to heterogeneous field conditions (Pang *et al*, 2003). The highest bacterial deposition rates are also observed at soil textural interface zones, where colloids are more likely to encounter dead end pores and be subject to straining (Bradford *et al*, 2005). As this is a problem with almost all models, heterogeneous soil column experiments are needed to bridge the knowledge gap between homogenous columns typically used at the laboratory scale, and true field conditions (Bradford *et al*, 2004).

Models that focus on the transport of bacteria or similar colloids through fractured soil systems are especially rare in the literature. Even in relatively intact soils, transport is likely to occur through an interconnected network of pores with a diameter large enough to allow bacterial transport, rather than the soil matrix (Foppen *et al*, 2008). One conceptual model specially tailored to fracture flow is demonstrated by Chrysikopoulos and Abdel-Salam (1997) which describes the modeling of colloid deposition within saturated fractures. This model is difficult to apply to laboratory or field scale fractured systems as both the spatial properties of the fracture network, and the sorptive properties of colloids within the network are difficult to characterize with much accuracy.

Because of the inherent variability in bacterial transport modeling, a certain amount of error is acceptable between modeled predictions and experimental results. Estimates within one order of magnitude may be acceptable for bacterial transport modeling purposes (Martin *et al*, 1992).

3.8 Design of laboratory column experiments to identify fate and transport parameters

To investigate and define the relevant fate and transport parameters required for contaminant transport modeling purposes at the laboratory scale, constant head column permeation tests may be used. These tests allow one-dimensional flow through a column of a test soil, allowing material properties (such as column volume, moisture content, compaction condition, porosity, soil composition, etc), hydraulic head, hydraulic gradient, contaminant concentration and flow rate to be controlled and measured.

Fluid containing a known concentration of a contaminant may be applied to the contaminant free test column during a permeation test. A simplified, generic column test schematic is shown in Figure 3.1. Periodic measurement of the effluent volume and effluent contaminant concentration can yield a breakthrough curve, where the concentration of the contaminant leaving the column is plotted as a function of time or pore volumes of flow.

The breakthrough curve may be broken into two distinct regions: the head, and tail. The head is the region from zero contamination in the effluent until steady state breakthrough is reached (concentration of solute in influent is constant). The tailing region is that following steady state breakthrough when the permeating fluid is changed to a contaminant free solution. Figure 3.2 (continuous source) and Figure 3.3 (pulsed source) shows several standard breakthrough curve characteristics typically seen in column experiments. For the pulsed source example (Figure 3.3), the pulse permeation length was set to five pore volumes. Data points at pore volume values below five would be located in the head region of the effluent breakthrough curve, while data points located after five would be located in the tailing region.

To acquire a complete contaminant transport profile, a pulse style permeation experiment is required. In this type of experiment, the soil column is first permeated with a contaminated solution, followed by permeation with a clean, contaminant free solution. This would ideally occur after effluent concentrations had reached steady state, such as when effluent C/C_o is equal to one, or full breakthrough had occurred. Completing this experimental protocol results in a breakthrough curve data set containing both the head and tail regions, providing much more information about the transport of the contaminant

through the test column compared to the head region alone. While equilibrium models do not require the tailing region of the breakthrough curve to fit the relevant modeling parameters, this region is necessary when considering the time dependant or irreversible sorption parameters of the kinetic and straining models.

To investigate the importance of straining, reversal of flow experiments are required in addition to pulse experiments. In these cases, flow is reversed by switching the effluent and influent lines, so that a contaminant free solution permeates from the base of the column through the top. Effluent collected in this matter is expected to contain colloids that were trapped as a result of physical processes rather than via physiochemical sorption. This can allow an estimate of the relative population of microbes sorbed to the soil particles compared to those strained/filtered by the soil particles.

To investigate the distribution of a contaminant within the column, the permeated columns may be disassembled and sampled along their length for the given contaminant. This provides a spatial distribution profile of the contaminant within the system.

Detailed methods for the preparation of the soil columns and the calculation of the relevant fate and transport parameters for this research are outlined in the following section.

Table 3.1 - Comparison of the various modeling theories described in this chapter.

Model	Equilibrium	Kinetic	Classic colloid filtration theory	Straining
Sorption	instantaneous / reversible	first-order, reversible	first-order, irreversible	first-order reversible/irreversible
Required parameters	Retardation factor Longitudinal dispersivity first-order decay coefficient zero order production Coefficient Porosity Bulk density Pore velocity	Kinetic attachment coefficient Kinetic detachment coefficient Longitudinal dispersivity first-order decay coefficient zero order production coefficient	Collector contact efficiency. Collector attachment efficiency. Mean collector diameter Longitudinal dispersivity Porosity Pore velocity first-order decay coefficient zero order production coefficient	Kinetic attachment coefficient Column Length first-order straining coefficient Depth dependant straining function Calibrated fitting parameter first-order decay coefficient zero order production coefficient
Data required	Breakthrough curve Batch sorption analysis	Pulse breakthrough curve Kinetic sorption analysis	Grain size analysis Kinetic sorption analysis	Pulse breakthrough curve Reversal of flow test Distribution profile Grain size analysis Kinetic sorption analysis
Advantages	Simplest available model All transport parameters may be fit to breakthrough curve Only requires head region of breakthrough curve to define parameters	Better than equilibrium model when describing tailing region of breakthrough curve Bacterial sorption rates are expected to be kinetic-like	Allows estimation of transport parameters in advance Performs well when utilized in uniform, sandy soils	Incorporates physical straining in transport parameters Can give excellent performance in situations where straining is an important removal mechanism
Disadvantages	Assumes desorption occurs at the same rate as sorption Tailing region of breakthrough curve expected to mirror head region Does not consider grain size influences Assumes complete desorption will occur	Does not consider straining Requires pulse permeation to differentiate sorption and desorption	Does not consider straining or preferential flow paths Cannot account for size exclusion, soil heterogeneity, bacterial population heterogeneity Complicated methodology to calculate the Collector contact efficiency. Model must be calibrated to to each experimental system	Can confuse the influence of straining to variations in the colloid population sorption rate Requires extensive data Collection to differentiate sorption and straining Model must be calibrated to each experimental system

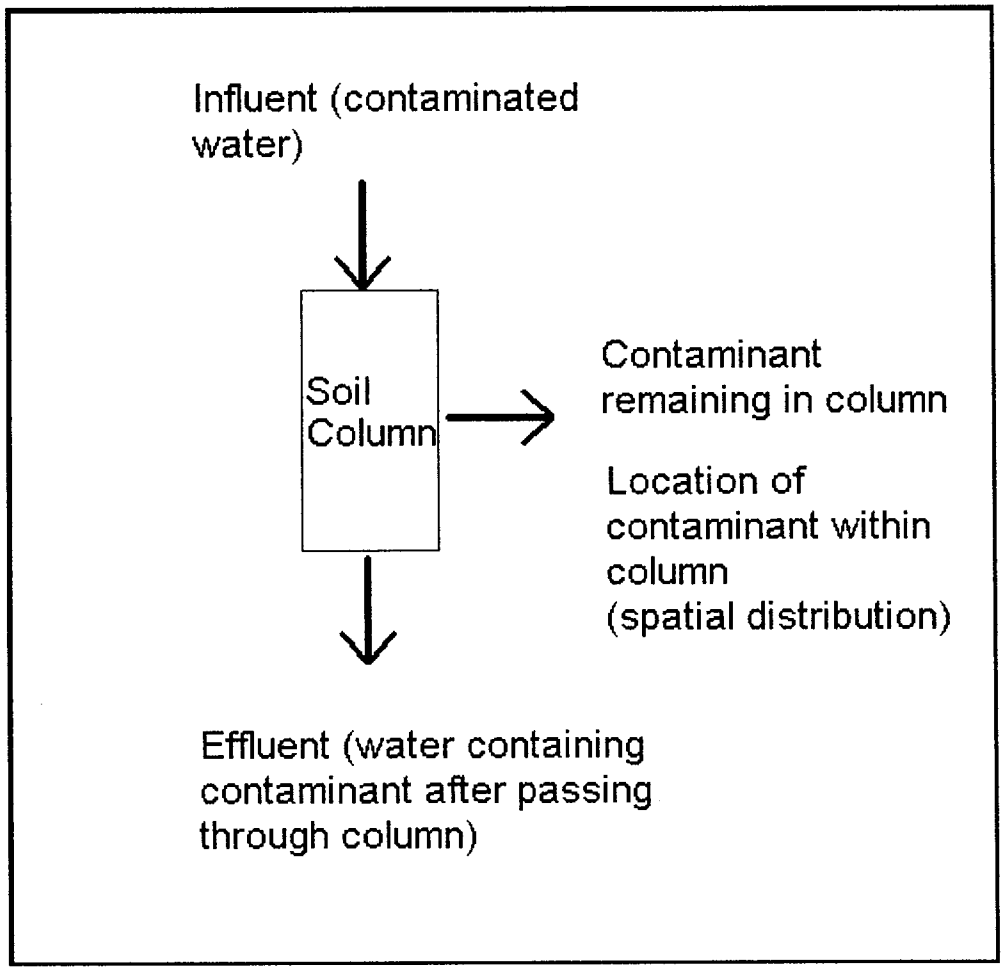

Figure 3.1 - Simplified column experiment schematic

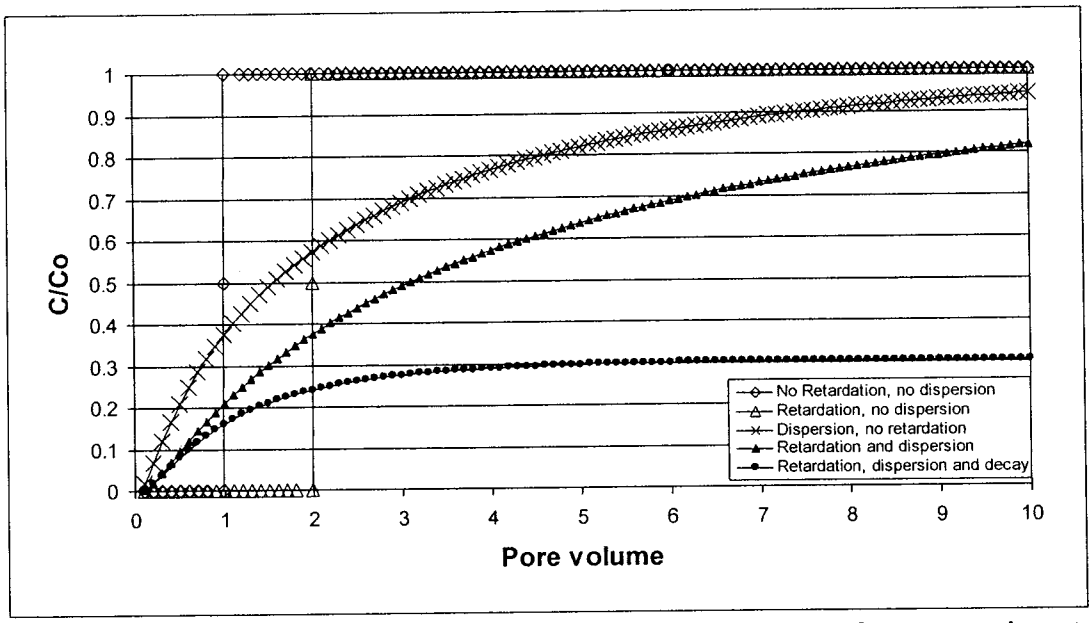

Figure 3.2 – Typical breakthrough curve characteristics seen in column experiments (continuous effluent source)

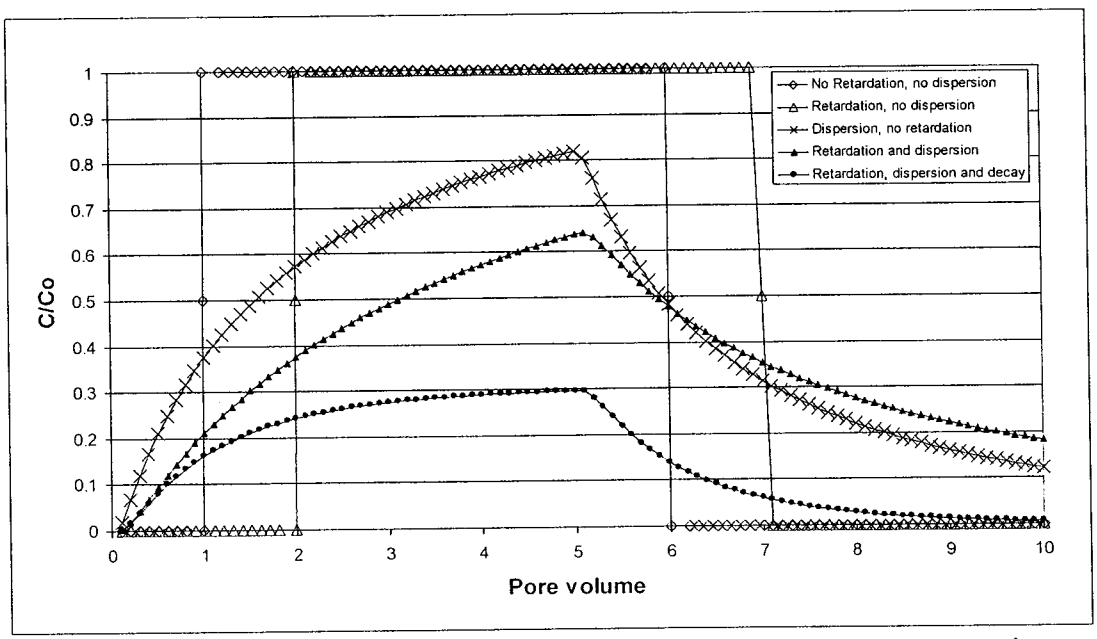

Figure 3.3 – Typical breakthrough curve characteristics seen in column experiments (pulsed effluent source (5 pore volumes))

Chapter 4 - Column Test Methods

4.1 Introduction

As described in the introduction for this thesis, existing column test and batch sorption data, and column test data generated as a part of this research were used to assess and develop the fate and transport models examined in this research. The experimental methods used in the previous studies are described in Miller (2004), Wong and Enns (2005), Scott and Nyguyen (2006), Lukacs *et al* (2007), and Rosa (2007). Methods used for the column tests carried out for this research, largely derived from the previously used methods, are described in the following sections. For this research project, column tests were carried out on compacted sand, compacted 90% sand / 10% silt mixed material columns, compacted silt, compacted clay, and normally consolidated clay. The clay columns were investigated as intact controls to contrast with the freeze-fractured clay columns investigated in the previous studies.

The column test setup used for this research is shown schematically in Figure 4.3, and is pictured in Figure 4.4. The column tests are conducted as constant head permeability tests. The chemicals, in this case suspended microbes, or interest are added to the influent reservoir and effluent samples are collected at regular intervals and analyzed to define the breakthrough curve.

4.2 Column preparation

4.2.1 Soil preparation and compaction

Soil columns were prepared following standard proctor methodology (ASTM D 698). The soil material properties such as the optimum water content and the specific gravity of the soil were determined in previous studies (Miller, 2004. Wong and Enns, 2005. Scott and Nguyen, 2006. Lukacs *et al*, 2007). The optimum water contents reported in those studies were used as the target for compaction in this research. The optimum water contents for the tested soils are listed in Table 4.1.

The medium quartz sand was filtered through a #20 sieve (0.85 mm), washed with tap water to remove dust and other contaminants that could affect sorption, and oven dried to remove moisture. The dry silt and Kam red clay (referred to from here on as "clay") were pulverized with a Los Angeles abrasion machine and filtered through a #40 sieve (0.45 mm) to remove clods. The silt was oven dried prior to the compaction, while the clay was not due to concerns that heat treatment would alter the clay's physio-chemical properties. The water content of the clay at storage condition was determined by measuring the mean mass difference between three approximately 10 g samples of the material before and after oven drying. The difference between this value and the optimal water content yields the amount of water required to bring the material to the target water content. The oven dried sand and silt was expected to have negligible water content, and the amount of water required to reach the optimal for compaction was calculated by assuming an initial water content of zero. The sand and silt columns were brought to the optimal water content from the dried state immediately preceding compaction, while the

clay soil was prepared two days in advance, and stored within sealed plastic bags until compaction. This was done to allow moisture to equilibrate through the clay material before compaction.

Compaction was performed by first applying a thin layer of lithium grease to the inside wall of a 15 cm high, 4" diameter (10.1cm inside diameter) clear PVC cylinder. The cylinder was then secured to a compaction apparatus, which provided a secure base plate for compaction. The base of the column contained a moistened sheet of 4" filter paper, or folded paper towel to prevent the soil material from moving through the base of the column. The entire apparatus was then weighed to provide an initial measure of the system without soil (Figure 4.3). Approximately 7 cm of loose soil material was then added to the column, followed by compaction via 25 drops with a standard 5.5 lb Proctor hammer. An additional layer of loose soil was added, and the compaction effort was repeated until 3 compacted soil layers were formed. The apparatus was then weighed, and the mass of the soil was determined by subtracting the mass of the empty apparatus from this value. A ruler was then used to measure the distance of the soil sample from the top ridge of the column at 6 locations along the top of the soil surface. The mean of this value was subtracted from the total column height to give the height of the soil column. A 5-10 g soil sample was then taken from the top of the soil column, and used to verify the compacted soil moisture content. These measurements were then used to calculate the various soil properties required for modeling purposes. A summary of these calculations is found in section 4.9.

The normally consolidated clay control column was prepared in a similar manner to the methodology of Scott and Nguyen (2006). The clay material was then mixed with a

enough water to bring the moisture content above the liquid limit (72%). The clay slurry was then added to the prepared compaction apparatus. A 1.5kg compaction hammer was then placed on top of the soil material to apply a surcharge of roughly 4 kPa, and the column was placed within a tub of tap water to prevent desaturation of the soil. Water was also added to the void space above the soil sample, and topped-up as needed. The volume of the consolidating clay was monitored by measuring the movement of the hammer into the column as the soil sample shrunk due to water leaving the clay matrix. After movement of the hammer was no longer observed (roughly 10 days from first pouring) the material properties were calculated (section 4.9), and the column was prepared for permeation. The compacted clay control column was treated in a similar manner to the consolidated clay column following the compaction, though no additional consolidation was observed.

4.2.2 Assembly of permeation apparatus

Soil permeater top and base plates were used to mount the soil columns for testing. The permeater plates contained fittings points for an influent line and an overflow line in the top plate, and an effluent line in the base plate. Ottawa sand was used in place of a porous stone in the base of the apparatus due to concerns that the stone could impede bacterial transport in unexpected ways. A moistened section of 4" diameter filter paper (Whatman grade #4) was placed on top of the Ottawa sand layer to prevent migration of the soil material through the column. Plumber's putty was placed in a ring along the edges of the filter paper to form a watertight seal between the base plate and soil column

edges. Because of concerns that the filter paper may impede bacterial transport in the sand columns, this was replaced with a fine zinc filter mesh in these columns.

The prepared soil column was removed from the compaction apparatus, and the bottom edge of the column was wiped clean to remove excessive soil from this area. The paper towel or filter paper used during compaction was discarded, and the column was placed into the base of the prepared soil permeater. The top edge of the column was then wiped clean, and lined with plumber's putty. The column top plate was then placed on top of the apparatus, and tightened. An image and schematic of a prepared column is shown in Figures 4.1 and 4.4. Distilled water was then allowed to flow into the column to prevent drying of the soil surface, and to check for any potential leaks.

4.2.3 Preliminary permeation testing

Before bacterial permeation was performed, preliminary permeation testing of the columns was conducted with distilled water to ensure proper operation of the system. This allowed the identification of leaks or unexpected flow characteristics to be identified and remedied before the bacterial permeation experiments. Minor faults such as pinhole leaks could be remedied by tightening the plate bracket screws, or through the addition of more plumbers putty to the affected area. Serious problems that resulted in destabilization of the soil sample (i.e. a failure in the filter paper / zinc mesh layer) resulted in the decommissioning of the affected column. Preliminary permeation also provides a baseline measure of the hydraulic conductivity and related properties of the columns. An

image and schematic of the prepared column attached to the permeation apparatus is shown in Figures 4.2 and 4.5.

Testing was conducted by permeating the columns with distilled water. The maximum flow rate of the system was determined by permeating an assembled, soil free column, and was found to be approximately 30 ml/s. As it was later determined that the distilled water could permeate the columns at this limit, it was decided to add a second control valve to the effluent line of the column. This control valve could then be used to control the flow rate of the column. Following the preliminary testing of the columns, the flow was stopped by closing the influent and effluent line valves. The columns were stored in this manner until the bacterial permeation experiments.

As the flow rate through the sand was at a similar magnitude to the maximum flow rate of the permeation system (estimated by testing the apparatus without a sample), it was decided to limit the flow rate within these columns using a control valve located in the effluent pipe. A flow rate of approximately 5 ml/s was achieved by gradually closing the control valve until this flow rate was reached. Flow could then be started or stopped by fully opening or closing another valve in the effluent line.

4.2.4 Sanitization of the reservoir and tubing

Following the preliminary permeation testing of the system, the reservoir and related tubing was sanitized. This involved flushing the system with bleach (sodium hypochlorite, 5% solution) followed by rinsing with several liters of sterile distilled water and a final rinse with 70% ethanol. This method was used as the vinyl chloride piping

and HDPE reservoirs would be destroyed by the high temperatures and pressures of the autoclaving process.

4.3 *E. coli* cell culture preparation

4.3.1 *E. coli* strain background

All previously conducted and current column tests conducted for this research utilized the same non-pathogenic strain of *E. coli*, labeled as S-17-1λ (pJB29) (Rosa, 2007). This particular strain contains a genetically modified plasmid containing genes for the production of the green fluorescence protein (Gfp), Ampicillin resistance (β-lactamase) and Kanamycin resistance (*nptII*). The strain also has an intrinsic resistance to Streptomycin. These modifications allow this strain to survive exposure to these particular antibiotics while potentially contaminating species are eliminated, and also allows the plated *E. coli* colonies to be easily identified visually via ultraviolet light.

4.3.2 Preparation of the minimal salt media

Because it is desirable to control the growth of bacteria within the reservoir, a nutrient limited suspension medium is required. Deionized water is not acceptable for this purpose as the osmotic gradient between the cells and the surrounding environment may be too great for the cell to survive, resulting in death. To overcome this problem, a sterile minimal salt media (MSM) solution was utilized. This solution is both nutrient limited to

prevent population growth, and contains sufficient salt content to prevent population loss through osmotic stress. The MSM was produced by bringing deionized water to the following salt concentrations.

- 170ppm KH_2PO_4 (Potassium phosphate monobasic)
- 99ppm $MgSO_4$ (Magnesium Sulphate)
- 5.6ppm $FeSO_4$ (Iron Sulphate)
- 74.9ppm NH_4Cl (Ammonium Chloride)
- 649.7ppm K_2PO_4 (Di-potassium hydrogen orthophosphate)

The final MSM solution contained 999.2ppm salt content, and has a pH 6.9. Following preparation, the solution was sterilized by autoclaving. The MSM recipe used for the current column tests is identical to the recipe used in all of the previously conducted column tests.

4.3.3 Agar plate and antibiotic preparation

The plating medium used to grow the *E. coli* was a standard tryptic soy agar (TSA) (25 g tryptic soy broth (TSB) medium mixed with 15 g agar in one liter of deionized water). TSA was used instead of Luria-Bertani (`) growth medium used in previous experiments as it was determined that colony growth was more rapid on TSA compared to LB. The required volume of this solution was mixed in an appropriately sized Erlenmeyer flask, capped with loose aluminum foil, and sterilized for one hour by autoclaving. An estimate of the required volume was approximately 10 ml of agar per 10cm Petri dish. Following sterilization, the agar medium was maintained at a liquid

consistency by placing the freshly autoclaved flask in a 55°C water bath. Once the medium had cooled to the hot water bath temperature (approximately 10 minuets for a 100 ml volume) the antibiotics were added. This was done by adding a 0.22 μm filtered stock solution of Ampicillin sodium salt (10 mg/ml) and Kanamycin monosulphate (5 g/ml) suspended in deionized water at a ratio of 1 μl antibiotic stock to 1 ml TSA.

The warm agar was then poured into sterile Petri dishes within a biosafety cabinet to prevent contamination by airborne particles. The agar was allowed to cool and solidify before replacing the lid of the Petri dish. The capped Petri dishes were then stacked and sealed within a labeled plastic bag, and stored under refrigeration until plating. It was estimated that the prepared antibiotics would decay slowly with time, and that after a period of two weeks post preparation, the prepared plates and antibiotic stock would no longer be adequate.

4.3.4 Culture preparation

To refresh a culture and select against cells which had lost the genes required for antibiotic resistance and the Gfp protein, a frozen culture or culture grown on older TSA medium was first plated on a freshly prepared TSA plates described in the previous section. The older or frozen stock was streak-plated to isolate individual colonies, and incubated at 37°C overnight. The temperature of 37°C is used as it is the optimum for the growth of *E. coli*. Following incubation, the inoculated plate was sealed with tape, and refrigerated to prevent excessive growth. This was done to maintain the refreshed culture for near term future use, and prevent overgrowth of the plated colonies.

4.3.5 Cell suspension preparation

To prepare the bacterial culture for the permeation experiments, a large quantity of cells was required. To achieve this, a standard Luria-Bertani (LB) nutrient broth solution was prepared. The volume of broth utilized was dependant on the quantity of cells required for a particular trial, and ranged from 200-500 ml. Previous trials had determined that 100 ml of inoculated broth provides enough cells for a final concentration of 10^{10} cells/L (10^{7} CFU/ml) in the final permeation stock solution.

The LB broth was prepared following manufacturers guidelines (25 g/L in deionized water) and was sterilized by autoclave. Once the LB broth had cooled to roughly room temperature, the antibiotic stock (Ampicillin sodium salt (10 mg/ml) and Kanamycin monosulphate (5 mg/ml)) was added at a ratio of one µl antibiotic stock per one ml of nutrient broth. The broth was then inoculated with an isolated *E. coli* colony using a heat sterilized inoculating loop. The inoculated broth was then transferred to an incubator, and maintained at 37°C overnight while being agitated at 100 rpm.

Following incubation, cells were separated from the nutrient broth by centrifugation at 8000rpm (average of 6555 G) at 4°C. This caused the formation of a "pellet" of cells at the bottom of the centrifuge container. The supernatant solution was discarded, and the pellet was resuspended into a similar volume of sterile MSM solution. This process was repeated for two additional cycles to ensure removal of the nutrient broth.

4.3.6 Preparation of the permeation influent reservoir

After the final centrifugation and resuspension, the cells were added to the sanitized reservoir, which contained the desired sterile MSM volume for permeation along with bromide (0.3723 g/l Potassium Bromide yielding a 250ppm bromide concentration) a tracer dye (10 mg/l Bromothymol blue) and antibiotics (one ml antibiotic stock per liter of influent). Cells were kept in solution with the use of a magnetic stir plate located below the reservoir (Figure 4.1), with a sterilized magnetic stir bar located within the reservoir. The air intake of the reservoir was filled with autoclaved cotton and capped loosely to filter microbes which could contaminate the reservoir.

4.4 Bacterial permeation

After preparation of the influent reservoir containing the *E. coli* suspension, the bacterial permeation test could begin. Prior to permeation, a sample from the reservoir was taken to determine the influent *E. coli* concentration. The distilled water on top of the soil column was first removed by gently pouring through the overflow (clay and silt columns) or by opening the effluent and overflow valves and allowing an air void to form until just above the soil surface (sand and 90% sand / 10% silt columns). The different techniques were used as the water above the clay and silt columns would require days to pass through the column, while occurring in minuets for the sand and 90% sand / 10% silt columns. The clay and silt columns were also cohesive enough to resist disturbance or shifting due to the pouring procedure, unlike the sand and 90% sand / 10% silt columns.

Care was taken with either technique to avoid disturbing and desaturating the soil sample. The resulting air void was then replaced with the bacteria solution by slowly filling the column through the influent line, and allowing the displaced air to flow out the overflow fitting.

The actual permeation was then started by opening the influent and effluent valves. A Chronograph was also started at the onset of permeation. The following sampling regiment was conducted for the tested soils:

Intact clay columns

The intact clay columns were sampled once a day by collecting the effluent within 250 ml weighed flasks (consolidated) 15 ml graduated cylinders (compacted) and 15 ml sterile centrifuge tubes (reservoir). The volume of effluent was determined by measuring the weight of the flask before and after effluent collection. It was assumed that one gram was equivalent to one ml. One ml samples were taken from the sample vessels and stored under refrigeration in sterile 1.5 ml centrifuge tubes for bacterial plate counting and bromide analysis. Excess fluid from the collection vessels was then emptied into a biohazard collection reservoir, and the vessels were then sanitized with 70% ethanol. A pair of collection vessels was used for each column, which allowed the current collection vessel to be immediately replaced with a sanitized collection vessel following sample collection. The collection time and volume was recorded for each column effluent.

Silt columns

Silt column effluent samples were acquired in a similar manner to the intact consolidated clay effluent samples. Plating was performed immediately after the effluent volume was measured. One ml samples were taken and stored in 1.5 ml centrifuge tubes for later bromide analysis.

Sand and 90% sand / 10% silt columns

Sand column effluent samples were acquired by collecting effluent in assembled racks of 72 autoclaved 15 ml test tubes. The filled racks were weighted before sample collection to assess the dry weight of the test tubes before permeation. Samples were collected in a regular pattern with every sixth test tube marked for analysis. Following the collection of 72 test tubes, three sterilized and weighed 125 ml flasks were filled with effluent. Later experiments collected a fourth flask to extend the permeation volume slightly. The time to fill the test tubes and each individual flask was recorded. Volume measurements were acquired by weighing the filled rack or flasks, and subtracting the dry weight. This methodology is similar to that used by Lukacs *et al* (2007).

Following the bacterial permeation experiment, the influent and effluent valves were closed to stop permeation. The column could then be prepared for a pulse experiment, or for soil sampling.

4.5 Pulse experiments

Since the previous experiments conducted for this program utilized continuous source column permeation, pulse experiments for the sand, silt, and 90% sand / 10% silt

columns were conducted. This was to add breakthrough data which could be used to estimate the non-equilibrium transport parameters, which require a tailing region (Reddy and Ford, 1996).

To perform the pulse type source experiment, the selected columns were first permeated with the bacterial suspension as described in section 4.4, followed by permeation with a sterile MSM solution. Following the change to the clean MSM influent solution, the effluent was sampled following the same regiment as outlined for the *E. coli* in section 4.4. The MSM reservoir was kept at the same height as the bacterial reservoir to avoid significant changes in the hydraulic head (Figure 4.1). The bacterial solution was flushed from the upper surface of the soil column by opening the overflow and MSM reservoir influent lines, and collecting approximately 1.5 liters of MSM effluent through the overflow. Permeation was then achieved by closing the overflow valve, and opening the effluent valve. Sampling was conducted in the same manner and at the same intervals as the bacterial permeation.

4.6 Column soil sampling

After the permeation experiments were completed, the sealed columns were transported to the microbiology lab for disassembly and soil sampling. The permeameter top plate was first detached, and the remaining permeation fluid was removed by tipping the column and pouring into a collection reservoir. The soil column was then removed from the plastic casing by lifting the cylinder, and allowing the intact soil sample to slide out the column bottom by gravity. The soil column was then laid on its side, and split

longitudinally using a scoopula sanitized with 70% ethanol. Splitting, rather than cutting, was done in an effort to prevent vertical smearing of the soil during column disassembly.

Soil samples were then collected from 12-25 points from within the column depending on the required sample resolution. This corresponded to 3-5 horizontal samples collected at the top, bottom, and every 0.33 to 0.25 relative depth interval in between. One gram samples of soil material were excised from the target location using a metal scoopula that was sanitized between each location using 70% ethanol. These weighed samples were then added to labeled 1.5 ml centrifuge tubes containing 950 µl of sterilized MSM. These samples were stored under refrigeration at 4°C until plating.

The purpose of the column soil samples was to investigate the retention of the *E. coli* bacteria within the column. The available data covered a variety of location sampling methodologies, such as the grid-like pattern used in this research, or an "I" shaped pattern with single samples taken at each layer, and additional measurements at the top and bottom soil boundaries. For comparison, the measured values were averaged, and the mean values were used for comparison. If available, the specific location of the sample was used to infer additional details, such as the presence of interface flow (presence of *E. coli* only found in samples taken proximal to the edge of the soil column).

4.7 E. coli Plating

The quantification of the effluent bacteria concentrations was accomplished by a drop plate counting technique. This procedure was completed in a biosafety cabinet to avoid contamination of the plates with airborne particulates. Samples were first vortexed briefly to resuspend cells into the solution sample. The samples were then diluted in a

series of sterile 1.5 ml centrifuge tubes by pipetting 100 µl of the undiluted sample stock into 900 µl of sterile MSM solution. The diluted sample was then vortexed briefly to ensure adequate mixing of the solution. Pipette tips were discarded between dilutions to prevent cross contamination. This was repeated to provide a total dilution series of 1, 1/10, 1/100, 1/1000, 1/10,000, or 4 orders of dilution.

The drop plating procedure was conducted by adding six separate five µl drops from each dilution to a labeled section of the prepared TSA plates. A single pipette tip was used, and the dilutions were plated in order of most dilute to least dilute. It was found that a maximum of four samples and their dilution series could be fit onto an individual plate by separating each section into quadrants. After dropping, the plates were allowed to air dry in the biosafety cabinet before being capped, and incubated overnight at 37°C.

After incubation, individual cells had multiplied into visually discernable colonies. These were then tabulated under a long wave UV lamp, where the *E. coli* colonies would fluoresce due to the presence of the Gfp protein. The dilution used for counting was that which provided approximately 5-50 discernable colonies.

4.8 Bromide effluent sampling analysis

Bromide analysis was conducted on the same effluent and stock samples used for the plate counting to provide matched sample times. Samples were prepared in 5 ml plastic vials by diluting 500 µl of a given effluent sample into 4.5 ml of distilled water. The vial was then capped with a filter stopper. Sample sets were submitted to the

Lakehead University Centre for Analytical Service, and were analyzed for bromide content via ion chromatography.

4.9 Column soil properties, permeation hydraulic and E. coli counting related calculations

4.9.1 Column properties

Data collected from the soil column preparation and effluent measurements were used to calculate several values required for modeling purposes. The necessary data from the soil compaction data included the sample height, sample diameter, sample mass and moisture content. Sample height was determined using the formula:

$$L = L_c - L_s$$

(Eqn 4.1)

Where (L) is the height of the soil sample in meters, (L_c) is the total height of the polyvinyl chloride (PVC) cylinder in meters, and (L_s) is the average height in meters of the space between the top of the soil sample, and the top of the plastic cylinder, measured using a ruler at six points through this region.

The mass of the sample was determined using the formula:

$$M_s = M_{se} - M_c$$

(Eqn 4.2)

Where (M_s) is the mass of the soil sample, (M_{se}) is the mass of the assembled compaction apparatus with the soil sample, and (M_e) is the mass of the assembled compaction apparatus before the addition of soil. The measurement units were kilograms.

The diameter of the soil sample was taken by measuring the average inner diameter of the plastic cylinder with an electronic caliper. This value was determined to be 10.1cm. This value was consistent across all measured cylinders, including those from the previous experiments. As the previous studies utilized a range of values from 9.8cm to 10.3cm, the associated data were updated with this correct value.

Soil moisture content was calculated using the formula:

$$w = \left(\frac{M_w}{M_d} - 1 \right) 100$$

(Eqn 4.3)

Where (w) is the percent moisture content of the sample, (M_w) is the mass of the moist soil sample and (M_d) is the mass of the oven dried soil sample.

The volume of the sample was calculated using the formula:

$$V = L\left(\frac{d}{200} \right)^2 3.14$$

(Eqn 4.4)

Where (V) is the sample volume in cubic meters, (d) is the diameter of the soil sample in cm, and (L) is the height of the soil sample in meters.

The wet density of the sample was calculated using the formula:

$$\rho_T = \left(\frac{1000 M_s}{V} \right)$$

(Eqn 4.5)

Where (ρ_T) is the density in Mg/m^3.

The Dry density could then be calculated using the formula:

$$\rho_d = \left(\frac{\rho_T}{1 + \frac{w}{100}} \right)$$

(Eqn 4.6)

Where (ρ_d) is the dry density in Mg/m^3

The unit weight of the samples was then calculated by multiplying ρ_d or ρ_t by the acceleration rate of gravity (9.81 m/s) to convert the density value (Mg/m^3) to kilonewtons/m^3).

The void ratio was calculated using the formula:

$$e = \left(\frac{Gs\rho_w}{\rho_d} \right) - 1$$

(Eqn 4.7)

Where (e) is the unitless void ratio, (ρ_w) is the fluid density in g/ml, and (Gs) is the specific gravity of the soil solids. The values of the specific gravities used are 2.65 for sand, 2.7 for silt, and 2.75 for clay (Rosa, 2007). The specific gravity of the 90% sand / 10% silt was calculated by using a weighted average of the sand and silt specific gravities, resulting in a value of 2.66.

As the moisture content data were missing for some of the older data, an alternative method was sought to calculate this value. Assuming that the compacted samples were fully saturated, the void ratio may be calculated using the formula:

The porosity of the samples was then calculated using the formula:

$$\eta = \left(\frac{e}{e-1} \right) 100$$

(Eqn 4.8)

Where (η) is the unitless porosity as a percentage value.

The volume of voids could then be calculated using the formula:

$$V_v = [\eta V]10^6$$

(Eqn 4.9)

Where (V_v) is the volume of voids in ml, and 10^6 is a constant used to convert the volume from m^3 to ml.

4.9.2 Hydraulic calculations

The parameters calculated using the equations presented in the previous section was utilized with the effluent data collected from the permeation experiments to assess the relevant hydraulic parameters. The hydraulic conductivity was calculated using the formula:

$$k = \frac{Q\left(\frac{L}{h}\right)}{At}$$

(Eqn 4.10)

Where (k) is the hydraulic conductivity in cm/s, (Q) is the effluent volume collected over the collection period in ml, (L) is the height of the column in cm, (A) is the cross sectional area of the column (cm^2), (h) is the head loss in cm, found by measuring the distance from the surface of the influent in the reservoir to the base of the column, and (t) is the time interval in seconds.

The pore volumes of flow were calculated using the equation

$$PV = \left(\frac{Q_t}{V_v} \right)$$

(Eqn 4.11)

Where (PV) is the cumulative pore volumes passed through the column at time step (t), (Q_t) is the total cumulative volume of effluent in ml at time (t), and (Vv) is the volume of voids of the column test sample in ml.

4.9.3 *E. coli* colony counts

To calculate the concentration of bacteria in the effluent and soil samples, it is necessary to convert the plate count values into the required value. This was accomplished using the formula:

$$C = C_m (200) D_f$$

(Eqn 4.12)

Where (C) is the concentration of bacteria per ml sample volume, (C_m) is the mean number of *E. coli* colonies in the six 5 µl drops of the dilution series, and (Df) is the

dilution factor (1 for an undiluted sample, 10 for a sample diluted 10 fold, 100 for a sample diluted 100 fold, etc)

The concentration of bacteria could then be converted to the dimensionless relative concentration format of C/C_o, where (C_o) is the mean concentration of cells in the reservoir, and (C) is the quantity of cells in the given sample (effluent or soil). The results of the bromide analysis were also converted to the C/C_o format following an identical methodology.

By converting the effluent data to PV and C/C_o, a general dimensionless breakthrough curve may be plotted. The *E. coli* and bromide breakthrough data and soil sample *E. coli* results of the previously conducted experiments, and the experiments conducted during the course of this thesis research are given in the next chapter.

Table 4.1 - Optimum water contents for compaction of the tested soils

Soil material	Water content (%)
Clay	31
Silt	15.5
Sand	9.5
90% sand / 10% silt	8

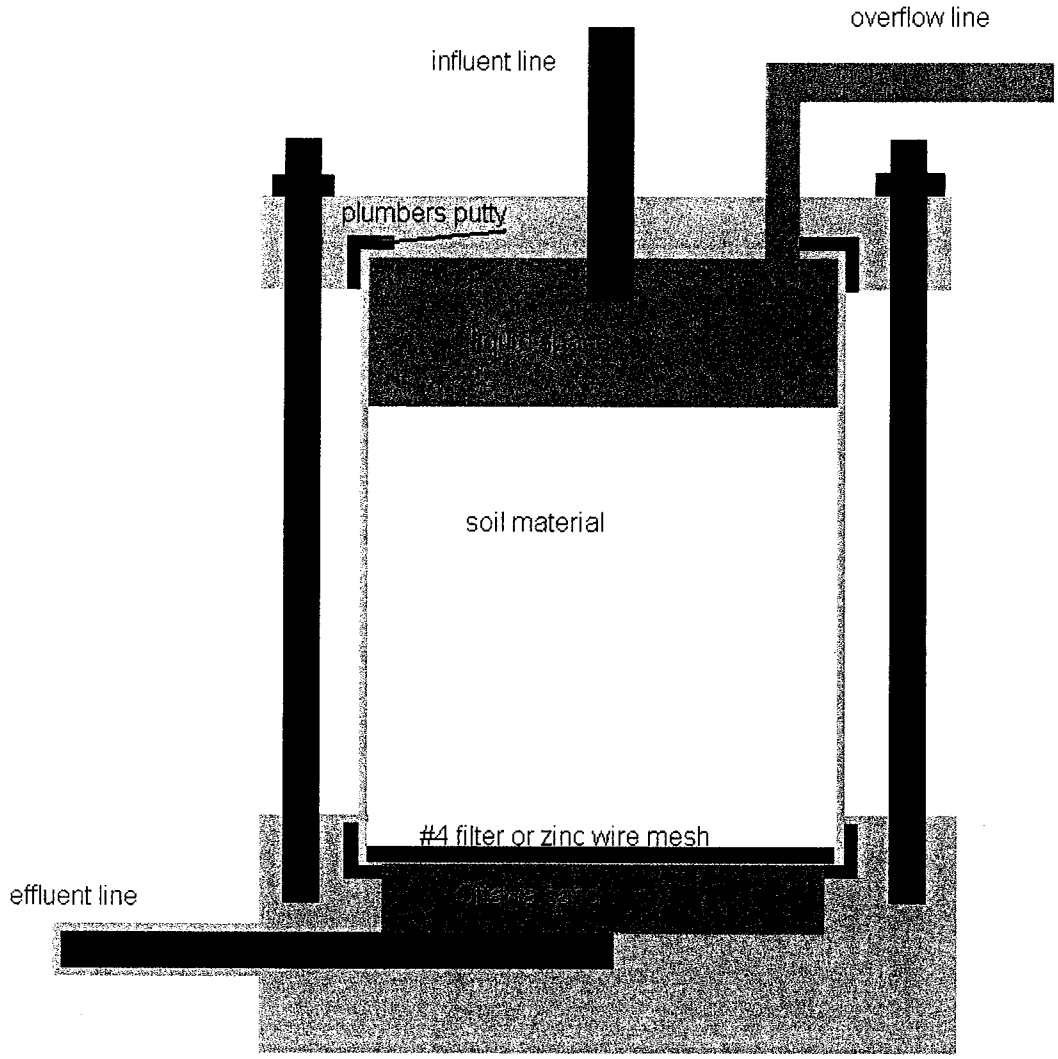

Figure 4.1 - Schematic of the assembled permeameter

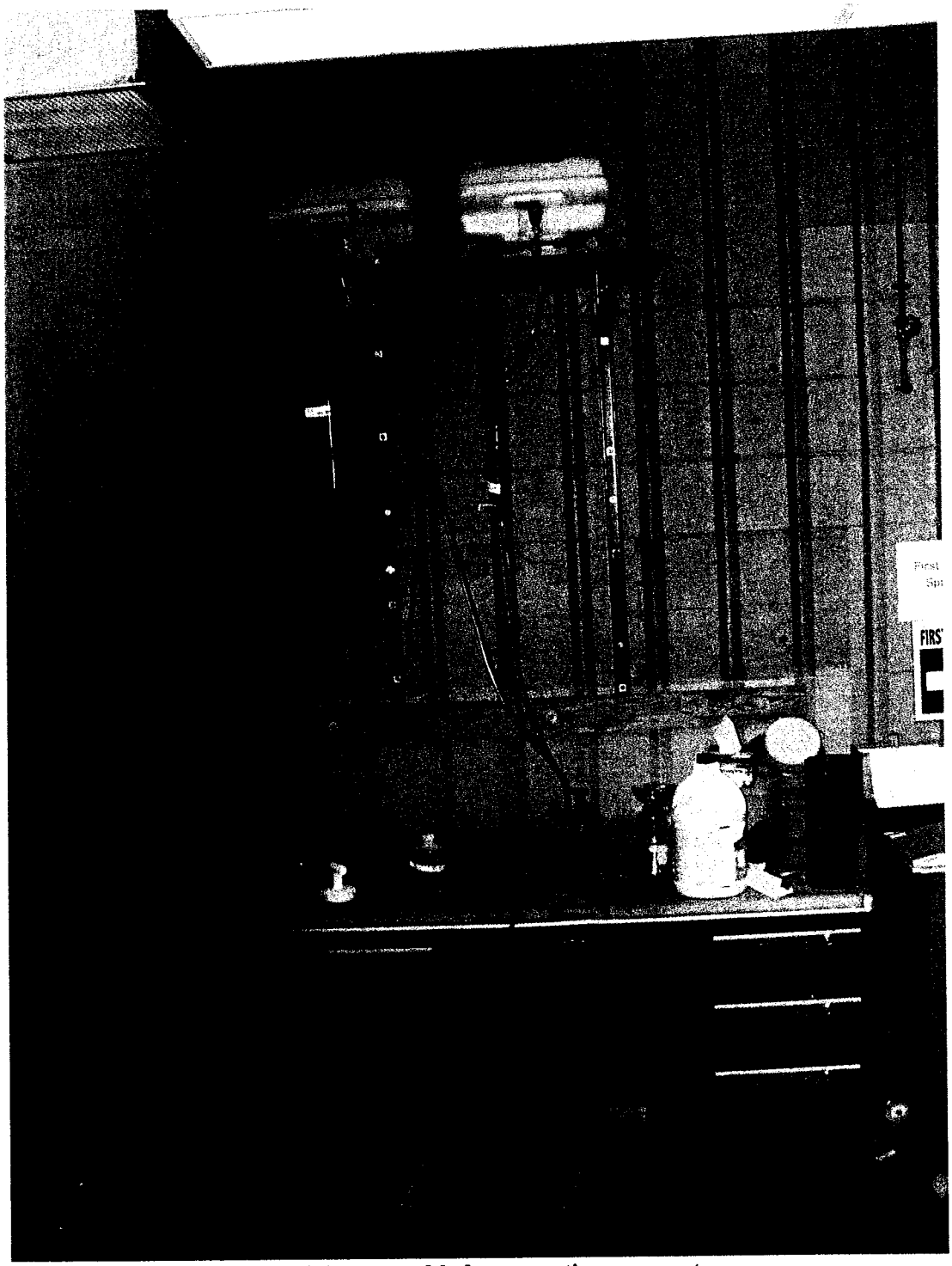

Figure 4.2 – Photograph of the assembled permeation apparatus.

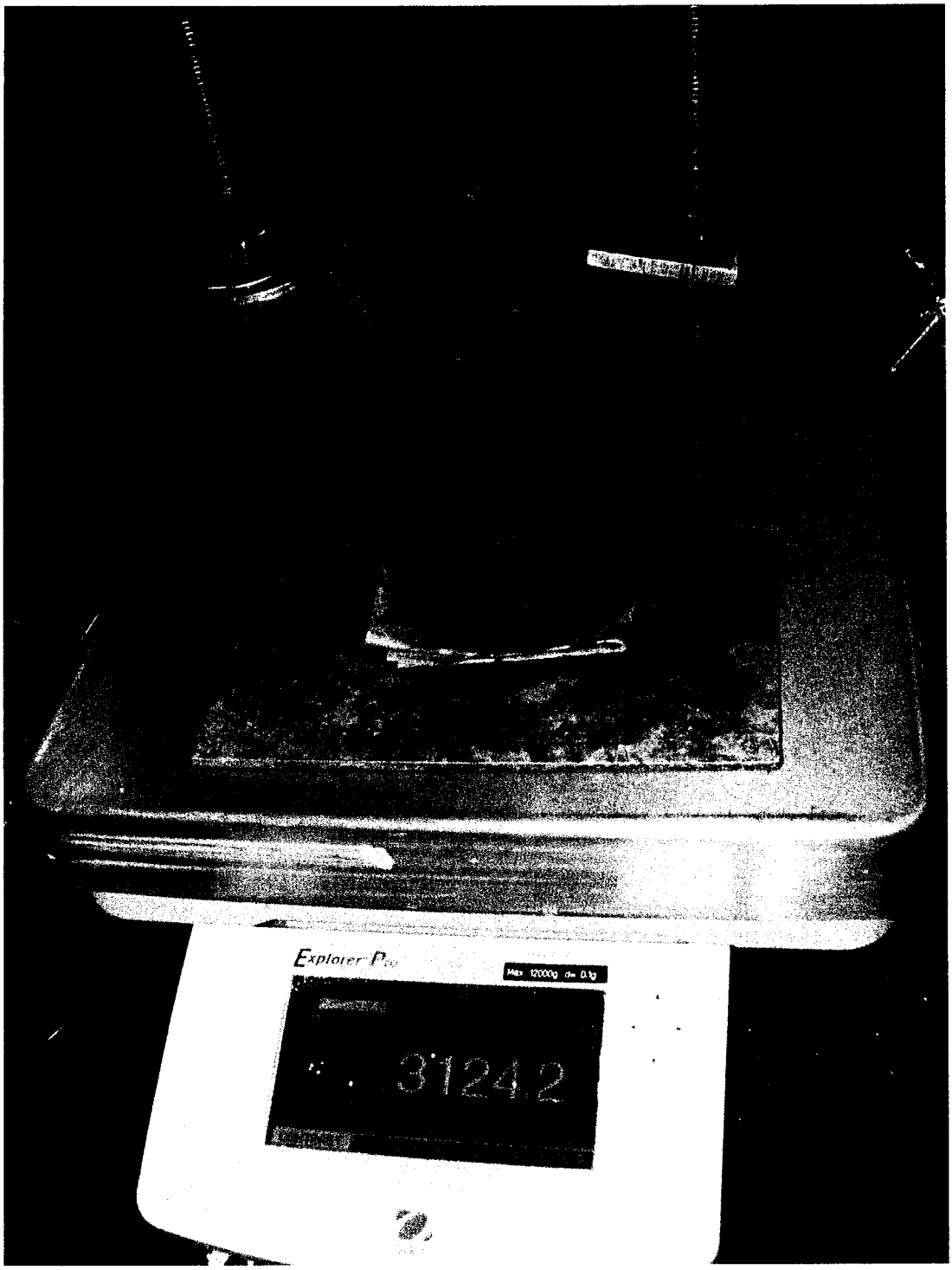

Figure 4.3 - Weighing of the assembled compaction apparatus prior to the addition and compaction of soil.

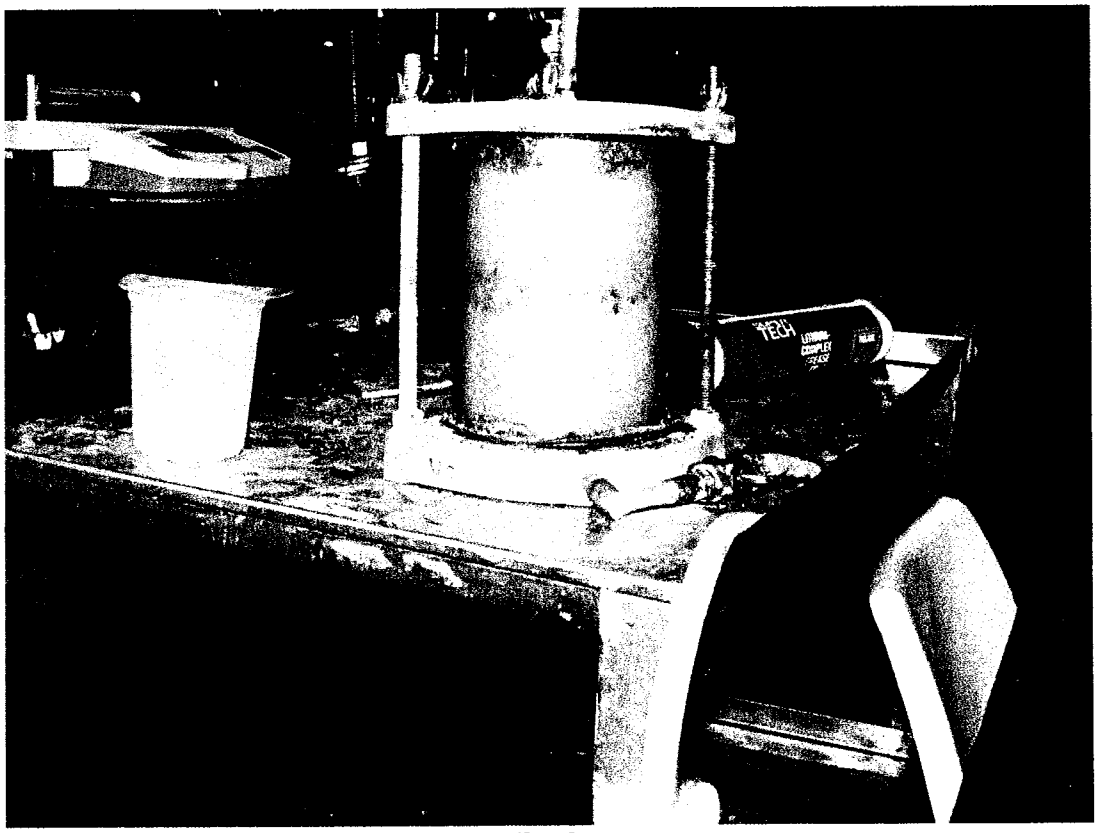

Figure 4.4 - Prepared and assembled soil column.

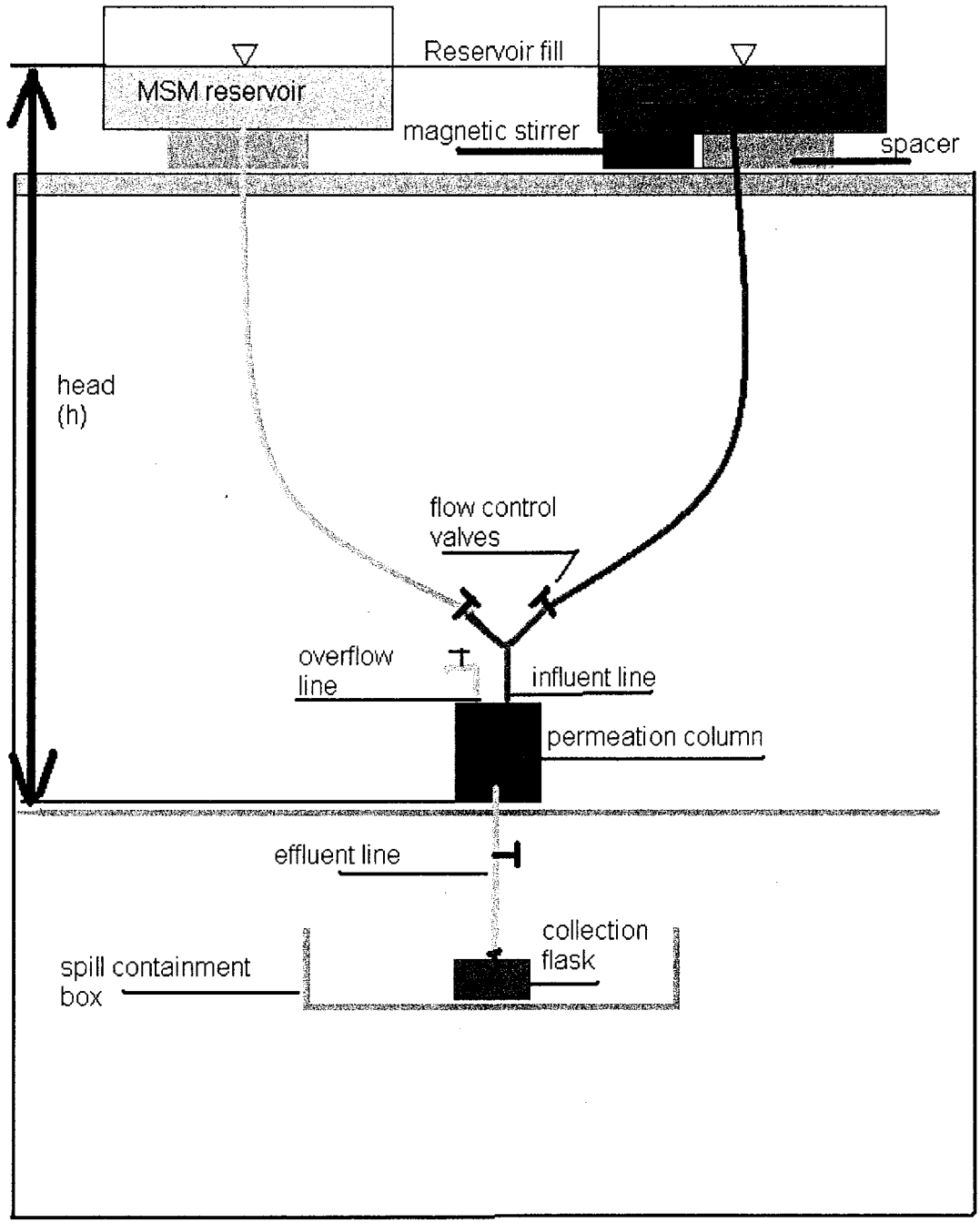

Figure 4.5 - Schematic of the assembled permeation apparatus

Chapter 5 - Column Test Results

5.1 Previously collected data

5.1.1 Column properties

Summaries of the soil column properties from the previously conducted experiments are shown in Tables 5.1, 5.2, 5.3 and 5.4 for the freeze-fractured compacted clays, freeze-fractured normally consolidated clays, compacted sand, and compacted 90% sand / 10% silt columns, respectively. These values differ slightly from those in the associated projects as all properties were recalculated using a column diameter of 10.1cm. Source data were taken from the raw data sheets of the associated experiments.

5.1.2 Soil grain size distribution

The soil grain size distribution for the soils tested in the batch sorption experiments by Rosa (2007) are summarized in Figure 5.1. Only the sand, silt, and red clay soil materials were utilized in the experimental test columns.

5.1.3 Bromide breakthrough curves

The bromide breakthrough curves for the previously tested soil columns are shown in Figures 5.2, 5.3, 5.4 and 5.5 for the compacted sand, compacted 90% sand / 10% silt, freeze-fractured compacted clay, and freeze-fractured normally consolidated clay columns respectively. These values differ slightly from the reported values in the associated documents due to the updated material properties being used to recalculate the corresponding pore volumes of flow.

5.1.4 *E. coli* breakthrough curves

The *E. coli* effluent breakthrough curves for the previously tested soil columns are shown in Figures 5.6, 5.7, 5.8 and 5.9 for the compacted sand, compacted 90% sand / 10% silt, freeze-fractured compacted clay, and freeze-fractured normally consolidated clay columns respectively. These values differ slightly from the reported values in the associated documents due to the updated material properties being used to recalculate the corresponding pore volumes of flow.

5.1.5 *E. coli* longitudinal distribution profiles through the soil columns

The *E. coli* distribution profiles, measured following column permeation, are shown in Figures 5.10, 5.11, 5.12 and 5.13 for the compacted sand, compacted mixed 90% sand / 10% silt, freeze-fractured compacted clay, and freeze-fractured normally

consolidated clay columns respectively. As the columns varied in height, the resulting data were normalized to the relative column height of each individual column. This was accomplished by dividing the distance to the base of the soil column at the sample location by the total column height (i.e. a sample collected at 8 cm from the column base in a 12 cm column, or 10 cm from the base in a 15 cm column would both have a relative height of 0.67). C/C_0 was calculated in a similar manner to the effluent counts (section 4.9.3). As the data sets varied from 1-5 samples at a given height, the values reported within the figures are the mean of the total measured *E. coli* concentrations from the given height within the soil column.

It should be noted that the soil samples also contained an unknown quantity of pore fluid in addition to the soil material. This means that the measured values are a unknown combination of both the quantity of *E. coli* recovered from the soil phase, and the quantity contained within the liquid pore spaces.

5.1.6 *E. coli* batch sorption data

The *E. coli* batch sorption data were acquired from the research of Rosa, (2007). As the batch sorption data for the sand experiments exhibited a confusing distribution profile at higher *E. coli* concentration values, only those data points for concentration values below 1 x 10^6 CFU/ml were used for this research to determine sorption isotherm parameters. The silt and Kam red clay batch sorption parameters were determined using the entire sorption data set. The Freundlich and Langmuir model parameters determined by fitting to the batch sorption data, were combined with the porosity and dry density

data for the corresponding columns, and used to calculate unique retardation factors for each column using equations 3.8 and 3.9. As the target (C_o) *E. coli* cell concentration was 10^7 cells/ml, this was utilized as the (C) variable within these formulas. As batch sorption experiments were not conducted with the 90% sand / 10% silt mixed material, a retardation factor for these columns was estimated by using a weighted average of the retardation factors for the sand and silt material. The resulting retardation factors using the Freundlich and Langmuir sorption isotherm models are shown in Tables 5.5 and 5.6, respectively.

5.1.7 Hydraulic conductivity measurements

The hydraulic conductivity measurements of the previously collected column data is shown in Figures 5.14, 5.15, 5.16, 5.17 for the compacted sands, compacted 90% sand / 10% silt, freeze-fractured normally consolidated clays and freeze-fractured compacted clay columns, respectively. The average hydraulic conductivity values are summarized in Table 5.7.

5.1.8 Survival and growth of *E. coli* within the reservoir and soil medium

The survival of *E. coli* within the MSM solution and within the clay soil was investigated by Rosa, 2007. An increase in the cell population was not observed during the experiment, indicating that population growth was not occurring within the reservoir or clay columns. The population of cells within the MSM reservoir tended to decrease by

67% after a time period of seven days, indicating the necessity of refreshing the cell suspension stock solution periodically. The clay survival trial indicated that the cell population dropped by 2-3 orders of magnitude over the 21 day trial period, and roughly 1.5 orders of magnitude over a 7 day period (Rosa, 2007).

5.2 Currently collected data

5.2.1 Column properties

A summary of the column properties from the experiments conducted during the course of this research are shown in Tables 5.8, 5.9 and 5.10 and 5.11 for the intact clay columns, compacted sand, compacted 90% sand / 10% silt, and compacted silt columns respectively.

5.2.2 Bromide breakthrough curves

The bromide breakthrough curves for the column experiments conducted during the course of this research are shown in Figures 5.18, 5.19 and 5.20 for the compacted sands, compacted 90% sand / 10% silts, and the compacted silt columns, respectively.

5.2.3 *E. coli* breakthrough curves

The *E. coli* effluent breakthrough curves of the column experiments conducted during this project are shown in Figures 5.21, 5.22 and 5.23 for the compacted sands, compacted 90% sand / 10% silts, and the compacted silt columns, respectively. No *E. coli* was detected in the effluents of the control clay columns.

5.2.4 *E. coli* longitudinal distribution profiles through the soil columns

The *E. coli* distribution profiles of the column experiments conducted during this research are shown in Figures 5.24, 5.25, 5.26 and 5.27 for the intact control clay columns, compacted sands, compacted 90% sand / 10% silts, and the compacted silt columns, respectively. Similar to section 5.1.5, the individual column heights were normalized and reported as the relative column height. C/C_o was calculated in a similar manner to the effluent counts (section 4.9.3). The mean value of the samples collected at each relative height interval was used for the reported values.

5.2.5 Hydraulic conductivity measurements

The hydraulic conductivity measurements of the column experiments conducted during this study are shown in Figures 5.14, 5.15, 5.28, and 5.29. Average hydraulic conductivity values are shown in Table 5.11.

5.3 *Discussion of the results*

5.3.1 Compacted / normally consolidated clay control columns

No *E. coli* breakthrough was observed in the compacted or normally consolidated clay control columns. Despite this, the presence of *E. coli* was found in several of the distribution profile measurements of the consolidated clay control (Figure 5.30) suggesting that *E. coli* migration through the column was occurring despite the lack of fracture flow paths from freeze thaw cycles. On closer inspection, it was found that the samples containing *E. coli* were all acquired from locations proximal to the edge of the column (i.e. no presence of *E. coli* inside the matrix). This indicates that *E. coli* did not migrate through the intact clay materials. The small presence of *E. coli* at the base of this column despite not being present in the column effluent may indicate contamination of the column during the disassembly procedure, or partial interface flow, or possibly migration.

It was also observed over the course of the control clay experiment (roughly 3 months from initial pouring to column disassembly) that void spaces had begun to form in the lithium grease used to prevent interface flow (Figure 5.31). Complete interface flow from the top to the bottom of the column due to these void formations was not suspected as the hydraulic conductivity remained stable through the experiment, and *E. coli* was not detected in the effluent samples. It is possible that partial interface flow due to this phenomenon may have contributed to the observed presence of *E. coli* in the distribution profile measurements along the sides of the column. As it would appear that decay or migration of the lithium grease into the column could occur over extended time

periods, long term column studies may be susceptible to interface flow. As *E. coli* was not found within the distribution profile measurements which were not located on the edges of the column, it would appear that the intact clays are impervious to *E. coli* cells.

5.3.2 Compacted sand columns

The compacted sand columns were assembled using the same material and technique utilized by Lukacs *et al* (2007). The target moisture content of these columns was 8.5% to produce columns similar to their reported data. During preliminary permeation tests with distilled water, it was evident that the compacted sand columns had significantly higher flow rates (10-30 ml/s) than those reported by Lukacs *et al* (2007) (1-5 ml/s), despite having similar material properties.

The sand columns for the current research utilized a fine, zinc wire mesh in place of the filter paper utilized by Lukacs *et al* (2007). As this material contains much larger pore spaces than filter paper, it was expected to have a minimal impact on flow rates or possible bacterial retention. This mesh was also used to contain the Ottawa sand located in the base of the permeation apparatus to prevent washout and destabilization of the soil sample.

Due to bleach contamination, the first 12 effluent samples of compacted sand column SP2 were rendered sterile, and could not be counted for bacterial concentrations. In sand column SP3, effluent samples 4, 5, and 6 were overgrown as the dilution series

utilized was too low for the observed breakthrough. Subsequently, these data points were omitted from the reported values and modeling and analyses.

5.3.3 Compacted silt column

The compacted silt columns were compacted at a target moisture content of 15.5% based on the optimum water content reported by Wong and Enns, (2005). A layer of filter paper was placed at the bottom of the soil column to limit silt migration from the soil sample.

During the course of the *E. coli* permeation of the columns, it was evident that significant bacterial contamination of the columns had occurred. An unknown bacterial species characterized by large, irregularly shaped colonies quickly outgrew any *E. coli* colonies, making colony counts difficult or impossible at high contamination levels (Figure 5.31). Colonies of this species also exhibited fluorescence, though it is quite possible that this may have been caused by *E. coli* cells incorporated into the colonies of the contaminating species. In an effort to control the growth of this contamination, modifications to the growth medium were tested. It was discovered that the contaminating species could outgrow the *E. coli* colonies in TSA plates containing 100 μg/ml streptomycin, Macconkey agar, membrane fecal coliform agar (M FC) without added Rosolic acid, and chrome *E. coli* agar. As the contaminant colonies appeared transparent and grey on the M FC agar while the *E. coli* colonies appeared dark blue, this allowed the identification of *E. coli* in mildly contaminated locations (Figure 5.32).

Because the effluent from column Silt R was heavily contaminated, *E. coli* counting could not be performed even on the M FC agar plates. Samples from this column were still collected and utilized for bromide analysis. The top surface of column Silt S was also heavily contaminated, and could not be accurately analyzed for colony concentrations.

5.3.4 Compacted 90 % sand / 10% silt columns

The compacted sand / silt columns were assembled in a similar manner and technique to those utilized by Lukacs *et al* (2007). The target moisture content was 8% to produce columns similar to their reported values. Similar to the compacted sand columns, the compacted 90 % sand / 10% silt columns had significantly higher flow rates than the values reported by Lukacs *et al* (2007), despite having similar material properties (Tables 5.7, 5.4 and 5.10). After permeating with *E. coli*, the flow rates of these columns dropped, and ultimately reached values approximately 2-3 times higher than those values reported by Lukacs *et al* (2007).

After *E. coli* permeation, it became evident that the columns for the current research experienced vastly different *E. coli* breakthrough curves compared to the columns of Lukacs *et al* (2007), despite having similar bromide breakthrough curves.

A possible explanation for these observed differences is a variation in the actual silt content of the columns, as it was observed that the silt tended to settle and stick to the edges of the mixing bowl used to prepare the moistened 90% sand / 10% silt mixture.

The columns used by Luckacs *et al* (2007) may therefore have contained less silt than the columns tested during this research. Another possible explanation is the presence of a preferential flow path created by displacing silt from the soil matrix by filling the column too quickly. This was observed in a preliminary test column after disassembly (Figure 5.33). If this was present within the columns analyzed by Lukacs *et al* (2007) this may have allowed the suspended *E. coli* cells a path through the column that would have minimizes access to the silt material.

As the initial pulse experiments were based on an expected full *E. coli* breakthrough of four pore volumes of flow, based upon the reported measurements of Lucaks *et a l* (2007), this proved to be too low of a permeation volume to observe full or steady state (stable effluent concentration) breakthrough. Consequently, column SSP3 was permeated with a pulse of 5 liters (approximately 17.5 PV) in an attempt to reach full or steady state breakthrough.

The contaminating colonies observed in the silt columns were also found in the 90% sand / 10% silt mixtures. The levels of contamination however, were not sufficient to impede colony counting during drop plate analysis with the TSA plates.

Table 5.1 - Freeze-fractured compacted clay column properties

Sample Label	CCA	CCB	CCC	CCD	average
Researchers	Scott & Nguyen	Scott & Nguyen	Lukacs et al	Lukacs et al	
Height (m)	0.067	0.073	0.081	0.085	0.077
Diameter (cm)	10.1	10.1	10.1	10.1	10.1
Weight of Sample (kg)	1.040	1.124	1.200	1.230	1.148
Moisture Content (%)	39.32	39.91	41.90	52.65	43.45
Volume (m^3)	538.92	587.77	647.83	676.66	612.80
Wet Density (Mg/M^3)	1.93	1.91	1.85	1.82	1.88
Dry Density (Mg/M^3)	1.39	1.37	1.31	1.19	1.31
Total Unit Weight (kN/m^3)	18.93	18.75	18.18	17.83	18.42
Dry Unit Weight (kN/m^3)	13.59	13.40	12.81	11.68	12.87
Specific Gravity	2.75	2.75	2.75	2.75	2.75
Void ratio (e)	0.985	1.013	1.106	1.310	1.104
Porosity	0.496	0.503	0.525	0.567	0.523
Volume of voids (ml)	267.48	295.73	340.25	383.74	321.80

Table 5.2 - Freeze-fractured normally consolidated clay column properties

Sample Label	NCCC	NCCD	NCCE	average
Researchers	Scott & Nguyen	Rosa et al	Rosa et al	
Height (m)	0.134	0.112	0.125	0.124
Diameter (cm)	10.1	10.1	10.1	10.1
Weight of Sample (kg)	1.786	1.562	1.730	1.692
Moisture Content (%)	48.07	50.15	50.78	49.67
Volume (m^3)	1074.88	894.47	1000.97	990.11
Wet Density (Mg/M^3)	1.66	1.75	1.73	1.71
Dry Density (Mg/M^3)	1.12	1.16	1.15	1.14
Total Unit Weight (kN/m^3)	16.30	17.13	16.95	16.79
Dry Unit Weight (kN/m^3)	11.01	11.41	11.24	11.22
Specific Gravity	2.75	2.75	2.75	2.75
Void ratio (e)	1.451	1.365	1.400	1.405
Porosity	0.592	0.577	0.583	0.584
Volume of voids (ml)	636.39	516.27	583.85	578.84

Table 5.3 - Compacted sand column properties

Sample Label Researchers	SnA Lukac et al	SnB Lukac et al	average
Height (m)	0.145	0.145	0.145
Diameter (cm)	10.1	10.1	10.1
Weight of Sample (kg)	2.251	2.129	2.190
Moisture Content (%)	9.90	9.36	9.63
Volume (m^3)	1161.13	1161.13	1161.13
Wet Density (Mg/M^3)	1.94	1.83	1.87
Dry Density (Mg/M^3)	1.76	1.68	1.72
Total Unit Weight (kN/m^3)	19.02	17.99	18.50
Dry Unit Weight (kN/m^3)	17.31	16.45	16.88
Specific Gravity	2.65	2.65	2.65
Void ratio (e)	0.502	0.581	0.541
Porosity	0.334	0.367	0.351
Volume of voids (ml)	388.18	426.49	407.34

Table 5.4 - Compacted 90% sand / 10% silt column properties

Sample Label Researchers	SSC Lukacs et al	SSD Lukacs et al	average
Height (m)	0.135	0.135	0.135
Diameter (cm)	10.1	10.1	10.1
Weight of Sample (kg)	2.166	2.159	2.163
Moisture Content (%)	8.30	7.94	8.12
Volume (m^3)	1081.05	1081.05	1081.05
Wet Density (Mg/M^3)	2.00	2.00	2.00
Dry Density (Mg/M^3)	1.85	1.85	1.85
Total Unit Weight (kN/m^3)	19.66	19.59	19.63
Dry Unit Weight (kN/m^3)	18.15	18.15	18.15
Specific Gravity	2.66	2.66	2.66
Void ratio (e)	0.438	0.438	0.438
Porosity	0.304	0.304	0.304
Volume of voids (ml)	329.17	329.03	329.10

Table 5.5 - Freundlich sorption isotherm parameters for the tested soils

	Sand	Silt	sand/silt	Com. Clay	Cons. Clay
K	1235.5	7566.7	n/a	5.12×10^{7}	5.12×10^{7}
N	0.554	0.617	n/a	0.273	0.273
R	3.83	59.87	9.05	287.85	224.80

Com. Clay – Freeze-fractured compacted clay columns
Cons. Clay – Freeze-fractured consolidated clay columns

Table 5.6 - Langmuir sorption isotherm parameters for the tested soils

	Sand	Silt	sand/silt	Com. Clay	Cons.Clay
K_L	5.09×10^{-6}	8.40×10^{-8}	n/a	2.59×10^{-7}	2.59×10^{-7}
M_L	$2.91 \times 10^{+6}$	$5.34 \times 10^{+8}$	n/a	$9.87 \times 10^{+9}$	$9.87 \times 10^{+9}$
R	1.03	81.05	9.03	498.71	389.41

Com. Clay – Freeze-fractured compacted clay columns
Cons. Clay – Freeze-fractured consolidated clay columns

Table 5.7 - Average hydraulic conductivity measurements for the experimental columns

Column	Average Hydraulic Conductivity (cm/s)
CCA	2.513×10^{-6}
CCB	3.288×10^{-6}
CCC	9.298×10^{-6}
CCD	5.481×10^{-6}
NCC	4.357×10^{-6}
NCD	1.810×10^{-5}
NCE	1.150×10^{-5}
SnA	1.176×10^{-3}
SnB	5.115×10^{-3}
SSC	2.022×10^{-4}
SSD	1.841×10^{-4}
NC Control	5.183×10^{-7}
CC Control	2.767×10^{-8}
Silt R	1.630×10^{-6}
Silt S	1.627×10^{-6}
SP1	4.442×10^{-3}
SP2	5.712×10^{-3}
SP3	4.929×10^{-3}
SSP1	3.792×10^{-4}
SSP2	3.461×10^{-4}
SSP3	4.654×10^{-4}

Table 5.8 - Intact clay control column properties

Sample	NCC control	CC Control
Researchers	Rosa and Burdenuk	Rosa and Burdenuk
Type	Normally Consolidated	Compacted Clay
Height (m)	0.111	0.098
Diameter (cm)	10.1	10.1
Weight of Sample (kg)	1.429	1.440
Moisture Content (%)	65.90	37.80
Volume (m^3)	884.86	784.76
Wet Density (Mg/M^3)	1.61	1.84
Dry Density (Mg/M^3)	0.97	1.33
Total Unit Weight (kN/m^3)	15.84	18.00
Dry Unit Weight (kN/m^3)	9.55	13.07
Specific Gravity	2.75	2.75
Void ratio (e)	1.825	1.065
Porosity	0.646	0.516
Volume of voids (ml)	571.66	404.69

Table 5.9 - Current sand column properties

Sand columns	SP1	SP2	SP3	average
Researchers	Burdenuk	Burdenuk	Burdenuk	
Height (m)	0.122	0.123	0.135	0.127
Diameter (cm)	10.1	10.1	10.1	10.1
Weight of Sample (kg)	1.907	1.911	2.052	1.96
Moisture Content (%)	8.00	9.10	6.80	7.97
Volume (m^3)	976.95	984.96	1081.05	1014.32
Wet Density (Mg/M^3)	1.95	1.94	1.90	1.93
Dry Density (Mg/M^3)	1.81	1.78	1.78	1.79
Total Unit Weight (kN/m^3)	19.15	19.03	18.62	18.93
Dry Unit Weight (kN/m^3)	17.73	17.45	17.43	17.54
Specific Gravity	2.65	2.65	2.65	2.65
Void ratio (e)	0.466	0.490	0.491	0.482
Porosity	0.318	0.329	0.329	0.325
Volume of voids (ml)	310.53	323.94	356.19	330.22

Table 5.10 - Current 90% sand / 10% silt column properties

Sand columns Researchers	SSP1 Burdenuk	SSP2 Burdenuk	SSP3 Burdenuk	Average
Height (m)	0.133	0.113	0.120	0.122
Diameter (cm)	10.1	10.1	10.1	10.1
Weight of Sample (kg)	2.139	1.805	1.964	1.969
Moisture Content (%)	7.35	7.35	8.17	7.62
Volume (m^3)	1065.04	904.88	960.93	976.95
Wet Density (Mg/M^3)	2.01	2.00	2.04	2.02
Dry Density (Mg/M^3)	1.87	1.86	1.89	1.87
Total Unit Weight (kN/m^3)	19.70	19.57	20.05	19.77
Dry Unit Weight (kN/m^3)	18.35	18.23	18.53	18.37
Specific Gravity	2.66	2.66	2.66	2.66
Void ratio (e)	0.422	0.432	0.408	0.42
Porosity	0.297	0.302	0.290	0.30
Volume of voids (ml)	316.06	272.84	278.49	289.13

Table 5.11 - Compacted silt column properties

Silt columns Researchers	Silt S Burdenuk	Silt R Burdenuk	average
Height (m)	0.102	0.097	0.100
Diameter (cm)	10.1	10.1	10.1
Weight of Sample (kg)	1.755	1.674	1.714
Moisture Content (%)	15.5	15.1	15.3
Volume (m^3)	816.79	776.76	796.78
Wet Density (Mg/M^3)	2.15	2.15	2.15
Dry Density (Mg/M^3)	1.86	1.87	1.87
Total Unit Weight (kN/m^3)	21.07	21.14	21.10
Dry Unit Weight (kN/m^3)	18.24	18.36	18.30
Specific Gravity	2.70	2.70	2.70
Void ratio (e)	0.452	0.442	0.447
Porosity	0.311	0.307	0.309
Volume of voids (ml)	254.18	238.25	246.22

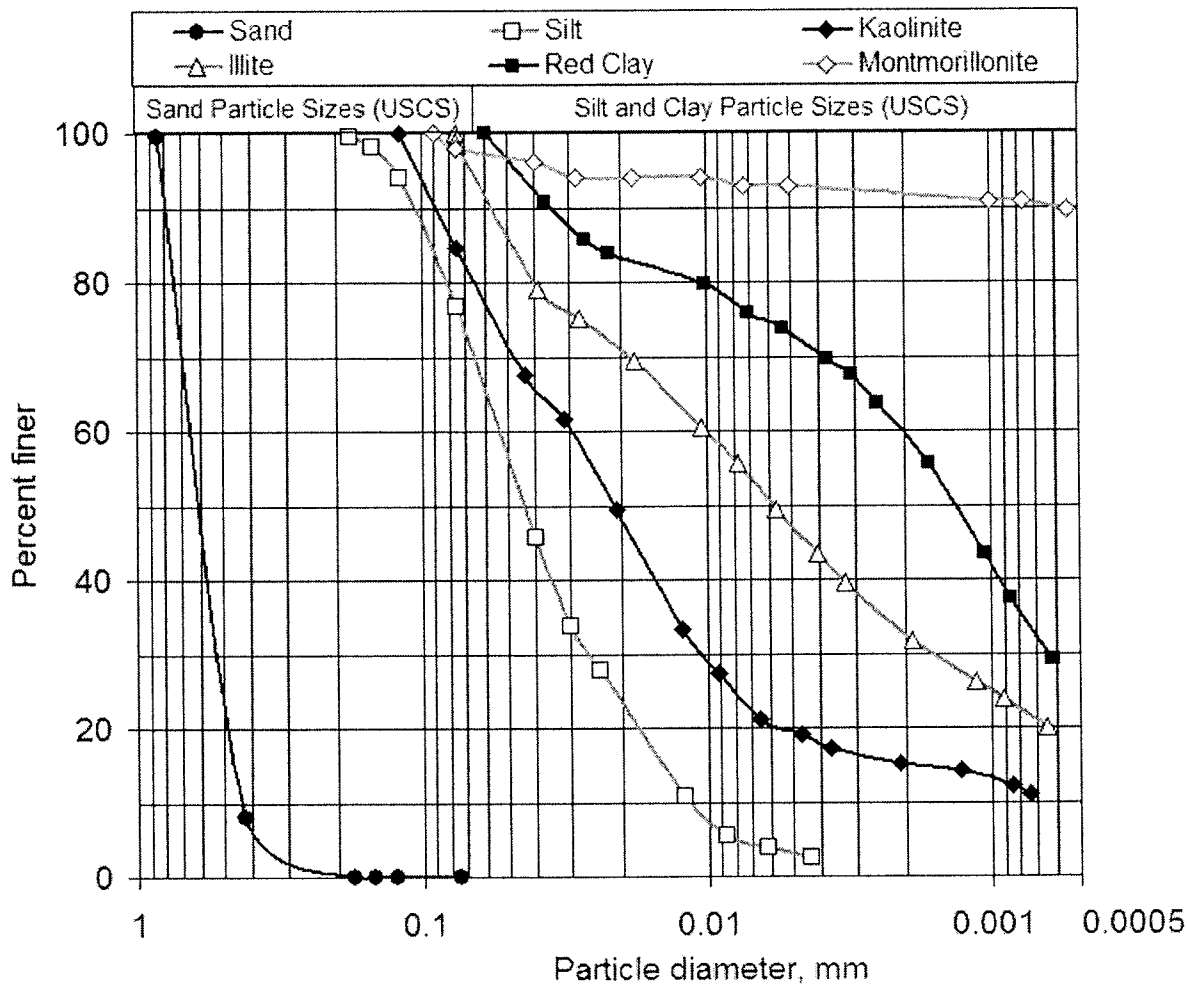

Figure 5.1 - Grain size distribution of soils tested during the batch sorption experiments. (Rosa, 2007)

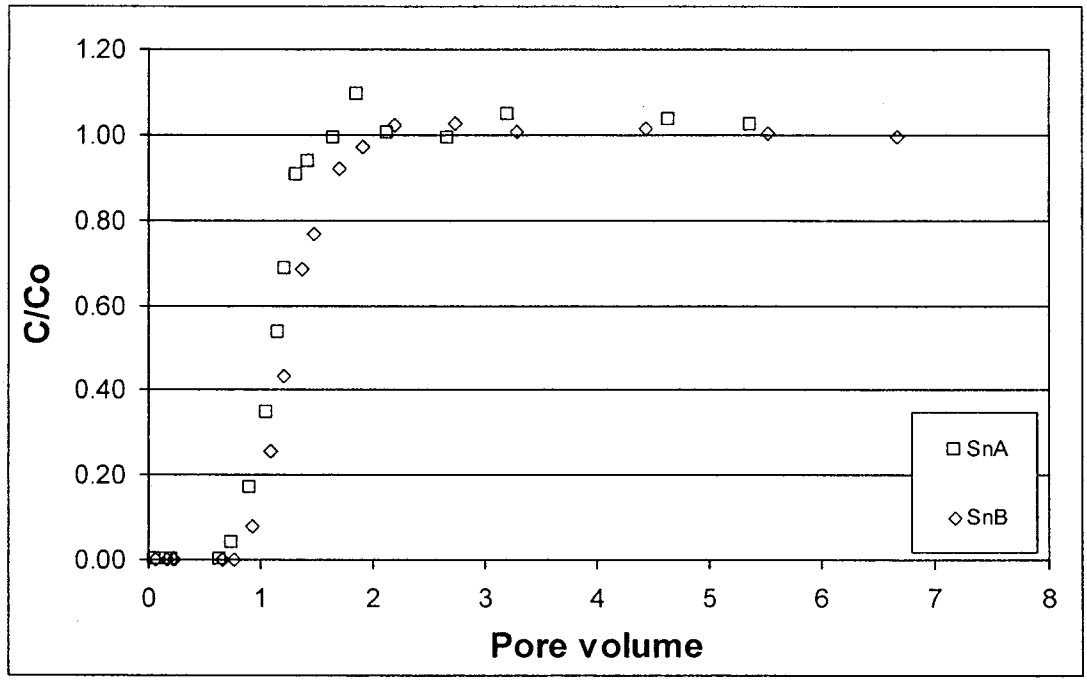

Figure 5.2 – Measured bromide breakthrough curves for the compacted sand columns collected during the previous experiments.

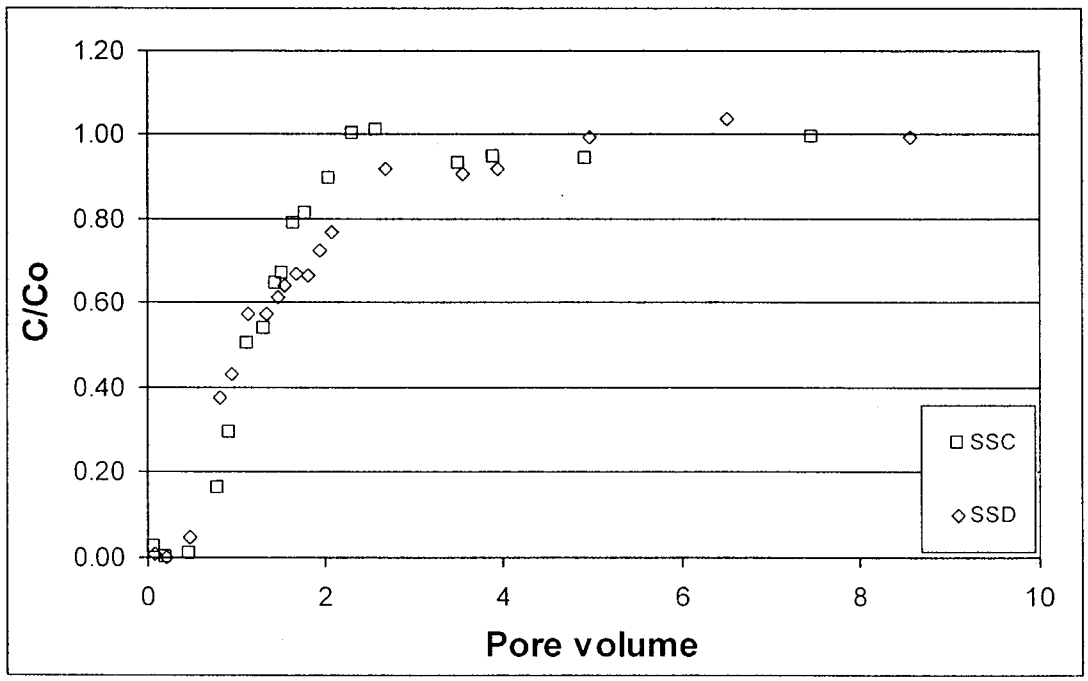

Figure 5.3 – Measured bromide breakthrough curves for the compacted 90% sand 10% silt mixed columns collected during the previous experiments.

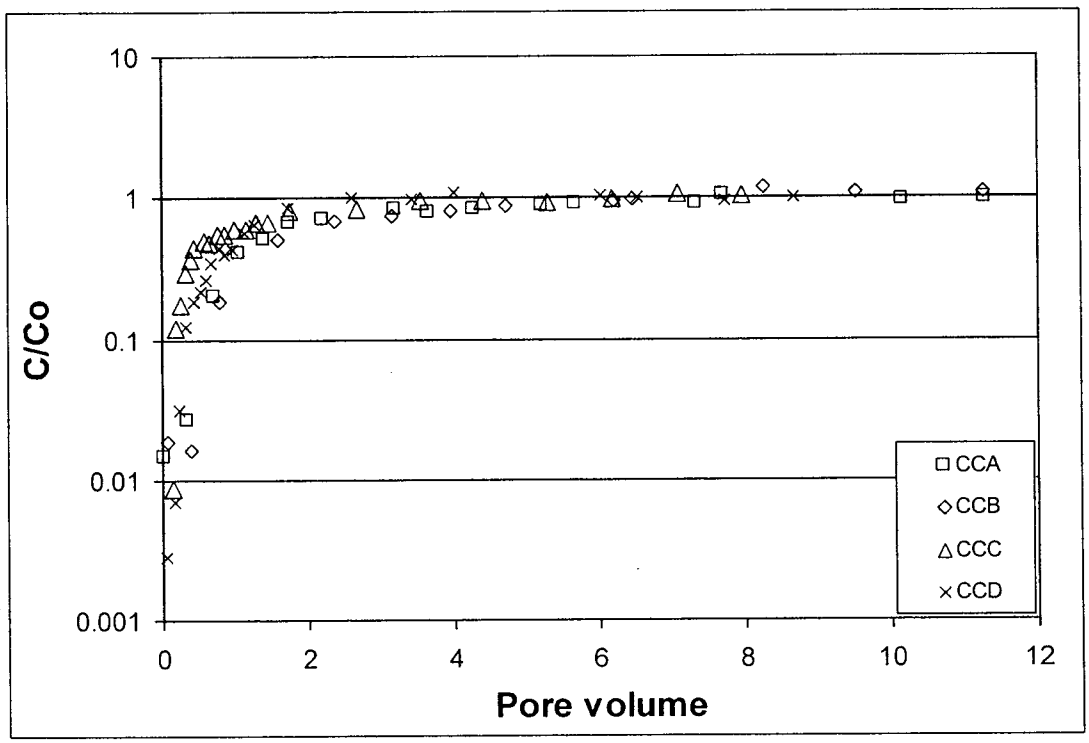

Figure 5.4 - Measured bromide breakthrough curves for the freeze-fractured compacted clay columns collected during the previous experiments.

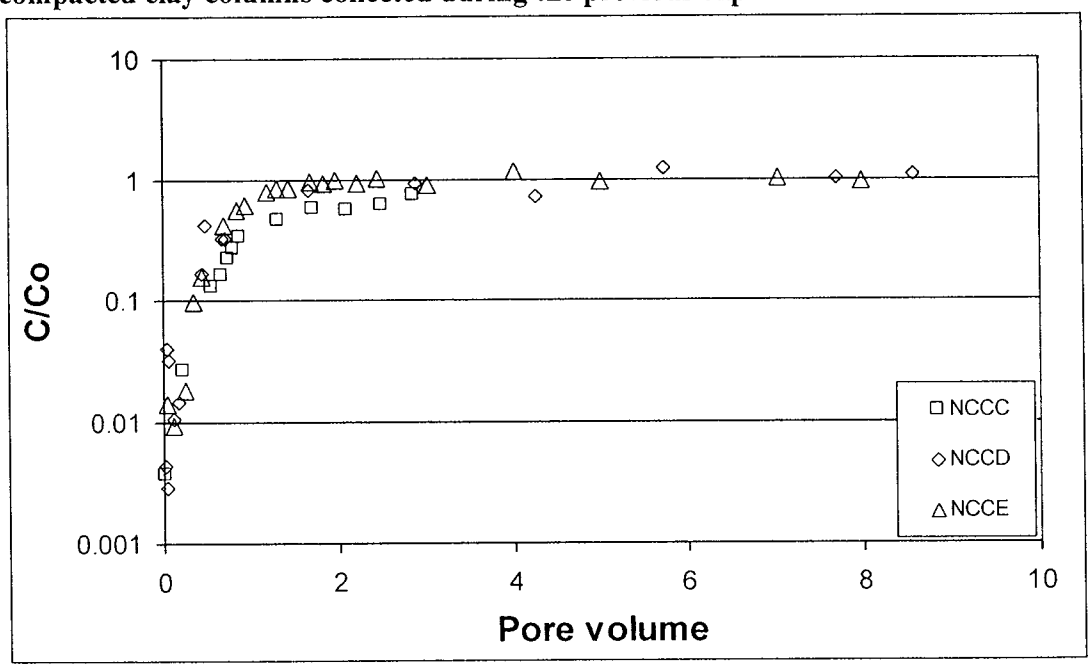

Figure 5.5 - Measured bromide breakthrough curves for the freeze-fractured normally consolidated clay columns collected during the previous experiments.

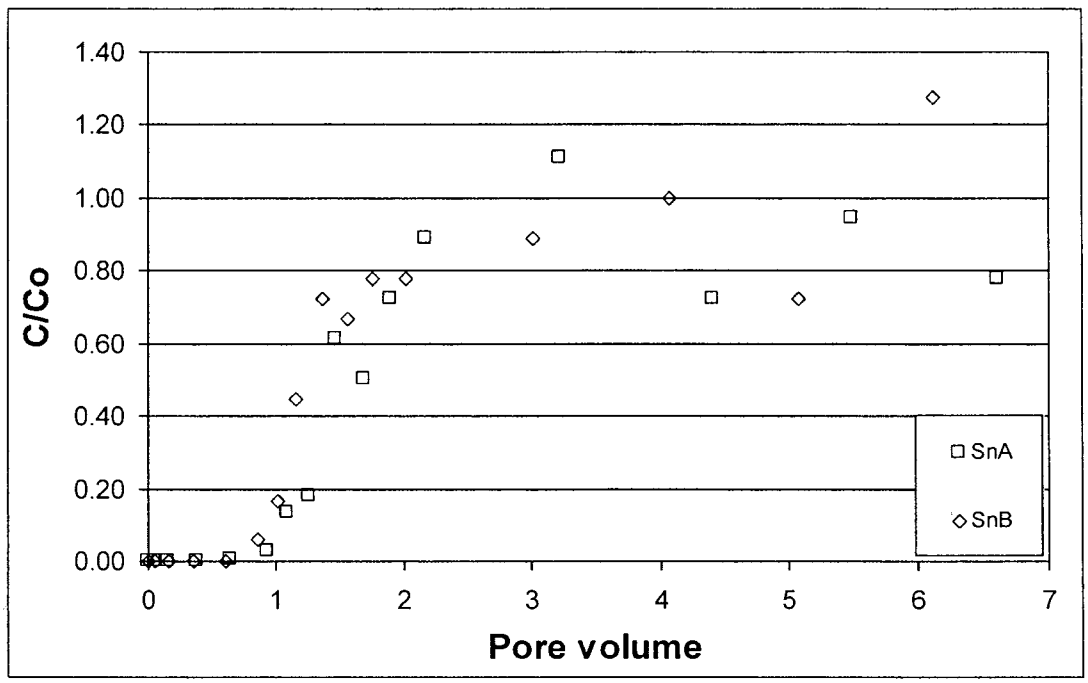

Figure 5.6 - Measured *E. coli* breakthrough curves for the compacted sand columns collected during the previous experiments.

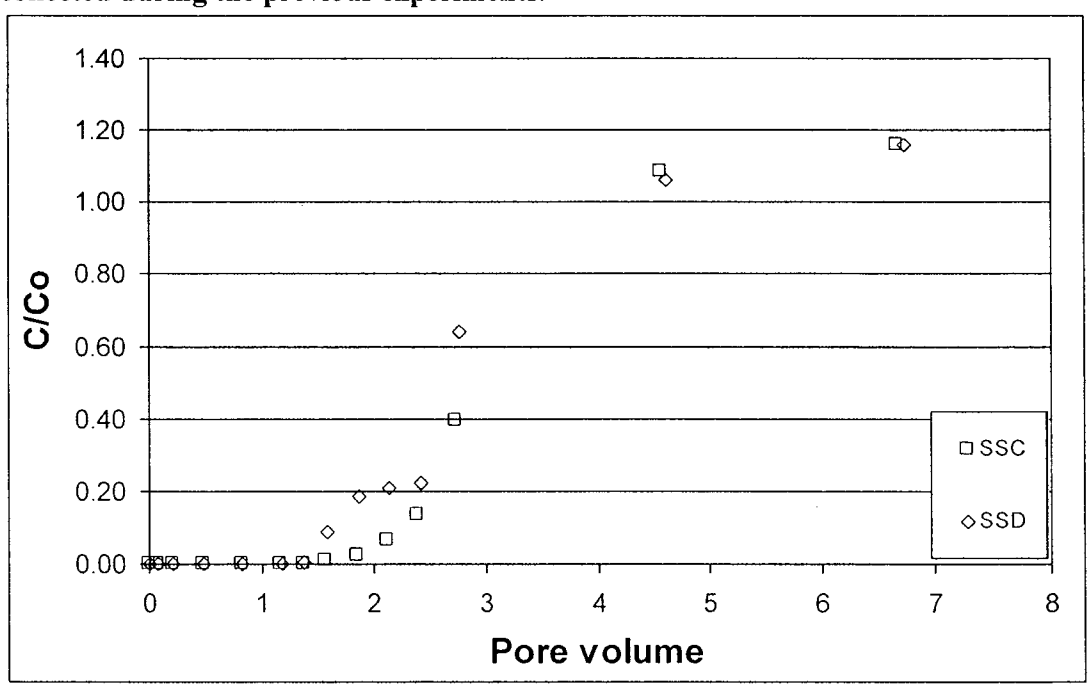

Figure 5.7 - Measured *E. coli* breakthrough curves for the compacted 90% sand / 10% silt columns collected during the previous experiments.

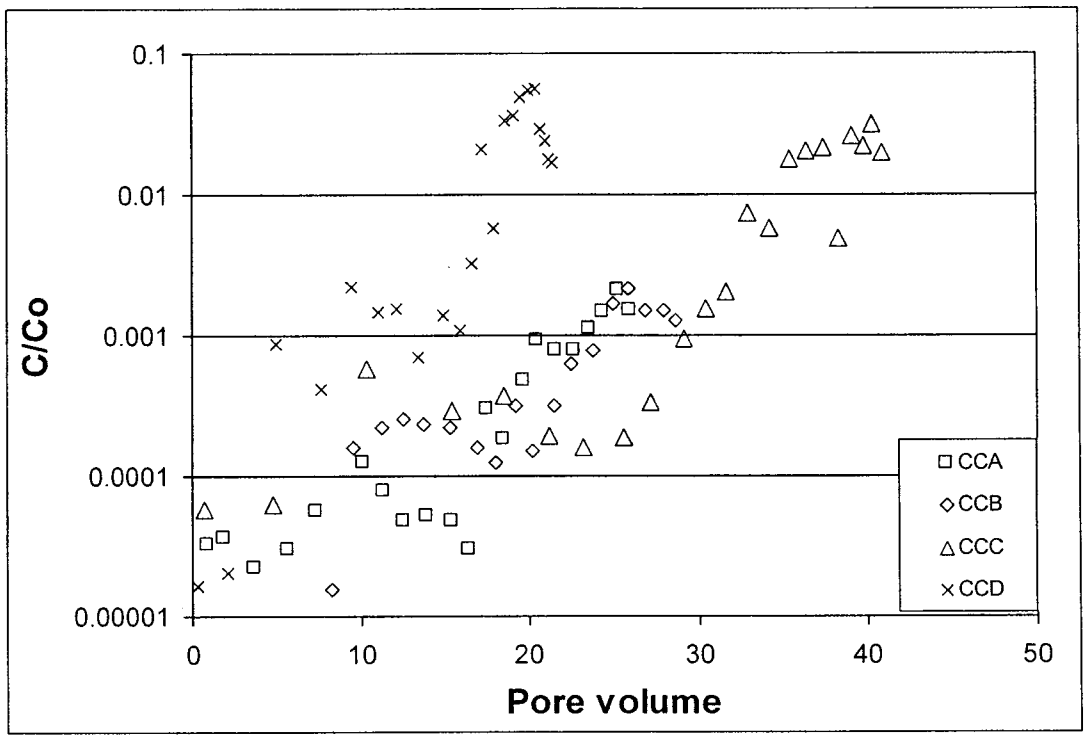

Figure 5.8 - Measured *E. coli* breakthrough curves for the freeze-fractured compacted clay columns collected during the previous experiments.

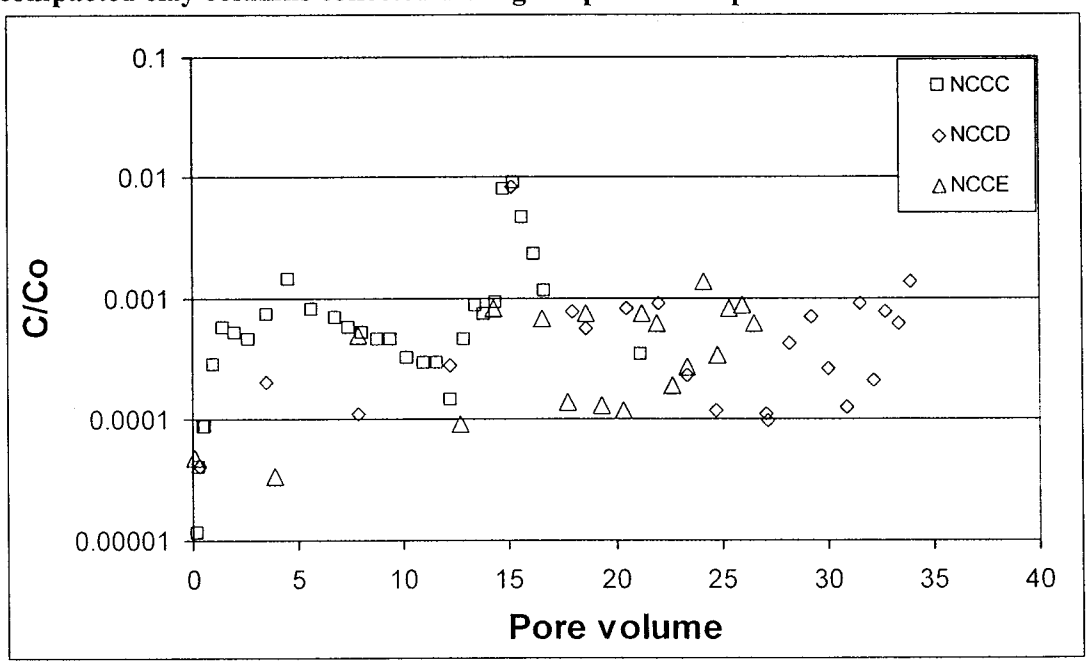

Figure 5.9 – Measured *E. coli* breakthrough curves for the freeze-fractured normally consolidated clay columns collected during the previous experiments.

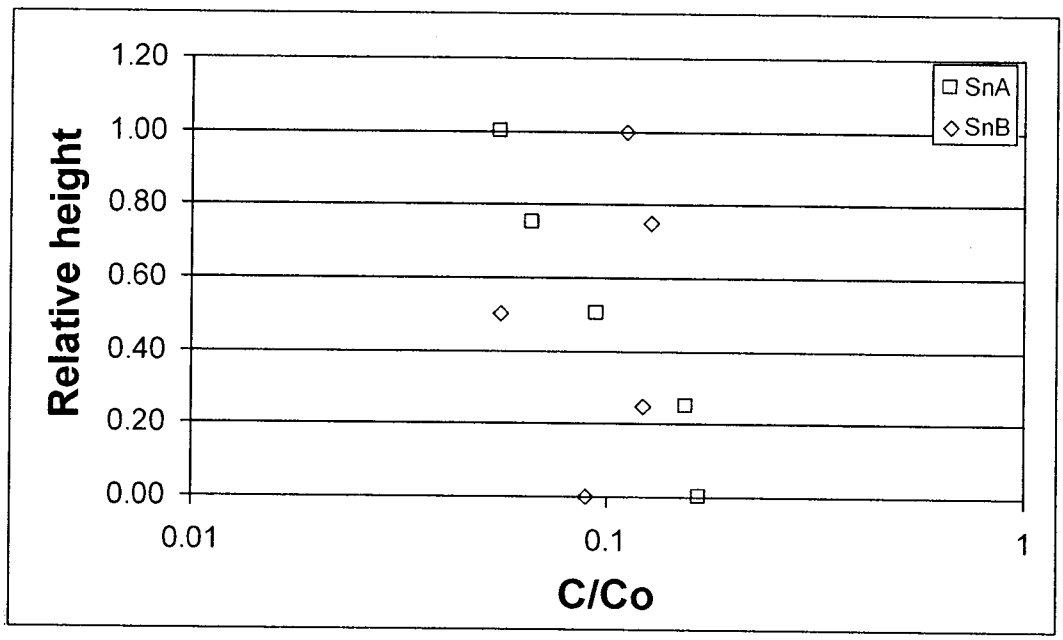

Figure 5.10 - Measured *E. coli* distribution profiles for the compacted sand columns collected during the previous experiments.

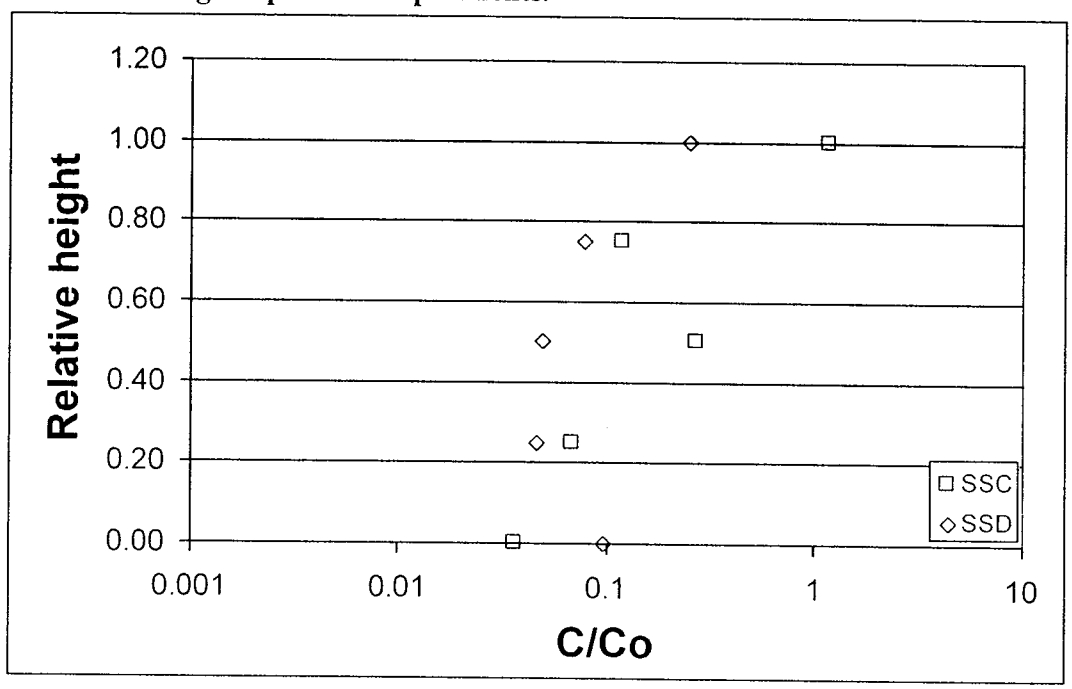

Figure 5.11 - Measured *E. coli* distribution profiles for the compacted 90% sand / 10% silt columns collected during the previous experiments.

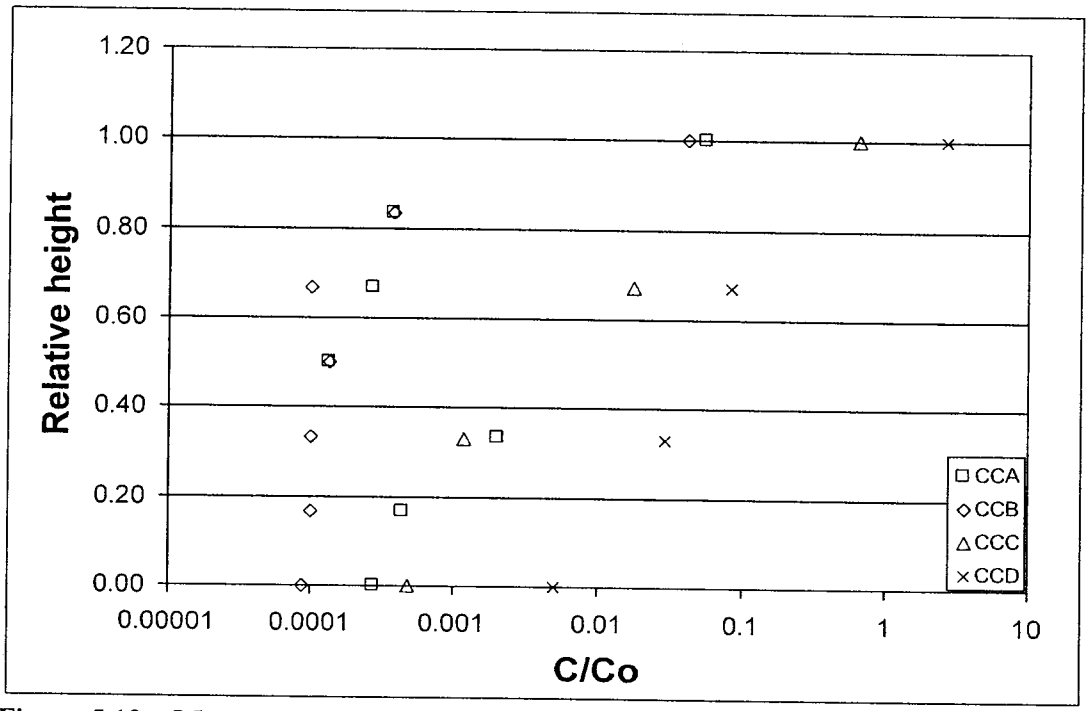

Figure 5.12 – Measured *E. coli* distribution profiles for the freeze-fractured compacted clay columns following permeation.

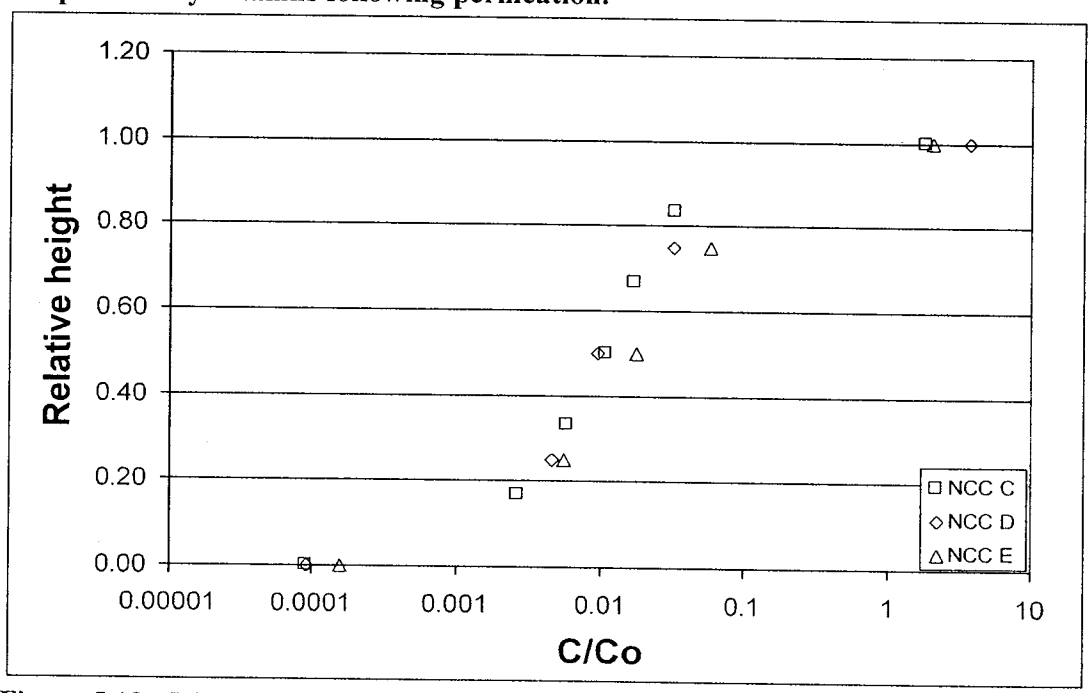

Figure 5.13 - Measured *E. coli* distribution profiles for the freeze-fractured normally consolidated clay columns collected during the previous experiments.

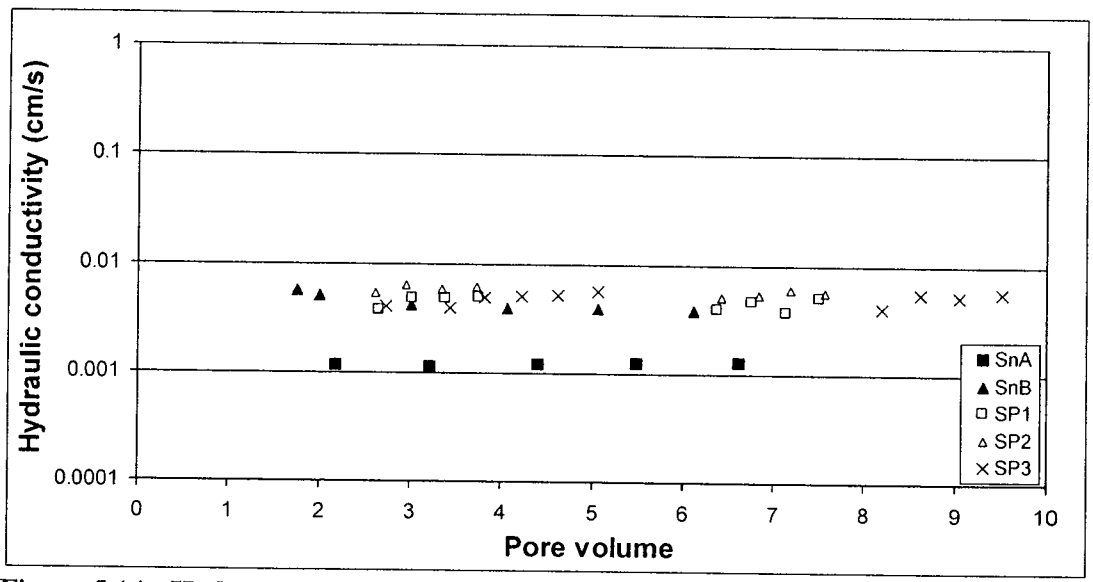

Figure 5.14 - Hydraulic conductivity measurements of the compacted sand columns.

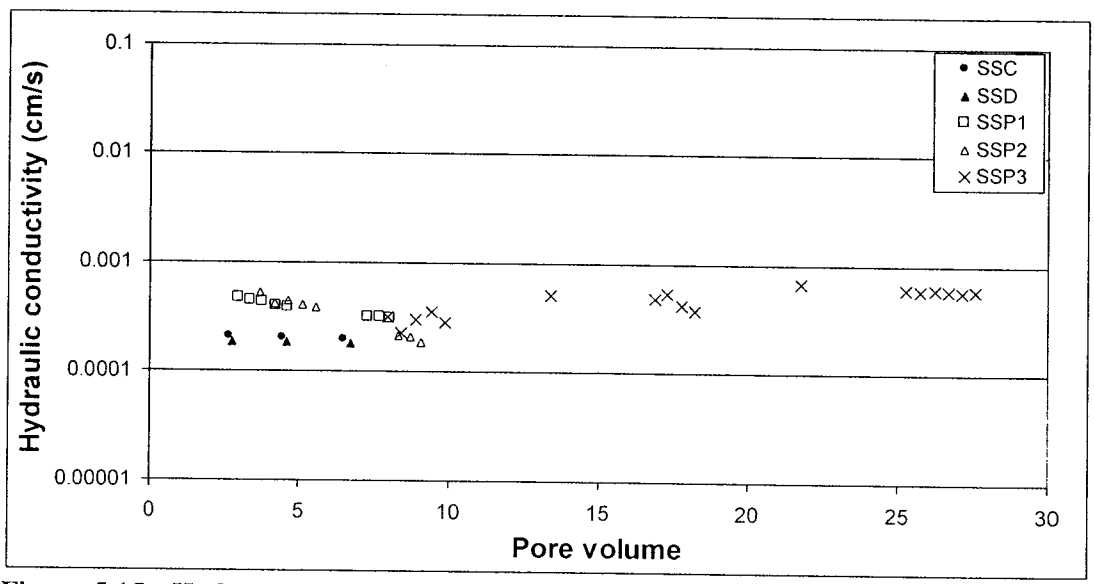

Figure 5.15 - Hydraulic conductivity measurements of the compacted 90% sand / 10% silt columns.

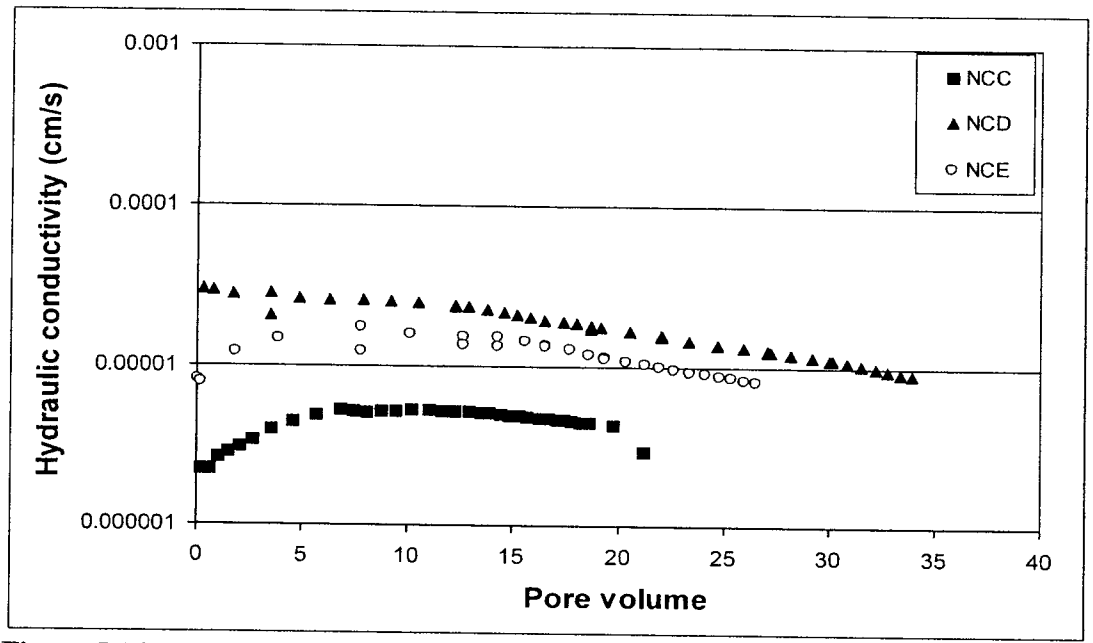

Figure 5.16 - Hydraulic conductivity measurements of freeze-fractured normally consolidated clay columns.

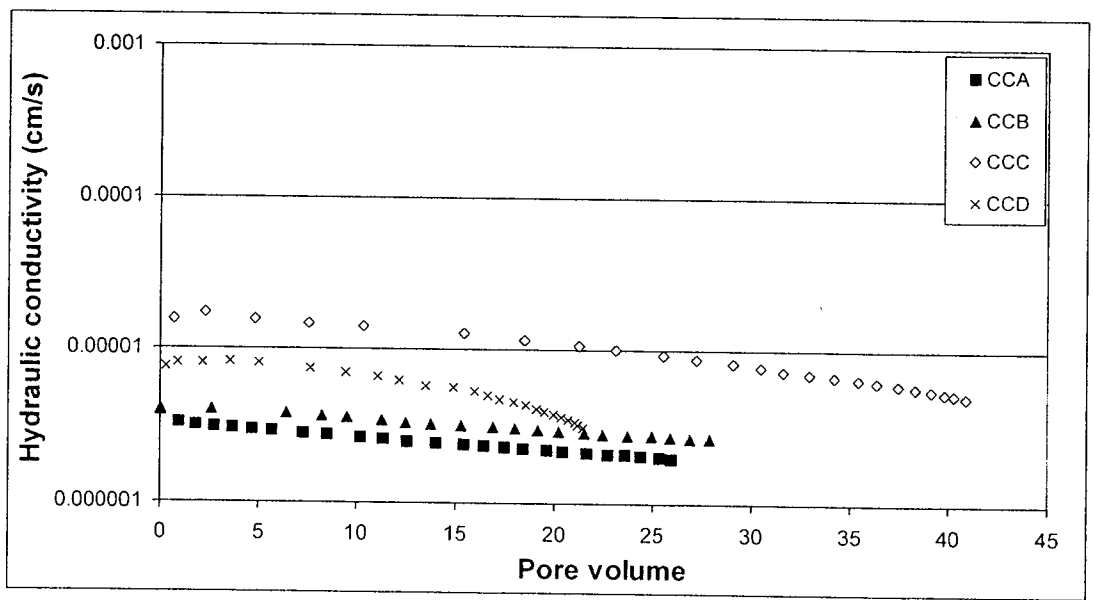

Figure 5.17 - Hydraulic conductivity measurements of freeze-fractured compacted clay columns.

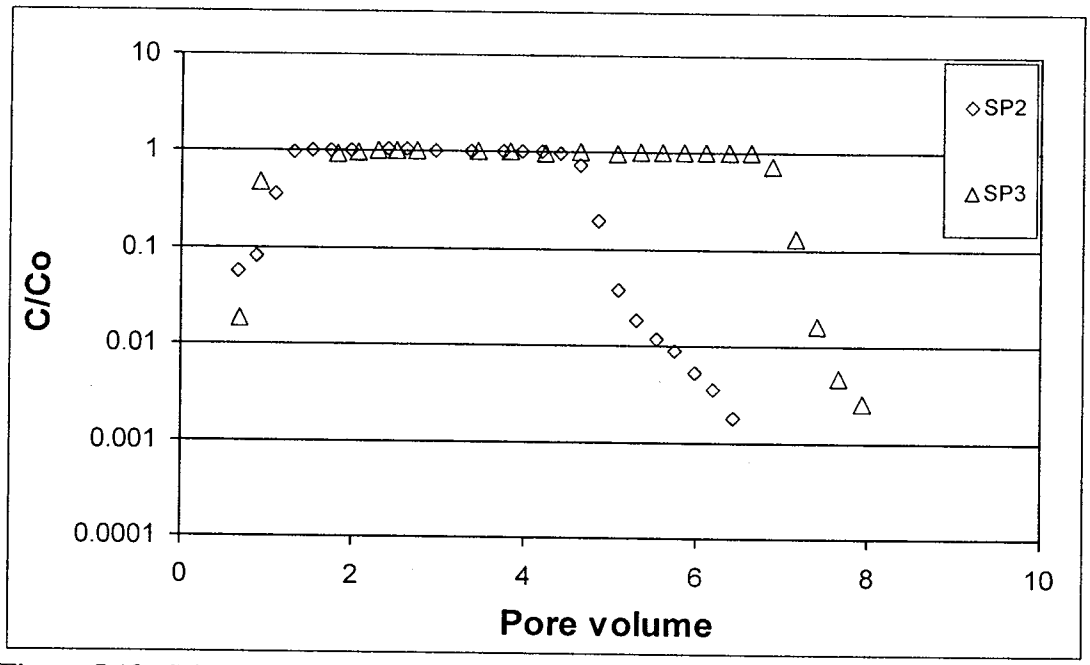

Figure 5.18 - Measured bromide breakthrough curves for the compacted sand pulse experiments conducted during the course of this study.

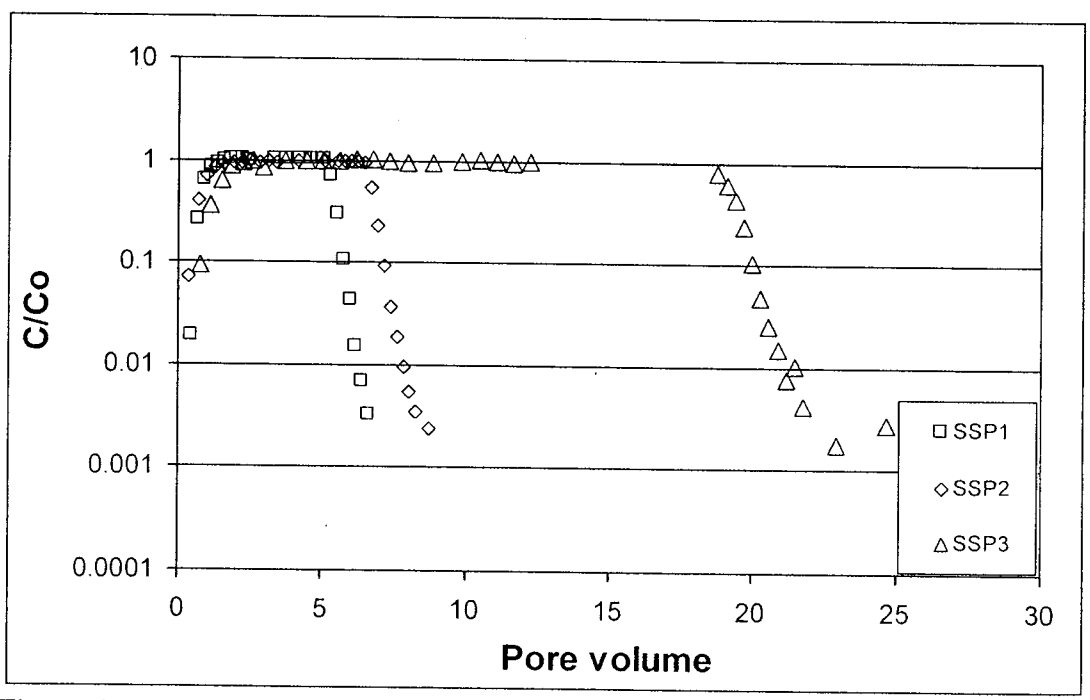

Figure 5.19 - Measured bromide breakthrough curves for the compacted 90% sand / 10% silt pulse experiments conducted during the course of this study.

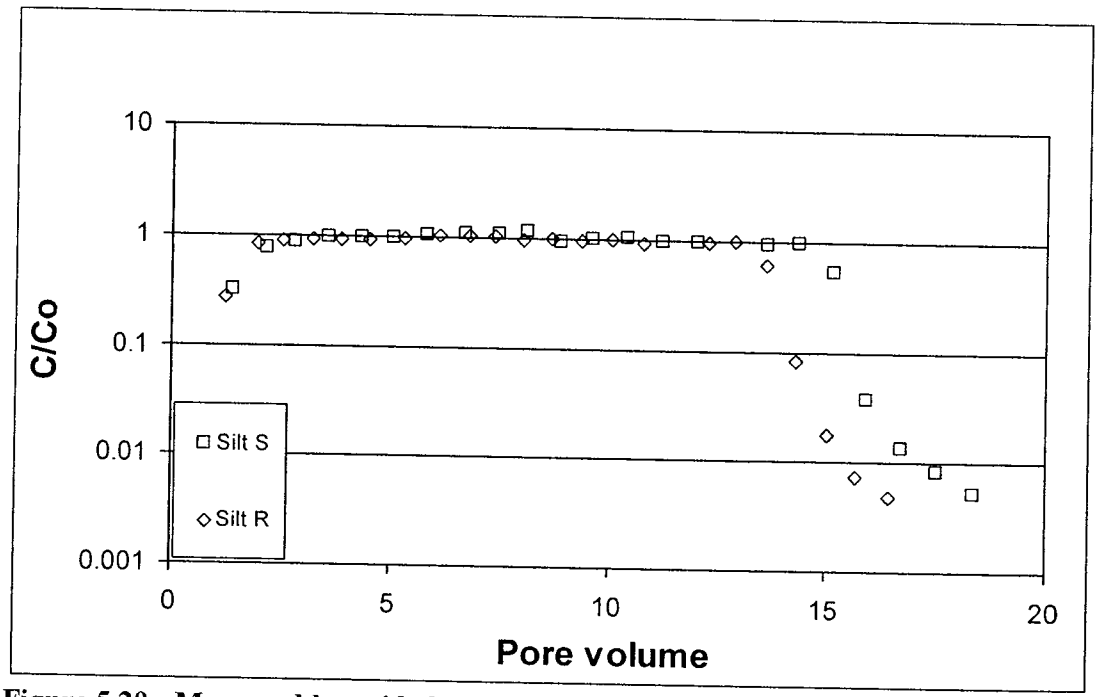

Figure 5.20 - Measured bromide breakthrough curves for the silt column experiments conducted during the course of this study.

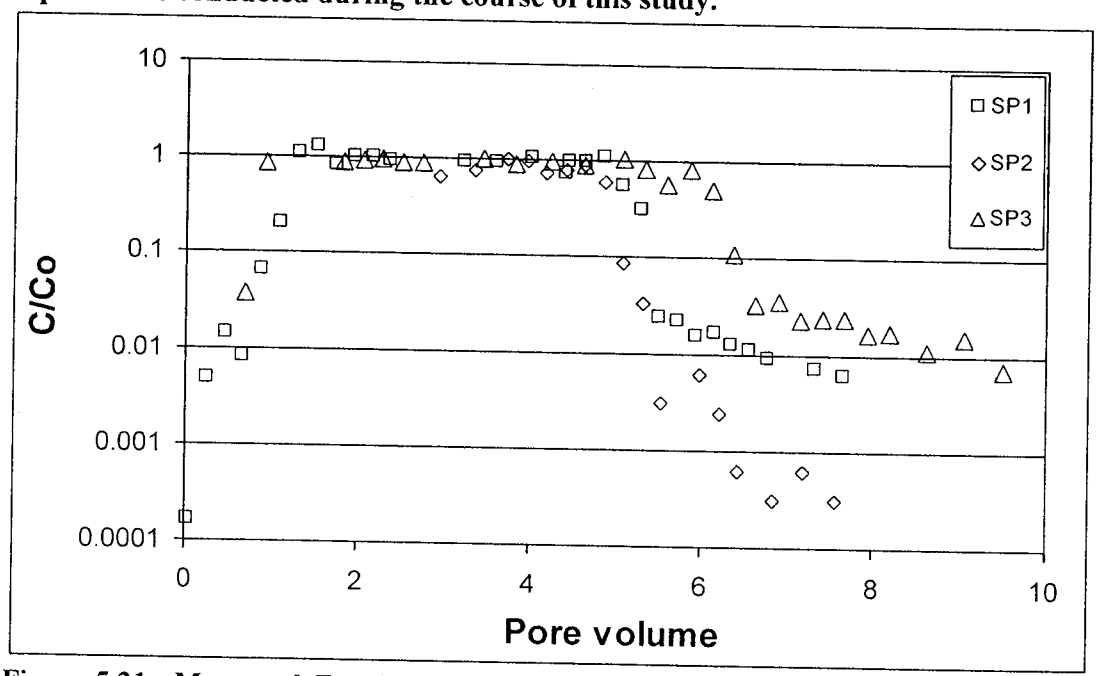

Figure 5.21 - Measured *E. coli* breakthrough curves for the compacted sand pulse experiments conducted during the course of this study.

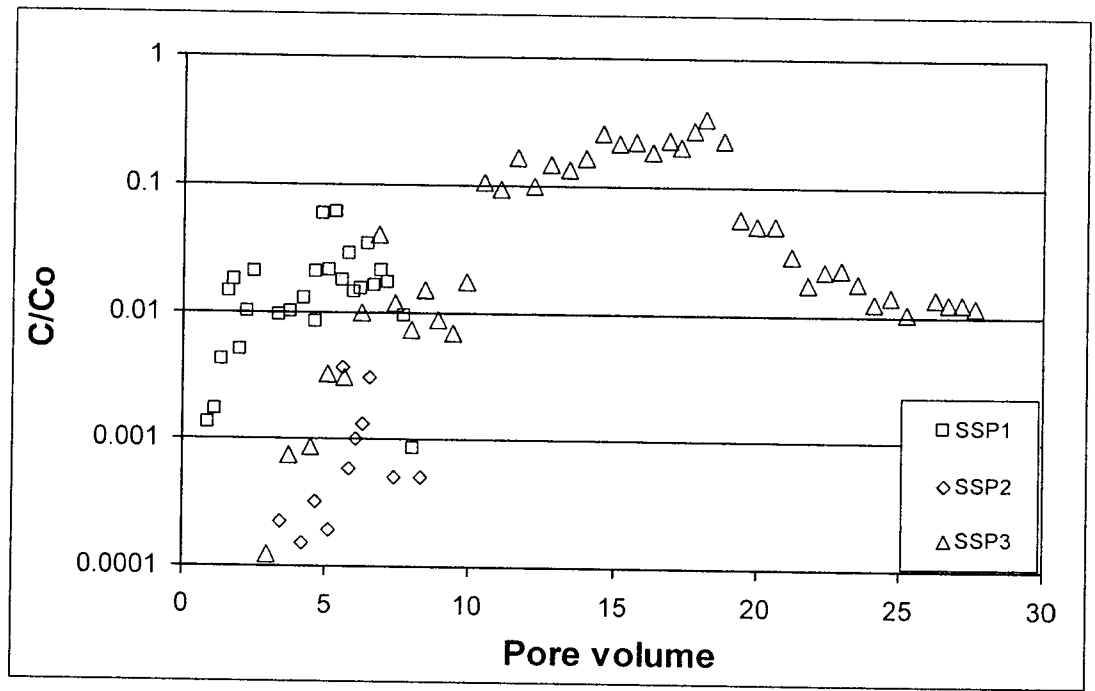

Figure 5.22 - Measured *E. coli* breakthrough curves for the compacted 90% sand / 10% silt pulse experiments conducted during the course of this study.

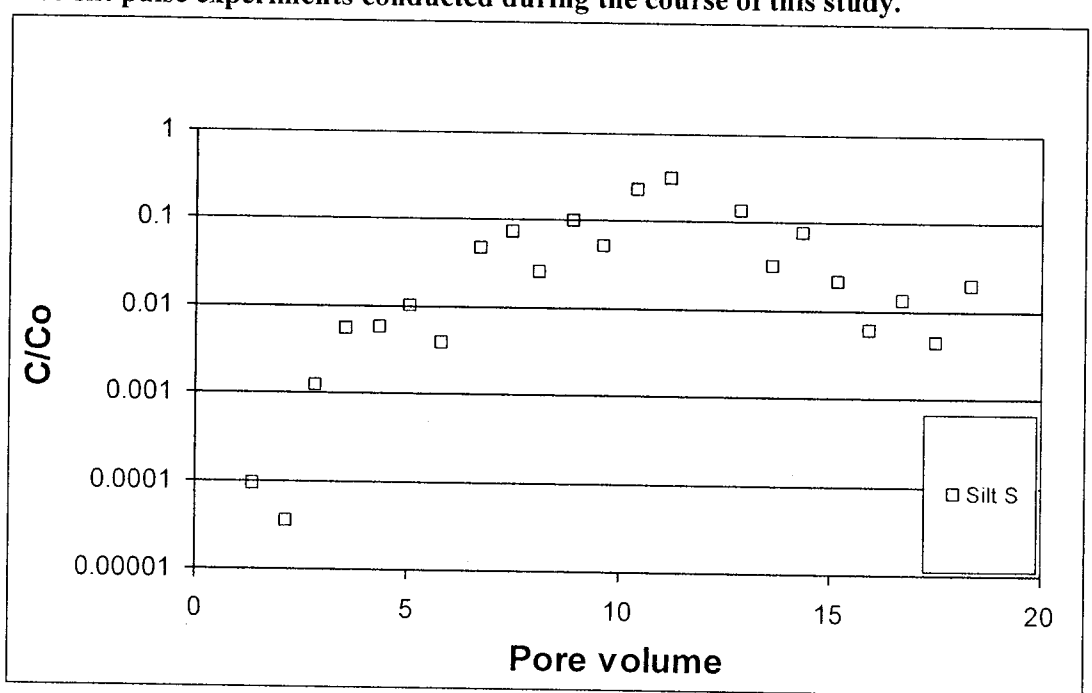

Figure 5.23 - Measured *E. coli* breakthrough curves for the silt column experiment conducted during the course of this study.

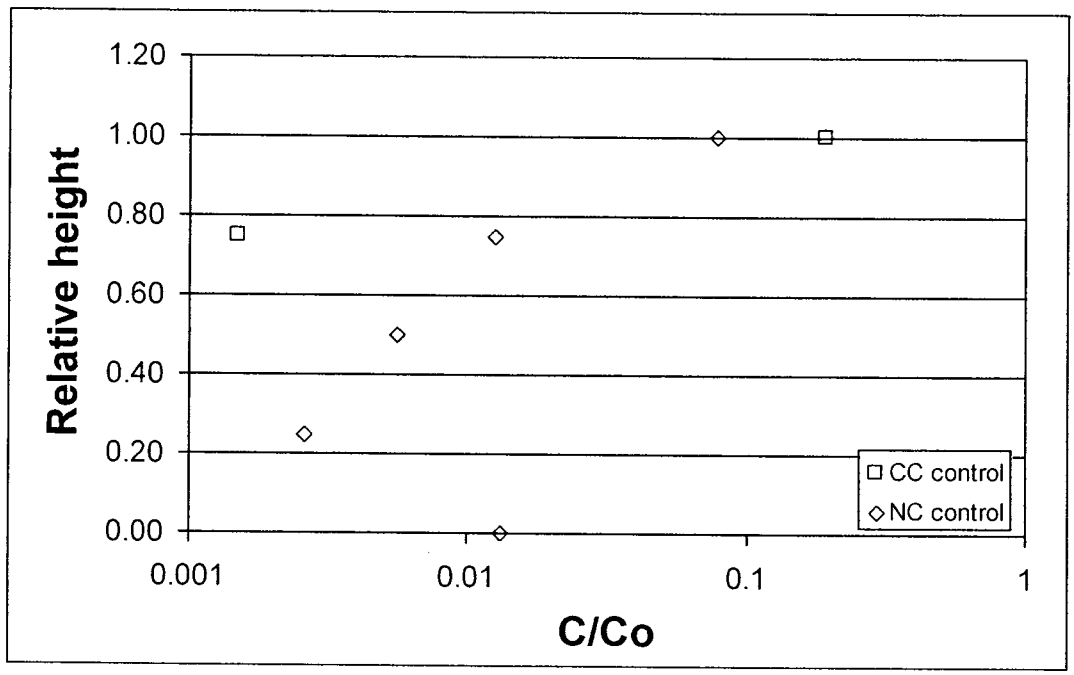

Figure 5.24 - Measured *E. coli* distribution profile for the intact clay control columns. Compacted control (CC) Normally consolidated control (NC).

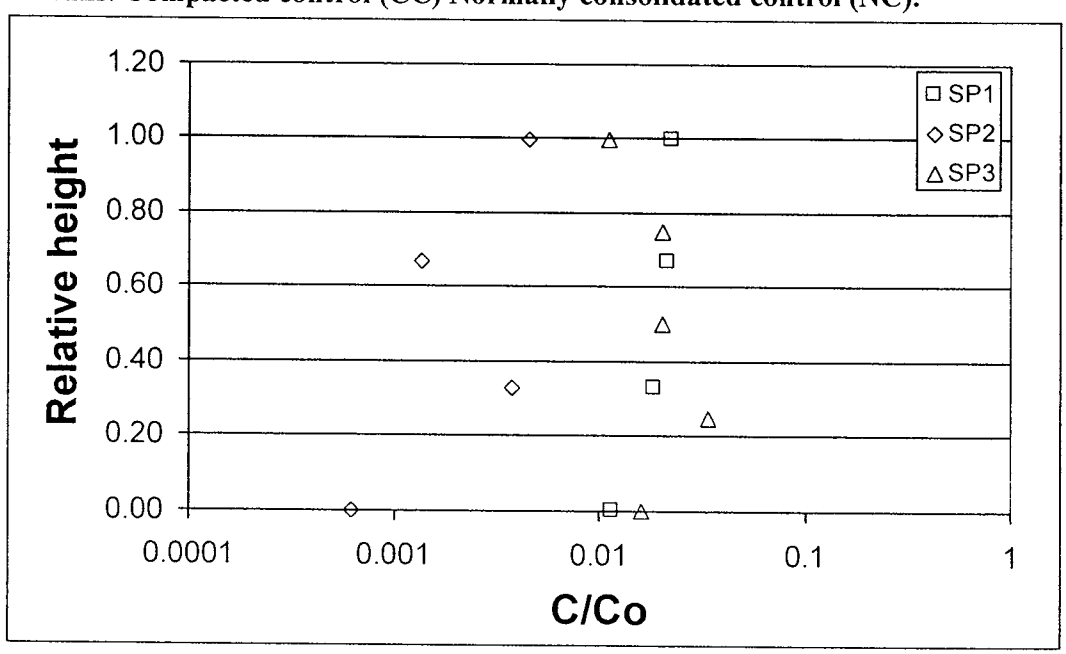

Figure 5.25 – Measured *E. coli* distribution profile for compacted sand pulse columns.

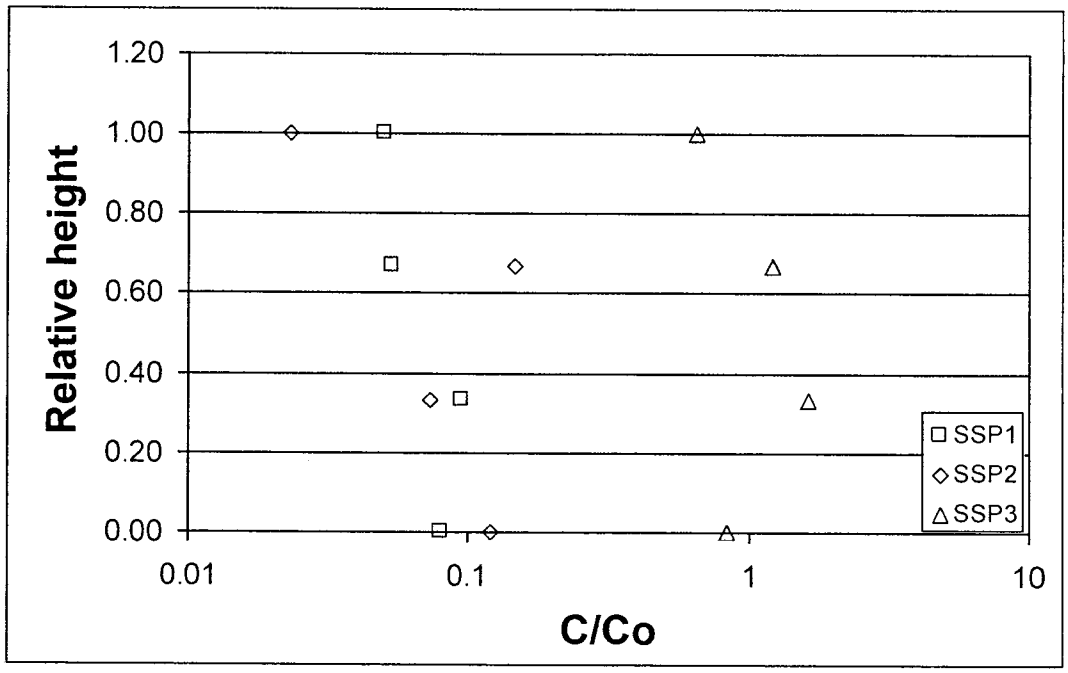

Figure 5.26 – Measured *E. coli* distribution profiles for the 90% sand / 10% silt pulse columns.

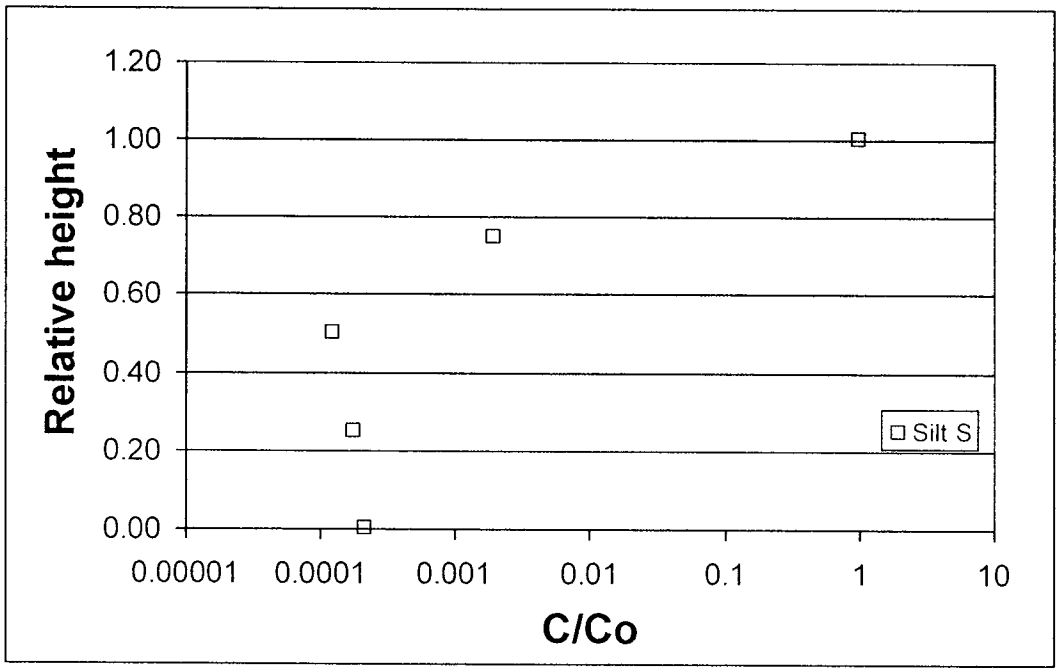

Figure 5.27 – Measured *E. coli* distribution profile for the compacted silt pulse column.

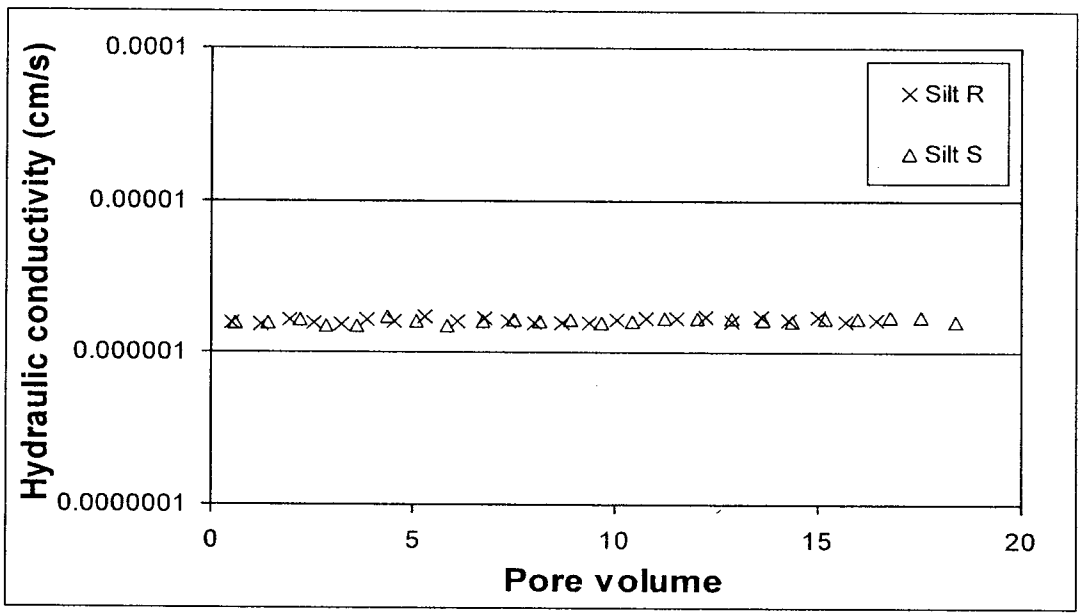

Figure 5.28 - Hydraulic conductivity measurements of compacted silt columns.

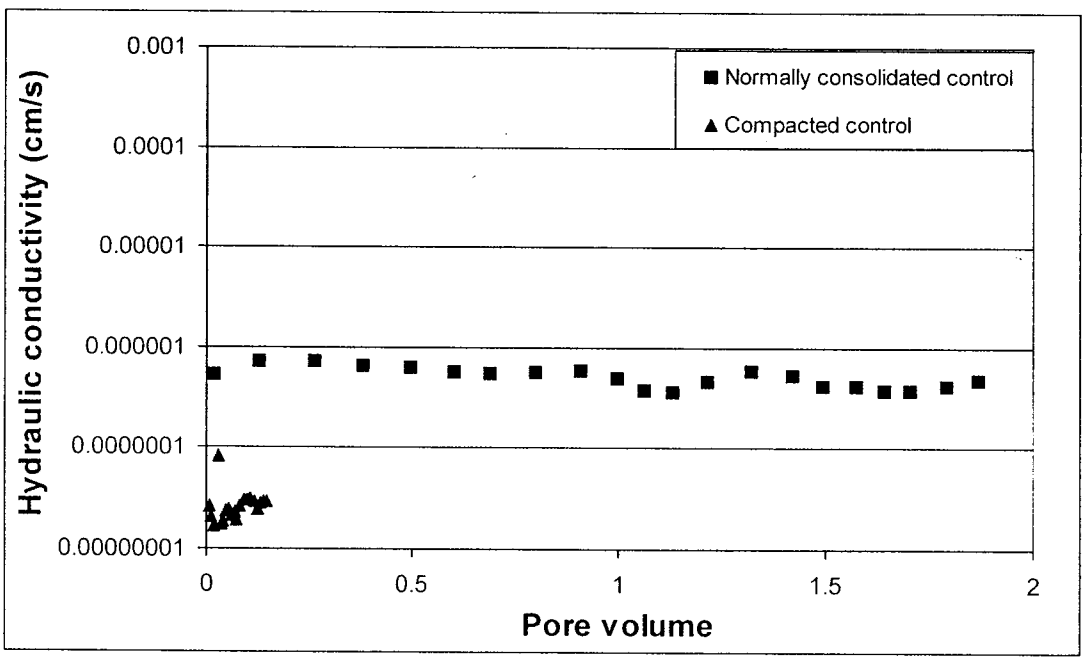

Figure 5.29 - Hydraulic conductivity measurements of control clay columns.

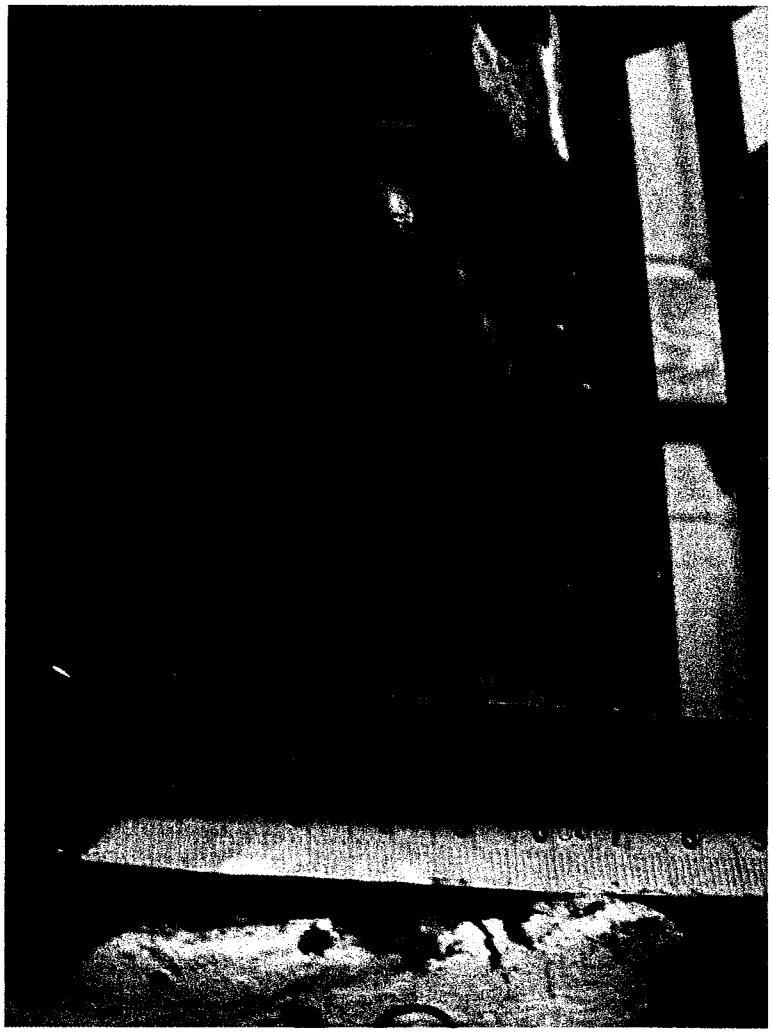

Figure 5.30 - Appearance of void spaces in the lithium grease used to prevent interface flow in the control clay columns.

Figure 5.31 - Contamination in effluent of silt columns. Column silt R (left) contained minimal contamination, while column Silt S (right) could not be analyzed for *E. coli* colonies due to extensive contamination.

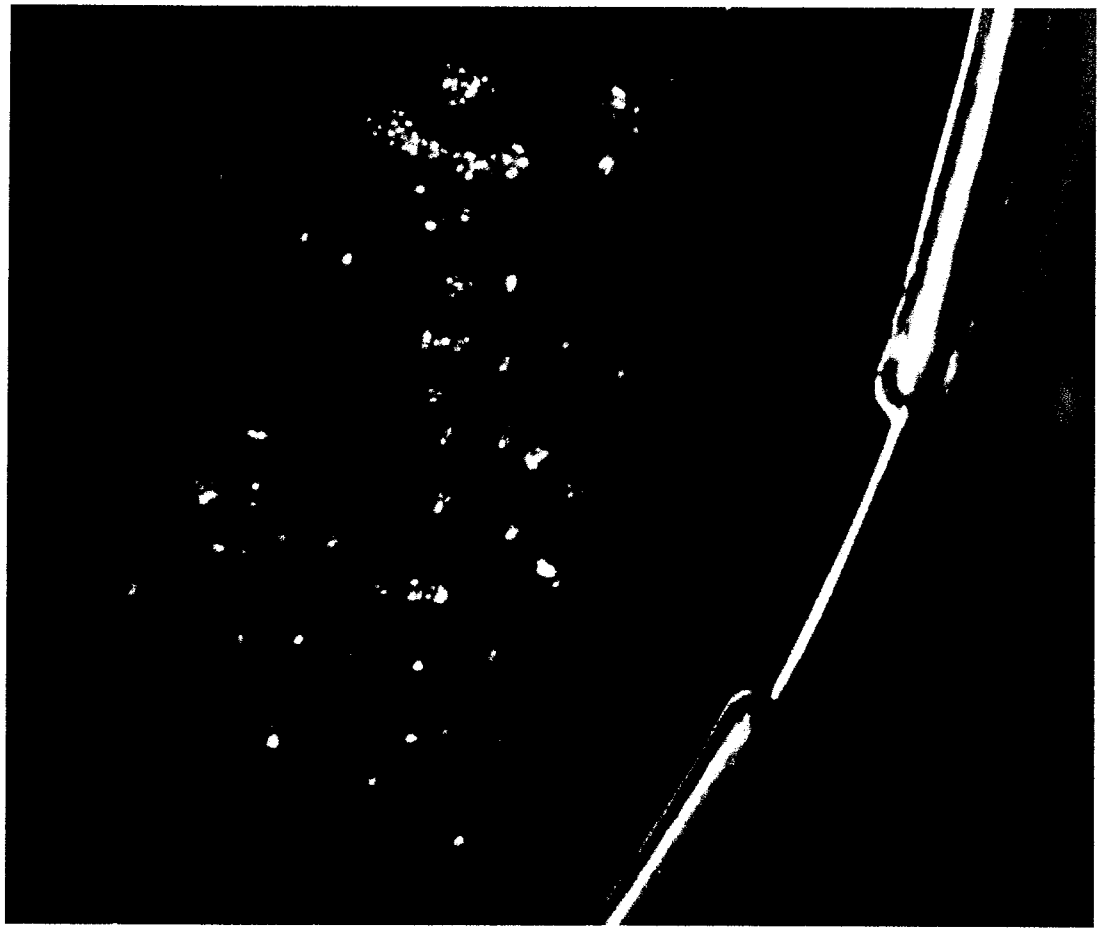

Figure 5.32 - Appearance of *E. coli* colonies and contaminating species as grown on M FC agar.

Figure 5.33 - Region of low silt content in 90% sand / 10% silt column formed by rapidly filling column with permeation fluid

Chapter 6 - Development and Application of Modeling Approaches for Analyses of Column Tests

6.1 Introduction

To assess and quantify the results of the column tests, it is necessary to develop a modeling approach that can account for and simulate the observed results. As the data covers a wide range of soil types, from medium sand to compacted clay, traditional models that may be suitable for one soil texture can come up short when applied to another. A goal is thus to generate a viable modeling approach that simulates the observed results of the column tests on the range of soil types. The applicability of the results of batch sorption tests on simulating *E. coli* transport through soil columns is also assessed.

Previous modeling efforts conducted by a related research group involved the use of an equilibrium transport model to simulate the breakthrough curves of *E. coli* and bromide through quartz sand and 90% sand/10% silt columns (Lukacs *et al*, 2007). Up until this point, no detailed modeling has been conducted on the freeze-fractured clay columns.

6.2 Suitability of available models to current data sets

As the combined data sets contain a wide range of data in both dimensional and non-dimensional formats, a variety of modeling techniques may be applied. This can allow defining breakthrough curves in the basic parameters of pore volumes of flow (PV) and relative concentration (C/Co), or including dimensional terms such as column length and time of measurement. In addition, the material properties of the test columns, such as the hydraulic conductivity, dry density or porosity can be defined, or these properties can be omitted; in this case the columns are treated as simple representative systems.

As the majority of this breakthrough data is focused on the head region of a continuous source breakthrough curve, this limits the applicability of several modeling theories. Equilibrium modeling theory is the strongest candidate to suit the majority of this data, while kinetic modeling theory has application to the pulse experiment data due to the inclusion of the tailing region of the effluent curve. Kinetic modeling theory may also be used with data sets limited to the head region of the breakthrough curve, though these results will be biased towards equilibrium-like sorption parameters (Reddy and Ford, 1996). Classic colloid filtration theory is of limited application to the mixed and freeze-fractured soil columns, as it cannot account for preferential flow paths or heterogeneous soil materials, and was not investigated during the course of this project. The physical straining model also cannot be used with the current data sets as this model requires both the analysis of data in the tailing region of the breakthrough curve to quantify the kinetic sorption properties, and reversal of flow experiments to quantify the fraction of colloids retained as a result of filtration or straining.

6.3 *Modeling software used for E. coli transport modeling*

Many commercial and public domain software packages have been developed to model contaminant fate and transport. The software packages can be used to identify fate and transport parameters, or if the fate and transport parameters are identified, to model contaminant fate and transport. To identify fate and transport parameters, column test breakthrough curves or field scale contaminant plumes can be fit or back analyzed. As many programs contain a variety of model theories, this also allows the comparison of various modeling techniques to a given data set. Some of the more commonly used programs for modeling bacterial fate and transport, and example papers include: PHREEQC (Foppen *et al*, 2008), MODFLOW (Foppen and Schijven, 2006) Hydrus 1D/3D (Gargiulo *et al*, 2007a Gargiulo *et al*, 2007b. Foppen et al, 2007a) and STANMOD (STudio of ANalytical MODels) (Dong *et al*, 2002. Pang *et al*, 2003. Hornberger *et al*, 1992. Levy *et al*, 2007. Bolster *et al*, 1998).

It was decided to focus the modeling endeavors on simplified one-dimensional systems using phenomenological modeling parameters. These types of models simplify the influences of multiple unknowns by attempting to quantify the net observed results rather than attempting to describe or define every particular variable. An example of this would be the modeling of a decay coefficient, which may be influenced by cell death, predation, irreversible sorption, local population size, nutrient availability or other environmental influences. As defining the contribution of each individual influence may be difficult or impossible, and the overall effect can also be heavily skewed by other yet unknown factors, a far simpler option is to focus on a phenomenological model for describing the decay coefficient as observed in experimental measurements.

The focus of the software modeling is within two modeling packages: Geostudio and STANMOD. These programs were chosen as they offer relatively simple equilibrium based transport models – the best type of model for use with the available data. As these models assume steady-state flow and uniform volumetric water content, experiments which violate these assumptions are unlikely to be valid when used with these models. More complex modeling software packages, such as PHREEQC or HYDRUS, requires additional modeling parameters not investigated in this research project.

6.4 STANMOD

The STANMOD (STudio of ANalytical MODels) modeling package is a public domain software suite which offers a variety of methods for evaluating solute transport using analytical solutions to the advection-dispersion equation (Eqn 3.1). As this research focused on relatively simple one-dimensional column tests, the subprograms contained within STANMOD that are most suitable for this type of modeling are CFITM (van Genuchten, 1980), CFITIM (van Genuchten, 1981), and CXTFIT (Toride *et al*, 1995). Since CXTFIT contains the same functionality as CFITM and CFITIM, as well as the capability to output data in both effluent and spatial distribution format, it was decided to focus the modeling efforts on this program.

To identify the required transport parameters to fit a given data set in an inverse model analysis, CXTFIT utilizes a least squares curve fitting algorithm. The software varies the selected transport parameters from an initial estimate to minimize the residuals between the measured values, and the corresponding simulated curve.

6.4.1 CXTFIT contaminant transport boundary conditions

CXTFIT allows the use of two contaminant transport related upper boundary conditions, and a semi-infinite lower boundary condition. The upper boundary conditions are a constant concentration (first type) and a flux averaged concentration (third type). The use of the flux averaged upper boundary condition over the constant concentration upper boundary condition is recommended when a solute is applied at a constant rate, due to the flux averaged boundary condition satisfying conservation of mass within the system (van Genuchten, 1981, Toride *et al*, 1995). It was found through trial and error that the flux averaged boundary condition provided a more accurate fitting of the bromide breakthrough curves (data not shown), and was used for the remainder of the modeling endeavors. As CXTFIT does not consider transient flow (variations in hydraulic head or flow rate) a steady state fluid flow condition is a required prerequisite of the represented model system within this program.

6.4.2 CXTFIT analytical solution for equilibrium transport

Within CXTFIT, the general advection-dispersion equation for equilibrium transport takes the form of:

$$R\frac{\partial C}{\partial t} = D\frac{\partial^2 C}{\partial x^2} - v\frac{\partial C}{\partial x} - \mu C + \gamma x$$

Eqn. 6.1

Where (R) is the retardation factor, (D) is the longitudinal dispersivity coefficient (L^2t^{-1}), (v) is the average pore water seepage velocity (Lt^{-1}), (μ) is the first-order decay term (t^{-1}), and (γ) is the zero order production term ($ML^{-3}t^{-1}$). The analytical solution for the equilibrium transport model using a flux averaged (third type) boundary condition and a semi-infinite lower boundary condition, with no contaminant production or preexisting contaminant within the system is given as (van Genuchten and Wierenga, 1986):

$$C = \frac{1}{2} erfc\left[\frac{RL - vt}{2(DRt)^{0.5}}\right] + \left(\frac{v^2 L}{\pi DR}\right)^{0.5} \exp\left[-\frac{(RL - vt)^2}{2(DRt)^{0.5}}\right]$$
$$- \frac{1}{2}\left(1 + \frac{vL}{D} + \frac{v^2 L}{DR}\right) \exp\left(\frac{vL}{D}\right) erfc\left[\frac{RL + vt}{2(DRt)^{0.5}}\right]$$

Eqn. 6.2

Where (R) is the retardation factor, (D) is the longitudinal hydrodynamic dispersion coefficient, (v) is the average pore water seepage velocity, and (L) is the permeation length (column length), and (t) is dimensional time (s^{-1}).

As CXTFIT is based in part on the earlier CFITM and CFITIM least squares curve fitting methodologies (Toride *et al*, 1995), the analytical solutions presented in van Genuchten, (1981) are essentially identical to those utilized by CXTFIT. This holds true only when the more complex features of CXTFIT, such as multiple pulse periods or multiple pulse solute concentrations, solute production, or stochastic analysis are not considered. The following dimensionless analytical solution presented in van Genuchten

(1981), is used by CXTFIT to generate an effluent breakthrough curve, or fit the associated transport parameters to experimental data:

$$C_e(T) = \frac{1}{2} erfc\left[\left(\frac{P}{4RT}\right)^{0.5}(R-T)\right] + \left(\frac{PT}{\pi R}\right)^{0.5} \exp\left[\left(-\frac{P}{4RT}\right)^{0.5}(R-T)^2\right]$$
$$-\frac{1}{2}\left(1+P+\frac{PT}{R}\right)\exp(P)erfc\left[\left(\frac{P}{4RT}\right)^{0.5}(R-T)\right]$$

Eqn. 6.3

Where (C_e) is the concentration of the effluent in solution, (T) is the total pore volumes at the measurement time (a "dimensionless" measure of time, where T=1 may be defined as the time required for one pore volume of effluent to permeate the column), (R) is the retardation factor, and (P) is the Peclet number, defined as seepage velocity (v) multiplied by the distance term (L) and divided by the hydrodynamic dispersion coefficient (D). In this situation, P is defined as the inverse of the hydrodynamic dispersion coefficient when pore velocity and column length are equal to one. This situation occurs when column height is described in non-dimensional relative height, and velocity is described as one column length of travel per pore volume of flow. This velocity term basically states that fluid located at the top of the column will arrive at the base of the column in the time required for one pore volume of fluid to flow through the column.

It should be noted that the dispersion coefficient is not truly a dimensionless parameters ($D = L^2T^{-1}$) however, it may be interpreted this way when the length (L) is expressed as dimensionless relative height, and dimensionless time (T = cumulative pore

volumes of flow) (i.e. D will now describe dispersion related spreading as the number of relative columns lengths over the time period required for one pore volume to permeate the column).

6.4.3 CXTFIT mobile-immobile model for non-equilibrium transport

CXTFIT also provides code to fit various non-equilibrium transport parameters such as a kinetic mass transfer coefficient and a dimensionless partitioning coefficient. This was investigated as it was likely that the immobile-mobile model incorporated into the program could provide a better model for the freeze-fractured clay columns compared to the basic equilibrium model. This could for example be used to estimate transport through the fractures (mobile) while assuming the intact clay matrix composes the immobile fraction.

In brief, the non-equilibrium transport equation introduces two additional modeling parameters to the general advection-dispersion equation. In the case of immobile and mobile flow paths, the dimensionless advection-dispersion equation takes the form (van Genuchten 1981):

$$\beta R \frac{\partial C_m}{\partial T} + (1-\beta) R \frac{\partial C_{im}}{\partial T} = D \frac{\partial^2 C_m}{\partial L^2} - \frac{\partial C_m}{\partial L}$$

Eqn. 6.4

$$(1-\beta)R\frac{\partial C_{im}}{\partial T} = \omega(C_m - C_{im})$$

Eqn. 6.5

Where the subscripts (m) and (im) designate the fractions of mobile and immobile pore fluid, (β) is a dimensionless fitting parameter which governs the partitioning (ratio of mobile to immobile porosity), (ω) is a dimensionless mass transfer coefficient signifying the rate of mass transfer between the mobile and immobile phases, and (T) is dimensionless time (cumulative pore volumes of flow). The values of ω and β may be calculated in advance using the equations (van Genuchten 1981):

$$\omega = \frac{aL}{\theta v}$$

Eqn. 6.6

Where (a) is a kinetic mass transfer coefficient (t^{-1}), (L) is the column length, (v) is pore water seepage velocity (Lt^{-1}), and (θ) is the total volumetric water content (L^3L^{-3}).

$$\beta = \frac{\theta_m + fP_b K_d}{\theta + P_b K_d}$$

Eqn. 6.7

Where (θ_m) is the fraction of volumetric water content in the mobile phase (L^3L^{-3}), (f) is the fraction of sorption sites at equilibrium with the fluid contained in the mobile

phase, (K_d) is the distribution coefficient, defined as the slope of a linear sorption isotherm, and (ρ_b) is the soil dry density (ML^{-3}). As can be seen with equation 6.7, by assuming all sorption sites are at equilibrium (f = 1), β reduces to a direct measure of the fraction of the porosity in the mobile phase.

The non-dimensional analytical solutions for this model are beyond the scope of this thesis, and the reader is best referred to van Genuchten, (1981) for additional details.

6.4.4 Effects of CXTFIT modeling parameters on breakthrough curve shape

To investigate the individual contributions of the five modeling parameters (retardation factor (R), dispersion coefficient (D) (relative column length / pore volume of flow), first-order decay coefficient (μ) (pore volume of flow^{-1}), the dimensionless partitioning variable (β) and the dimensionless mass transfer coefficient (ω)) on the shape of the resulting curve, a representative system was constructed within CXTFIT where the parameters could be varied to generate a variety of example curves. The equilibrium model was set to the values of R = 2, D = 0.5, μ = 0 (i.e. no decay), and a pulse duration of 10 pore volumes, within a dimensionless representative system. The mobile-immobile model was set to the default values of R = 2, D = 0.5, β = 0.5, ω = 1, and μ = 0. Other parameters were left in the default state (no initial concentration, no contaminant production (i.e. γ = 0)). As the system was input as a dimensionless representative system (L = relative column length (1), T = cumulative pore volumes of flow, V = 1 column length of travel / 1 pore volume of flow) the units reduce to a dimensionless form. The

effects of varying these parameters on the resulting modeled breakthrough curves are shown in Figures 6.1-6.5.

In brief, the dispersion coefficient (D) represents the longitudinal spreading of the contaminant plume over the length of the column. Low values represent plug-like flow, where the contaminant experiences minimal spreading and a sharp (abrupt) breakthrough curve, while high values represent early and most gradual breakthrough, and an extended tailing region within the breakthrough curve.

The retardation factor (R) governs the length of time required for a contaminant to pass through a column relative to a conservative tracer, which is not expected to interact with the soil medium and have a retardation factor of one. Values below one represent faster breakthrough than a conservative tracer, while values above one represent slower breakthrough compared to a conservative tracer. The retardation factor also affects the length of time a contaminant within the model system is subject to dispersion-like spreading.

The first-order decay coefficient (μ) describes the apparent removal of the contaminant from the model system, and the most striking effect of this parameter is controlling the peak, steady state effluent concentration of the contaminant. The decay coefficient may be interpreted as the combined effects of cell death, irreversible sorption, and filtration. Filtration is included in this variable as it would contribute to the apparent removal of bacteria from the system. Filtration is also better approximated with this variable compared to the batch-sorption calculated retardation factor, as filtration is not expected to occur within a batch sorption system.

The partitioning parameter (β) within the mobile-immobile model governs the relative amount of the total pore space contained in the mobile phase. High values indicate that the majority of the pore spaces contain mobile fluid, and at β=1, transport may be described entirely using an equilibrium transport model.

The mass transfer coefficient (ω) describes the rate of solute transfer between the mobile and immobile phases within the mobile-immobile model. Higher values represent rapid transfer between the phases, while low values represent negligible transfer. At extreme values, ω and β are capable of canceling one another. Very high or low values of β indicate that the pore fluid within the system is either completely mobile or immobile, suggesting that mass transfer is of negligible significance. Similarly, high values of ω suggest that mass transfer between the phases occurs at such a rapid rate, that the mobile and immobile phases behave as one unified phase.

6.4.4 Parameter estimations and constraints

As CXTFIT requires an initial estimation of the fitting parameters, an effort was made to calculate these values in advance using the following methods.

Pulse Length

As the previous experiments utilized continuous sources, the pulse length was set to an arbitrarily high value of 100 pore volumes to signify that permeation with bacteria was continuous over the data collection period. For the pulsed source experiments, this

value was set to the pore volume of effluent at which permeation was switched to the pure MSM solution. Pulse length was always defined, and was not fit in any modeling trial.

Dispersion Coefficient

To calculate the dispersion coefficient of the column, the bromide breakthrough curve was fit with the retardation factor constrained. As bromide is not expected to undergo sorption to soil particles, a retardation factor value of one was used. A similar methodology was undertaken with the *E. coli* transport experiments conducted by Harvey (1991) who calibrated both dispersivity and velocity values to their effluent bromide data. The same dispersivity value was used for both the equilibrium and mobile-immobile non-equilibrium model as dispersion is expected to be similar in both models (Reddy and Ford, 1996). For the modeling conducting for this research, it is assumed that the dissolved solute (bromide) and the suspended *E. coli* cells behave in a similar manner in transport through the column (i.e. the bromide represents conservative (non-sorbing) *E. coli* cells. This is the only way to independently asses the dispersion and retardation effects and parameters.

Retardation factor

Several methods were found to estimate the bacterial retardation factor. For the sand, similar published data could be used (Powelsen and Mills, 2001). It is also possible

to utilize batch sorption data to derive a retardation factor. As this was the focus of the previous work conducted by Rosa (2007), it was decided to utilize these data for modeling purposes. The retardation factor may be estimated from a linear sorption isotherm by using equation 3.7. As the best fitting isotherm for the batch sorption data was found to be a Freundlich isotherm, a retardation factor using this model may be calculated using equation 3.8. As the available data also allow the calculation of a Langmuir isotherm, this model was also used to calculate the corresponding retardation factor for this isotherm using the equation 3.9.

Partitioning parameter

The value of β is difficult to estimate in advance with the available data. For the freeze-fractured clay columns, it was possible to estimate the fracture porosity using the methodology of Scott and Nguyen (2005), based on the research of McKay *et al* (1993). In this method the fracture porosity is calculated using the following set of equations:

$$K_f = (2b)^2 \frac{\rho_w g}{12u}$$

Eqn. 6.8

Where (K_f) is the hydraulic conductivity of a fracture (cm/s), (2b) is the fracture aperture (cm), (ρ_w) is the fluid density, set as 1 g/ml for water, (g) is the acceleration of gravity, given as 981 cm/s^2, and (u) is the flow viscosity of the fluid, given as 0.0131 g/cm/s for water.

$$K_{XY} = \frac{2b}{2B} K_f + K_m$$

Eqn. 6.9

Where (K_{xy}) is the measured hydraulic conductivity of the model system (cm/s), (K_f) is the hydraulic conductivity of the fractured spaces (cm/s), (K_m) is the hydraulic conductivity of the intact clay matrix (cm/s), and (2B) is the distance between adjacent fractures (cm).

$$n_f = 2\frac{2b}{2B}$$

Eqn. 6.10

Where (n_f) is the fraction porosity as a fraction of total porosity.

The results of this analysis utilizing an assumed fracture spacing of 0.5cm are shown in Table 6.1. It was assumed that the hydraulic conductivity of the intact clay matrix was equivalent to the hydraulic conductivity of the intact control clay columns. The value of K_{xy} was assumed to be the average measured hydraulic conductivity of the freeze-fractured experimental clay columns. The assumed fracture spacing of 0.5 cm was based on the visual observations of Scott and Nguyen (2006).

The sand and 90% sand/10% silt columns were assumed to not contain immobile pore fluid based on preliminary modeling, which strongly favoured contaminant transport by the equilibrium model.

Mass transfer coefficient

In the clay columns, it was assumed that *E. coli* would not be able to enter the clay matrix, which would compose the immobile fraction of the column. To reflect this, the value of ω was set to a value of 1×10^{-5} to indicate negligible mass transfer between the phases.

6.5 Geostudio

The Geostudio software suite (GEO-SLOPE Int.) is a geotechnical modeling package which utilizes the finite element modeling method. Of interest to this project are the SEEP/W and CTRAN/W programs, which may be utilized to model groundwater flow and contaminant transport in saturated soil systems, respectively. Unlike STANMOD, Geostudio can not be used to fit transport parameters to an observed data set, as it lacks the capabilities to perform inverse modeling. However, as Geostudio allows model systems more complex than one-dimensional columns, material properties to be defined, and the presence of multiple materials, this software may be used to model situations more complex than the homogeneous soil columns assumed in CXTFIT.

The two-dimensional governing seepage equation utilized by SEEP/W in a steady fluid flow condition is as follows (GEO-SLOPE 2008b):

$$\frac{\partial}{\partial z}\left(kz\frac{\partial H}{\partial z}\right)+\frac{\partial}{\partial y}\left(k_y\frac{\partial H}{\partial y}\right)+Q=m_w\gamma_w\frac{\partial H}{\partial t}$$

Eqn 6.11

Where (H) is the total head (length), (k_z) is the hydraulic conductivity in the z direction (length / time) (k_y) is the hydraulic conductivity in the y direction (length / time), (Q) is the applied boundary flux (length^3 / time), (γ_w) is the unit weight of water (g/ml), (m_w) is the slope of the storage curve, and (t) is dimensional time (seconds).

The contaminant transport equation utilized by CTRAN/W is given as (GEO-SLOPE 2008b):

$$\theta\frac{\partial C}{\partial t}+\rho_d\frac{\partial S}{\partial C}\frac{\partial C}{\partial t}=\theta D\frac{\partial^2 C}{\partial z^2}-v\frac{\partial C}{\partial z}-\mu\theta C-\mu S\rho_d$$

Eqn 6.12

Where (v) is the seepage velocity (m/s), (S) is the concentration of contaminant sorbed to the solid phase (g/g), (C) is the concentration of contaminant in the liquid phase, (t) is dimensional time (seconds), (z) is the dimensional length (m), (μ) is the dimensional decay coefficient (s^{-1}) and (θ) is the volumetric water content.

The integration of these equations into the finite element mesh used by SEEP/W and CTRAN/W are explained further within the associated documentation (GEO-SLOPE 2008a and 2008b)

To define the bacterial transport parameters used in CTRAN/W, the equilibrium transport parameters fit in CXTFIT were used. This was done so that column models used by the two software packages may be directly compared. Using this method is also desirable as hand calculation methods may not be repeatable between researchers (van Genuchten, 1984).

6.5.1 Conversion of STANMOD outputs for entry into Geostudio

As the transport parameters output from STANMOD are in a non-dimensional format, they must first be converted to the dimensional format utilized by Geostudio. The methods here are similar to those utilized by Lukacs *et al* (2007). Because Geostudio utilizes length in meters, the associated column properties were converted to this unit system before being entered into the program. Other dimensional units were time measured in seconds, and mass measured in dimensionless relative mass. The dimensionless mass unit may be assumed to be synonymous with megagrams, and allowed density and sorption data to be entered without requiring recalculation (1 Mg/m^3 = 1 g/ml).

The dimensional value of the longitudinal dispersivity was calculated using the equation:

$$\alpha_L = LD$$

Eqn. 6.13

Where (α_L) is the dimensional longitudinal dispersivity (meters), (L) is column length (meters), and (D) is the dispersion coefficient calculated by fitting the term to the bromide breakthrough curve in CXTFIT (L^2T^{-1}).

The non-dimensional retardation factor was converted to the linear distribution coefficient using the equation:

$$K_d = \frac{\eta(Rd-1)}{\rho_d}$$

Eqn. 6.14

Where (K_d) is the distribution coefficient, defined as the slope of a linear sorption isotherm, (η) is the porosity of the soil column, (R) is the retardation factor, and (ρ_d) is the soil dry density in Mg / m^3. The k_d value was used to generate a linear sorption curve within the adsorption function section of CTRAN/W.

While a linear sorption isotherm may be directly calculated from the batch sorption data, this model typically fit the experimental batch sorption data very poorly ($R^2<0$), and suggested minimal difference between bacterial sorption to the various soil materials. As the Freundlich and Langmuir isotherms were used to generate the retardation factors used within the CXTFIT models, it was decided to generate a linear sorption isotherm using these comparable values. This also provides an added level of model parameter consistency between the programs.

Within Geostudio, the decay coefficient (μ) was required to be input as a dimensional half-life. From CXTFIT, the fit dimensionless decay coefficient was first converted to a dimensional form by the equation:

$$k_{dim} = \mu(f_r)$$

Eqn. 6.15

Where (k_{dim}) is the dimensional decay coefficient in seconds^{-1}, (μ) is the dimensionless decay coefficient in pore volumes^{-1} and (f_r) is a conversion factor, defined as the inverse of the flow rate in seconds/pore volume. The purpose of the f_r variable is to convert the decay coefficient from time in pore volumes to time in seconds/hours/day etc. The half life could then be calculated using the formula:

$$t_{\frac{1}{2}} = \frac{\ln(2)}{k_{dim}}$$

Eqn. 6.16

Other required parameters determined from the soil column test data are: The column dimensions, the average hydraulic conductivity in m/s, the porosity which was input as the saturated volumetric water content, and the dry density in Mg/M3. Boundary conditions included: a constant contaminant concentration of 1Mg/m^3 (1g/ml) at the top of the column to signify a C/Co of 1, a boundary condition at the base of the column (Qm = 0M/s, Qd>0) to signify unimpeded, free-flow of the contaminant out of the after

reaching this location, total hydraulic head equal to the measured elevation head from the column test experiments, and a total head of zero at the base of the column. To model the pulse experiments, a time dependant boundary condition was input as explained in the following section.

6.5.2 Integration of non-linear sorption isotherms and time dependant boundary conditions into CTRAN/W

The simplest method to import the non-linear sorption isotherms into CTRAN/W involves using equation 3.8 or 3.9 to calculate a corresponding retardation factor, and then using that value in equation 6.14 to calculate a linear distribution coefficient. This value may then be entered as a linear sorption isotherm with a slope of the distribution coefficient. The reason a linear isotherm was not directly fit to the batch sorption data was that the associated data was very non-linear in distribution.

As Geostudio allows the use of user written addin programs to expand some functions within the software, it was also possible to directly incorporate the Freundlich and Langmuir sorption isotherms from the batch sorption data. This was desirable as it could allow the direct modeling of the sorption isotherms defined by Rosa (2007). The addin programs were written in C#, and were input as the following:

```
//Langmuir Isotherm;

public class Langmuir
{
        public double KL; // KL input
```

```
        public double ML; // ML input
        public double Calculate (double x)
        {
                return ((KL*ML*x)/(1+(KL*x)));
        }
}
```

This program, once processed with the C# compiler included with the Geostudio developer's kit, allows the user to specify the K_L and M_L coefficients of a Langmuir sorption model. Geostudio will then calculate a corresponding Langmuir isotherm for all concentrations of a contaminant (x). The (x) term is utilized instead of (C) as (x) is the default independent variable within Geostudio addins, i.e. it is interpreted as the contaminant concentration within this example.

The corresponding Freundlich isotherm program was written as:

```
//Freundlich Isotherm;

public class Freundlich
{
        public double K; // K input
        public double N; // N input
        public double Calculate(double x)
        {
        double d, q;
         if (x < 0) x = 0;
                d = (System.Math.Pow(x,N));
                q = d*K;
                return (q);
        }

}
```

This model uses the slope of the Freundlich sorption model (K) and the exponent N to calculate the corresponding Freundlich isotherm for all concentrations of a contaminant. The (if (x < 0) x = 0;) statement was found to be essential to the operation of the program. This is due to a bug whereby CTRAN/W attempts to calculate negative contaminant concentration values, returning imaginary numbers, and an error when the program is executed (personal correspondence with GEO-SLOPE technical support).

When running the analysis using the Freundlich or Langmuir sorption isotherms within Geostudio, the contaminant boundary condition required an adjustment. This is because these sorption isotherms are dependant on the contaminant concentration in the permeating fluid, unlike the linear isotherm. To reflect the concentration used in these studies, the upper boundary condition within CTRAN/W was set to a contaminant concentration of $1 \times 10^{7} M/m^{3}$.

The time dependant boundary condition for the pulse source experiments was input using the program:

```
//Pulse
public class Pulse
{
  public double PrePulseMagnitude; // PrePulse Concentration
  public double PulseStart; // Pulse Start
  public double PulseMagnitude; // Pulse Concentration
  public double PulseEnd; // When Pulse Ends
  public double TailMagnitude; // Post Pulse Concentration

  public double Calculate(double x)
  {
     double d;
        if (x < 0) x = 0;
                        d = PulseMagnitude;
                        if (x < PulseStart)
                                d = PrePulseMagnitude;
```

```
                if (x > PulseEnd)
                        d = TailMagnitude;

    return (d);
  }
}
```

The five variables (PrePulseMagnitude, PulseStart, PulseMagnitude, PulseEnd and TailMagnitude) allow the user to specify the starting / ending time and concentration of a contaminant pulse, and any contaminant concentration at the boundary zone before and after the pulse, respectively. In the scenarios analyzed for this research, the PrePulseMagnitude, TailMagnitude and PulseStart variables were set to 0, the PulseMagnitude was set to 1, and the PulseEnd varitable was set to the time in seconds that the bacterial permeation was ended.

Table 6.1 - Estimation of the fracture porosity within the freeze-fractured clay columns

Column	2B (cm)	$K_{(x,y)}$ cm/s *	K_m (cm/s) **	2b (μm)	Kf (cm/s)	n_f (%)
CCA	0.50	2.513×10^{-6}	2.767×10^{-8}	58.40	2.128×10^{-3}	0.23
CCB	0.50	3.288×10^{-6}	2.767×10^{-8}	63.93	2.550×10^{-3}	0.26
CCC	0.50	9.298×10^{-6}	2.767×10^{-8}	90.56	5.118×10^{-3}	0.36
CCD	0.50	5.481×10^{-6}	2.767×10^{-8}	75.88	3.593×10^{-3}	0.30
NCC	0.50	4.357×10^{-6}	5.183×10^{-7}	67.50	2.844×10^{-3}	0.27
NCD	0.50	1.810×10^{-5}	5.183×10^{-7}	112.10	7.842×10^{-3}	0.45
NCE	0.50	1.150×10^{-5}	5.183×10^{-7}	95.82	5.730×10^{-3}	0.38

* Average hydraulic conductivity of experimental columns
** Average hydraulic conductivity of non-fractured control columns (compacted control column for CCA-CCD, normally consolidated control column for NCC-NCE)

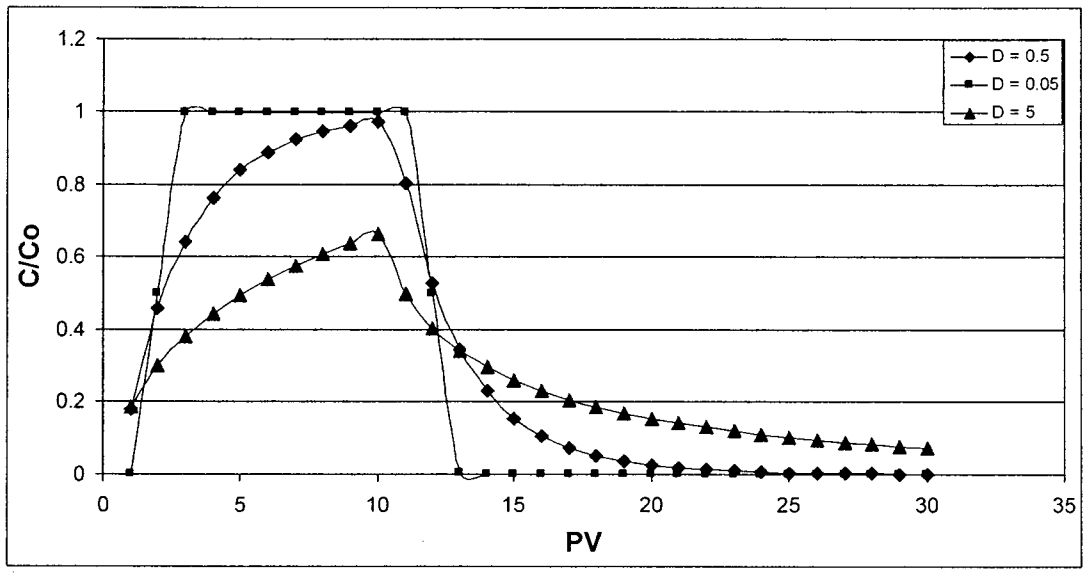

Figure 6.1 - Effects of the dispersion coefficient (D) value on the modeled effluent breakthrough curves.

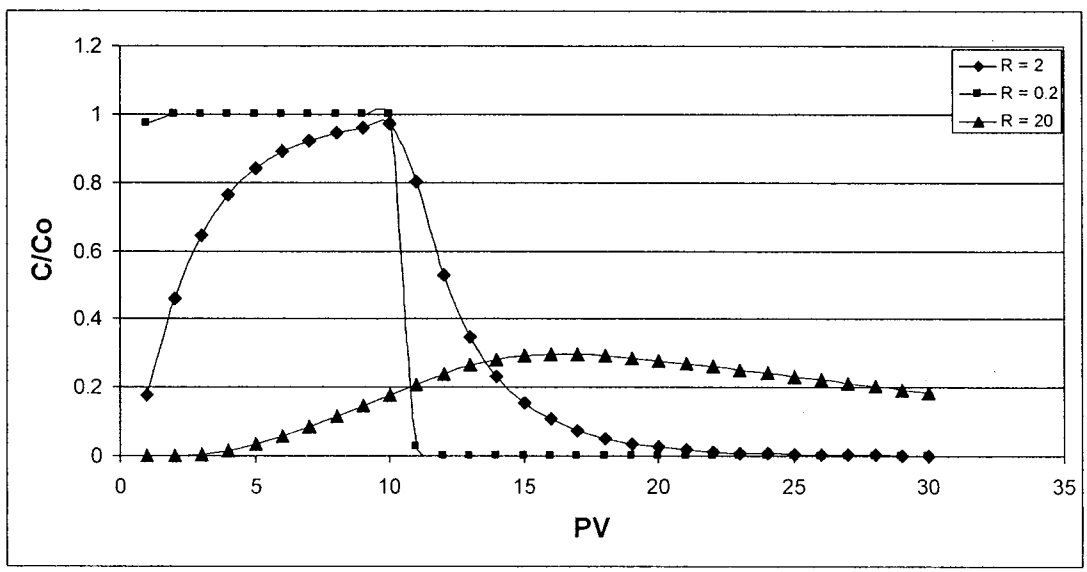

Figure 6.2 - Effects of the retardation factor (R) value on modeled effluent breakthrough curves.

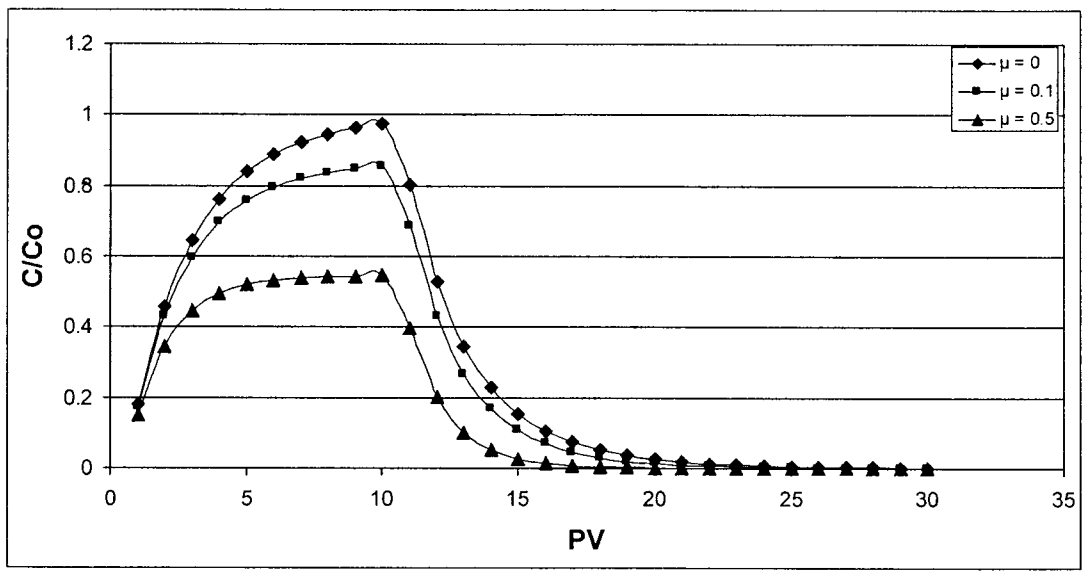

Figure 6.3 - Effect of the first- decay coefficient (μ) on modeled effluent breakthrough curves.

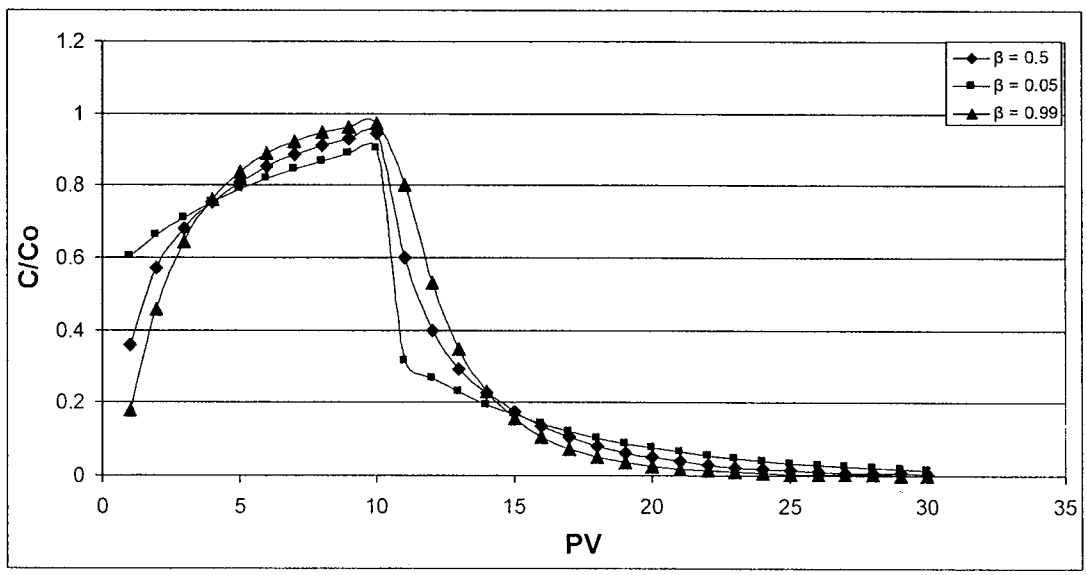

Figure 6.4 - Effect of the partitioning parameter (β) on effluent breakthrough curves.

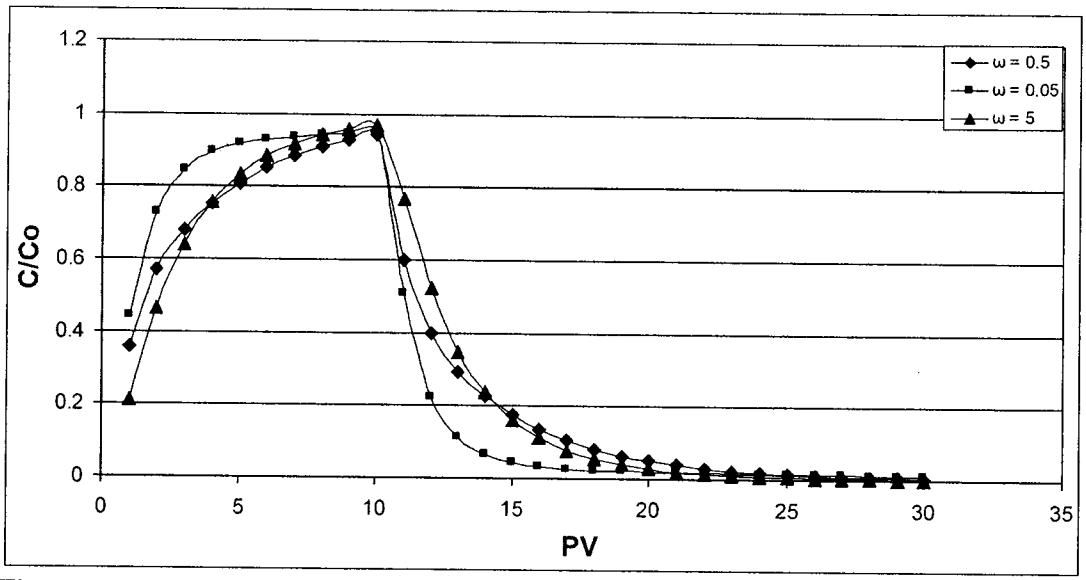

Figure 6.5 - Effects of the mass transfer coefficient (ω) on modeled effluent breakthrough curves.

Chapter 7 - Modeling Procedures and Results

7.1 Preliminary observations, program settings, model overviews

7.1.1 Selection of sorption isotherms for the estimation of the retardation factor.

During the preliminary modeling trials, it was observed that the Freundlich sorption model yielded transport parameters that provided a closer fir to the observed breakthrough curves of the silt and clay columns. The Langmuir sorption model, however, yielded transport parameters that gave a better fit to the observed breakthrough curves of the compacted sand samples when compared to the Freundlich model. The reason for this is unknown, though a large amount of scatter was observed in the sand sorption data set. As soil-free controls were not conducted during the batch sorption experiments of Rosa (2007) it is possible that factors unrelated to bacterial sorption to the soil may have influenced the reported values for the sand data, while being of minor consequence for the silt and clay. Consequently, the calculated retardation factors for the sand columns were calculated from the Langmuir model, while the clay and silt retardation factors were calculated from the Freundlich model.

7.1.2 Poor modeling performance of the Freundlich and Langmuir addins when used with the Geostudio model

Preliminary modeling of the bacterial breakthrough data using Geostudio with the sorption isotherm addins (section 6.5.2) produced simulation results which did not represent the experimental observations. Within systems representing the sand columns and the Langmuir sorption addin, simulated *E. coli* breakthrough times were approximately 2-3 times longer than the observed values. Using a similar methodology with the freeze-fractured clay column properties, and the Freundlich sorption addin, the model predicted no detectable *E. coli* in the column effluent for several centuries. Consequently, it is not possible at this time to generate viable *E. coli* transport simulations within Geostudio using the identified batch sorption parameters. It was still possible to generate viable models within Geostudio by using Eqn 6.14 to generate a linear distribution coefficient (K_d) from the retardation factors estimated using Eqn 3.8 and 3.9.

7.1.3 Modification of the estimated retardation factor in the mobile-immobile model.

Preliminary modeling within the mobile-immobile model suggested that the estimated retardation factor or partitioning parameter was underestimating the apparent value by two orders of magnitude. It was decided to interpret this phenomenon as an indication that the retardation of the *E. coli* bacteria within the fracture network is approximately 100 times higher than that predicted by the batch sorption analysis. A detailed discussion of this is outlined in section 8.2. Because the retardation factor for this

model was estimated by using this correction factor rather than being directly entered as the batch sorption retardation factor value, the transport parameters that best describe the transport of bacteria within the columns using this technique are not unique. It can be expected that a variety of retardation factor and decay coefficient value combinations would produce model results that simulate the measured data to a similar accuracy.

7.1.4 Common program settings for the CXTFIT model

The following program settings were consistent in all of the modeling procedures undertaken in CXTFIT.

-Dimensionless time (pore volumes), length (relative height) and concentration (relative concentration) parameters. Dimensionless parameters selected for all variables within the scale and space unit menu. Data input for the inverse parameter estimation modeling would then be input as total pore volumes of flow and relative concentration. Program model outputs would then be in total pore volumes of flow, relative concentration, and relative height.

-A third type inlet, resident concentration mode with a characteristic column length of one (third type upper boundary, section 6.4.1).

-No estimate for total contaminant mass as this data output was not utilized

-Maximum of 200 iterations for the inverse estimation problem

-Velocity parameter (average pore water seepage velocity) set as 1. While velocity is not specifically considered as an input parameter by the program when using pore volumes of flow and relative height for the temporal and scale units (Eqn 6.3) (i.e.

velocity is interpreted as one column length of travel per pore volume of flow), a positive value is required as a dummy variable. The default value of 0 caused a program error, while a value of 1 or any other positive value had no effect on the output.

-A step input concentration of 1 for the continuous source experiments, or a pulse input of the pulse duration (in pore volumes of flow) for the applicable pulse experiments

-Zero initial contaminant concentration within the model system

-Zero contaminant production ($\gamma = 0$)

-A fixed depth breakthrough curve at a value of 1. This indicates to the program that the data inputs from the column experiments were collected from the lower boundary (effluent) of the experimental columns.

7.1.5 Common program settings for the Geostudio bacterial transport model

The following program settings were consistently used in all of the modeling simulations conducted with Geostudio.

SEEP/W

-Conductivity ratio of 1 (indicates hydraulic conductivity is the same regardless of flow direction (i.e. isotropic hydraulic conductivity)) in a 0' direction (indicates that the hydraulic conductivity is defined by the x-y coordinate system, used as a default value)

-Coefficient of Volumetric Compressibility (Mv) value of 1×10^{-5} / kPa (Geostudio recommended default, does not affect model outputs)

CTRAN/W

-Transverse dispersivity of 5 x 10^{-5} m to indicate negligible contaminant transfer perpendicular to the direction of flow

-Diffusion function of 1 x 10^{-9} m^2/s to indicate negligible diffusion of the bacteria.

7.1.6 Comparing modeled data to experimental data

To compare the simulated results to the experimental measurements, a simple regression analysis was utilized to provide an indication of the model goodness of fit. The regression analysis compares the variability of the measured and simulated data sets using the equation:

$$R^2 = 1 - \frac{\Sigma(c_i - c_{avg})^2}{\Sigma(c_{mi} - c_i)^2}$$

Eqn 7.1

Where (R^2) is the coefficient of determination, (c_i) is the measured *E. coli* concentration (C/C_o) at a given time, (c_{avg}) is the mean *E. coli* concentration over the total experimental data collection set, (c_{mi}) is the modeled *E. coli* concentration at a given time. R^2 values of one indicate perfect fit between the model simulated values and the experimental measurements. An R^2 value of zero or less than zero indicates that the model is equal to or worse at describing the data set compared to a horizontal line drawn at the mean of the data values.

7.2 *General model overviews*

7.2.1 CXTFIT equilibrium model.

A general flowchart outlaying the CXTFIT equilibrium model and data sources is shown in Figure 7.1. The model utilizes three transport parameters: the retardation factor (R), dispersion coefficient (D), and decay coefficient (μ). The retardation factor was estimated using the batch sorption data (section 6.4.4), while the dispersion coefficient was estimated using breakthrough data from permeating the column with a non-sorbing tracer (bromide) as explained further in section 7.3.1. The decay coefficient was then fit to the experimental data measurements through inverse parameter modeling.

7.2.2 CXTFIT mobile-immobile model

A general flowchart outlaying the CXTFIT mobile-immobile model and data sources is shown in Figure 7.2. Similar to the CXTFIT equilibrium model, the retardation factor (R) and dispersion coefficient (D) were estimated using the batch sorption and bromide permeation data (sections 6.4.4 and 7.3.1). The dimensionless mass transfer coefficient (ω) was set to 10^{-5} to signify negligible mass transfer between the mobile (fractured) and immobile (matrix) phases. The dimensionless partitioning parameter (β) was calculated using the hydraulic conductivity data of the intact clay control columns, and the freeze-fractured clay columns (section 6.4.4). It was assumed that the fracture

porosity composed the mobile fraction of the total porosity, while the matrix composed the immobile fraction.

7.2.3 Geostudio equilibrium transport model.

A general flowchart outlaying the Geostudio equilibrium model and data sources is shown in Figure 7.3. The model outputs of the CXTFIT equilibrium model were converted to their dimensional form as explained in section 6.5.1. Soil material and hydraulic properties were acquired from the soil compaction and permeation experiments. As the sorption addins (described in section 6.5.2) were not effective at describing the observed transport of the bacteria through the model systems, the calculated retardation factors (section 6.4.4) were converted to a linearized distribution coefficient using Eqn. 6.14.

7.2.4 Distribution profile modeling

While the distribution profile measurements contained both cells contained both cells recovered from the solid phase, and cells contained within the pore fluid of the sample locations (section 5.1.5) the modeled distribution profile results are only those for the *E. coli* contained within the solid phase of the model systems. Cells contained within the pore fluid were not considered in the modeled results for two reasons: the actual measure of pore fluid within the measured soil samples could not be ascertained for comparison to the Geostudio models (which consider a fully saturated sample location

when considering solid and liquid contaminant concentrations), the porosity and moisture content of the soil is not considered by the CXTFIT model.

7.3 Bromide CXTFIT transport simulations for the identification of transport parameters

7.3.1 Bromide CXTFIT equilibrium transport simulations for the identification of the dispersion coefficient

The dispersion coefficient (D) for bromide was estimated by constraining the retardation factor value to a value of one (as bromide is a conservative, non-sorbing chemical), and the decay coefficient to zero. This meant that only the dispersion coefficient would be fit by the program. As steady state (i.e. full) bromide breakthrough was observed in all of the column tests, the complete data set from the head and tailing region was utilized for parameter estimation purposes when available. The results of this analysis for the previously conducted and currently conducted column experiments, and the associated coefficients of determination are shown in Table 7.1.

7.3.2 Bromide mobile-immobile transport model

The bromide mobile-immobile transport simulations were conducted using the same initial values (R=1, $\mu = 0$) as the bromide equilibrium transport model. The value of β was set to the fracture porosity value calculated using the methodology outlined in section 6.4.4 (Eqns 6.8-6.10) and the value of ω was set to 1×10^{-5} to signify minimal

mass transfer between the mobile and immobile phases. This mass transfer value was used as it was expected that *E. coli* would not be able enter the intact clay matrix.

The CXTFIT model using the mobile-immobile parameters was less effective than the bromide equilibrium transport model at simulating the observed breakthrough curves for the fractured clay columns. Allowing the program to optimize either the β or ω parameters resulted in the values of $\beta = 1$ or $\omega = 100$, which indicates that the system is best described using an entirely mobile, single phase equilibrium model.

7.4 E. coli transport simulations for the identification of transport parameters

7.4.1 *E. coli* CXTFIT equilibrium transport model

During the course of the modeling work, it became evident that the scatter inherent in several *E. coli* data sets (freeze-fractured compacted clays, freeze-fractured normally consolidated clays) made it impossible to form reliable models to simulate transport behaviour. In these circumstances, the resulting transport parameters from the model fitting would be at unacceptable extremes (for example retardation factor values in the millions combined with negligibly low dispersion coefficients). To remedy this, at least one parameter would be constrained to an estimated value as outlined in section 6.4.4. This also has the advantage of allowing a comparison of the transport parameters estimated using the methodologies outlined in section 6.4.4 to the optimized values as calculated by the inverse modeling procedure. A summary of the estimated dispersion values and retardation factors are shown in Table 7.2, along with the associated

coefficients of determination when compared to the *E. coli* column effluent measurements.

Because steady state *E. coli* breakthrough (i.e. effluent concentration measurements that are stable) was not observed in the 90% sand / 10% silt pulse column tests, only the head region of the breakthrough curve was utilized for bacterial transport parameter fitting purposes. This was required as a steady state breakthrough condition is required to properly differentiate the influences of retardation and decay on the resulting observations.

The estimated values of the retardation factor (R) and the dispersion coefficient (D) as outlined in section 6.4.4 were compared to the optimized values fit by the inverse modeling procedure. The fit retardation factor optimized to the simulation with an estimated dispersion coefficient is shown in Table 7.3, while the dispersion coefficient optimized to the estimated retardation factor is shown in Table 7.4.

The rate of population decay was estimated by inverse model fitting a first-order decay coefficient (μ) to the transport parameters estimated using the methodology described in section 6.4.4 (allowing the program to optimize this transport parameter to minimize the residuals between the model predictions and input data values). The results of this are shown in Table 7.5.

7.4.2 *E. coli* mobile-immobile transport model for freeze-fractured clay columns

The mobile-immobile transport model tended to produce less satisfactory fits to the observed data when compared to the equilibrium model in most circumstances. It was

also found that in the absence of decay ($\mu = 0$), and insignificant mass transfer between the mobile and immobile phases ($\omega = 1 \times 10^{-5}$) the mobile-immobile model produced identical results to a similar equilibrium transport model (β and ω not considered in the modeling theory) when the retardation factor was multiplied by the dimensionless partitioning coefficient (β). The likely explanation for this is that reducing the effective porosity reduces the availability of sorption sites. Allowing the program to fit a kinetic mass transfer coefficient (ω) to the estimated partitioning coefficient produced very low values ($10^{-8} - 10^{-4}$) for this term - consistent with the hypothesis of negligible mass transfer between the phases.

As it is more difficult to estimate the transport parameters within the CXTFIT mobile-immobile model compared to the simpler CXTFIT equilibrium model, an effort was made to modify the estimated transport parameters for this particular model. It was found through trial and error that the estimated retardation factor (methodology described in section 6.4.4) tended to be approximately 100 times lower than the values optimized by the CXTFIT inverse analysis when using the estimated fractured porosity as the (β) term. It is likely that the apparent retardation of the bacteria within the fracture network is higher than the estimated value due to influences such as ripening and biofilm production. As the dispersion coefficient (D) estimated by the bromide CXTFIT equilibrium simulations was based on the assumption that all pore spaces were available to the bromide, this is also likely to be in error when considering the *E. coli* which were assumed to be limited to the pore spaces composing the fractured porosity. Using the (D) value estimated by the bromide analysis as an initial estimate, and allowing the program to optimize this value while simultaneously fitting the decay coefficient (μ) provided a

superior simulation of the experimental results compared to the initial estimates alone. The results of this analysis are shown in Table 7.6.

7.4.3 Geostudio equilibrium transport simulations

The Geostudio equilibrium transport simulations were performed using the individual column properties and the transport parameters identified using the CXTFIT analyses. The transport parameters were converted to their dimensional equivalents as outlined in section 6.5.1. As the 90% sand / 10% silt column retardation factor was estimated by using a weighed average of the estimated sand and silt retardation factors weighed in a 90% sand / 10% silt ratio, this value was input as a linear sorption isotherm with a slope corresponding to the calculated distribution coefficient. The values of the calculated dispersion coefficients are shown in table 7.7. The remaining dimensional transport parameters and resulting coefficients of determination for the Geostudio modeling analysis are shown in Table 7.8. The simulation results within Geostudio were inferior to the CXTFIT equilibrium model results in all models with the exception of columns SSC and SSD.

7.5 Simulation of *E. coli* breakthrough curves using the transport parameters identified from the CXTFIT analysis

7.5.1 Compacted sand columns

The *E. coli* breakthrough curve simulation results for the compacted sand columns are shown in Figures 7.4-7.11. These figures contrast the modeled effluent concentrations of *E. coli* with the experimental measurements. The soil column *E. coli* distribution profile model results are shown in Figures 7.12-7.13. The distribution profiles for columns SP1-SP3 are not shown as neither the CXTFIT equilibrium model, nor the Geostudio model simulations simulated any bacteria remaining in the solid phase after the MSM pulse, contrary to the experimental observations (Figure 5.21). The retardation factors (R) and dispersion coefficients (D) estimated using the methodologies described in section 6.4.4, combined with the decay coefficients (μ) fit during the inverse analysis, produced breakthrough curve simulations that reasonably represented the experimental observations. The CXTFIT models were more accurate (R^2 0.75-0.97) at simulating the experimental data sets compared to the Geostudio model (R^2 0.71-0.83). However, the simulated column distribution profiles poorly represented the observed values, predicting no bacteria remaining in the columns after the MSM pulse, contrary to the experimental observations (Figures 5.10, 5.25). Another shortcoming of both the CXTFIT and Geostudio model was the inability to accurately simulate the observed *E. coli* concentrations within the tailing region of the breakthrough curve following the MSM pulse (Figures 7.7, 7.9, 7.11).

While the head regions of the pulsed-source experiments (columns SP1, SP2, SP3) conducted during this study had a high degree of repeatability for both bromide and *E. coli* analysis (Figure 5.18, 5.21) the head region of these breakthrough curves differed slightly from the experiments conducted by Lukacs *et al* (2007) (columns SnA and SnB, Figures 5.6, 5.10). The breakthrough of SnA and SnB broke sharply and tended to level off to a relative concentration of 0.7-0.8, followed by a more gradual climb to full breakthrough. The results of their sand column bromide permeation (Figure 5.6) also suggested full breakthrough of the bromide was delayed noticeably compared to the sand column bromide permeation in this study (Figure 5.18). This may suggest that the permeating fluid in their study was diluted with clean water remaining in the void space above their soil column. This could have occurred for example if a quantity of clean water remained above the soil sample when being filled with the permeating solution, or if the column was quickly filled allowing the influent to displace clean water in the upper reaches of the soil matrix.

7.5.2 Compacted 90% sand / 10% silt columns

The breakthrough curve simulated results for the compacted 90% sand / 10% silt columns are shown in Figures 7.14 - 7.18. The simulated distribution profiles are shown in Figures 7.19-7.23. The convex shape of the distribution profiles for the pulsed-source 90% sand / 10% silt column simulations (in particular columns SSP1 and SSP2, Figures 7.18, 7.19) is likely a result of the estimated location of the peak contaminant concentration. This may also be viewed in the simulated breakthrough curves, as the *E.*

coli effluent concentrations were predicted to continue to increase during the simulated time frame after the onset of the MSM pulse.

Overall, the equilibrium transport model does not adequately describe the observed *E. coli* breakthrough curves and distribution profiles of the 90% sand / 10% silt columns. These columns also had the highest relative variability in the fit retardation factors (2.63 - 55.6, Table 7.3) despite having similar soil properties (5.4, 5.10). Because high concentrations of bacteria were also found within the pulsed column following the MSM flush, this may also suggest that straining and related physical removal mechanisms played an important roll in limiting bacterial transport through these columns.

While the Geostudio equilibrium model simulation was more effective than the CXTFIT equilibrium model simulation at describing the observed effluent *E. coli* measurements of the continuous source columns (Tables 7.2, 7.5, 7.8) this trend was not seen in the pulsed-source experimental columns (SSP1, SSP2, SSP3).

7.5.3 Compacted silt columns

As column Silt R was rendered invalid due to bacterial contamination, only column Silt S was used for bacterial modeling purposes. The model breakthrough curve for this column is shown in Figure 7.25, while the simulated distribution profile is shown in Figure 7.25.

The equilibrium transport model was does not adequately describe the observed breakthrough curves or distribution profiles of the silt column. It is likely that the

combined influences of competition with the contaminating bacterial species within these columns, and physical straining of the *E. coli* cells may have greatly limited the applicability of the equilibrium model in this soil type.

7.5.4 Freeze-fractured compacted clay columns

The breakthrough curve model results for the freeze-fractured compacted clay columns are shown in Figures 7.26-7.29. The simulated distribution profiles are shown in Figures 7.30-7.33. The Geostudio equilibrium transport model was not capable of describing the observed breakthrough curves of these experimental columns (Table 7.8).

In two of the columns (CCA, CCB), the CXTFIT equilibrium transport model utilizing the transport parameters estimated using the methodology described in section 6.4.4, with a decay coefficient calculated using the inverse, parameter estimation method, produced a model simulation which accurately represented the observed effluent measurements (R^2 0.76-0.92, Table 7.5). This accuracy was not seen in columns CCC and CCD using a similar methodology (R^2 0.00-0.22, Table 7.5). It appeared that the estimated retardation factors for columns CCC and CCD were higher than the optimized values (Table 7.3) and that decay was not significant in these columns (Table 7.5). Similar to the unfractured sand and silt columns, the equilibrium transport model was not effective at describing the observed distribution profiles. In contrast, the mobile-immobile model was more effective in describing both the observed breakthrough curves and distribution profiles compared to the equilibrium model (Figures 7.26-7.33. Tables 7.5 and 7.6).

7.5.5 Freeze-fractured normally consolidated clay columns

The breakthrough curve simulation results for the freeze-fractured normally consolidated clay columns are shown in Figures 7.34-7.36. The simulated distribution profiles are shown in Figures 7.37-7.39. The CXTFIT and Geostudio equilibrium transport models were not suitable for describing the observed effluent breakthrough curves of the freeze-fractured consolidated columns (R^2 <0, with the exception of column NCC at 0.18 within the CXTFIT equilibrium model (Tables 7.5 and 7.8).

Similar to the freeze-fractured compacted clay columns; the mobile-immobile model was more accurate in describing both the effluent breakthrough curves and the distribution profiles of the experimental columns (Figures 7.34-7.39, Table 7.6).

7.6 Relationship between estimated dispersion value from bromide data, and fit dispersion value in the mobile-immobile model

As the dispersion coefficient (D) was fit in the *E. Coli* mobile-immobile model using the value estimated from the bromide analysis as an initial estimate (Table 7.1), an attempt was made to find a relationship between the value of this parameter estimated through the bromide analysis, and the value fit within the mobile-immobile model. With the exception of column NCC, which seemed to have both an abnormally high bromide dispersion coefficient value compared to the other freeze-fractured columns (Table 7.1) and an oscillating bacterial breakthrough curve that tended to confuse the parameter

fitting algorithm (Figure 5.9 or 7.31), a simple power relationship between the estimated value from the bromide breakthrough analysis, and the optimized value in the mobile-immobile model was found using the equation:

$$D_{mim} = 0.15(D_{brom})^{-1}$$

Eqn 7.2

Where (D_{mim}) is the fit dispersion value in the mobile-immobile model and (D_{brom}) is the fit dispersion value in the bromide breakthrough analysis. The R^2 value for this correlation is 0.84, indicating a high degree of fit.

Table 7.1 - Bromide dispersivity values estimated from the CXTFIT equilibrium model simulation

Column label	Fit dispersion coefficient (relative height^2 / PV)	Retardation Factor	R^2
CCA	1.14	1	0.98
CCB	1.11	1	0.94
CCC	6.52×10^{-1}	1	0.77
CCD	2.92×10^{-1}	1	0.98
NCC	2.04	1	0.94
NCD	3.05×10^{-1}	1	0.93
NCE	1.11×10^{-1}	1	0.92
SnA	3.63×10^{-2}	1	0.95
SnB	8.67×10^{-2}	1	0.89
SSC	2.28×10^{-1}	1	0.96
SSD	5.08×10^{-1}	1	0.99
Silt S	4.97×10^{-1}	1	0.91
SP1	n/a		n/a
SP2	1.68×10^{-2}	1	0.98
SP3	1.74×10^{-2}	1	0.97
SSP1	4.38×10^{-2}	1	0.96
SSP2	8.32×10^{-2}	1	0.94
SSP3	1.84×10^{-1}	1	0.98

*bromide data for column SP1 was not measured

Table 7.2 –Estimated* *E. coli* transport parameters for the CXTFIT equilibrium model, and coefficients of determination when applied to the experimental data.

Column label	Estimated dispersion coefficient (relative height^2 / PV)	Estimated Retardation Factor	R^2
CCA	1.14	320.05	0.84
CCB	1.11	311.48	<-2
CCC	0.652	285.22	0.21
CCD	0.292	241	<-2
NCC	2.04	217.63	<-2
NCD	0.305	231.32	0.26
NCE	0.111	225.61	<-2
SnA	0.036	1.03	0.49
SnB	0.087	1.03	0.83
SSC	0.228	9.05	0.09
SSD	0.508	9.05	0.04
Silt S	0.497	59.87	0.32
SP1	0.017	1.03	0.9
SP2	0.017	1.03	0.86
SP3	0.017	1.03	0.94
SSP1	0.044	9.05	0.75
SSP2	0.083	9.05	<-2
SSP3	0.184	9.05	<-2

* Methodology for estimation of parameters described in section 6.4.4

Table 7.3 – Estimated* retardation factors contrasted with values optimized for the *E. coli* effluent measurements.

Column label	Estimated dispersion coefficient (relative height^2 / PV)	Estimated Retardation Factor	Optimized retardation factor	R^2 Optimized value	% difference**
CCA	1.140	320.05	378.00	0.93	18.11
CCB	1.110	311.48	404.00	0.73	29.70
CCC	0.652	285.22	218.00	0.73	-23.57
CCD	0.292	241	80.30	0.56	-66.68
NCC	2.040	217.63	338.00	0.00	55.31
NCD	0.305	231.32	228.00	0.24	-1.44
NCE	0.111	225.61	96.30	0.49	-57.32
SnA	0.036	1.03	1.54	0.91	49.51
SnB	0.087	1.03	1.28	0.91	24.27
SSC	2.28E-01	9.05	3.19	0.82	-64.75
SSD	5.08E-01	9.05	2.63	0.80	-70.94
Silt S	0.497	59.87	51.20	0.27	-14.48
SP1	0.017	1.03	1.11	0.92	7.77
SP2	0.017	1.03	1.14	0.89	10.68
SP3	0.017	1.03	1.04	0.94	0.97
SSP1	4.38E-02	9.05	8.17	0.46	-9.72
SSP2	8.32E-02	9.05	15.60	0.83	72.38
SSP3	1.84E-01	9.05	55.60	0.58	514.36

* Methodology for estimation of parameters described in section 6.4.4

**Percent difference between estimated and optimized value

Table 7.4 – Estimated* dispersion coefficients (Table 7.1) contrasted with values optimized for the *E. coli* effluent measurements

Column label	Estimated dispersion coefficient (relative height^2 / PV)	Estimated Retardation Factor	Optimized dispersion (relative height^2 / PV)	R^2 Optimized value	% difference**
CCA	1.14	320.05	0.900	0.93	-21.05
CCB	1.11	311.48	0.766	0.71	-30.99
CCC	0.652	285.22	1.050	0.70	61.04
CCD	0.292	241	4.720	0.47	1516.44
NCC	2.04	217.63	1.030	-0.08	-49.51
NCD	0.305	231.32	0.312	-0.24	2.30
NCE	0.111	225.61	0.442	-0.28	298.20
SnA	0.0363	1.03	1.160	0.73	3095.59
SnB	0.0867	1.03	0.247	0.85	184.89
SSC	0.228	9.05	1.125	0.23	393.42
SSD	0.508	9.05	1.570	0.11	209.06
Silt S	0.497	59.87	21.500	0.16	4225.96
SP1	0.017	1.03	0.021	0.91	23.53
SP2	0.0168	1.03	0.041	0.87	145.83
SP3	0.0174	1.03	0.057	0.94	224.71
SSP1	0.0438	9.05	0.063	-0.42	44.52
SSP2	0.0832	9.05	0.017	0.96	-79.69
SSP3	0.184	9.05	116.00	0.35	62943.48

* Methodology for estimation of parameters described in section 6.4.4

**Percent difference between estimated and optimized value

Table 7.5 - Decay coefficients (μ) fit to the experimental data using the predicted transport parameters (Table 7.2). These values were utilizes for the CXTFIT equilibrium transport model

Column label	Dispersion coefficient (relative height^2 / PV)	Estimated Retardation Factor	μ (PV^{-1})	R^2
CCA	1.14	320.05	11.8	0.92
CCB	1.11	311.48	16.1	0.76
CCC	0.652	285.22	0	0.22
CCD	0.292	241	0	0.00
NCC	2.04	217.63	23	0.18
NCD	0.305	231.32	2.05×10^{-5}	-0.26
NCE	0.111	225.61	0	<-2
SnA	0.0363	1.03	0.304	0.75
SnB	0.0867	1.03	0.109	0.86
SSC	0.228	9.05	2.18×10^{-6}	0.09
SSD	0.508	9.05	1.55×10^{-6}	0.04
Silt S	0.497	59.87	0.413	-0.29
SP1	0.017	1.03	6.38×10^{-2}	0.91
SP2	0.0168	1.03	0.142	0.90
SP3	0.0174	1.03	0.10	0.97
SSP1	0.0438	9.05	2.72×10^{-7}	-0.69
SSP2	0.0832	9.05	8.19	0.47
SSP3	0.184	9.05	2.37	0.37

Table 7.6 – Mobile immobile transport parameters and resulting coefficients of determination when compared to the original data set.

Column label	Fit dispersion coefficient (relative height^2 / PV)	Estimated Retardation Factor	μ (PV^{-1})	β	R^2
CCA	0.144	32005	7.06	0.0023	0.93
CCB	0.176	31148	8.96	0.0026	0.77
CCC	0.138	28522	0	0.0036	0.80
CCD	0.373	24100	0.388	0.0030	0.56
NCC	0.419	21763	13.1	0.0027	0.21
NCD	0.893	23132	35.2	0.0045	0.15
NCE	1.31	22561	44.1	0.0038	0.18

Table 7.7 - Distribution coefficient (K_d) values (Mg/m^3) for the Geostudio model simulation inputs

Column label	K_d (Mg/m^3)
CCA	114.3
CCB	114.3
CCC	114.3
CCD	114.3
NCC	114.3
NCD	114.3
NCE	114.3
SnA	0.006
SnB	0.007
SSC	1.325
SSD	1.324
Silt S	9.851
SP1	0.005
SP2	0.006
SP3	0.006
SSP1	1.277
SSP2	1.306
SSP3	1.235

Table 7.8 - Geostudio model inputs* for *E. coli* transport modeling

Column label	Longitudinal Dispersion (m)	Hydraulic conductivity (m/s)	Decay half life ($t_{1/2}$) (s)	column height (m)	head (m)	porosity	Dry density (Mg/m^3)	R^2 No decay ($t_{1/2}$ = 0)	R^2 with decay
CCA	7.67×10^{-2}	2.513×10^{-8}	4103	0.0673	1.62	0.496	1.39	<-2	<-2
CCB	8.15×10^{-2}	3.288×10^{-8}	2724	0.0734	1.62	0.503	1.37	<-2	<-2
CCC	5.27×10^{-2}	9.298×10^{-8}	0	0.0809	1.55	0.525	1.31	<-2	n/a
CCD	2.47×10^{-2}	5.481×10^{-8}	0	0.0845	1.55	0.567	1.19	<-2	n/a
NCC	2.74×10^{-1}	4.357×10^{-8}	6855	0.134	1.62	0.592	1.12	<-2	<-2
NCD	3.41×10^{-2}	1.810×10^{-7}	0	0.112	1.51	0.577	1.16	<-2	n/a
NCE	1.39×10^{-2}	1.150×10^{-7}	0	0.125	1.5	0.583	1.15	<-2	n/a
SnA	5.26×10^{-3}	1.176×10^{-5}	780	0.145	1.62	0.334	1.76	0.40	0.71
SnB	1.26×10^{-2}	5.115×10^{-5}	789	0.145	1.62	0.367	1.68	0.79	0.83
SSC	3.08×10^{-2}	2.022×10^{-6}	0	0.135	1.62	0.304	1.85	0.54	n/a
SSD	6.86×10^{-2}	1.841×10^{-6}	0	0.135	1.62	0.304	1.85	0.81	n/a
Silt S	5.07×10^{-2}	1.627×10^{-8}	0	0.102	1.58	0.311	1.86	-0.82	n/a
SP1	2.07×10^{-3}	4.442×10^{-5}	809	0.122	1.58	0.318	1.81	0.80	0.81
SP2	2.07×10^{-3}	5.712×10^{-5}	286	0.123	1.58	0.329	1.78	0.78	0.81
SP3	2.35×10^{-3}	4.929×10^{-5}	545	0.135	1.58	0.329	1.78	0.71	0.78
SSP1	5.83×10^{-3}	3.792×10^{-6}	0	0.133	1.58	0.297	1.87	<-2	n/a
SSP2	9.40×10^{-3}	3.461×10^{-6}	80	0.113	1.58	0.302	1.86	<-2	<-2
SSP3	2.21×10^{-2}	4.654×10^{-6}	171	0.12	1.58	0.290	1.89	<-2	<-2

*Parameter estimation methods summarized in section 6.5.1

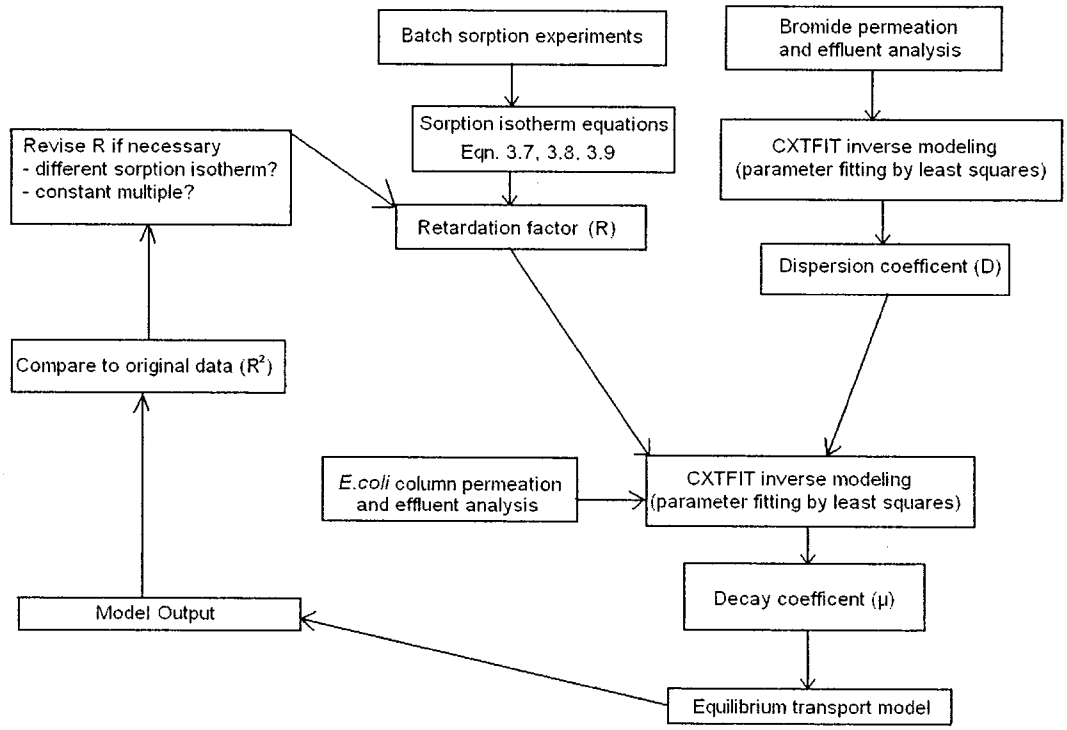

Figure 7.1 – Flowchart overview of the CXTFIT equilibrium transport model and related data sources.

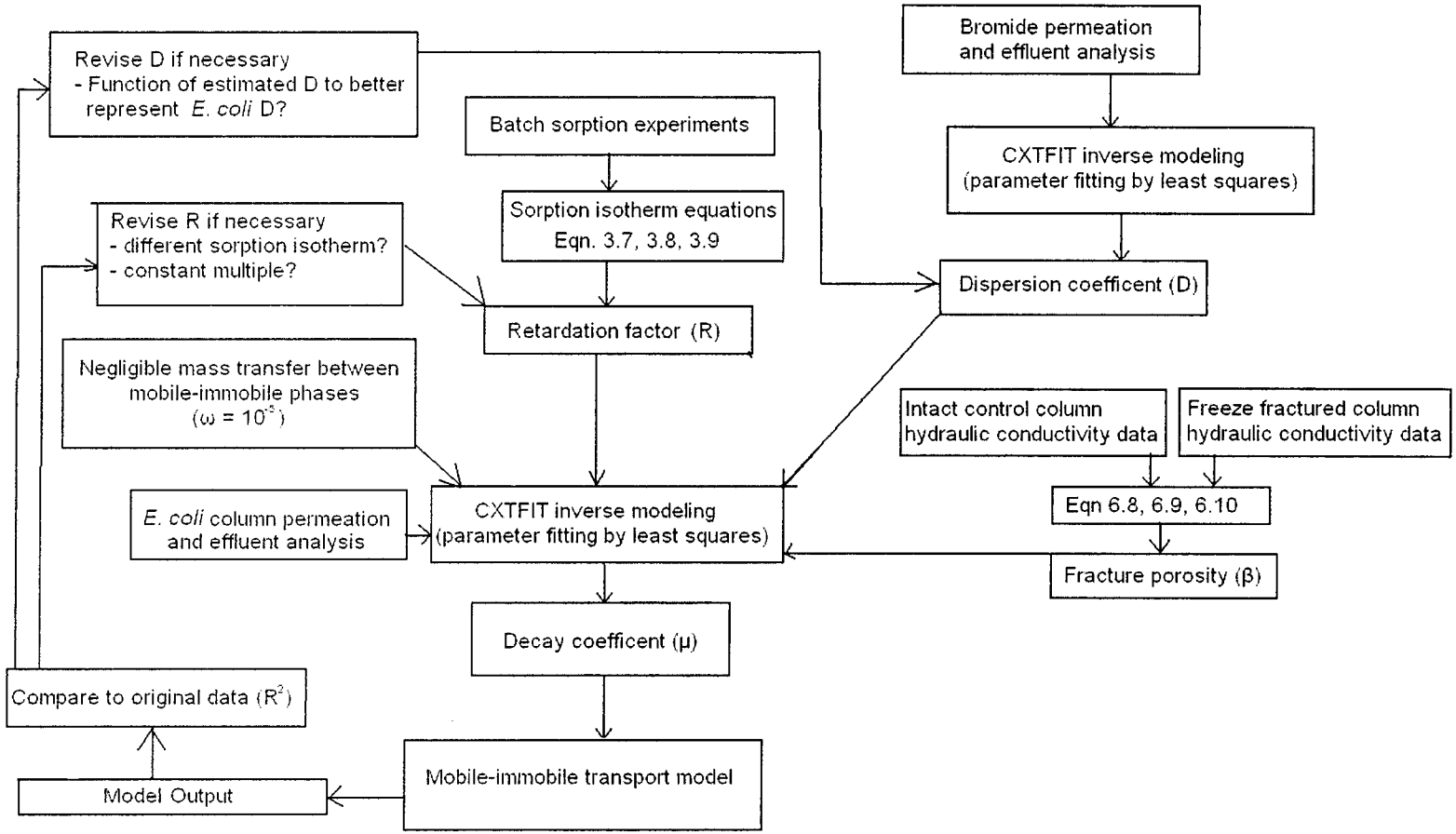

Figure 7.2 – Flowchart overview of the CXTFIT mobile-immobile transport model and related data sources.

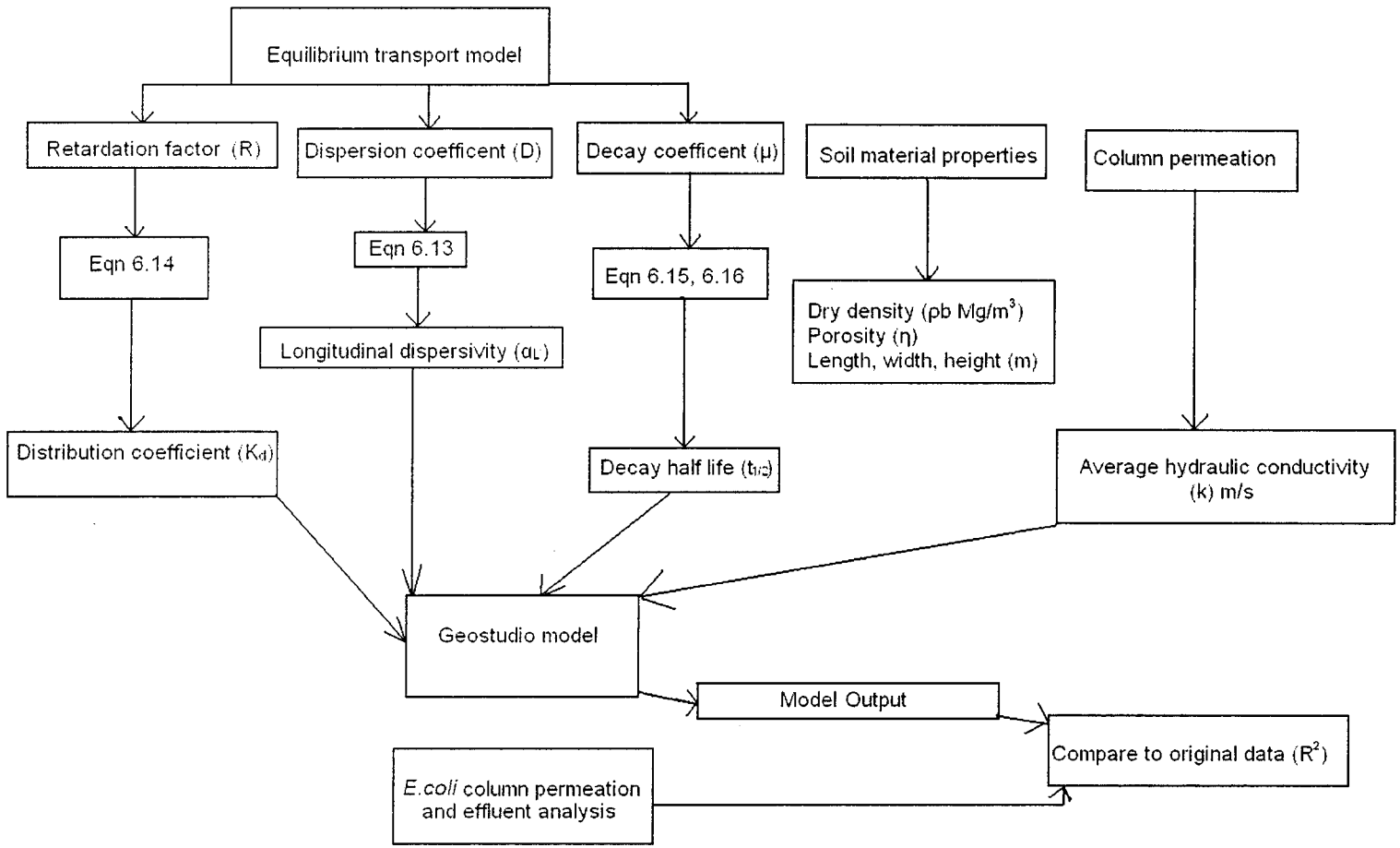

Figure 7.3 – Flowchart overview of the Geostudio equilibrium transport model and related data sources.

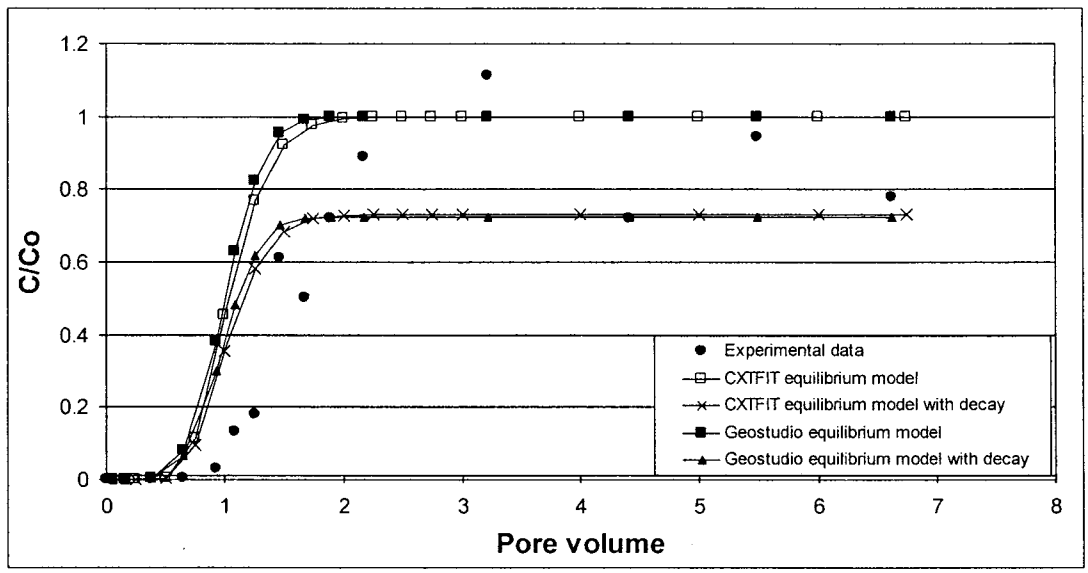

Figure 7.4 – Column SnA *E. coli* effluent measurements and corresponding models.

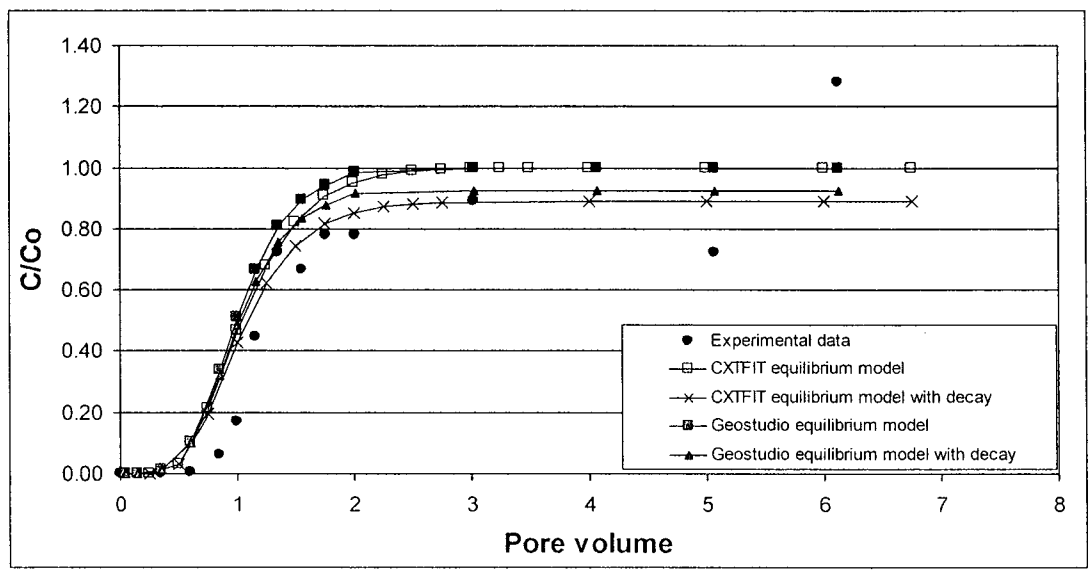

Figure 7.5 – Column SnB *E. coli* effluent measurements and corresponding models.

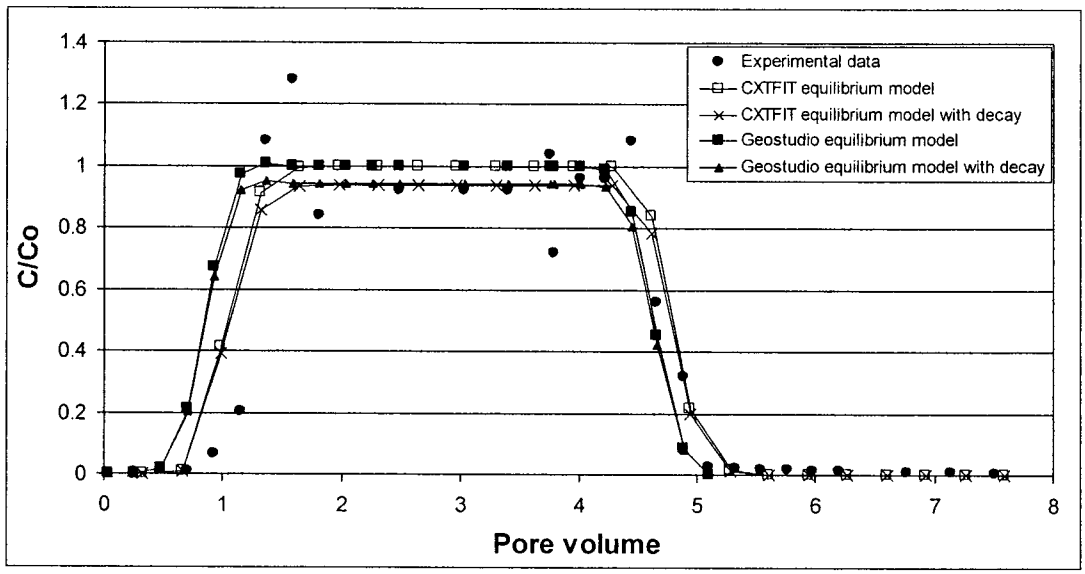

Figure 7.6 – Column SP1 *E. coli* effluent measurements and corresponding models.

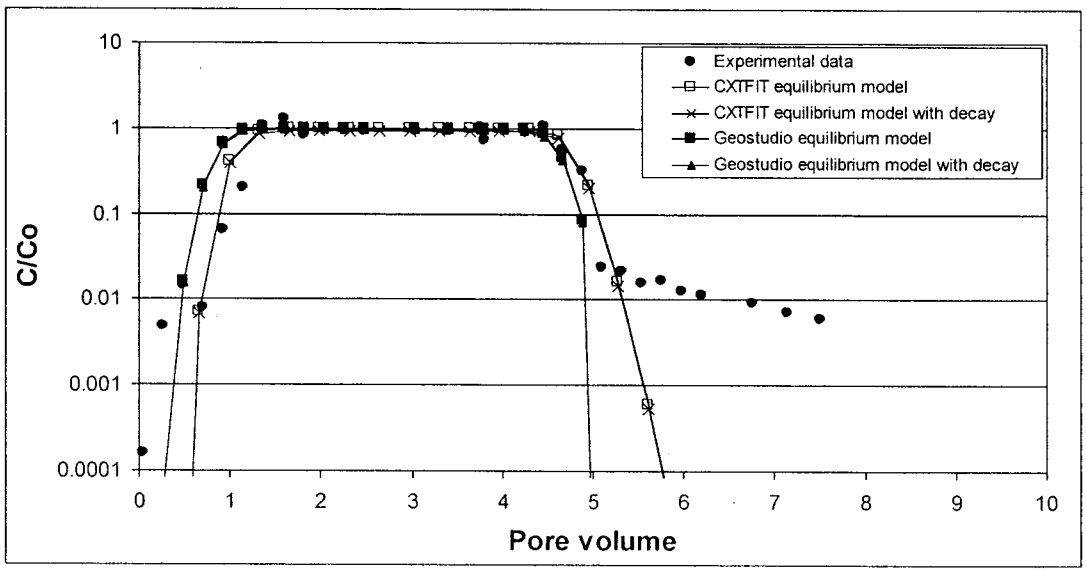

Figure 7.7 – Column SP1 *E. coli* effluent measurements and corresponding models - Log C/Co axis.

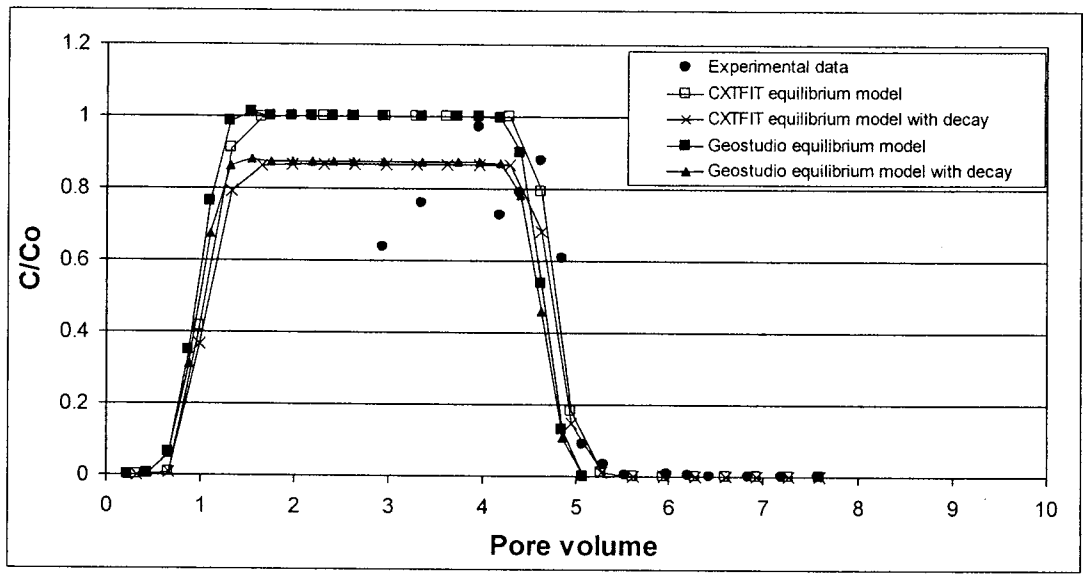

Figure 7.8 – Column SP2 *E. coli* effluent measurements and corresponding models.

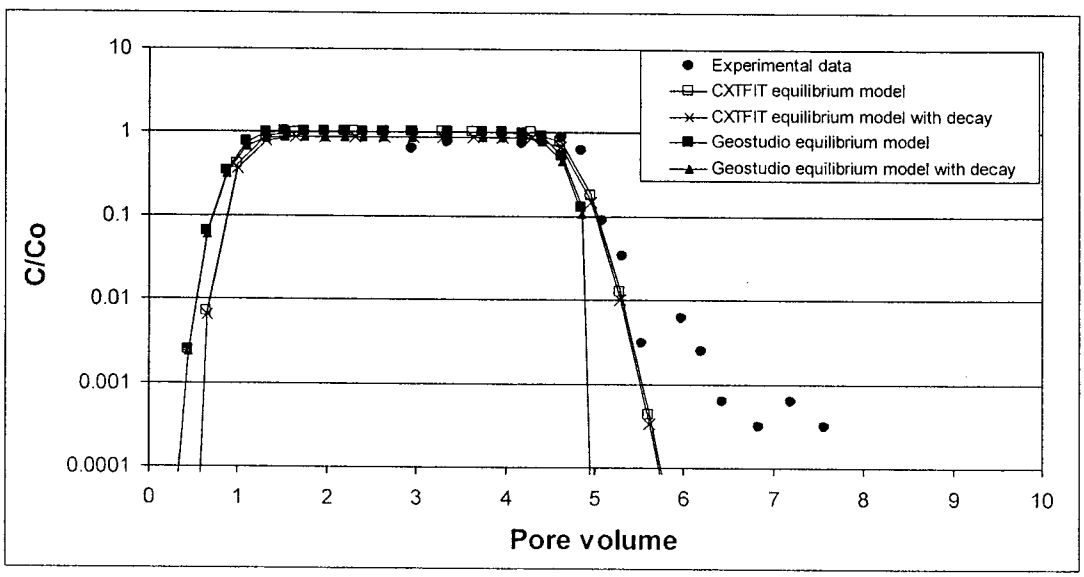

Figure 7.9 – Column SP2 *E. coli* effluent measurements and corresponding models - Log C/Co axis.

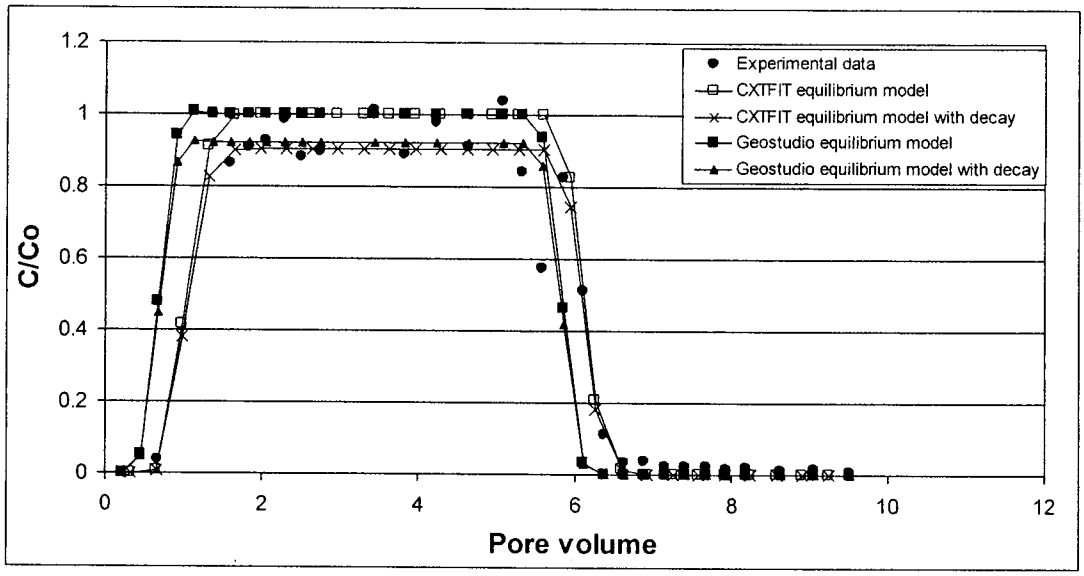

Figure 7.10 – Column SP3 *E. coli* effluent measurements and corresponding models.

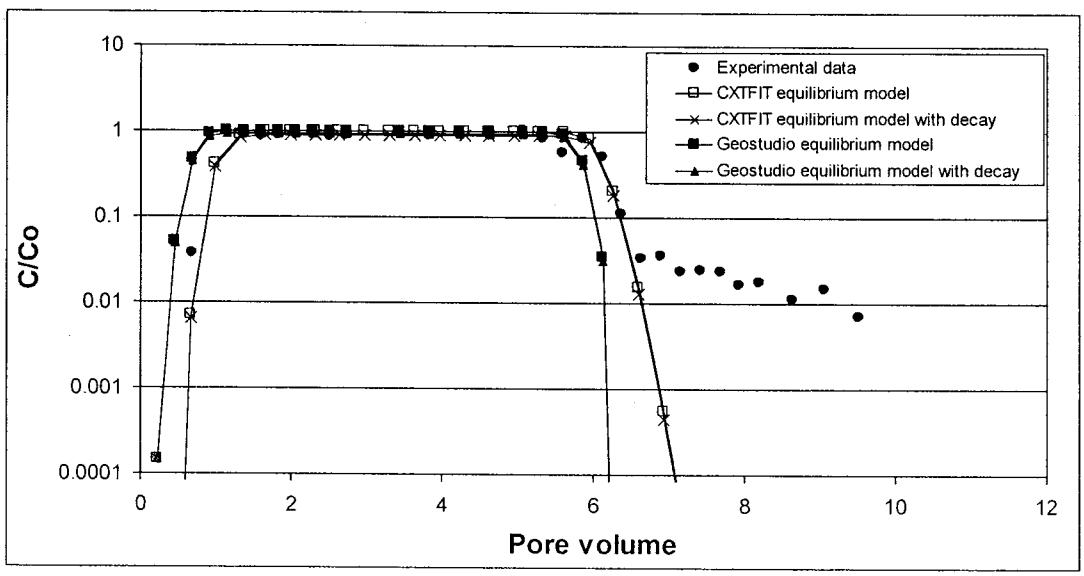

Figure 7.11 – Column SP3 *E. coli* effluent measurements and corresponding models - Log C/Co axis.

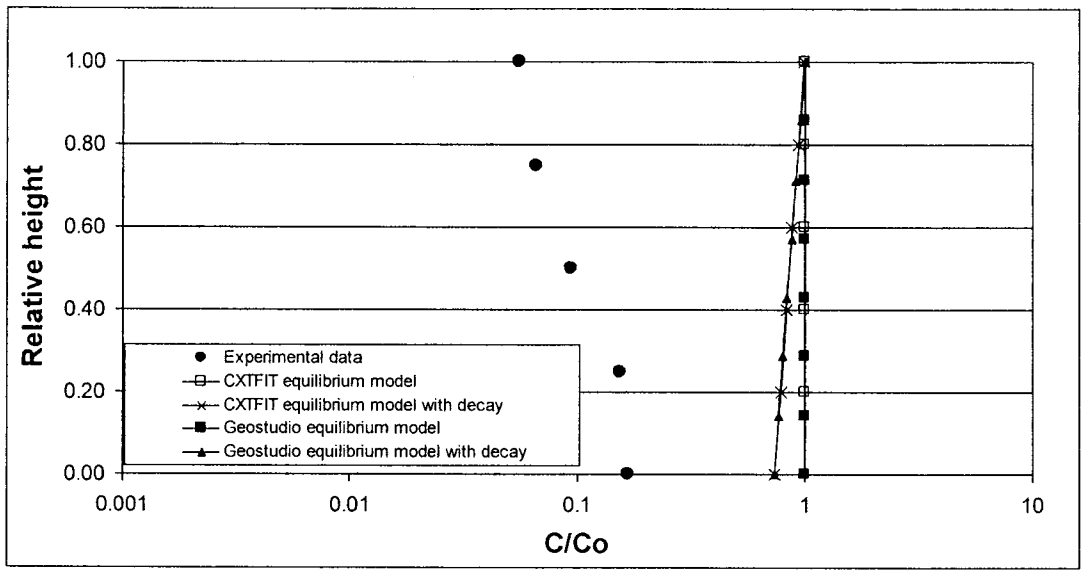

Figure 7.12 – Column SnA *E. coli* distribution profile measurements and corresponding models.

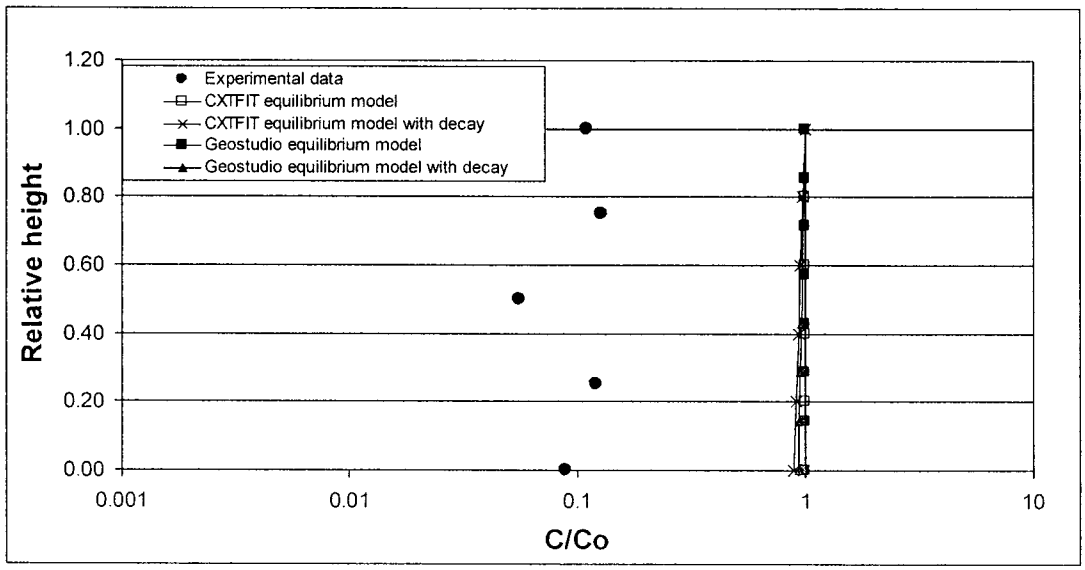

Figure 7.13 – Column SnB *E. coli* distribution profile measurements and corresponding models.

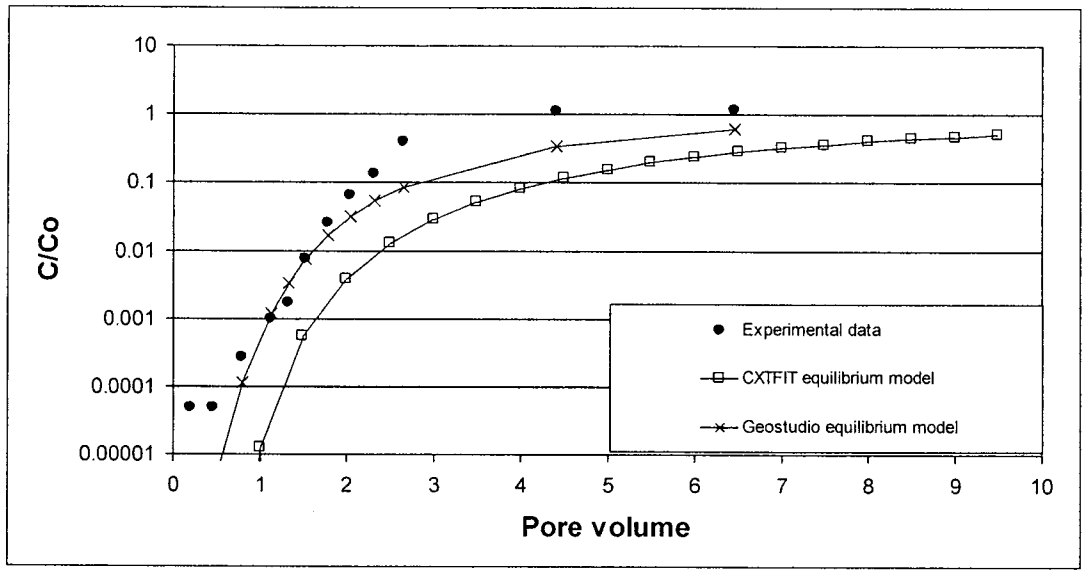

Figure 7.14 – Column SSC *E. coli* effluent measurements and corresponding models.

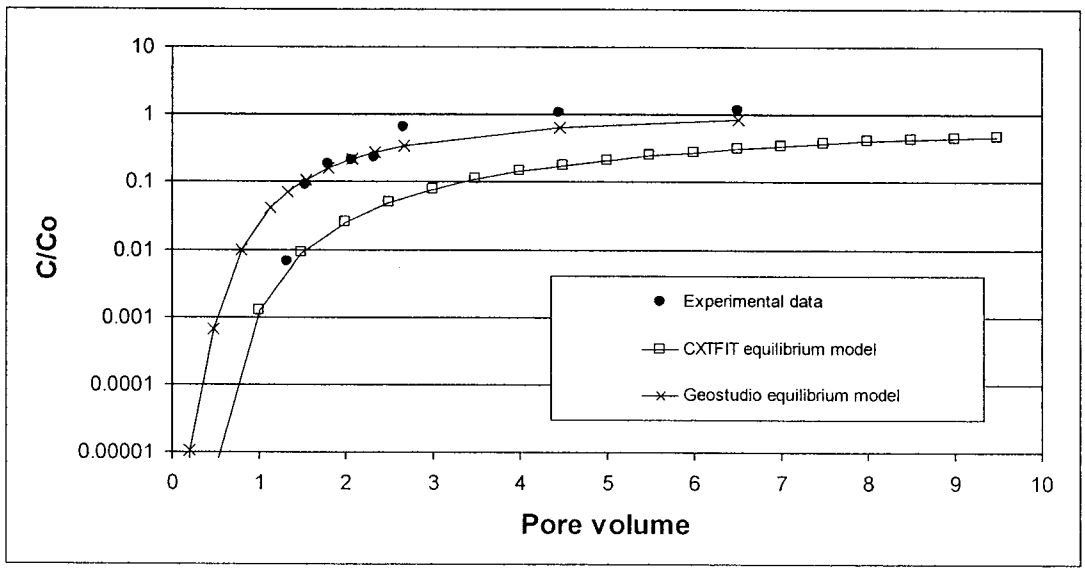

Figure 7.15 – Column SSD *E. coli* effluent measurements and corresponding models.

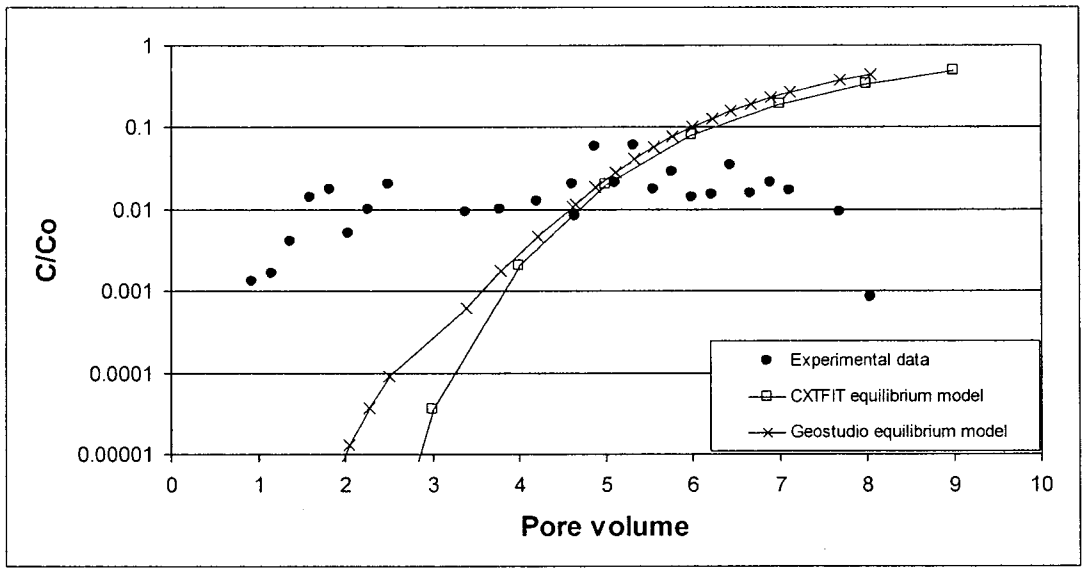

Figure 7.16 – Column SSP1 *E. coli* effluent measurements and corresponding models.

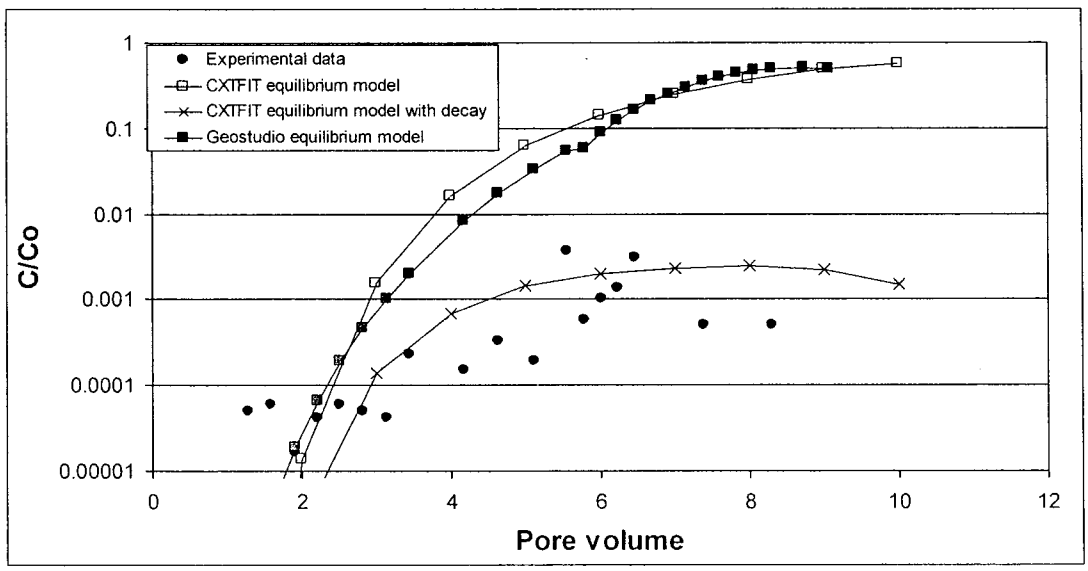

Figure 7.17 – Column SSP2 *E. coli* effluent measurements and corresponding models.

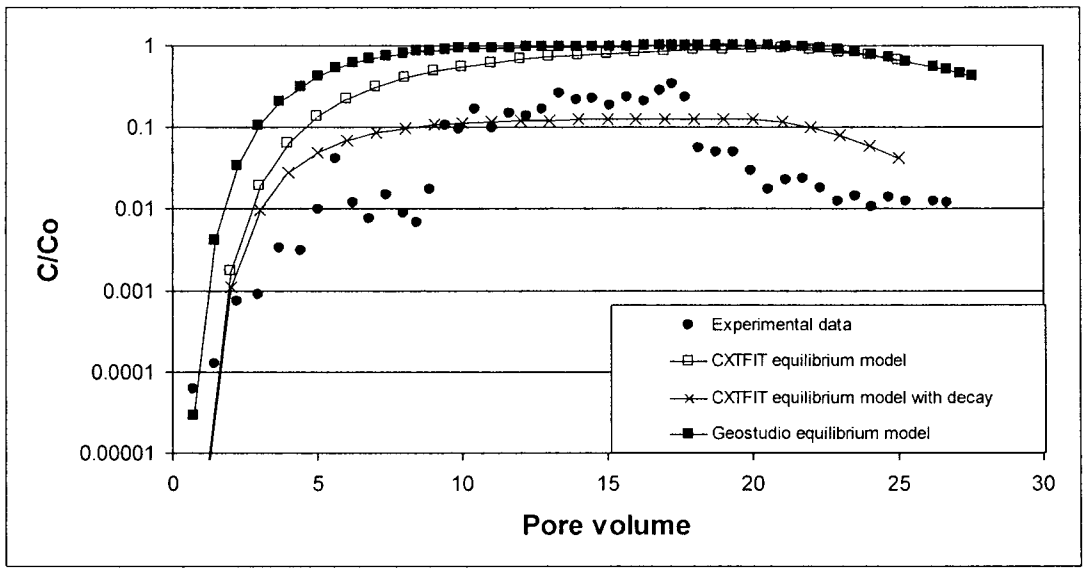

Figure 7.18 – Column SSP3 *E. coli* effluent measurements and corresponding models.

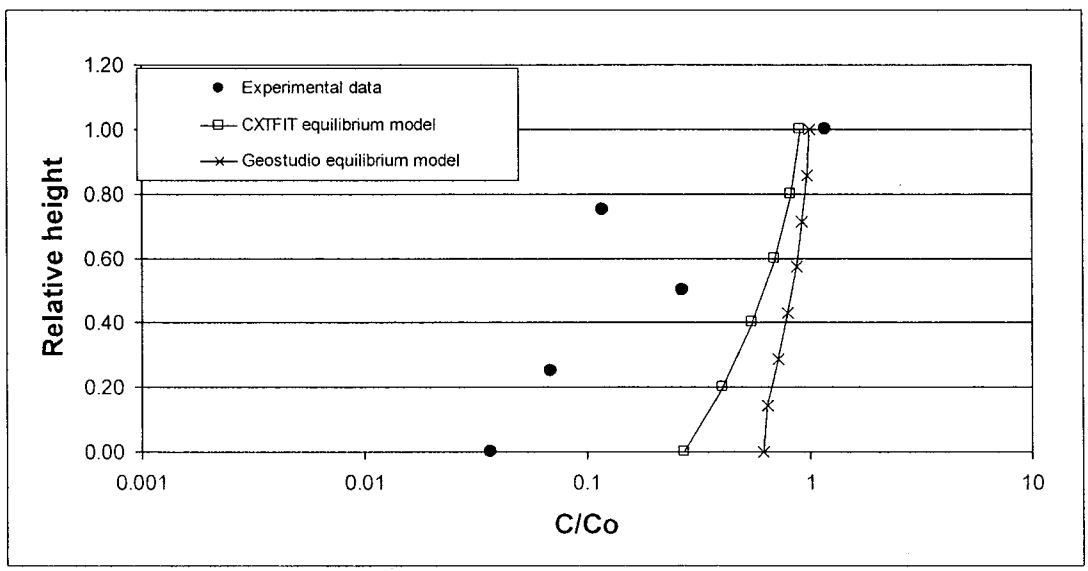

Figure 7.19 – Column SSC *E. coli* distribution profile measurements and corresponding models.

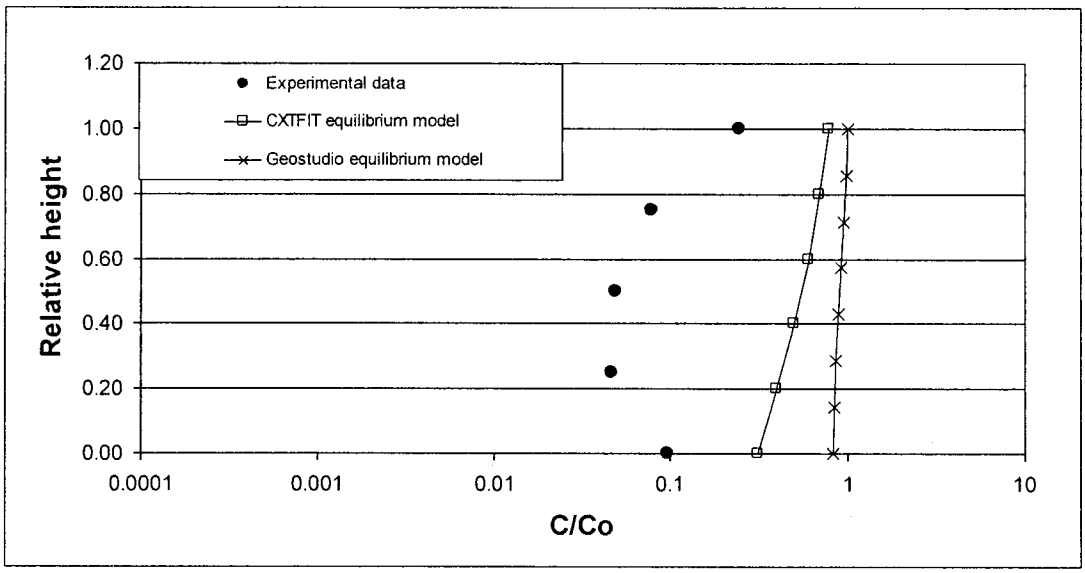

Figure 7.20 – Column SSD *E. coli* distribution profile measurements and corresponding models.

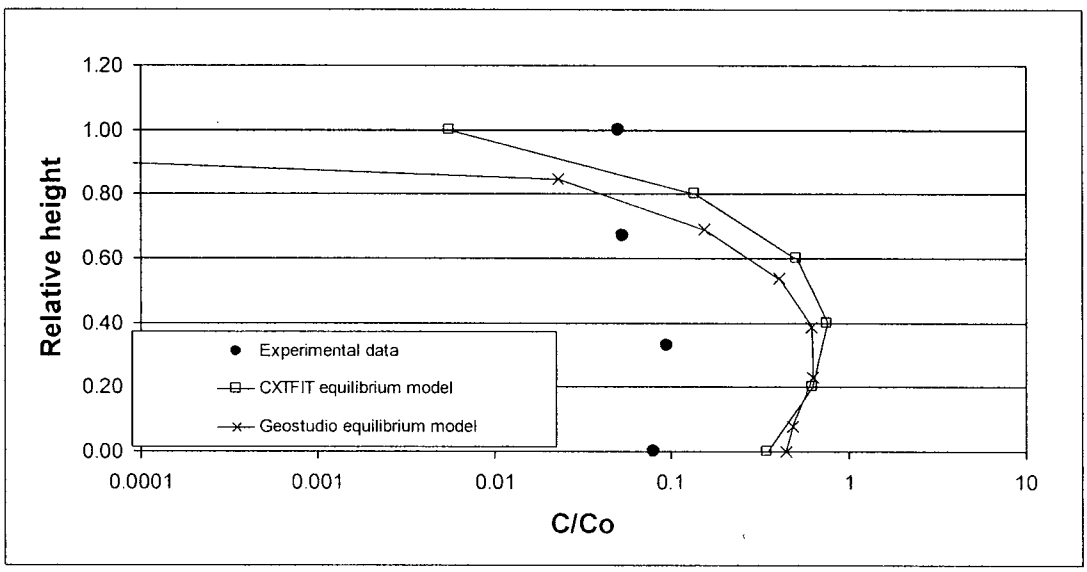

Figure 7.21 – Column SSP1 *E. coli* distribution profile measurements and corresponding models.

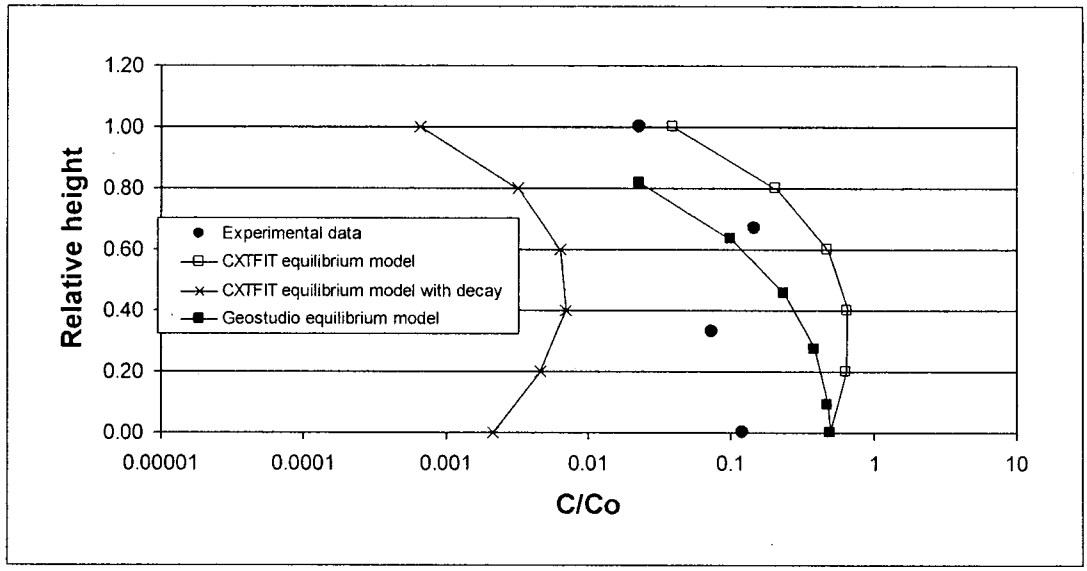

Figure 7.22 – Column SSP2 *E. coli* distribution profile measurements and corresponding models.

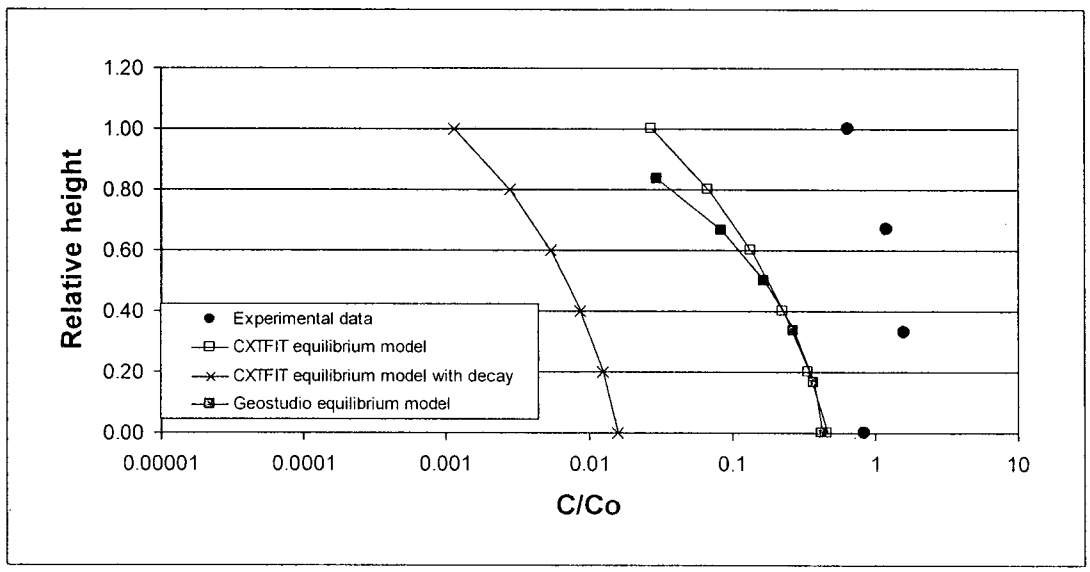

Figure 7.23 – Column SSP3 *E. coli* distribution profile measurements and corresponding models.

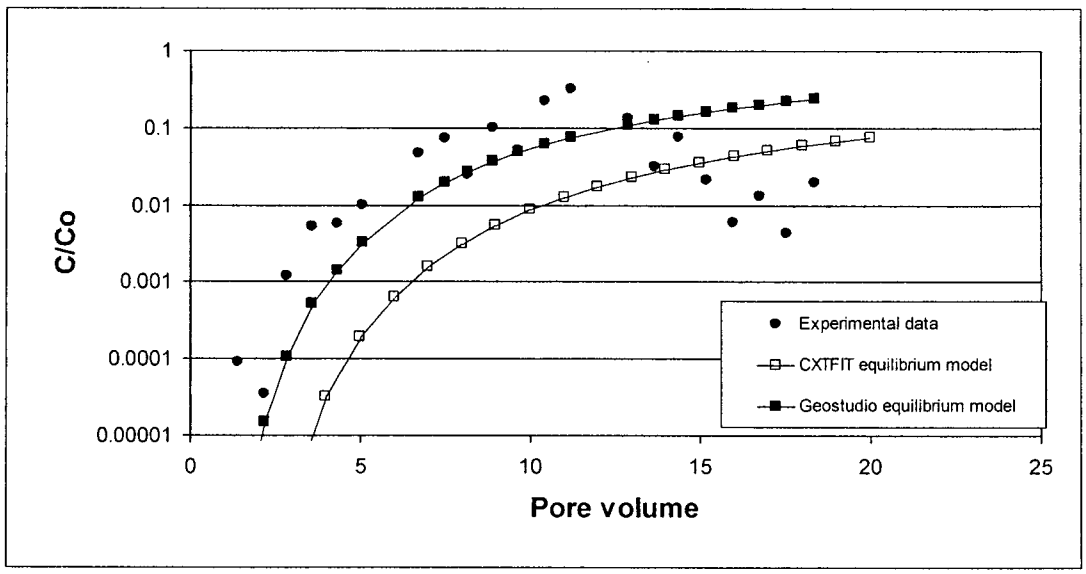

Figure 7.24 – Column Silt S *E. coli* effluent measurements and corresponding models.

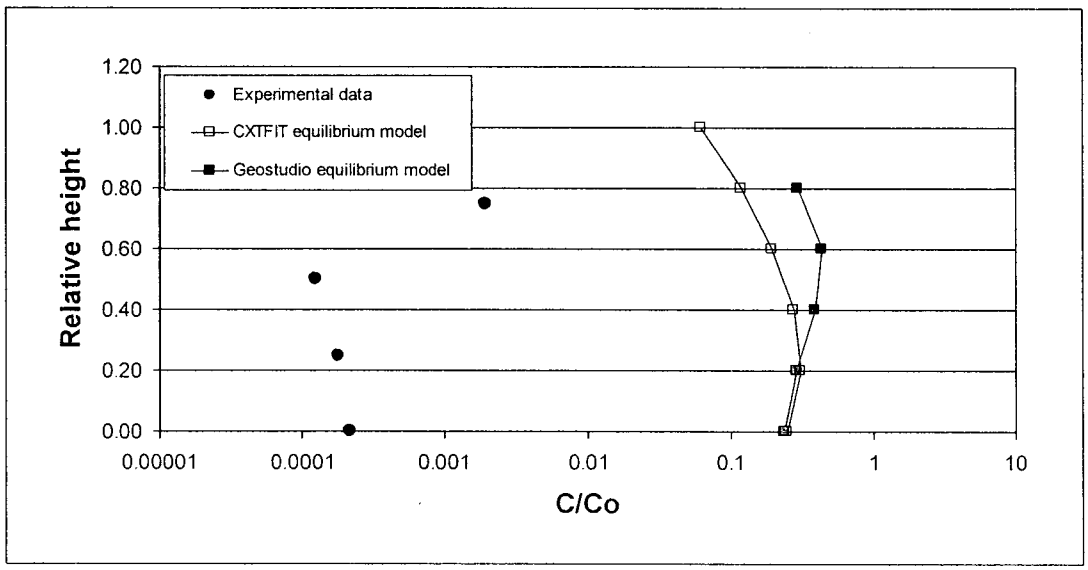

Figure 7.25 – Column Silt S *E. coli* distribution profile measurements and corresponding models.

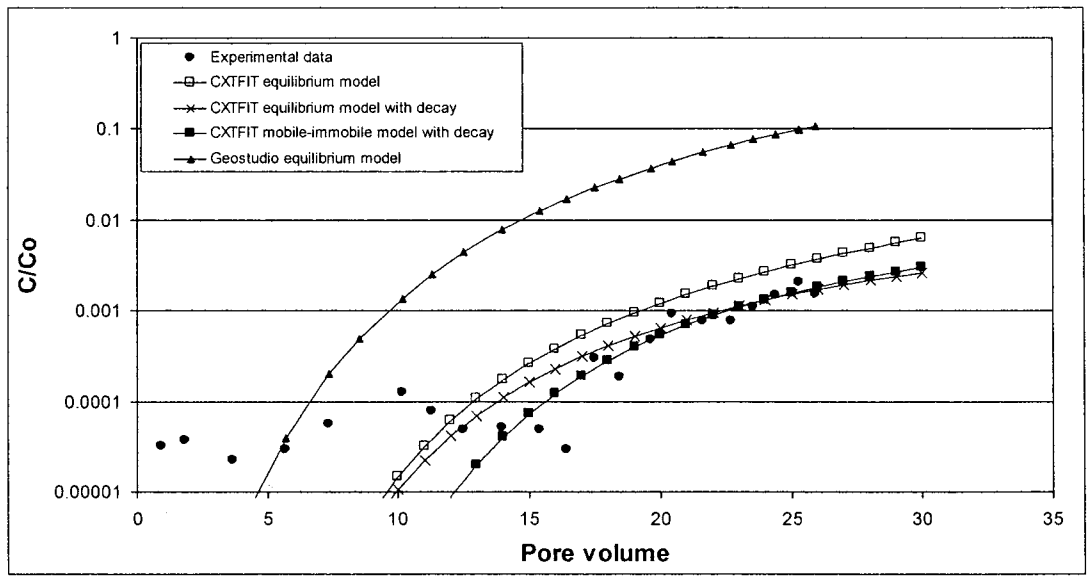

Figure 7.26 – Column CCA *E. coli* effluent measurements and corresponding models.

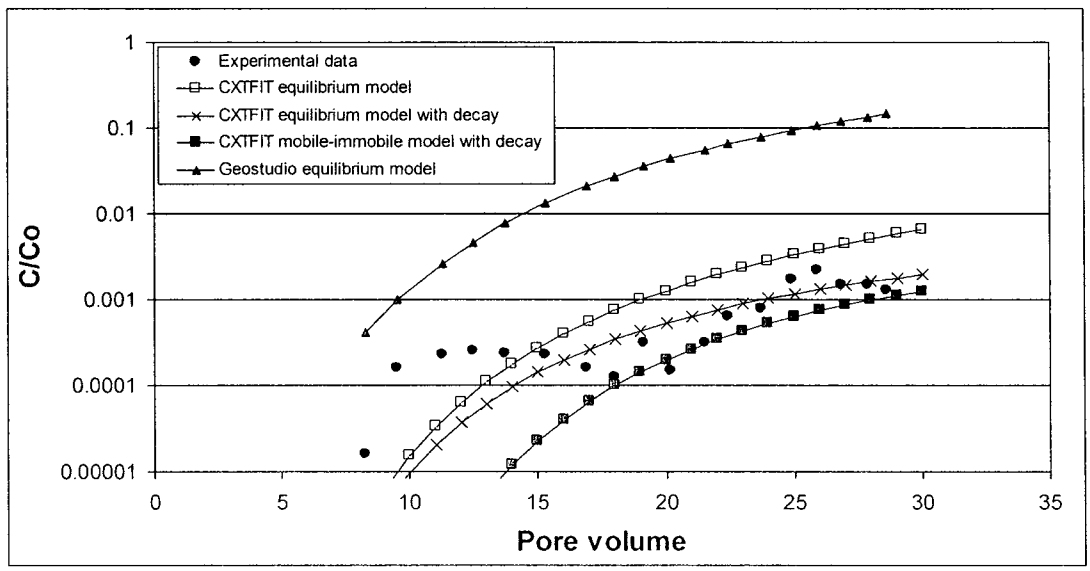

Figure 7.27 – Column CCB *E. coli* effluent measurements and corresponding models.

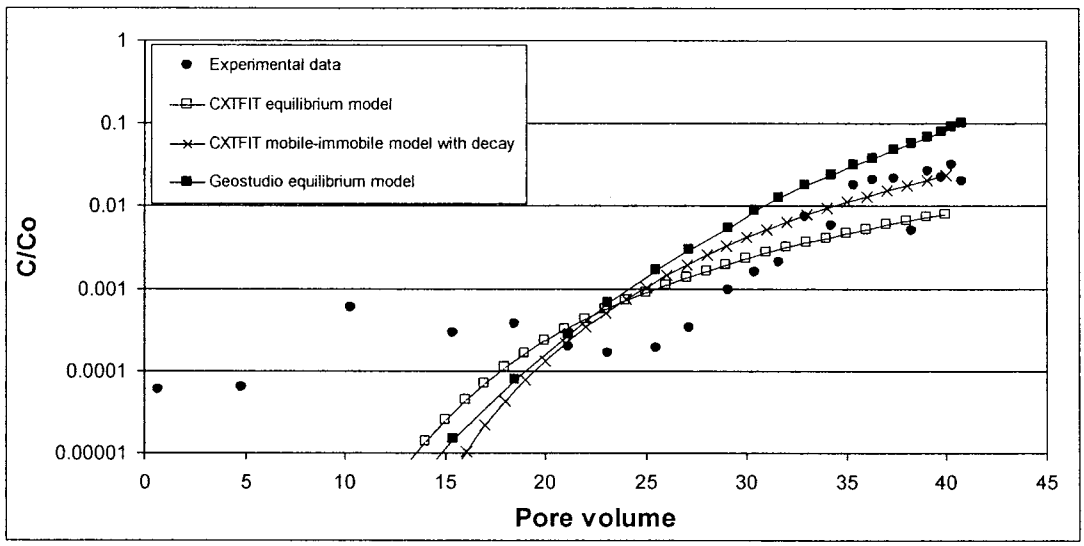

Figure 7.28 – Column CCC *E. coli* effluent measurements and corresponding models.

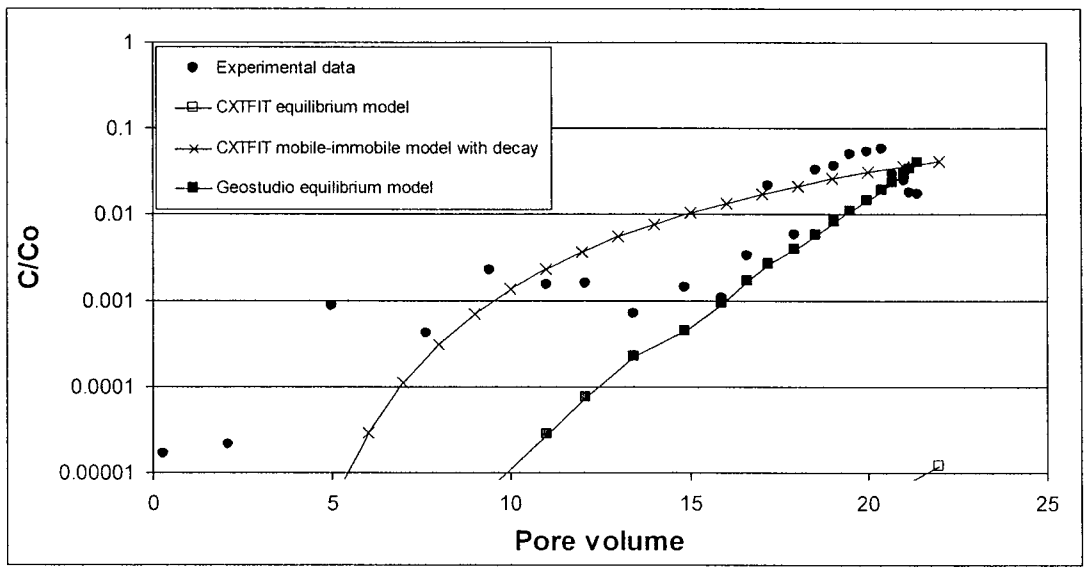

Figure 7.29 – Column CCD *E. coli* effluent measurements and corresponding models.

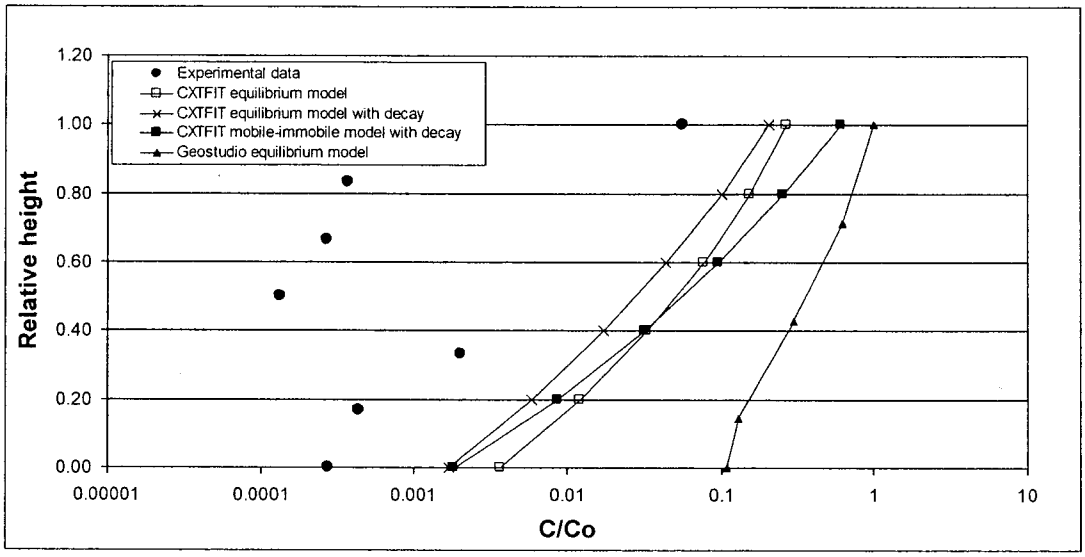

Figure 7.30 – Column CCA *E. coli* distribution profile measurements and corresponding models.

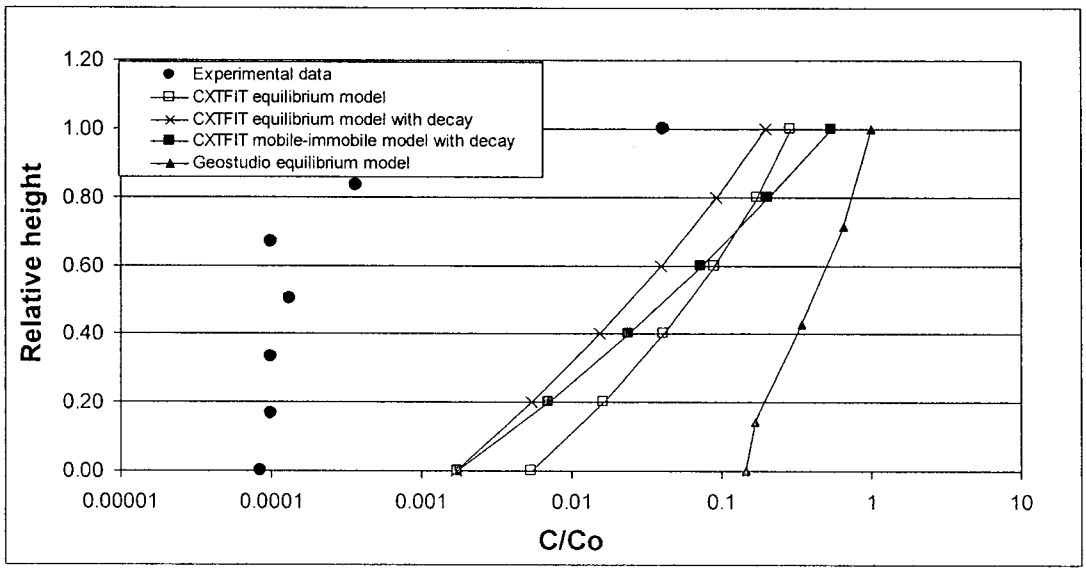

Figure 7.31 – Column CCB *E. coli* distribution profile measurements and corresponding models.

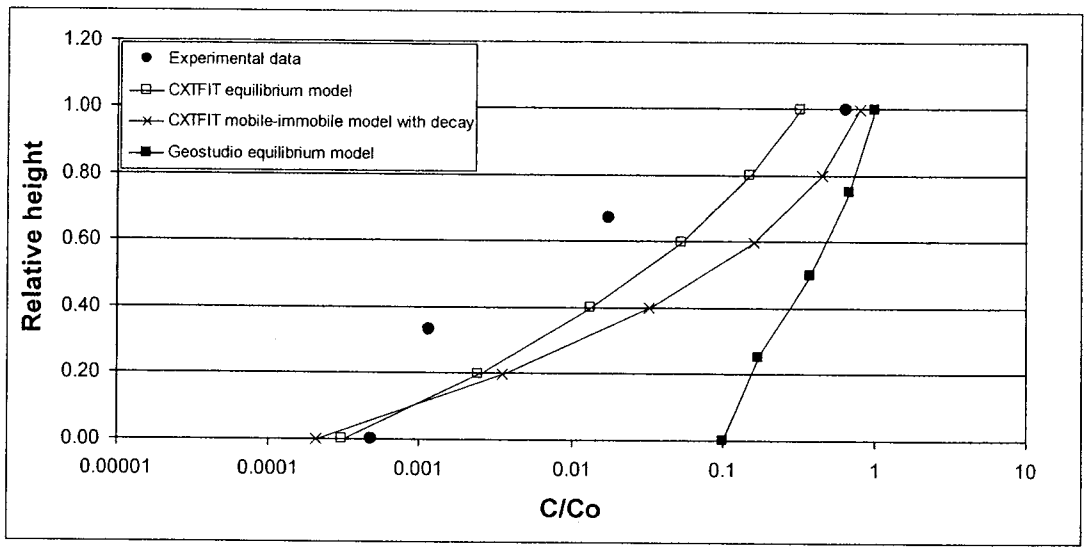

Figure 7.32 – Column CCC *E. coli* distribution profile measurements and corresponding models.

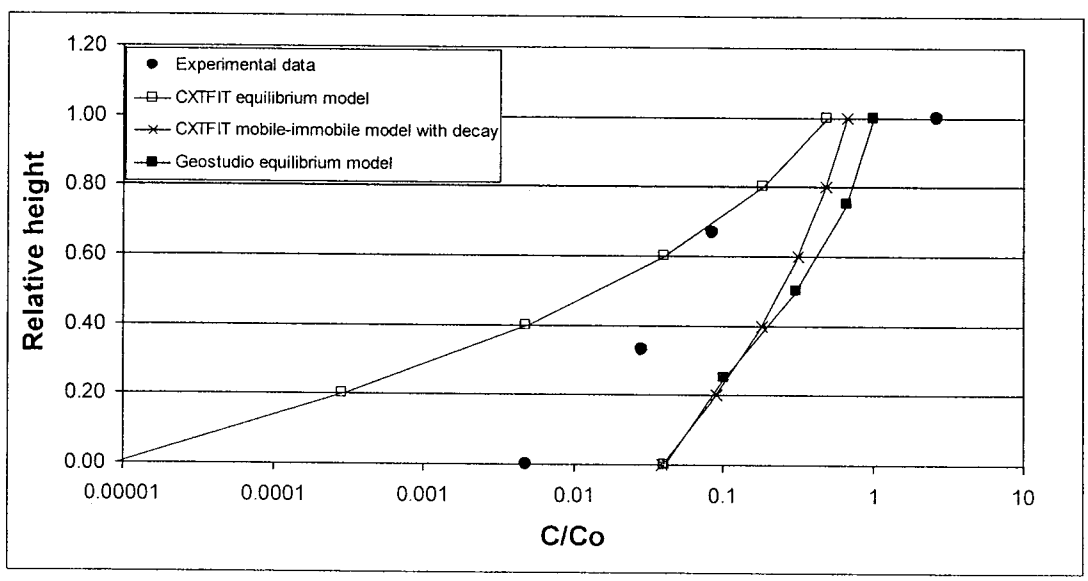

Figure 7.33 – Column CCD *E. coli* distribution profile measurements and corresponding models.

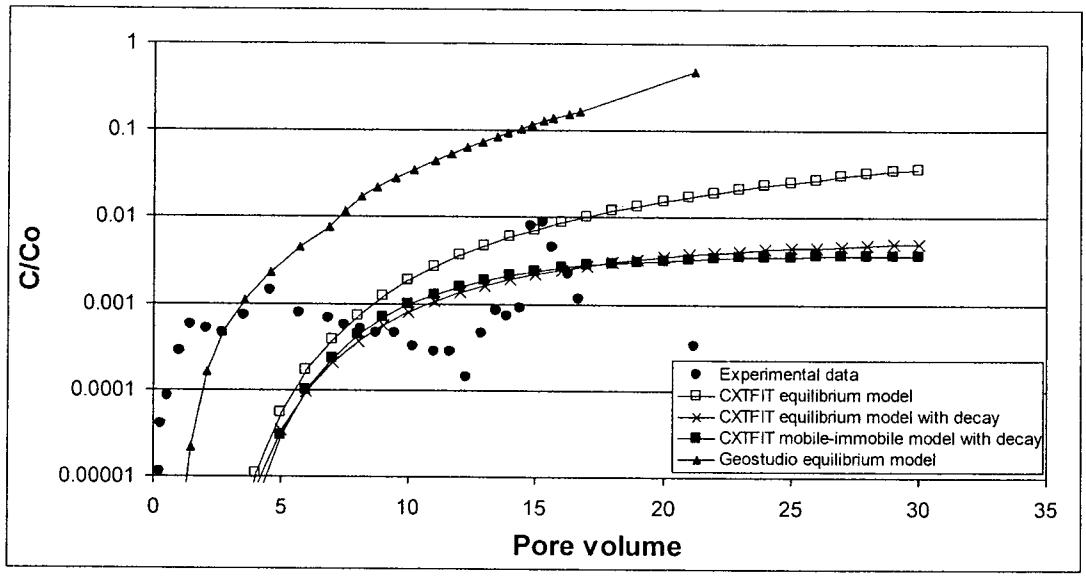

Figure 7.34 – Column NCC *E. coli* effluent measurements and corresponding models.

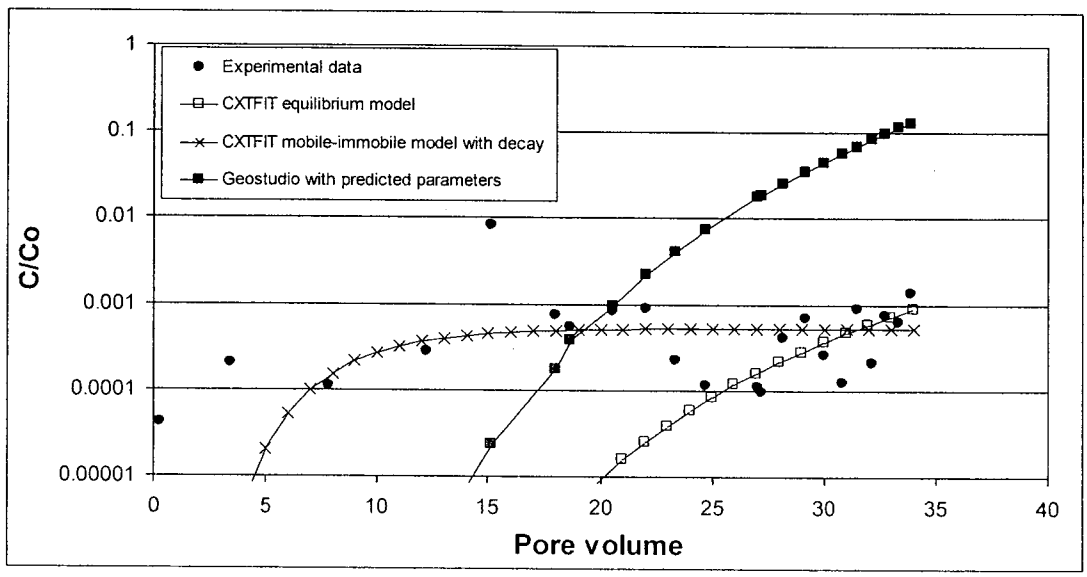

Figure 7.35 – Column NCD *E. coli* effluent measurements and corresponding models.

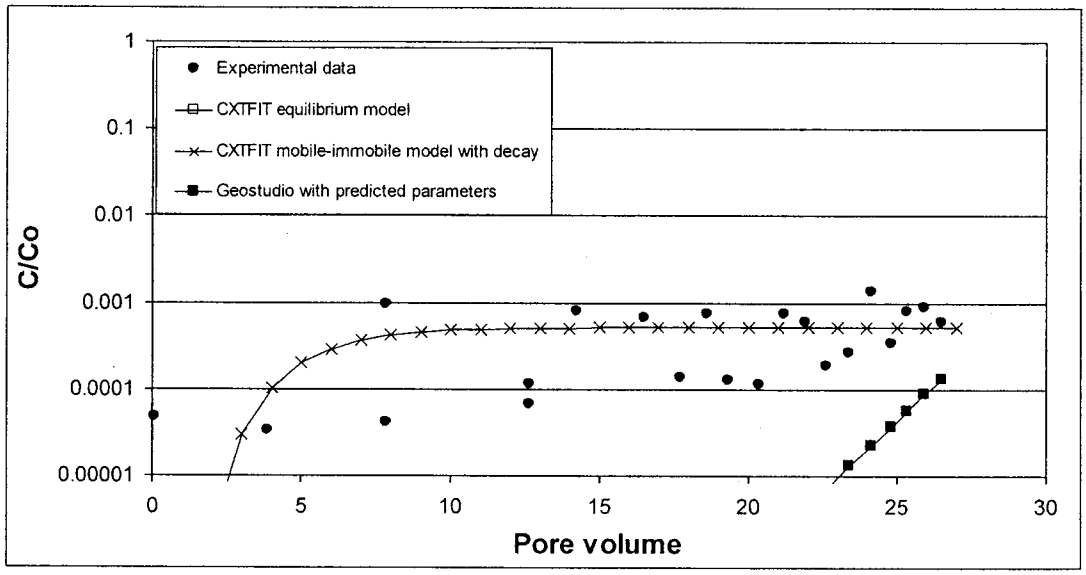

Figure 7.36 – Column NCE *E. coli* effluent measurements and corresponding models.

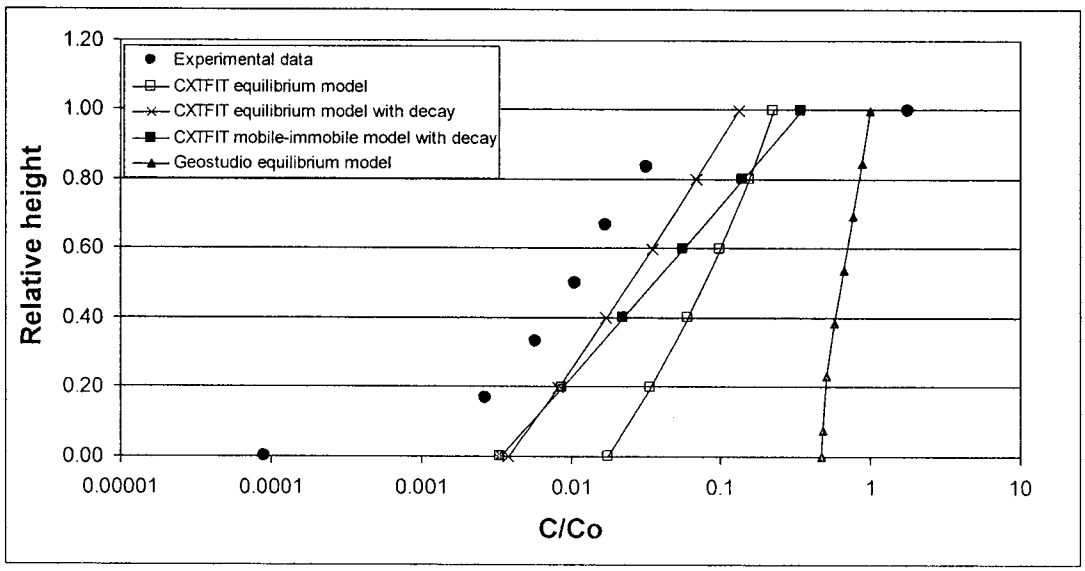

Figure 7.37 – Column NCC *E. coli* distribution profile measurements and corresponding models.

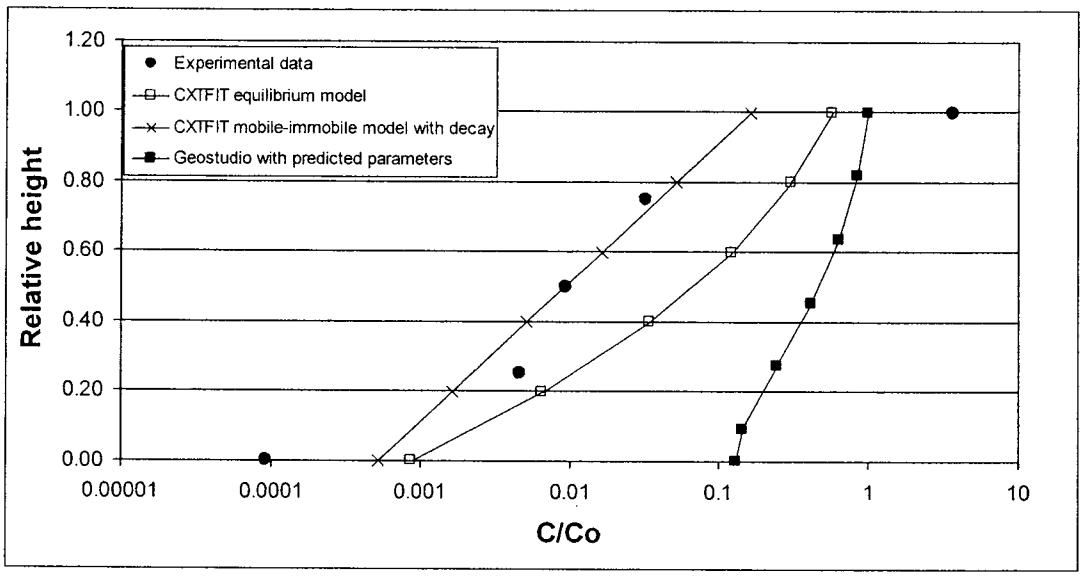

Figure 7.38 – Column NCD *E. coli* distribution profile measurements and corresponding models.

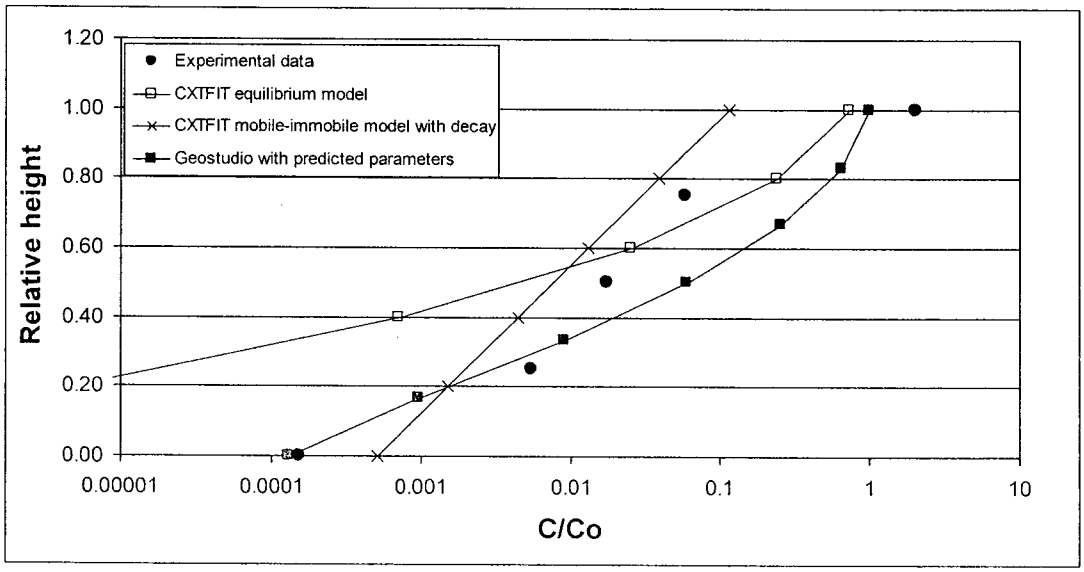

Figure 7.39 – Column NCE *E. coli* distribution profile measurements and corresponding models.

Chapter 8 - Discussion

8.1 Applicability of models

During the course of this study, it became apparent that the dimensionless transport parameters used in the CXTFIT equilibrium model did not typically convert well into the dimensional format used by Geostudio. The reason for this is unknown, though it may be due to the inclusion of the hydraulic conductivity parameters which are not considered by the CXTFIT model. The exceptions to this trend were the compacted sand columns; both the CXTFIT and Geostudio simulations fix the observed data well. In general, Geostudio tended to produce earlier breakthrough curves than CXTFIT for the remaining column sets when decay was not considered. Incorporating the dimensionless decay coefficient from CXTFIT into Geostudio was only effective in the sand columns. When used to model the other column materials, the Geostudio models predicted no *E. coli* breakthrough within the time frames used during the experimental periods. In general, the coefficients of determination for the Geostudio models were lower than those of the CXTFIT models.

8.1.1 Applicability of models – compacted sands

For the sand columns, the equilibrium model of both CXTFIT and Geostudio reasonably simulated both the observed *E. coli* effluent concentrations and peak C/Co of the observed columns. The models did not reasonably simulate the tailing region of the measured *E. coli* effluent profile following a pulse with MSM solution, or the measured *E. coli* distribution profile data from the soil column post test. The simulations suggested that the *E. coli* would desorb or leave the system at a higher rate than was observed in the actual column tests. This suggests that a kinetic sorption term is required in modelling bacterial transport through these soils to account for the fraction of bacteria that desorb at a slower rate than simulated by a purely equilibrium sorption theory. Trial modeling attempts with CXTFIT using a two-site chemical non-equilibrium model were more successful than the equilibrium model at simulating the measured effluent concentrations within the tailing region. Because the available data does not allow the estimation or fitting of kinetic transport parameters outside of the pulse experiments (described in section 3.4), this model is of limited application to the data sets containing data from the head region of an effluent breakthrough curve only.

The modelled distribution profiles differed substantially from the measured profiles. Within the continuous source columns (SnA and SnB) the measured bacterial soil concentrations were approximately one order of magnitude lower than the simulated concentrations. For the pulse experiments (Sp1, Sp2, Sp3) all models predicted zero bacteria remaining in the columns following the application of the MSM pulse, in contrast to the experimental columns where relative *E. coli* (C/C_0) concentrations of

0.0006-0.02 were observed. This discrepancy is likely a limitation of the entirely reversible sorption assumed in the equilibrium model. Limitations in applying the equilibrium transport theory to the tailing region of an effluent curve have also been reported in other studies (Dong *et al*, 2002).

The use of a calculated retardation factor from the batch sorption data is questionable in these soils. Using a Freundlich sorption isotherm model to analyses the batch sorption data gave a retardation factor of 9.75, approximately one order of magnitude higher than suggested by the Langmuir model and by the column test results. Other studies have observed bacterial breakthrough before that of a conservative tracer in sand or mixed columns (Jiang *et al*, 2007, Dong *et al*, 2002, Levy *et al*, 2007. Hornberger *et al*, 1992) suggesting that a retardation factor of less than one may be expected for bacteria within these and similar column experiments (indicating preferential flow).

Based on these results, it is recommended the basic equilibrium transport model with a column test calibrated decay term is sufficient for simulating the head region of an *E. coli* breakthrough curve in a medium sand soil. This approach for example may be utilized to calculate safe setback distances from sewage sources or contaminated waterways. This method may be utilized in both the CXTFIT modeling software and the Geostudio modeling software.

8.1.2 Applicability of models – compacted 90% sand / 10% silts

The equilibrium model was inadequate in simulating the breakthrough curves of the compacted 90% sand / 10% silt columns. The large difference between the observed

breakthrough curves of the column tests conducted by Lukacs *et al* (2007) and the column experiments conducted during this study are puzzling. As the soil material properties between the columns were similar, it is likely that the discrepancy may have been caused by differences in the column preparation or permeation procedures. Levy *et al* (2007) also observed significant variation in bacterial transport properties within test columns of similar material properties. They suggested that layers of fines or organic material present in some columns may make it impossible to model some columns. It is also possible that a variable amount of the wet silt may have "stuck" to the mixing equipment used for the soil preparation in the study conducted by Lukacs *et al* (2007), which could have reduced the apparent quantity of silt within the column. However this is only speculation and the exact reason for the observed differences between the columns cannot be determined at this time.

Similar to the sand columns, the models tended to overestimate the amount of bacteria remaining in the column by approximately one order of magnitude. The exception is column SSP3 which contained significantly higher quantities of bacteria within the distribution profile measurements compared to the remaining columns and model simulations. This was despite having an extended MSM flush following the bacteria permeation. This may be interpreted as evidence of significant filtration and straining occurring within the column rather than purely equilibrium or kinetically based sorptive processes.

At this time the use of the equilibrium transport model for estimating bacterial transport through mixed 90% sand / 10% silt columns is not recommended. This,

however, is a limitation similar to other transport models such as CCFT (Levy *et al*, 2007).

8.1.3 Applicability of models – compacted silts

Similar to the mixed 90% sand / 10% silt columns, the equilibrium transport model with a fit decay coefficient was not able to reasonably simulate the *E. coli* breakthrough characteristics of the silt columns (R^2 -0.29).

Similar to the sand and mixed 90% sand / 10% silt columns, the simulated *E. coli* distribution profiles of the post-test silt column were higher than those observed in the experimental results. The equilibrium modelled results were approximately two orders of magnitude higher than the observed results, while the modified mobile-immobile model simulated a distribution profile approximately one order of magnitude higher than the observed. There are two likely explanations for this discrepancy; competition/predation from the contaminating bacteria may have accelerated the rate of *E. coli* decay within the column, or *E. coli* transport was predominantly through preferential flow paths which were not located in the regions sampled for the distribution profile analysis.

8.1.4 Applicability of models – freeze-fractured normally consolidated clays

Similar to the silt and 90% sand / 10% silt columns; the equilibrium transport model did not reasonably simulate the observed breakthrough curves of the freeze-fractured consolidated clay columns (R^2 0.18 -<-2). These columns are characterized by

fast breakthrough within the first pore volume of flow, to a near steady state *E. coli* effluent concentration. Extensive scatter and oscillation in the measured data sets make it difficult to reliably observe trends.

The mobile-immobile model is able to better simulate the observed effluent breakthrough curves of these columns. However, the low R^2 values (0.13-0.21) of this model suggest that it remains unsuitable for these particular columns. The first-order decay coefficients (μ (PV^{-1})) optimized to the estimated transport parameters also suggest a wide range of removal rates within these columns, from (μ = 0-23) in the equilibrium models, to (μ = 13.1-46.9) in the mobile-immobile models. As scatter within the experimental data is a consistent problem with the entire consolidated column data sets, these results are questionable and may not accurately represent *E. coli* transport through these columns.

The effluent breakthrough curves tended to be characterized by fast breakthrough (less than 0.5 PV) and effluent concentrations that appeared to oscillate between relative concentrations of 0.0001-0.001. Linear regression analysis of the freeze-fractured normally consolidated data sets suggested a very slowly increasing *E. coli* concentration trend (slope of 10^{-4} C/C_0 / PV for column NCC, 2 x 10^{-5} C/C_0 / PV for column NCE) or even a decreasing *E. coli* effluent concentration trend (slope of -2 x 10^{-5} C/C_0 / PV for column NCD). In contrast, the freeze-fractured compacted clay columns showed a definitive increasing concentration trend with increasing pore volumes of flow. While such flat breakthrough curves are not expected when permeating a column with a continuous source of contaminant, there are several explanations for this observation. It is possible that the scatter within these data masks the observable trends (for example, the

removal of one potential outlier in the NCD data set caused the linear regression analysis to generate a positive slope). It is also possible that filtration contributed strongly to the observed results. This could occur if the *E. coli* cells were only capable of moving through a subset of the fracture network, while the MSM solution (filtered and strained of cells) was capable of moving through both the entire fracture network, and the intact matrix. While the fractures capable of transporting the *E. coli* cells may individually shown full breakthrough ($C/C_o = 1$) the cells transported through these fractures would be diluted in the effluent due to the excess of clean MSM emitted from the fractures incapable of transporting cells. This may also explain the high μ values observed in these columns, as filtration can contribute to the apparent decay within the system.

The goodness of fit analysis (section 7.1.6) compares the residuals of the model simulated results to the experimental data set, as well as a horizontal line where all values are sets as the mean of the data values. Applied to a column test, this horizontal line may be interpreted as immediate and steady state (constant effluent concentration) breakthrough. Because the experimental data seems to follow a trend similar to this value rather than a traditional column breakthrough curve (increasing trend towards full breakthrough with a constant contaminant source), this can explain the low R^2 values of the resulting models (i.e. the mobile-immobile model is only slightly better at describing the variance in the data set compared to a horizontal line placed at the mean observed concentration). It is important to note that this observation may be an artefact produced by the duration of the experimental period being too short. Extended permeation of these columns would likely result in observed effluent concentrations that are more similar to a traditional breakthrough curve.

The *E. coli* distribution profile model results tended to be approximately 0.5 orders of magnitude higher than the experimental results. This was a closer approximation of the experimental observations than the models for the sand, 90% sand / 10% silt, and silt columns, which tended to generate results that were one to two orders of magnitude higher than the experimental observations. The reason for this is observation unknown at this time.

8.1.5 Applicability of models – freeze-fractured compacted clays

The freeze-fractured compacted clay column test results show significant variation between tests conducted by the two research groups (Scott and Nguyen, 2006. Lukacs *et al*, 2007). Consequently, columns CCA and CCB were modelled relatively accurately by the CXTFIT equilibrium transport model (R^2 of 0.92 and 0.76) while columns CCC and CCD were poorly modelled (R^2 0.22 and 0.00). The mobile-immobile simulations resulted in similar accuracy for columns CCA and CCB (R^2 of 0.93 and 0.77) while forming good-satisfactory simulations of columns CCC and CCD (R^2 of 0.80 and 0.56). The optimized first-order decay coefficients (PV^{-1}) of columns CCA and CCB were similar (μ of 11.8 and 16.8 in the equilibrium model, μ of 7.06 and 8.96 in the mobile-immobile model), while columns CCC and CCD were similar (μ of 0 in the equilibrium model, μ of 0.0112 and 0.205 in the mobile-immobile model). This difference in μ is likely the result of the data set suggesting steady state breakthrough had occurred in columns CCA and CCB, while not yet occurring in columns CCC and CCD. These modelled differences may also be the result of significant differences in the

material properties, as columns CCA and CCB were denser, less porous, possessed a lower moisture content, lower hydraulic conductivity and lower fracture porosity than columns CCC and CCD (see Table 5.1, Figure 5.31). It would appear that the equilibrium model is capable of describing bacterial transport through freeze-fractured compacted clay columns with similar properties to columns CCA and CCB, while becoming weaker with columns similar to CCC and CCD, which possess material properties closer to the freeze-fractured normally consolidated columns.

The modeled post test *E. coli* soil distribution profiles were similar to those predicted by the sand models, with the modelled results typically one order of magnitude higher than the observed values.

8.2 Comparison of simulation results to similar data in the literature

As the majority of research in the literature focuses on bacterial transport through sand columns or intact field samples, comparisons to several of the experimental results are lacking. In Table 8.1, the model parameters determined from this research are compared to the parameters determined in similar work by Pang *et al* (2003) and Powelsen and Mills (2001) who investigated *E. coli* transport through saturated sand columns with a similar methodology to that used for this research. Both the optimized and estimated retardation factors are for this research are very similar to the values reported by Powelsen and Mills (2001) while lower than those reported by Pang *et al* (2003). This is to be expected as the pumice sand utilized by Pang *et al* (2003) possesses a higher surface area and a higher porosity than other sandy aquifer materials. These

properties are thought to enhance microbial sorption, contact, and residence time within pumice sands relative to comparable quartz sands (Pang *et al,* 2003).

To compare the dispersion and decay coefficient results from this research to the values reported by Pang *et al* (2003) and Powelsen and Mills (2001), it was necessary to convert the transport parameter values into the same units. To do this, the values from this research project and the values reported by Pang *et al* (2003) were converted into the format used by Powelsen and Mills, (2001). The dimensional dispersivity value for the Geostudio model was multiplied by the average seepage velocity of the associated column and reported in the units of cm^2/hr, while the dimensional decay coefficient was converted from PV^{-1} to $hours^{-1}$. The results of this comparison are shown in Table 8.1.

The dispersion coefficient values from this research project tended to be several times lower, and the decay coefficients several times higher than the values reported by Pang *et al*, (2003) and Powelsen and Mills (2001). This is likely the result of the sand permeation experiments for this research being conducted at much higher flow rates, or through shorter column lengths than these comparable studies. If the transport parameter results of these similar studies could be converted to the format used in this research project (decay and flow expressed as PV^{-1}) it is likely that the results would appear more similar. This is best exemplified through the decay coefficient, which often considers both temporal influences (apparent decay through a reduction in the population as a function of time) and dimensional influences (apparent decay through a reduction in the population through filtration / straining, a function of travel length). Assuming straining is the only factor affecting the decay rate, and occurs at a similar function of travel length between a 100 cm column with a pore seepage velocity of 1cm/s and an identical column

with a pore seepage velocity of 0.1cm/s, it would appear that the faster flowing column removes the contaminant at a greater rate than the low flowing column (i.e. 100 seconds to remove a given contaminant in the high flow rate columns compared to 1000 seconds in the slow flow rate column). By normalizing these flow rates to PV^{-1} (i.e. as a function of normalized permeation volume rather than time) the resulting decay coefficients are likely to be identical.

The Freundlich sorption isotherm used in this study also seems to underestimate the retardation factor of the tested soils when compared to similar experimental results in the literature. Guber *et al* (2005) investigated the sorption of *E. coli* to field samples of a fine-silt soil material, and arrived at the Freundlich coefficients of K = 24.4 and N = 1.335, which when utilized with the *E. coli* concentration and material properties used in this research yields an expected retardation factor of 43,535 for the silt, 14,116 for the normally consolidated clay and 18,188 for the compacted clay. A similar study by Gantzer *et al* (2001) reported Freundlich values of K = 55.3 and N = 1.07 for a clay loam soil, which when used with the concentration and soil material properties used in this research, results in retardation factor values of 1,105 for the silt, 359 for the normally consolidated clay columns and 462 for the compacted clay columns. The higher retardation factor values for the silt columns when these modeling values are used (Eqn.3.8) is the result of the higher dry density and lower porosity of the silt columns compared to the compacted and consolidated clays (Tables 5.10, 5.1, 5.2). Levy *et al* (2007) also report a mean retardation factor of 14,000 from analysis of *E. coli* transport in their experimental columns, using a combination of classic colloid filtration theory and a CXTFIT mobile-immobile model within a soil composed of intact glacial outwash

material. This is interesting as their soil material was composed primarily of sand and gravel, with approximately 10% of the soil material composed of silt and clay, implying that the observed retardation factors may be primarily the result of variations in soil structure rather than the availability of sorption sites.

Another limitation of using batch sorption data to calculate retardation factors is that in this methodology all soil surfaces are available for sorption. Realistically, only a fraction of the total soil surfaces within a given soil column may be accessible to bacteria due to preferential flow paths and size exclusion. The retardation factor calculated from the batch sorption data may be at best an estimate of bacterial retardation through a laboratory soil column or in a field scenario, rather than an accurate evaluation of this parameter.

In the mobile-immobile model, the effective porosity of the system is reduced by assuming all transport occurs within the fractured porosity ($\beta = n_f$) as estimated from the methodology of McKay *et al* (2003) (see section 6.4.4. Eqns 6.8, 6.9, 6.10). Since reducing the effective porosity of the system had the effect of reducing the retardation factor by the same proportional amount when mass transfer between the mobile and immobile phases is insignificant (Eqn 6.4), the apparent discrepancy between the measured and adjusted retardation factor values may reflect either errors in the estimation of the fracture porosity or retardation factor. If the error is within the β value, then back-calculating through equations 6.8-6.10 would suggest fracture spacing (2B) on the micrometer scale, with a 10 fold reduction in fracture apertures (2b). This would suggest that bacterial transport is not expected to occur within the freeze-fractured clay columns as the fracture apertures would be smaller than the 20 μm threshold of mechanical

filtration (as described in section 2.2.2). While there is likely some error in the fracture porosity estimations (i.e. the fracture spacing is not likely to be regular at 0.5cm intervals, and all fractures are not likely to be identical), it is unlikely that the clay columns possess the fracture system suggested by optimizing the β parameter to the data set. As the estimated retardation factor values within the mobile-immobile model system seem to be roughly two orders of magnitude lower than the retardation factor values reported by Levy *et al* (2007), which is the same proportional adjustment required for either the estimated β value or the estimated retardation factor, the error is likely to be contained within the estimated retardation factor value.

A noticeable situation between the mobile-immobile model and the equilibrium transport model is the similar accuracy of the two models when applied to columns CCA and CCB despite the large difference in model retardation factor values. The main difference between the equilibrium models and the mobile-immobile models is that the mobile-immobile model assumes that contaminant transport only occurs within the fracture network, while the equilibrium model assumes that contaminant transport occurs throughout the entire pore network. As only a small percentage of the total pore volume is considered mobile within the examined freeze-fractured clay columns, it is implied that many "fracture" pore volumes have passed through the fracture network for every total pore volume of flow (which considered both the mobile fracture pore volumes and matrix pore volume). At the fracture microcosm level, the higher number of fracture pore volumes required for breakthrough to be observed in the effluent implies a higher retardation factor (i.e. on the range of 10^4 within the freeze-fractured columns observed in this study).

From a phenomenological standpoint, the retardation factor estimated through the batch sorption analysis and used in the equilibrium model is more correct as it indicates a closer approximation of the apparent retardation of a contaminant within a complete soil sample (i.e. the retardation of *E. coli* within the entire soil column). From the more mechanistic mobile-immobile model, the higher retardation factor is more correct as it better represents the actual retardation of the *E. coli* within the pore spaces which participate in the contaminant transport (i.e. the retardation of *E. coli* transported within a single fracture).

8.3 *Interpretation of simulation results*

8.3.1 Distribution profiles

The soil column *E. coli* distribution profile simulation results seem to indicate that the equilibrium transport models tend to overestimate the measured soil *E. coli* concentrations by one order of magnitude, with the exception of the freeze-fractured normally consolidated clay columns, silt, and 90% sand / 10% silt columns. It is possible that the differences between the simulated and measured values are a result of the data collection technique rather than errors in the model assumptions. For the data collection technique, it is assumed that all bacteria contained in a given soil sample will desorb from the solid phase and enter the clean MSM solution for analysis. However, equilibrium sorption theory implies that a certain quantity will remain sorbed onto the solid phase. In equilibrium batch sorption theory, it is also assumed that the bacterial cells will undergo

instantaneous, reversible sorption, and this sorption theory does not account for kinetically controlled desorption rates which may be many times slower or negligible compared to the forward sorption rate. For the plate counting technique, it is also assumed that plated cells are formed from independent and isolated cells, when in fact the colony may have formed from a group of amalgamated cells joined to the same suspended soil particle or biofilm fragment. It is possible that these and similar factors combine to cause a measured undercount of the soil profile samples by an order of magnitude. Cell death may also account for some of the observed error.

The better agreement between the simulated and measured *E. coli* distribution profiles in the freeze-fractured normally consolidated clay columns, and column CCC of the compacted clay column set may be a result of the incorporation of the suspended clay material in the plating procedure. This would allow cells sorbed to the solid phase to be counted along with cells suspended in the MSM solution. This is not expected to occur in the sand samples, where the larger sand grains are not suspended or incorporated in the plated solution.

The column measurements which showed higher measured than simulated *E. coli* distribution profile data (particularly column SSP3) may indicate that significant straining or other physical processes were occurring. Strained bacteria may not necessarily be sorbed to soil particles, and would easily be resuspended in solution, as opposed to cells which must desorb first.

8.3.2 Qualitative interpretation of sand column results

Based on the model results for the sand columns, it may be concluded that bacteria transport through this soil type may be explained primarily through the first-order decay coefficient term rather than through the retardation or dispersivity terms (i.e. *E. coli* transport through these soil columns was adequately simulated (R^2 0.75-0.97) with minimal retardation (R=1.03) low dispersion coefficient (D = 0.00168 - 0.0867 L^2T^{-1}) Table 7.5). Foppen *et al*, (2005), summarizes several papers by Matthess *et al* which suggest that bacterial transport through laboratory sand soils is aptly described using a first-order filtration coefficient, calculated from pore water velocity and grain size analysis, and incorporated into the advection-dispersion equation. As the modeling simulation results seem to suggest that the most important transport parameter is the first-order decay coefficient, it would appear that techniques capable of providing estimates for the value of this term are of a much greater importance for modeling purposes compared to those that provide estimates of dispersion or retardation within these soils. The low dispersion coefficients within these soils also suggest that the influence of hydrodynamic dispersion is minor, leading support for filtration based theories such as CCFT (Tufenkji, 2007).

To address the discrepancy between the equilibrium model predictions and measured *E. coli* values within the effluent and distribution profiles of the sand columns, a kinetic transport model may be investigated. Preliminary modeling through inverse parameter fitting the kinetic transport parameters to the observed *E. coli* breakthrough curves proved capable of simulating the tailing region much more accurately than the equilibrium model (data not shown). As the current data limits the applicability of kinetic

models to the sand and possibly sand/silt columns, this approach was not investigated in detail for this research project. However, the data collected from the pulsed source columns may be used in future experiments which attempt to model bacterial fate and transport using a kinetic approach.

Classic colloid filtration theory (section 3.5) which was not investigated during the course of this experiment may also be used to verify or contrast the modeled or measured *E. coli* distribution profile results within the sand columns. This could be accomplished by calculating the associated transport parameters within the CCFT model (Eqn 3.11 – 3.13) and defining the attachment efficiency as the constant multiple required to convert the k_{att} transport parameter calculated in Eqn 3.13, to an optimized kinetic attachment value calculated through an inverse modeling methodology using Eqn 3.11 and 3.12 and the experimental data.

8.3.3 Qualitative interpretation of compacted mixed 90% sand / 10% silt and compacted silt column results

The 90% sand / 10% silt columns exhibit the greatest variation of measured and optimized transport parameters from both the bromide and *E. coli* breakthrough curves. It would appear that small differences in column preparation procedures can lead to very different bacterial transport properties for these soil materials. The reasons for the observed differences between the column experiments conducted for this study and the experiments conducted by Lukacs *et al* (2007) can only be speculated. Based on the high retention of *E. coli* within the pulsed-source columns following MSM permeation, it is expected that straining and filtration play a much more important roll in governing

transport through the mixed 90% sand / 10% columns compared to equilibrium-based transport processes.

At this time, it is difficult to form an opinion on bacterial transport modeling through the compacted silt columns with the current methodology. Based on the geometrical suffusion security (Eqn 2.1) and using the grain size analysis table (Figure 5.1) with an expected *E. coli* cell diameter of 2 μm (White, 1984), the silt possesses an expected geometrical suffusion security value of 1.28. The value is quite close to the 1.5 threshold expected for straining to be significant (Foppen *et al*, 2005). Other researchers predict that straining is significant at geometrical suffusion security values below this threshold (Bradford *et al*, 2003). From this, it would appear that straining based models would be far more likely to be applicable to this soil material than the current equilibrium based model. As this time, it may only be concluded that *E. coli* cells are capable of being transported through this soil material.

As bacterial contamination rendered results from the duplicate silt column (column Silt R) invalid, it is also possible that the same contamination in the upper reaches of this experimental column may have affected the experimental results by competing with, or blocking pore access to the *E. coli*. The lack of reliable *E. coli* permeation data for the silt material in the previously conducted experiments also hampers the ability to draw conclusions about bacterial transport through this soil type.

8.3.4 Qualitative interpretation of freeze-fractured clay column results

As bacterial breakthrough was not observed in the clay control columns, it may be concluded that fractures created by the freeze-thaw procedure are responsible for the observed bacterial breakthrough in these columns. The early breakthrough (<0.5 pore volumes) is also indicative that bacterial transport occurs through a small fraction of the total pore volume.

The decay coefficient (μ), which is interpreted as the combined influence of death, predation, straining and irreversible sorption, appears to be much higher in the normally consolidated columns as opposed to the compacted clay columns. It is possible that the less dense and less homogeneous nature (the upper region of the normally consolidated columns were noticeably softer and more gel-like than the lower regions) of the consolidated columns allowed greater potential for self healing of the fracture network. This could occur if the softer regions of the normally consolidated columns migrated into a portion of the freeze-fractured spaces following the thaw and subsequent permeation, which would act to reduce pore sizes and increase the potential for filtration and straining to occur.

The denser, freeze-fractured compacted clay columns (CCA and CCB) exhibited similar transport properties, but differed substantially from the softer compacted columns (CCC and CCD). The fracture analysis (Table 6.1) suggests that CCA and CCB possess smaller average fracture apertures (2b) than CCC and CCD, which could contribute to enhanced filtration and straining, resulting in larger optimized values of the decay coefficient (μ). The small decay coefficients optimized in columns CCC and CCD,

despite having material properties and fracture apertures similar to those of the freeze-fractured normally consolidated columns, may indicate that the compaction procedure enhances the ability for bacteria and similar colloids to move through these fractured soils.

8.4 Proposed model for the estimation of *E. coli* transport in freeze-fractured clay soils

The proposed model for estimating bacterial transport through the freeze-fractured clay columns is a modification of the general mobile-immobile model, and takes the form:

$$G\frac{\partial C_m}{\partial T} = D\frac{\partial^2 C_m}{\partial L^2} - \frac{\partial C_m}{\partial L} - \mu C$$

Eqn 8.1

$$G = (R\beta)100$$

Eqn 8.2

As *E. coli* mass transfer is not expected between the mobile and immobile pore fractions (as *E. coli* cells are expected to be too large to enter to clay matrix (Θ = infinity, clay d_{10} smaller than *E. coli* d_m) this was confirmed with the control clay columns) the second term within the general mobile-immobile model (Eqn 6.4) reduces to zero, and is omitted. The (G) term (unitless) may be described as the apparent retardation factor of bacteria within the fractures of the soil system, and is a function of the batch sorption test estimated retardation, factor using the methodology of Rosa (2007), and the fracture

porosity estimated from the methodology of McKay et al, (1993). The bacterial dispersion coefficient (D) may be approximated from the dispersion coefficient of a conservative tracer using equation 7.2.

8.5 Application of model: Calculating safe setback distances from a source of E. coli bacteria.

To calculate the safe setback distance from a pathogenic bacteria source, such as a compromised septic tank or leaking sewage lagoon, representative one-dimensional model systems were constructed in CXTFIT. These systems were composed of the average equilibrium transport properties for the sand columns, and the average mobile-immobile transport properties of the freeze-fractured compacted clay columns, and freeze-fractured normally consolidated clay columns. The properties for the mobile-immobile model were calculated using equations 8.1, 8.2 and 7.2 with an assumed fracture spacing of 0.5cm. The goal of this modeling is to simulate one-dimensional transport and calculate the distance required to achieve a 7 order reduction in the bacterial concentration from a point source.

The transport parameters were calculated using the average material properties of the columns (Tables 5.1, 5.2 and 5.3) are listed in Table 8.2. The modeling results are given in Table 8.3. The average height is the mean height of the associated columns (Tables 5.1, 5.2, 5.3) and the column length required is the average column height multiplied by the relative height required for a 7 log reduction in bacterial effluent concentrations.

Assuming that the freeze-fractured clay column experiments may be extrapolated to arbitrary lengths, it would appear that the freeze-thaw weathering simulated in the test columns is not sufficient to allow high levels of *E. coli* through dense compacted clay liners, or through normally consolidated clay soils. Freeze-fractured low-density compacted clay liners would seem to be at a higher risk of bacteria containment failure. Note that the transport parameters used for this analysis were derived from permeation durations of approximately 3 weeks, and that longer test durations may show higher breakthrough of *E. coli.* It is also possible that straining related mechanisms dominate the removal of *E. coli* within these soil systems, which are predicted to become less effective with increasing column lengths (i.e. the chance of encountering dead end pores is greatest in the beginning of the soil column, and lowest near the bottom of the column due to the consolidation of the flow paths to the larger pore spaces (Bradford, 2003)). The estimated setback distance of 14.28m for the sand material is remarkably similar to the 15m setback distance between a septic tank and a surface water body as outlined in a source cited by Pang et al (2003).

To investigate the contribution of each individual parameter within the mobile-immobile model on the estimated setback distances, a simple sensitivity analysis was conducted by varying each input parameter by +100%/- 50% (double and half the predicted values) (Table 8.4). For columns, the parameter which had the largest effect on the required setback distance was the decay coefficient. In general, increasing the apparent retardation (through an increase in the retardation factor or the fracture porosity) decreases the estimated setback distance, increasing the mobile-immobile dispersion

coefficient tends to increase the setback distance required, and increasing the decay coefficient decreases the setback distance required.

8.6 Model shortcomings and knowledge gaps

The equilibrium transport models have shown significant weakness in explaining the observed breakthrough curves of soils other than compacted mediums sands and dense, freeze-fractured compacted clay columns. It is suspected that bacterial transport in the other soil materials is dominated by processes that cannot be adequately represented by the equilibrium transport theory and modeling methodology. Results also show that the equilibrium model is incapable of accurately simulating the bacterial soil column distribution profile and the bacterial concentrations in the tailing region of a pulsed breakthrough curve. This limitation has also been reported by other researchers (Levy *et al*, 2007. Hornberger *et al*, 1992. Gargiulo *et al*, 2007a).

A major hurdle to refining the current modeling approach and investigating similar models is the lack of pulsed-source experiments conducted on the freeze-fractured clay material. As the experimental columns were many times shorter than the one meter depth requirement for soil liners in Ontario (Ontario *Ministry of Agriculture, Food and Rural Affairs*, 2002) it is difficult to assess the risk of bacterial migration through these engineered barriers. Future experiments should be conducted on a variety of column lengths with a goal of investigating the depth dependant straining function of these soils, and the risk potential for bacterial transport at regulated lengths. This would provide a much greater understanding of the potential for bacterial transport through these freeze-

fractured systems up to and beyond the one meter liner requirement. It is also desirable to better understand the properties of the fractured system (i.e. fracture spacing and aperture) and the roles of fracture flow and matrix diffusion for *E. coli* transport in these systems.

As the modeling simulations have examined the transport of one *E. coli* strain, suspended in a nutrient limited media, permeating under controlled column experiments, it is difficult to confidently extend the simulated results to other scenarios. The bacteria used in these column tests may possess different transport properties compared to more pathogenic strains, and may differ substantially from other bacterial species. Waste effluents containing *E. coli* and other potentially pathogenic microbes are also likely to contain nutrient sources capable of sustaining the growth of these and competing bacteria. Guber *et al*, (2005) have also shown that particulate matter, such as suspended manure particles can compete with *E. coli* for sorption sites, which can affect the transport properties. Consequently, it is generally impossible to use the results of one set of experiments to all sets of microbes of concern (Yates and Yates, 1988).

Table 8.1 - Comparison of estimated parameters from this research with literature values

Researchers	Material	Influent source	R estimated (section 6.4.4)	R (optimized to data)	D (section 6.4.4) (Relative column length)	D_{dim} cm^2/h	μ PV^{-1}	μ_{dim} $Hour^{-1}$
Lukacs et al, 2007	Quartz Sand	continuous	1.03	1.54	0.036	0.008	0.30	3.200
Lukacs et al, 2007	Quartz Sand	continuous	1.03	1.28	0.087	0.054	0.11	3.165
Burdenuk, 2009	Quartz Sand	Pulse	1.03	1.11	0.017	0.014	0.06	3.086
Burdenuk, 2009	Quartz Sand	pulse	1.03	1.14	0.017	0.017	0.14	8.720
Burdenuk, 2009	Quartz Sand	pulse	1.03	1.04	0.017	0.015	0.10	4.580
Pang et al, 2003	Pumice Sand	continuous		1.31		0.083		0.592
Pang et al, 2003	Pumice Sand	pulse		1.92		0.083		0.219
Powelsen and Mills, 2001	Quartz Sand	continuous		1.22		0.135		0.023
Powelsen and Mills, 2001	Quartz Sand	continuous		1.03		0.15		0.029

Table 8.2 - Modeling parameters used for one-dimensional representative field systems

	Average R (Batch sorption data)	Average D (Bromide permeation)	G (Eqn 8.2) Average (unitless)	D_{mim} (Eqn. 7.2) (relative height^2 / PV)	Average Decay Coefficient (PV^{-1})
FF Dens. Comp. Clay	315.8	1.125	77.298	0.133	8.010
FF Soft. Comp. Clay	263.110	0.472	87.490	0.372	0.120
FF Cons. Clay	224.853	0.819	82.862	0.639	31.733
Comp Sand.	1.030	0.035			0.144

Table 8.3 - Transport distance required for a seven log reduction in bacterial concentrations from a continuous effluent source.

	Distance required (relative height)	Average column height (cm)	Distance required (m)
FF Dens. Comp. Clay	3.21	7.0	0.2
FF Soft. Comp. Clay	130	8.3	10.8
FF Cons. Clay	2.30	12.4	0.3
Comp Sand.	112.46	12.7	14.3

FF Dens. Comp. Clay - Average values for experimental columns CCA and CCB (Table 5.1)
FF Soft. Comp. Clay - Average values for experimental columns CCC and CCD (Table 5.1)
FF Cons. Clay - Average values for experimental columns (Table 5.2)
Comp Sand. - Average values for experimental compacted sand columns (Table 5.3, 5.8

Table 8.4 - Sensitivity analysis of mobile-immobile modeling parameter estimated inputs on modeled setback distances

soil	G (Eqn 8.2)	D_{mim} (Eqn 7.2)	μ	Distance Required (relative column lengths) G +100%	G -50%	D_{mim} +100%	D_{mim} -50%	μ +100%	μ -50%	Range of values (relative column lengths)	Range of values (meters)
FF. Dens. Comp. clay.	77.30	0.13	8.01	3.2	3.2	3.3	2.8	2	5.45	2 - 5.45	0.14 - 0.38
FF. Soft. Comp. clay.	87.49	0.37	0.12	158	140	141	138	73	275	73 - 275	6.1 - 22.8.
FF. Cons. clay.	82.86	0.64	31.73	2.3	2.3	3.1	1.75	1.55	3.5	1.55 - 3.5	0.19 – 0.43

FF Dens. Comp. Clay - Average values for experimental columns CCA and CCB (Table 5.1)
FF Soft. Comp. Clay - Average values for experimental columns CCC and CCD (Table 5.1)
FF Cons. Clay - Average values for experimental columns (Table 5.2)

Chapter 9 - Conclusions and Recommendations

9.1 Conclusions

The experimental pulsed source permeation procedures undertaken during this research have proven important for the identification of the transport parameters and limitations with the current modeling methodology. It is anticipated that future experiments conducted using the methods outlined for this research will allow more in-depth analysis of the factors which influence bacterial transport in the studied soils. The pulsed source sand column data for example, could form the basic framework for a future project which may focus on describing the transport of *E. coli* using kinetic transport parameters.

Potential sources of error, such as soil displacement within the mixed 90% sand / 10% silt columns (Figure 5.33) or inadequate removal of the clean, initial permeating solution have also been identified and discussed. Weaknesses in the established methods, such as the potential for error due to the inclusion of pore fluid in the methodology used for the *E. coli* distribution sampling procedure have also been identified.

During the course of this research, it has been demonstrated that a basic, non-dimensional equilibrium transport model with a dispersion coefficient estimated from bromide breakthrough results, and a retardation factor estimated from a batch sorption isotherm with a first-order decay coefficient derived from breakthrough curve fitting, is suitable for estimating one-dimensional breakthrough and potential setback distances in a

medium quartz sand system. This model also shows potential application in dense, well compacted freeze-fractured clay systems, although more research is needed to investigate this phenomenon. This model shows little to no application in estimating the breakthrough curves of mixed 90% sand / 10% silt, silt, or normally-consolidated freeze-fractured clay columns. The equilibrium model also fails to predict with reasonable accuracy, residual bacterial distribution profiles or effluent concentrations after a MSM pulse through the column. It is suspected that this is primarily due to the influence of straining, irreversible sorption, preferential flow paths, experimental variability, and other factors not addressed in the simple equilibrium model.

At this time, it is not possible to use the transport parameters estimated using the methodologies outlined in section 6.4.4, and converted for input into the Geostudio modeling program following the methodologies outlined in section 6.5.1. Geostudio was only capable of simulating *E. coli* transport through the compacted sand columns to the same level as CXTFIT. As Geostudio was not capable of simulating the transport of *E. coli* through the-fractured clay systems, it was not possible to simulate a two-dimensional model system such as a freeze-fractured clay liner similar to the example shown in Figure 1.1. Instead, one-dimensional, continuous source transport through freeze-fractured clay materials was simulated by extrapolating the mobile-immobile model to arbitrary lengths. It is possible that dimensional transport parameter fitting within CXTFIT, where the column dimensions and pore velocity are defined, may produce estimated transport parameter that may be entered into Geostudio more seamlessly. Preliminary modeling with a dimensional CXTFIT equilibrium model indicated a high degree of similarity between the bromide transport parameters of the dimensional and non-dimensional model

formats; however, when applied to the *E. coli* data sets, the resulting transport parameters estimated from the more mechanistic approach of the dimensional format differed noticeably from the non-dimensional format. This is likely due to the nature of suspended colloids such as bacterial cells, which behave differently than dissolved contaminants, which equilibrium models are better suited for.

Based on the modeled results, which were calibrated to the measured data collected over a limited time frame (~21 days), it would appear that a transport distance of 0.14 – 0.38 m is sufficient to reduce bacterial concentration levels by a factor of 10^7 through systems representing the freeze-fractured dense compacted clay, and 0.19 – 0.43 m is sufficient to reduce bacteria concentrations by 10^7 within systems representing the freeze-fractured consolidated clay columns. In systems representing the freeze-fractured soft compacted clay columns, a much larger distance of 6.1 – 22.8 m was required to reduce the bacteria concentrations by a similar magnitude. It is important to note that these results are based on the extrapolated observations of laboratory columns, and may not properly represent the results of long term permeation, or the fracture networks present in field scenarios. Longer experimental permeation periods may also different results if used to calibrate the models.

To address the limited application of the equilibrium model in the freeze-fractured clay columns, a mobile-immobile model with equilibrium sorption was utilized. The mobile-immobile model assumed that the entire mobile fraction is contained within the fracture spaces (fracture porosity), and that mass transfer between the phases is negligible. To estimate the fraction of mobile pore fluid, the method of McKay *et al* (1993) was used with an estimated fracture spacing of 0.5 cm, and hydraulic conductivity

values measured from both intact control, and freeze-fractured experimental columns. The results of this analysis yielded the estimated fracture porosity as a percentage of the total porosity, which was input as the dimensionless partitioning parameter within the modeling program. Preliminary fitting analysis indicated that this value was roughly 100 times smaller than the optimized, curve fit value when the batch sorption estimated retardation factor and bromide estimated dispersion coefficient were utilized. As the retardation factor and dimensionless partitioning parameter combine into the same term (G, the apparent retardation within the fracture spaces (dimensionless)) within the model, this apparent error may be due to inaccuracies in the methodology of calculating the retardation factor, as other studies have suggested that these values are approximately two orders of magnitude higher than the estimated values based on the batch sorption data. It is also likely that the increase in the required retardation factor is an artifact of the mobile-immobile model theory, in which only a small fraction of the total pore volume participates in the contaminant transport. This would imply that many "fracture pore volumes" have passed through the column for every total pore volume. Using an estimated correction value (R x 100), a model optimized (inverse parameter estimate analysis within CXTFIT) dispersion coefficient and a first-order decay coefficient, simulations with coefficients of determination (R^2) between 0.56-0.93 for the freeze-fractured compacted clay columns, and 0.13-0.21 for the freeze-fractured consolidated columns were generated. A simple power relationship between the estimated dispersion values, derived from fitting the dispersion coefficient to the measured effluent breakthrough curve of bromide, and the optimized value for the for the observed *E. coli* effluent measurements, is shown in equation 7.2.

The modeling results suggest that filtration and related removal mechanisms are related to the compaction condition and material properties of the freeze-fractured clay systems. It would appear that the greatest risk of bacterial transport as a result of freeze fracture formation occurs in low density compacted clay materials. It is suspected that these soils possess larger fracture apertures than denser compacted clay soils, while the less cohesive and non-uniform nature of the consolidated columns allows a more rapid self healing of the clay matrix to occur following thaw.

9.2 Recommendations

To address knowledge gaps in the current research data, it is recommended that the following experimental endeavours be conducted:

Bacterial pulse experiments with the freeze-fractured consolidated and compacted clay columns should be conducted. These experiments should cover a range of column lengths with the goal of describing the depth dependant straining function within these soils. It is suspected that a mobile-immobile straining based model would result in much more reliable and effective representation of the experimental column results than the equilibrium based mobile-immobile model used in this research project. It is also suspected that a straining related model would explain the high bacteria retention and limited breakthrough that were observed in the silt and 90% sand / 10% silt columns.

Continuous source or pulse source type experiments with high and low density freeze-fractured compacted clay columns should be conducted. This may confirm or refute the hypothesis that the calculated dry-density of the freeze-fractured clay is an important indicator of the magnitude of the risk for *E. coli* transport.

Additional continuous source or preferably pulse source type experiments with the freeze-fractured consolidated clay as the current data sets contain excessive scatter. This limits the ability to make both reliable conclusions about the available data and fit corresponding models. It may also be fruitful to investigate the effect of bacteria permeation on the column transport parameters by permeating the column with a second bromide pulse following bacterial permeation (Levy *et al*, 2007). This may also lead to an estimate of the bacterial dispersion coefficient that accounts for ripening.

A major knowledge gap within the literature is the lack of available batch sorption or kinetic sorption related data for *E. coli* and various soil materials. For this project, the retardation factor of the 90% sand / 10% silt columns by weighting the associated values from the sand and silt sorption data in the proportions used. It cannot be said for certain if a batch sorption experiment conducted with soil mixed in these proportions will yield similar as the estimated value. As soil free controls were not utilized in the batch sorption experiments conducted by Rosa (2007), a correction curve calibrated with this control data may also explain the scatter present in the sand sorption data.

As the current models tend to overestimate the measured values of the *E. coli* distribution profiles by an order of magnitude, it is quite possible that the soil sampling methodology, based upon completely reversible equilibrium sorption is flawed. An alternative method that is more capable of quantifying sorbed rather than suspended cells should be investigated.

References

Abichou, T., Benson, C., Friend, M., Wang, X., 2002. "Hydraulic conductivity of a Fractured Aquitard." Evaluation and Remediation of Low Permeability and Dual Porosity Environments. ASTM STP 1415 M.N. Sara and L.G. Everette, Eds., ASTM International, West Conshohocken, PA.

Abu-Ashour, J., Joy, D.M., Lee, H., Whiteley, H.R., Zelin, S., 1994. "Transport of microorganisms through soil." Water, Air and Soil Pollution. 75:141-158.

Albinger, O., Biesemeyer, B.K., Arnold, R.G., Logan, B.E., 1994. "Effect of bacterial heterogeneity on adhesion to uniform collectors by monoclonal populations." FEMS Microbiology Letters 124:321-326

Avery, L., Hill, P., Killham, K., Jones, D.L., 2004. "*Escherichia coli* O157 survival following the surface and sub-surface application of human pathogen contaminated organic waste to soil." Soil Biology and Biochemistry. 36(12):2101-2103

Bales, R.C., Li, S., Yeh, T.-C.J., 1997. "Bacteriophage and microsphere transport in saturated porous media: Forced-gradient experiment at Borden, Ontario. Water Resource Management. 33(4):639-648.

Baygents, J.C., Glynn, J.R., Albinger, O., Biesemeyer, B.K., Ogden, K.L., Arnold R., G., 1998. "Variations of Surface Charge Density in Monoclonal Bacterial Populations: Implications for Transport through Porous media." Environmental Science and Technology. 32:1596-1603.

Becker, M.W., Collins, S.A., Metge, D.W., Harvey, R.W., Shapiro, A.M., 2004. "Effect of cell physicochemical characteristics and motility on bacterial transport in groundwater." Journal of contaminant hydrology. 69:195-213.

Berg, H.C., 2003. "*E. coli* in motion." Published by Springer, New York. ISBN: 978-0-387-00888-2

Bergey, D.H., Holt, J.G., 1994. "Bergey's Manual of Determinative Bacteriology." Published by Lippincott Williams & Wilkins, Baltimore. ISBN 0683006037, 9780683006032

Beutin, L., Geier, D., Steinruck, H., Zimmermann, S., Scheutz, F., 1993. "Prevalence and Some Properties of Verotoxin (Shiga-Like Toxin)-Producing *Escherichia coli* in Seven Different Species of Healthy Domestic Animals." Journal of Clinical Microbiology. 31(9):2483-2488.

Bolster, C.H., Hornberger, G.M., Mills, A.L., 1998. "A method for calculating bacterial deposition coefficients using the fraction of bacteria recovered from laboratory columns." Environmental Science and Technology. 32:1329-1332.

Bos, R., Van der Mei, H.C., Busscher, H.J., 1999. "Physio-chemistry of initial microbial adhesive interactions - its mechanisms and methods for study." FEMS Microbiology Reviews. 23:179-230.

Boyce, T., Swerdlow, D.L., Griffin, P.M., 1995. "*Escherichia coli* O157:H7 and the Hemolytic–Uremic Syndrome." The New England Journal of Medicine. 333(6):364-368.

Bradford, S.A., Bettahar, M., 2006. "Concentration dependant transport of colloids in saturated porous media." Journal of Contaminant Hydrology. 82:99-117.

Bradford, S.A., Bettahar, M., Simunek, J., van Genuchten, M., T., 2004. "Straining and Attachment of Colloids in Physically Heterogeneous Porous Media." Vadose Zone Journal. 3:384-394

Bradford, S.A., Simunek, J., Bettahar, M., Tadassa, Y.F., van Genuchten, M.T., Yates, S.R., 2005. "Straining of colloids at textural interfaces." Water Resources Research. W10404. 41:1-17

Bradford, S.A., Simunek, J., Bettahar, M., van Genuchten, M, Yates, S, 2003. "Modeling Colloid Attachment, Straining, and Exclusion in Saturated Porous Media." Environmental Science and Technology. 37:2242-2250.

Bradford, S.A., Simunek, J., Bettahar, M., van Genuchten, M.T., Yates, S.R., 2006. "Significance of straining in colloid deposition: Evidence and implications." Water Resource Research. W12S15 42:1-16

Bradford, S.A., Simunek, J., Walker, S.L., 2006. "Transport and straining of *E. coli* O157H7 in saturated porous media." Water Resource Research. W12S12. 42:1-12

Bradford, S.A., Yates, S.R., Bettahar, M., Simunek, J., 2002. "Physical factors affecting the transport and fate of colloids in saturated porous media." Water Resources Research, 38(12):1327-1338

Camesano, T.A., Logan, B.E., 1998. "Influence of Fluid Velocity and Cell Concentration on the Transport of Motile and Nonmotile Bacteria in Porous Media." Environmental Science and Technology. 32:1699-1708.

Camesano, T.A., Unice, K.M., Logan, B.E., 1999. "Blocking and ripening of colloids in porous media and their implications for bacterial transport." Colloids and Surfaces A: Physicochemical and Engineering Aspects. 160:291-308.

Chen, G., Strevett, K.A., 2001. "Impact of surface thermodynamics on bacterial transport." Environmental Microbiology, 3(4):237-245.

Chen, G., Strevett, K.A., 2003. "Impact of carbon and nitrogen conditions on *E. coli* surface thermodynamics." Colloids and Surfaces B: Biointerfaces. 28:135-146

Chrysikopoulos, C.V., Abdel-Salam, A., 1997. "Modeling colloid transport and deposition in saturated fractures." Colloids and Surfaces. 121:189-202

Clement, T.P., Peyton, B.M., Skeen, R.S., Jennings, D.A., Peterson, J.N., 1997. "Microbial growth and transport in porous media under denitrification conditions: experiments and simulations." Journal of Contaminant Hydrology. 24:269-285.

Conboy, M.J., Goss, M.J., 2000. "Natural Protection of groundwater against bacteria of fecal origin." Journal of Contaminant Hydrology. 43:1-24

Craun, G.F., 1985. "Summary of Waterborne Illness Transmitted through Contaminated Groundwater." Journal of Environmental Health. 48(3):122-127.

Dong, H., Rothmel, R., Onstott, T.C., Fuller, M.E., DeFlaun, M.F., Streger, S.H., Dunlap, R., Fletcher, M., 2002. "Simultaneous Transport of Two Bacterial Strains in Intact Cores from Oyster, Virginia: Biological Effects and Numerical Modeling." Applied and Environmental Microbiology. 68(5):2120-2132

Feng, P., Weagant, S.D., Grant, M.A., 2002. "Enumeration of *Escherichia coli* and the Coliform Bacteria." Bacteriological Analytical Manual, 8th Edition, Revision A, Chapter 4. US Food and Drug Administration.

Foppen, J.W., Schijven, J.F., 2006. "Evaluation of data from the literature on the transport and survival of *Escherichia coli* and thermotolerant coliforms in aquifers under saturated conditions." Water Research. 40:401-426.

Foppen, J.W., van Herwerden, M., Schijven, J., 2007a. "Measuring and modeling straining of *Escherichia coli* in saturated porous media." Journal of Contaminant Hydrology. 93:236-254.

Foppen, J.W., van Herwerden, M., Schijven, J., 2007b. "Transport of *Escherichia coli* in saturated porous media: Dual mode deposition and intra-population heterogeneity." Water Research. 41:1743-1753.

Foppen, J.W.A., Mporokoso, A., Schijven, J.F., 2005. "Determining straining of *Escherichia coli* from breakthrough curves." Journal of Contaminant Hydrology. 76:191-210.

Foppen, J.W.A., van Herwerden, M., Kebtie, M., Noman, A., Schijven, J.F., Stuyfzand, P.J., Uhlenbrook, S., 2008. "Transport of *Escherichia coli* and solutes during

waste water infiltration in an urban alluvial aquifer." Journal of Contaminant Hydrology. 95(1-2):1-16.

Fuller, M.E., Dong, H., Mailloux, B.J., Onstott, T.C., DeFlaun, M.F., 2000. "Examining Bacterial Transport in Intact Cores From Oyster, Virginia: Effect of Sedimentary Facies Type on Bacterial Breakthrough and Retention." Water Resource Research. 36(9):2417–2431.

Gagliardi, J.V., Karns, J.S., 2000. "Leaching of *Escherichia coli* O157:H7 in Diverse Soils under Various Agricultural Management Practices." Applied and Environmental Microbiology. 66(3):877-883.

Gannon, J.T., Manilal, V.B., Alexander, M., 1990. "Relationship of cell surface properties and Transport of bacteria through soil." Applied and Environmental Microbiology, 57(1):190-193.

Gantzer, C., Gillerman, L., Kuznetsov, M., Oron, G., 2001. "Adsorption and survival of faecal coliforms, somatic coliphages and F-specific RNA phages in soil irrigated with wastewater." Water Science and Technology. 43(12):117-124

Gargiulo, G., Bradford, S.A., Simunek, J., Ustohal, P., Vereecken, H., Klumpp, E., 2007a. "Transport and Deposition of Metabolically active and Stationary Phase

(*Deinococcus radiodurans*) in Unsaturated Porous media." Environmental Science and Technology. 41:1265-1271

Gargiulo, G., Bradford, S., Simunek, J., Ustohal, P., Vereecken, H., Klumpp, E., 2007b. "Bacteria transport and deposition under unsaturated conditions: The role of the matrix grain size and the bacteria surface protein." Journal of Contaminant Hydrology. 92:255-273

Gauthier, F., Archibald, F., 2001. "The Ecology of "Fecal Indicator" bacteria commonly found in Pulp and Paper Mill Water Systems." Water Research, 35(9):2207-2218

GEO-SLOPE Int. Ltd, 2008a. "Contaminant modeling with CTRAN/W 2007." Electronic copy included with software package. pp 99-105

GEO-SLOPE Int. Ltd, 2008b "Seepage modeling with SEEP/W 2007." Electronic copy included with software package. pp 264-266

Gerba, C.P., Smith, J.E. Jr, 2005. "Sources of Pathogenic Microorganisms and Their Fate during Land Application of Wastes." Journal of Environmental Quality. 34:42-48

Ginn, T.R., Wood, B.D., Nelson, K.E., Scheibe, T.D., Murphy, E.M., Clement, T.P., 2002. "Processes in microbial transport in the natural subsurface." Advances in water resources. 25:1017-1042

Grant, S.B., Pendroy, C.P., Mayer, C.L., Bellin, J.K., Palmer, C.J., 1996. "Prevalence of Enterohemorrhagic *Escherichia coli* in Raw and Treated Municipal Sewage." Environmental Microbiology. 62(9):3466-3469.

Griffin P.M., 1995 "*Escherichia coli* O157:H7 and other enterohemorrhagic *Escherichia coli*." In: Blaser MJ, Smith PD, Ravdin JI, Greenberg HB, Guerrant RL, eds. Infections of the gastrointestinal tract. New York: Raven Press, 739-61.

Gross, M., Albinger, O., Jewett, D.G., Logan, B.E., Bales, R., Arnold, R.G., 1995. "Measurement of bacterial collision efficiencies in porous media." Water Research. 29(4):1151-1158

Gross, M.J., Logan, B.E., 1995. "Influence of Different Chemical Treatments on Transport of *Alcaligenes paradoxus* in Porous Media." Applied and Environmental Microbiology. 61(5):1750-1756

Guber, A.K., Shelton, D.R., Pachepsky, Y.A., 2005. "Transport and retention of Manure-Borne Coliforms in Soil." Vadose Zone Journal. 4:828-837

Harvey, R.W., 1991. "Use of colloid filtration theory in modeling movement of bacteria through a contaminated sandy aquifer." Environmental Science and Technology. 25:178-185

Hassen, A., Jamoussi, F., Saidii, N., Mabrouki, Z., Fakhfakh, E, 2003. "Microbial and copper adsorption by smectitic clay - An experimental study." Environmental Technology. 24:1117-1127

Hornberger, G.M., Mills, AL., Herman, J.S., 1992. "Bacterial Transport in Porous Media: Evaluation of a Model Using Laboratory Observations."

Hrudey, S.E., Huck, P.M., Payment, P., Gillham, R.W., Hrudey, E.J., 2002. "Walkerton: Lessons learned in comparison with waterborne outbreaks in the developed world." Journal of environmental Engineering and Science. 1:397-407

Jewett, D.G., Hilbert, T.A., Logan, B.e., Arnold, R.G., Bales, R.C., 1995. "Bacterial transport in laboratory columns and filters: influences of ionic strength and pH on collision efficiency." Water Research. 29(7):1673-1680

Jiang, G., Noonan, M.J., Buchan, G.D., Smith, N., 2007. "Transport of *Escherichia coli* through variably saturated sand columns and modeling approaches." Journal of Contaminant Hydrology. 93:2-20

Kjartanson, B.H., Eigenbrod, K.D., Leung, K.T., Rosa, B.A., 2005. "Transport of *E. coli* through fractured high plastic clay and compacted silt." CGS conference proceedings, #537.

Kölbel-Boelke,J., Anders, E.M., Nehrkorn, A., 1988. "Microbial communities in the saturated groundwater environment II: Diversity of bacterial communities in a Pleistocene sand aquifer and their in vitro activities." Microbial Ecology. 16(1):31-48

Levy, J., Sun, K., Findley, R.H., Farruggoa, F.T., Porter, J., Mumy, K.L., Tomaras, J., Tomaras, A., 2007. "Transport of *Escherichia coli* bacteria through laboratory columns of glacial-outwash sediments: Estimating model parameter values based on sediment characteristics." Journal of Contaminant Hydrology. 89:71-106

Leon-Morales, C.F., Leis, A.P., Strathmann, M., Flemming, H-C., 2004. "Interactions between laponite and microbial biofilms in porous media: implications for colloid transport and biofilm stability." Water Research. 38:3614-3626

Logan, B.E., 1999. "Environmental Transport Processes" Published by John Wiley and Sons, Inc, New York. ISBN 0471188719, 9780471188711

Logan, B.E., Camesano, T.A., DeSantis, A.A., Unice, K.M., Baygents, J.C., 1999. "Comment on "A Method for Calculating Bacterial Deposition Coefficients Using the Fraction of Bacteria Recovered from Laboratory Columns." Environmental Science and Technology. 33:1316-1317.

Logan, B.E., Jewett, D.G., Arnold, R.G., Bouwer, E.J., O'Melia, C.R., 1995. "Clarification of Clean-Bed Filtration Models." Journal of Environmental Engineering. 121(12):869-873.

Lukacs, C., Smith, T., Steane, B., 2007. "*E. coli* Transport through Sand and Sand-Silt Mixtures." Lakehead University Degree Project.

Macler, B., Merkle, J., 2000. "Current knowledge on groundwater microbial pathogens and their control." Hydrogeology Journal. 8:29-40.

Mailloux, B.J., Fuller, M.E., 2003. "Determination of In Situ Bacterial Growth Rates in Aquifers and Aquifer Sediments." Applied ad Environmental Microbiology. 69(7):3798-3808

Marshall, K.C., 1992. "Biofilms: An Overview of Bacterial Adhesion, Activity and Control at Surfaces." ASM news. 58(4):202-207

Martin, R.E., Bouwer, E.J., Hanna, L.M., 1992. "Application of Clean-Bed Filtration Theory to Bacterial Deposition in Porous Media." Environmental Science and Technology. 26:1053-1058

Maurer, J.J., Brown, T.P., Steffens, W.L., Thayer, S.G., 1998. "The Occurrence of Ambient Temperature-regulated Adhesins, Curli, and the Temperature-sensitive Hemagglutinin Tsh amoung Avian *Escherichia coli*." Avian Disease. 42:106-118

Mcdowell-Boyer, L.M., Hunt, J.R., Sitar, N., 1986. Particle Transport Through Porous Media." Water Resources Research. 22(13):1901-1921

McKay, L.D., J.A. Cherry and R.W. Gillham 1993. "Field experiments in a fractured clay till: 1. hydraulic conductivity and fracture aperture." Water Resources Research 29(4):1149-1162.

McMurry, S.W., Coyne, M.S., Perfect, E., 1998. "Fecal Coliform Transport through Intact Soil Blocks Amended with Poultry Manure." Journal of Environmental Quality, 27:86-92.

Miller, S., 2004. "Permeation of *E. coli* bacteria through a fractured high plastic clay." Civil Engineering degree project. Lakehead University.

Morley, L.M., Hornberger, G.M., Mills, A.L., Herman, J.S., 1998. "Effects of transverse mixing on transport of bacteria through heterogeneous porous media." Water Resources Research. 34(8):1901-1908

National Research Council (U.S.). Committee to Assess the Performance of Engineered Barriers, National Academies Press (COR), 2007. "Assessment of the Performance of Engineered Waste Containment Barriers." Published by National Academies Press. ISBN 0309108098, 9780309108096

Nelson, K.E., Massoudieh, A., Ginn, T.R., 2007. "*E. coli* fate and transport in the Happel sphere-in-cell model." Advances in Water Resources. 30:1492-1504

O'Connor, D.R., 2002. "Report of the Walkerton Inquiry: The Events of May 2000 and Related Issues." Ontario Ministry of the Attorney General. ISBN: 0-7794-2559-6

Olsen, A., Jonsson, A., Normark, S, 1989. "Fibronectin binding mediated by a novel class of surface organelles on *Escherichia coli*." Nature. 338:652-655.

Olsen, M.S., Ford, R.M., Smith, J.A., Fernandez, R.J., 2006. "Mathematical Modeling of Chemotactic Bacterial Transport through a Two-Dimensional Heterogeneous Porous medium." Bioremediation journal. 10(1-2):13-23

Ontario Ministry of Agriculture, Food and Rural Affairs, 2002. "Compacted soil liners", NSTS-07b.

Ontario Ministry of the Environment, June 2003 "Technical Support Document for Ontario Drinking Water Standards, Objectives and Guidelines." Ontario Ministry of the Environment. Publication 4449e01.

Pachepsky, Y.A., Sadeghi, A.M., Bradford, S.A., Shelton, D.R., Guber, A.K., Dao, T., 2006. "Transport and Fate of manure-borne pathogens: Modeling perspective." Agricultural Water Management. 86:81-92.

Pang, L., Close, M., Goltz, M., Sinton, L., Davies, H., Hall, C., Stanton, G., 2003. "Estimation of septic tank setback distances based on transport of *E. coli* and F-RNA phages." Environment International. 29:907-921.

Pekdeger, A., Matthess, G., 1983. "Factors of Bacteria and Virus Transport in Groundwater." Environmental Geology. 5(2):49-52.

Peterson, T.C., Ward, R.C., 1989. "Development of a bacterial transport model for coarse soils." Water Resources Bulletin, American Water Resources Association. 25(2):349-357

Phifer, M.A., Drumm, E.C., Wilson, G.V., 1994. "Effects of Post Compact Water Content Variation on Saturated Conductivity." Hydraulic Conductivity and Waste Transport in Soil. ASTM STP 1142. David E. Daniel and Stephen J. Trautwein,

Eds., American Society for Testing and Materials, Philadelphia,. ISBN 0803114427

Powelson, D.K., Mills, A.L., 2001. "Transport of *Escherichia coli* in Sand Columns with Constant and Changing Water Contents." Journal of Environmental Quality. 30:238-245.

Rajagopalan, R., Tien, C., 1976. "Trajectory analysis of deep-bed filtration with the sphere-in-cell porous media model." American Institute of Chemical Engineers Journal. 22(3):523-533

Reddy, H.L., Ford, R.M., 1996. "Analysis of biodegradation and bacterial transport: Comparison of models with kinetic and equilibrium bacterial adsorption." Journal of Contaminant Hydrology. 22. :271-287.

Redman, J.A., Walker, S.L, Elimelech, M., 2004. "Bacterial Adhesion and Transport in Porous Media: Role of the Secondary Energy Minimum." Environmental Science and Technology. 38:1777-1785

Rockhold, M.L, Yarwood, R.R., Selker, J.S., 2004. "Coupled Microbial and Transport Processes in Soils" Vadose Zone Journal. 3:368-383.

Rogers, B., Logan, B.E., 2000. "Bacterial Transport in NAPL-Contaminated Porous Media." Journal of Environmental Engineering. 126(7):657-666.

Rosa, B.A., Kjartanson, B.H., Leung, K.T., 2007. "Sorption of *ESCHERICHIA COLI* to Clay Barrier Materials." Proceedings of the 60th Canadian Geotechnical Conference, Ottawa, Ontario, October 21-24, 2007.

Rosa, B.A., 2007. " The Transport of Escherichia coli Through Soil." Lakehead University. Masters thesis, Biology.

Sakthivadivel, R., 1969. "Clogging of a granular porous medium by sediment." Hydraulic Engineering Laboratory, University of California, Berkeley, Report HEL 15–17

Schelde, K., Moldrup, P., Jacobsen, O.H., de Jonge, H., de Jonge, L.W., Komatsu, T., 2002. "Diffusion-Limited Mobilization and Transport of Natural Colloids in Macroporous Soil." Vadose Zone Journal. 1:125-136

Schijven, J.F. and Hassanizadeh, S.M., 2000. "Removal of viruses by soil passage: Overview of Modeling, Processes, and Parameters." Critical Reviews in Environmental Science and Technology. 30(1):49-127

Scott, R., Nguyen, H., 2006. "*E. coli* transport through fractured clay." Civil Engineering degree project. Lakehead University.

Sharma, H.D., Reddy, K.R., 2004. "Geoenvironmental Engineering, Site Remediation, Waste Containment, and Emerging Waste Management Technologies." John Wiley & Sons, Inc., Hoboken, New Jersey.

Simunek, J., He, C., Pang, L., Bradford, S.A., 2006. "Colloid-Facilitated Solute Transport in Variably Saturated Porous Media: Numerical Model and Experimental Verification." Vadose Zone Journal. 5:1035-1047.

Sjogren, R.e., 1994. "Prolonged survival of an environmental *Escherichia coli* in laboratory soil microcosms." Water, Air and Soil Pollution. 75:389-403.

Stoddard, C.S., Coyne, M.S., Grove, J.H., 1998. "Fecal Bacteria Survival and Infiltration through a Shallow Agricultural Soil: Timing and Tillage Effects." Journal of Environmental quality. 27:1516-1523.

Surette, M.G., Miller, M.B., Bassler, B.L., 1999. "Quorum sensing in *Escherichia coli*, Salmonella typhimurium and Vibrio harveyi: A new family of genes responsible for autoinducer production." The Proceedings of the National Academy of Sciences USA. 96:1639-1644.

Tong, M., Johnson, W.P., 2007. "Colloid Population Heterogeneity Drive Hyperexponential Deviation from Classic Filtration Theory." Environmental Science and Technology. 41:493-499.

Toride, N., F. J. Leij, and M. Th. van Genuchten, 1995. "The CXTFIT code for estimating transport parameters from laboratory or field tracer experiments." Version 2.0, Research Report No. 137, U. S. Salinity Laboratory, USDA, ARS, Riverside, CA

Tufenkji, N., 2007. "Modeling microbial transport processes in porous media: Traditional approaches and recent developments." Advances in Water Resources. 30:1455-1469.

Tufenkji, N., Elimelech, M., 2004. "Correlation equation for predicting single-collector Efficiency in Physicochemical Filtration in Saturated Porous Media." Environmental Science and Technology. 38:529-536.

Tufenkji, N., Miller, G.F., Ryan, J.N., Harvey, R.W., Elimelech, M., 2004. "Transport of *Cryptosporidium* Oocysts in Porous Media: Role of Straining and Physicochemical Filtration." Environmental Science and Technology. 38:5932-5938.

Unice, K.M., Logan, B.E., 2000. "The insignificant role of hydrodynamic dispersion on bacterial transport." Journal of Environmental Engineering. 126(6):491-500.

van Genuchten, M. Th., 1981 "Non-equilibrium transport parameters from miscible displacement experiments". Research Report No. 119, U. S. Salinity Laboratory, USDA, ARS, Riverside, CA,.

van Genuchten, M.T., 1980. "Determining transport parameters from solute displacement experiments." Research Report No.118 United States department of Agriculture. Science and Education Administration, U.S. Salinity Lab, Riverside California.

van Genuchten, M.T., Wierenga, P.J., 1986. "Solute dispersion coefficients and retardation factors." Methods of Soil Analysis, Part 1. Physical and Mineralogical Methods. Agronomy Monograph. no. 9. 2nd edition. American Society of Agronomy. 1025-1052

Vargas, C., Ortega-Guerrero, A., 2004. "Fracture hydraulic conductivity in the Mexico City clayey aquitard: Field piezometer rising-head tests." Hydrogeology Journal. 12(3):336-344

Vidal, O., Longin, R., Prigent-Combaret, C., Dorel, C., Hooreman, M., Lejeune, P., 1998. "Isolation of an *Escherichia coli* K-12 Mutant Strain Able to Form Biofilms on

Inert Surfaces: Involvement of a New ompR Allele That Increases Curli Expression." Journal of Bacteriology. 180(9):2442-2449

Walker, S.L., Hill, J.E., Redman, J.A., Elimelech, M., 2005. "Influence of Growth Phase on Adhesion Kinetics of *Escherichia coli* D21g." Applied and Environmental Microbiology. 71(6):3093-3099.

White, R.E., 1984. "The Transport of Chloride and Non-Diffusible Solutes Through Soil." Irrigation Science. 6:3-10

Wong, K., Enns, T, 2005. "Transport of E-coli bacteria through clay and silt." Civil Engineering degree project. Lakehead University.

Yao, K, Habibian, M.T., O'melia, C.R., 1971. "Water and Waste Water filtration: Concepts and Applications." Environmental Science and Technology. 5(11):1105-1112

Yates, M.V., Yates, S.R., 1988. "Modeling Microbial Fate in the Subsurface Environment." CRC Critical reviews in environmental control. 17(4):307-344

Young, C.C., Greenfield, M., 1922. "Observations on the viability of the bacterium *coli* group under natural and artificial conditions." American Journal of Public Health. 13:270-273